Multitemporal Mapping of Burned Areas in Mixed Landscapes in Eastern Zambia

Lonesome Malambo

Dissertation submitted to the faculty of the
Virginia Polytechnic Institute and State University
in partial fulfillment of the requirements for the degree of

Doctor of Philosophy
In
Geospatial and Environmental Analysis

Conrad D. Heatwole, Chair

James B. Campbell

Valerie A. Thomas

Randolph H. Wynne

29th October, 2014

Blacksburg, VA

Keywords: Remote sensing, Burned area mapping, Multitemporal analysis, Fuzzy clustering, Scan line corrector error, Landsat gap-filling, Zambia.

Multitemporal Mapping of Burned Areas in Mixed Landscapes in Eastern Zambia

Lonesome Malambo

ABSTRACT

Fires occur extensively across Zambia every year, a problem recognized as a major threat to biodiversity. Yet, basic tools for mapping at a spatial and temporal scale that provide useful information for understanding and managing this problem are not available. The objectives of this research were: to develop a method to map the spatio-temporal seasonal fire occurrence using satellite imagery, to develop a technique for estimating missing data in the satellite imagery considering the possibility of change in land cover over time, and to demonstrate applicability of these new tools by analyzing the fine-scale seasonal patterns of landscape fires in eastern Zambia. A new approach for mapping burned areas uses multitemporal image analysis with a fuzzy clustering algorithm to automatically select spectral-temporal signatures that are then used to classify the images to produce the desired spatio-temporal burned area information. Testing with Landsat data (30m resolution) in eastern Zambia showed accuracies in predicting burned areas above 92%. The approach is simple to implement, data driven, and can be automated, which can facilitate quicker production of burned area information. A profile-based approach for filling missing data uses multitemporal imagery and exploits the similarity in land cover temporal profiles and spatial relationships to reliably estimate missing data even in areas with significant changes. Testing with simulated missing data from an 8-image spectral index sequence showed highly correlated (R^2 of 0.78-0.92) and precise estimates (deviations 4-7%) compared to actual values. The profile-based approach overcomes the common requirement of gap-filling methods that there is gradual or no change in land cover, and provides accurate gap-filling under conditions of both gradual and abrupt changes. The spatio-temporal progression of landscape burning was evaluated for the 2009 and 2012 fire seasons (June-November) using Landsat data. Results show widespread burning (~ 60%) with most fires occurring late (August-October) in the season. Fire occurrence and burn patch sizes decreased with increasing settlement density and landscape fragmentation reflecting human influences and fuel availability. Small fires (< 5ha) are predominant and were significantly under-detected (>50%) by a global dataset (MODIS Burned Area Product (500m resolution)), underscoring the critical need of higher geometric resolution imagery such as Landsat imagery for mapping such fine-scale fire activity.

To Phyllis, Evan and Ethan

Acknowledgements

I would like to express my deepest appreciation to my advisor, Dr. Conrad Heatwole, who has been a great mentor for me both in my academic work and life in general. I have learned great lessons from my interaction with you. Thank you very much for giving me the great chance to carry out this research, for your professional guidance, funding, and for your enduring trust in my commitment to finishing my PhD degree.

I also extend my gratitude to my committee members Dr. James B. Campbell, Dr. Valerie Thomas and Dr. Randolph Wynne for their brilliant, challenging but helpful comments that reinforced by dissertation. Dr. Campbell, thank you very much for accommodating my many impromptu visits and for whetting my appetite for spatial analysis, Dr. Thomas for your insightful and detailed feedback and Dr. Wynne for always encouraging me to reach out and network.

I would like to thank all the staff members in the department of Biological Systems Engineering who have always offered their help. Special thanks to the department head, Dr. Mary Leigh Wolfe and her assistant Ms. Barbara Taylor, for facilitating scholarship and grants, even at short notice, that helped me travel to carry out field work in Zambia and attend academic conferences. Thanks to Denton Yoder for helping with computing issues and for being an easy person to talk to. Thank you for the coffees too.

Finally, I would like to express my heartfelt thanks to my family for their patience and encouragement during the course of my research. To my wife, Phyllis, who believed and stood by me through out and was always my support in the moments when I felt hopeless, to my two boys, Evan and Ethan, for giving me the reason to live and work harder. To mum and dad, thank you very much for your love and sacrifices you made on my behalf. Thank you also to my mother in law for the sacrifice you made to help us take care of our new born, without it, it would have been harder to carry out my research. Thank you to my brother, Kelvin, my sisters, Linda, Lynn, Lister and Lonely, my sister in law, Glenda for your prayers and encouragement. I love you all.

Table of Contents

List of Figures

List of Tables

Chapter 1
The Challenge of Mapping Landscape Fires

1.1 ROLE OF FIRE IN THE ENVIRONMENT

1.1.1 Fire occurrence

Fires are widespread seasonal events in many regions around the world and affect millions of hectares of vegetated land every year. Estimates from satellite imagery of the total global burned area between 2000 and 2008 ranged from 330 to 431 million hectares with the majority, about 250 million hectares, occurring in Africa (FAO, 2007; Giglio et al., 2010; Giglio et al., 2006; Tansey et al., 2008). Future projections from climate change models show increasing trends in global fire activity leading to an increase in global burned area (Doerr et al., 2006; Pechony and Shindell, 2010). The majority of fires in the tropics and subtropics, and in some temperate-boreal transition zones, are caused by human activities usually associated with land-use practices and changes (Goldammer et al., 2001; Pereira et al., 1999). In many cases, especially in developing countries where fire management is inadequate, these fires burn out of control eventually covering large areas (Chuvieco, 1999). In Boreal biomes and in a few temperate and tropical biomes, lightning is also a significant source of fire (Lafon and Grissino-Mayer, 2007).

1.1.2 Fire effects

Fire can play an integral role in the function of ecosystems. In fire-dependent ecosystems such as savannas, it helps maintain biodiversity, productivity and recycling of nutrients (Cochrane and Ryan, 2009; Goldammer and De Ronde, 2004). Fire may also be detrimental to the normal functioning of ecosystems if it is excessive or occurs in a fire-sensitive ecosystem. Fire can cause excessive heating of the soil and local environment contributing to plant mortality, reduced surface cover, and impairment of soil structure leading to ecosystem and watershed damage (Chuvieco, 1999; DeBano et al., 1998; Miller and Yool, 2002). The burning of plant biomass also contributes to air and water pollution through the deposition of burned biomass and release of large amounts of sulfur dioxide and particulates into the atmosphere (Innes et al., 2000). Thus, resource managers and policy makers must evaluate the positive against and the negative impacts of fire so net benefit is realized from the interaction of fire and the environment (DeBano et al., 1998; FAO, 2007).

The effects of fire can be observed at various spatial and temporal scales (DeBano et al., 1998; Geraci et al., 2009; Lhermitte et al., 2011). At a small scale, fire can impact soil structure, plant nutrition, species composition and competition, and the cumulative effect of these can lead to changes in composition, structure and function of ecosystems at a landscape level. Further, these impacts can lead to changes in vegetation distribution and atmospheric chemistry at regional or global scales (Lentile et al., 2006; Lhermitte et al., 2011). The timing of fire also influences fire impacts on ecosystem resources which are a function of varying fire intensity and individual plant phenology cycles (Cochrane and Ryan, 2009; Gillanders et al., 2008). In the tropics, fires burning late in the dry season tend to burn more intensely thus are more damaging because of the dry biomass and hot weather compared to those burning early in the season (Goldammer et al., 2001). Fires also tend to be more destructive if they occur at certain critical points in plant's cycle. For instance, fire can hamper regeneration of it occurs at seed set versus if it occurs during the plant's dormant or senescent periods (Cochrane and Ryan, 2009). Therefore, better understanding of fire disturbance in a given area requires an appreciation of where, how often, and when fire occurs (Pereira, 2003; Pricope and Binford, 2012). The combination of such information with other relevant ecosystem information can enable a wide variety of fire related impacts to be assessed (Geraci et al., 2009). Because of that, there is need for mapping of burned areas and collection of related ecosystem information (French et al., 2008; Roy et al., 2002). Burned area maps are a vital input to a number of terrestrial and atmospheric fire impact assessments. Burned area maps enable co-location of the burning with affected vegetation so localized assessments such as plant mortality, vegetation regeneration, soil degradation can be carried out (Pereira, 2003). Burned area is also an important input in climate modelling where it is used with available fuel load and burn efficiency information to estimate trace gases or aerosol emissions into the atmosphere (Geraci et al., 2009; Smith et al., 2007). In regions where fire often causes human and infrastructure losses, burned area information can be used to assess the economic impact of the fire (Chuvieco, 1999). All these applications underscore the need for the availability of reliable burned area information in the management of natural resources.

1.2 OBTAINING BURNED AREA INFORMATION USING REMOTE SENSING TECHNIQUES

Remote sensing presents the only practical way of collecting information on burned areas from a local to global level (Roy et al., 2002). The capability of mapping fire patterns at regular time intervals makes it a more suitable for collecting such information than field observation (Flasse et al., 2004). The regular data capture allows the study of spatial and temporal occurrence of fire and associated interactions with the ecosystem and environment in a more complete way (Archibald et al., 2010). By capturing data across a wider range of the electromagnetic spectrum than can be seen by humans, remote sensing permits the extraction of a wider range of fire-related information than is possible with other methods (Coppin et al., 2004; Flasse et al., 2004).

1.2.1 Spectral characterization of fire response

Generally, remote sensing methods are based on developing a relationship or correlation between variations on the Earth's surface and spectral variations observed from remote sensors (Campbell and Wynne, 2011; Flasse et al., 2004). In the case of mapping burned areas, physical changes due to fire such as loss of vegetation, charring of the surface and relative temperature rises (Flasse et al., 2004) can be related to observed spectral changes that enable the discrimination of burned areas from unburned ones (Pereira et al., 1999). A number of studies have documented the characteristic spectral responses to fire in the different regions (visible, near-infrared, mid-infrared and thermal) of the electromagnetic spectrum and these have enabled the application of wide array of approaches to mapping burned areas. In the visible spectrum, a general reduction of reflectance after a fire has been observed in many studies. However, deviations from this pattern have been reported and are usually associated with prevailing factors such as soil background reflectance, combustion completeness (presence of white ash), and vegetation structure (grassland vs forest) any of which may result in an increase in reflectance (Pereira et al., 1999; Roy and Landmann, 2005). The near-infrared region has also been extensively used to discriminate burned areas and is considered more effective than the visible region (Koutsias et al., 1999). Because unburned vegetation has very high reflectance in this region and very low reflectance after a fire (Lentile et al., 2006), there is a marked decrease in reflectance which provides for better discrimination of burned areas. This characteristic is the basis for the design of burn-specific spectral indices such as the normalized burn ratio (Key and Benson, 2003). In the mid-infrared portion, the loss of water or moisture from plants causes a general increase in reflectance from the pre-fire state (Trigg and

Flasse, 2001). The mid-infrared region suffers minimal atmospheric scattering compared to the visible and near-infrared (NIR) spectra region making sensing in this region more attractive (Pereira et al., 1999). The thermal region has been used by basing classification on the relative temperature rise of a burned area to surrounding unburned areas (Flasse et al., 2004). The suitability of a method is thus constrained by the availability of data since all satellite imagery does not capture data in all these wavelength bands (Pereira et al., 1999).

1.2.2 Remote sensing data for mapping burned areas

Due to differences in fire severity, burn completeness, land cover type, phenology and the persistence of the burn signal since fire, burned areas can exhibit wide spectral, spatial and temporal variability which complicates burned area mapping (Bastarrika et al., 2011; Pereira, 2003; Roy and Landmann, 2005). In addition, the general spatial heterogeneity of the landscape also raises questions on the optimum scale of imagery to characterize fire events (Koutsias et al., 1999). These two aspects are of vital importance in the application of remote sensing for burned area mapping and determine the suitable data, in terms of spatial, spectral and temporal resolution, and to some extent the techniques for retrieving the required burn information (Jensen, 2007; Koutsias et al., 1999). Coarse spatial resolution data (250m to 1km ground sample distance) from sensors such as Advanced Very High Resolution Radiometer (AVHRR), Moderate Resolution Imaging Spectro-radiometer (MODIS) or SPOT VGT have been extensively used to generate active fire (Giglio et al., 2009; Justice et al., 2002) and burned area (Boschetti et al., 2009) information. The daily imaging frequency in the case of MODIS enables the characterization of the daily and seasonal patterns of burning at a regional or global level which is useful in the study of fire patterns and their inter-relation with environmental and anthropogenic factors at regional scales (Archibald et al., 2010; Pricope and Binford, 2012). However, such coarse data are limited for local more detailed mapping of fire especially in the fragmented landscapes were fire sizes tend to be small (Kull and Laris, 2009; Sá et al., 2007). To meet this need, higher spatial resolution data such as Landsat are needed and are increasingly being used to generate burned area maps (Bastarrika et al., 2011; Laris, 2005). These data provide a more detailed view of the landscape and therefore burn estimates and derivatives such as carbon emissions are much better than what can be obtained using coarse resolution imagery (Eva and Lambin, 1998; Pereira, 2003). The now

free archive of Landsat data enables multitemporal burn mapping which has not been widely explored before because of the high cost of acquiring the imagery (Giri et al., 2013).

1.2.3 Burned area mapping methods

Remote sensing methods for mapping burn areas are usually classified in terms of the number of images used in the analyses (Koutsias et al., 1999; Quintano et al., 2011), with the three primary approaches summarized as the following.

1) Single image approaches, where one post fire image is used. Supervised techniques such as object based classification (Gitas et al., 2004), classification and regression trees (CART) (Cassidy, 2007), support vector machines and neural networks (Cao et al., 2009), or unsupervised techniques such as clustering (Laris, 2005), have mostly been applied.

2) Bitemporal methods, where both a pre-fire and post-fire image are used and detection is based on temporal change of the spectral signature of the burned area from its unburned state. Thresholding of differenced spectral index data such as the normalized burn ratio (NBR) (Key and Benson, 2003) is primarily used to discriminate burned from unburned areas (Koutsias et al., 1999).

3) Multitemporal or time series approaches, where more than two images are used for the analyses (Quintano et al., 2006). In this category supervised neural networks (Al-Rawi and Casanova, 2001; Gomez and Martin, 2011) and physical models such the Bi-Directional Reflectance Model-Based Expectation change detection approach (Roy et al., 2002) have been applied

Factors such as phenological changes, persistence of the burn signal, and time since the fire point to the need for a temporal dimension in burn mapping. Thus, it should not be surprising that use of single or bitemporal approaches often leads to the confusion of burned areas with spectrally similar land covers such as wetlands or with phenological changes during the fire season (Cassidy, 2007). Given that landscape burning is a dynamic event, burn data obtained through single and bitemporal approaches are less informative at capturing the spatio-temporal patterns of fire (Thackway et al., 2013). The use of multiple images over a fire season or over a chosen timespan can significantly overcome such limitations and provide a more comprehensive way of mapping spatio-temporal distribution of burned areas (Lhermitte et al., 2011; Lu et al., 2004).

1.3 OBJECTIVES

Developing countries such as Zambia face difficulties in monitoring their natural resources such as forests due to budgetary constraints, lack of qualified personnel for monitoring activities and sometimes low political will to address issues pertaining to the environment. As such, there is often little or no effective management of natural resources, and disturbances such as forest fire go uncontrolled (Goldammer and De Ronde, 2004). Fire is increasingly recognized as one of the major threats to biodiversity in Zambia (Forestry Department, 2013; Kokwe and Mickels-Kokwe, 2012; Vinya et al., 2011). Widespread fire activity in the dry season results in the proportion of burned land exceeding 50% in many regions of the country (Archibald et al., 2010). Fire activity in Zambia also ranks highest in terms of monthly fire radiative energy release power (FRP) which measures the strength of fires. This has vital implications for biomass emissions, given the direct relationship of FRP to the rate of biomass consumption (Ichoku et al., 2008). However, little has been done to control the frequent occurrence of fires and there is lack of reliable burned information to study fire impacts at local scales (Pricope and Binford, 2012; Zimsky et al., 2010).

More effective management could be aided through the use of remote sensing fire products (Goldammer and De Ronde, 2004). However, currently available global datasets are not locally relevant because of the coarse spatial resolution. Fires in many regions of Africa occur as many widely dispersed small events and there is a high potential to miss them or over-estimate the burned areas with these coarse data (Goldammer and De Ronde, 2004; Kull and Laris, 2009). The main study area in Eastern Zambia is a mixed landscape with wide land cover variation ranging from large homogenous areas of woodland and grassland to highly settled, fragmented areas dominated by cropland, shrubs and fallow. Thus, burned areas sizes may vary considerably (Lafon and Grissino-Mayer, 2007). Fires in agricultural fields are limited in size by small crop field sizes which may not be detectable with course imagery data, thus missing subtle but important changes in fire distribution (Loboda et al., 2007; Randerson et al., 2012). Effective remote sensing data and techniques are needed to characterize the fine to broad-scale burn patterns in such mixed land use landscapes.

The goal of this study was to develop methods for mapping the fine-scale mosaic of burning created by fragmented fire events using higher spatial resolution (30 m ground sample distance) Landsat data. With ready access to Landsat scenes spanning the fire season there is the possibility

of developing multitemporal burn mapping methods that would be able to better characterize seasonal fire activity. However, the usability of these data is often hampered by missing data due to cloud cover and sensor specific problems such as the scan-line corrector (SLC) error in Landsat 7 (Brooks et al., 2012). Therefore, effective methods for gap-filling are also needed to make these data more useful for assessing environmental disturbances such as fire. Existing gap filling methods (Chen et al., 2011; Scaramuzza et al., 2004; Zhu et al., 2012) are not designed to model abrupt changes in the landscape such as is due to fire, thus conceptually cannot adequately estimate missing data under these conditions. With multitemporal data there is great potential to model these changes more accurately (Thackway et al., 2013) to provide better estimates for missing data. This research was structured as three independent but related studies which are developed and described in Chapters 2 - 4. The three primary objectives of these studies are expressed in the following:

1) Develop a method for fine scale mapping of the spatio-temporal progression of burned areas in Eastern Zambia over a fire season using multitemporal Landsat imagery.

2) Develop and evaluate a change-preserving gap filling method for estimating missing values in a multitemporal spectral index derived from Landsat data to provide a method that can accurately estimate missing values even under abrupt change due to fire.

3) Characterize the spatial and temporal patterns of landscape fires across three physiographic regions in the Eastern Province of Zambia, and assess variability in burn patterns as a function of land cover, topography and settlement density.

1.4 REFERENCES

Al-Rawi, K.R., Casanova, J.L., 2001. A neural network approach for mapping burned areas using post-fire and multi-temporal NOAA-AVHRR images, in: Buchroithner, M. (Ed.), Decade of Trans-European Remote Sensing Cooperation. Swets & Zeitlinger, Lisse, The Netherlands, pp. 189-192.

Archibald, S., Scholes, R.J., Roy, D.P., Roberts, G., Boschetti, L., 2010. Southern African fire regimes as revealed by remote sensing. International Journal of Wildland Fire 19, 861-878.

Bastarrika, A., Chuvieco, E., Martín, M.P., 2011. Mapping burned areas from Landsat TM/ETM+ data with a two-phase algorithm: Balancing omission and commission errors. Remote Sensing of Environment 115, 1003-1012.

Boschetti, L., Roy, D., Hoffmann, A.A., 2009. MODIS Collection 5 Burned Area Product - MCD45 User's Guide, Retrieved 03/08, 2011, from http://modis-fire.umd.edu/Documents/MODIS_Burned_Area_User_Guide_2.0.pdf.

Brooks, E.B., Thomas, V.A., Wynne, R.H., Coulston, J.W., 2012. Fitting the multitemporal curve: A fourier series approach to the missing data problem in remote sensing analysis. Geoscience and Remote Sensing, IEEE Transactions on, 1-14.

Campbell, J.B., Wynne, R.H., 2011. Introduction to remote sensing. Guilford Press, New York.

Cao, X., Chen, J., Matsushita, B., Imura, H., Wang, L., 2009. An Automatic method for burn scar mapping using support vector machines. International Journal of Remote Sensing 30, 577-594.

Cassidy, L., 2007. Mapping the annual area burned in the wetlands of the Okavango panhandle using a hierarchical classification approach. Wetlands Ecology and Management 15, 253-268.

Chen, J., Zhu, X., Vogelmann, J.E., Gao, F., Jin, S., 2011. A simple and effective method for filling gaps in Landsat ETM+ SLC-off images. Remote Sensing of Environment 115, 1053-1064.

Chuvieco, E., 1999. Remote sensing of large wildfires in the European Mediterranean Basin. Springer, Berlin; New York.

Cochrane, M., Ryan, K., 2009. Fire and fire ecology: Concepts and principles, Tropical Fire Ecology. Springer Berlin Heidelberg, pp. 25-62.

Coppin, P., Jonckheere, I., Nackaerts, K., Muys, B., Lambin, E., 2004. Digital change detection methods in ecosystem monitoring: A review. International Journal of Remote Sensing 25, 1565-1596.

DeBano, L.F., Neary, D.G., Folliott, P.F., 1998. Fire's effects on ecosystems. J. Wiley, New York.

Doerr, S.H., Shakesby, R.A., Blake, W.H., Chafer, C.J., Humphreys, G.S., Wallbrink, P.J., 2006. Effects of differing wildfire severities on soil wettability and implications for hydrological response. Journal of Hydrology 319, 295-311.

Eva, H., Lambin, E.F., 1998. Remote sensing of biomass burning in tropical regions: Sampling issues and multisensor approach. Remote Sensing of Environment 64, 292-315.

FAO, 2007. Fire management : global assessment 2006 : a thematic study prepared in the framework of the Global forest resources assessment 2005. Food and Agriculture Organization of the United Nations, Rome.

Flasse, S.P., Trigg, S.N., Ceccato, P.N., Perryman, A.H., Hudak, A.T., Thompson, M.W., Brockett, B.H., Dramé, M., Ntabeni, T., Frost, P.E., Landmann, T., Roux, J.L.l., 2004. Remote sensing of vegetation fires and Its contribution to a fire management Information system. Global Fire Management Center, Freiburg.

Forestry Department, 2013. About Forestry Department Retrieved 9/9, 2013, from http://www.ministryoflands.gov.zm/index.php/forestry.

French, N.H.F., Kasischke, E.S., Hall, R.J., Murphy, K.A., Verbyla, D.L., Hoy, E.E., Allen, J.L., 2008. Using Landsat data to assess fire and burn severity in the North American boreal forest region: An overview and summary of results. International Journal of Wildland Fire 17, 443-462.

Geraci, R., Csiszar, I., Justice, C., Goldammer, J.G., van Lierop, P., Sessa, R., 2009. Fire Disturbance - Assessment of the status of the development of the standards for the Terrestrial Essential Climate Variables. Global Terrrestrial Observing System, Food Agriculture Organization (FAO), Rome, pp. 1-10.

Giglio, L., Loboda, T., Roy, D.P., Quayle, B., Justice, C.O., 2009. An active-fire based burned area mapping algorithm for the MODIS sensor. Remote Sensing of Environment 113, 408-420.

Giglio, L., Randerson, J.T., van der Werf, G.R., Kasibhatla, P.S., Collatz, G.J., Morton, D.C., DeFries, R.S., 2010. Assessing variability and long-term trends in burned area by merging multiple satellite fire products. Biogeosciences 7, 1171-1186.

Giglio, L., van der Werf, G.R., Randerson, J.T., Collatz, G.J., Kasibhatla, P., 2006. Global estimation of burned area using MODIS active fire observations. Atmos Chem Phys 6, 957-974.

Gillanders, S.N., Coops, N.C., Wulder, M.A., Gergel, S.E., Nelson, T., 2008. Multitemporal remote sensing of landscape dynamics and pattern change: Describing natural and anthropogenic trends. Progress in Physical Geography 32, 503-528.

Giri, C., Pengra, B., Long, J., Loveland, T.R., 2013. Next generation of global land cover characterization, mapping, and monitoring. International Journal of Applied Earth Observation and Geoinformation 25, 30-37.

Gitas, I.Z., Mitri, G.H., Ventura, G., 2004. Object-based image classification for burned area mapping of Creus Cape, Spain, using NOAA-AVHRR imagery. Remote Sensing of Environment 92, 409-413.

Goldammer, J.G., De Ronde, C., 2004. Wildland Fire Management Handbook for Sub-Sahara Africa. Global Fire Management Center, Freiburg.

Goldammer, J.G., Frost, P.G., Jurvélius, M., Kamminga, E.M., Kruger, T., Moody, S.I., Pogeyed, M., 2001. Community participation in integrated forest fire management: Experiences from Africa, Asia and Europe, Communities in Flames. Proceedings of an International Conference on Community Involvement in Fire Management. FAO Regional Office for Asia and the Pacific, Balikpapan, Indonesia, pp. 25-28.

Gomez, I., Martin, M.P., 2011. Prototyping an artificial neural network for burned area mapping on a regional scale in Mediterranean areas using MODIS images. International Journal of Applied Earth Observation and Geoinformation 13, 741-752.

Ichoku, C., Giglio, L., Wooster, M.J., Remer, L.A., 2008. Global characterization of biomass-burning patterns using satellite measurements of fire radiative energy. Remote Sensing of Environment 112, 2950-2962.

Innes, J.L., Beniston, M., Verstraete, M.M., 2000. Biomass burning and its inter-relationships with the climate system. Kluwer Academic Publishers, Dordrecht; Boston.

Jensen, J.R., 2007. Remote sensing of the environment : An earth resource perspective. Pearson Prentice Hall, Upper Saddle River, NJ.

Justice, C.O., Giglio, L., Korontzi, S., Owens, J., Morisette, J.T., Roy, D., Descloitres, J., Alleaume, S., Petitcolin, F., Kaufman, Y., 2002. The MODIS fire products. Remote Sensing of Environment 83, 244-262.

Key, C.H., Benson, N.C., 2003. The normalized burn ratio (NBR): A Landsat TM radiometric measure of burn severity. US Geological Survey Northern Rocky Mountain Science Center.

Kokwe, M., Mickels-Kokwe, G., 2012. Forest management practices with potential for REDD+ in Zambia. Ministry of Lands, Natural Resources and Environmental Protection, Lusaka, Zambia.

Koutsias, N., Karteris, M., Fernández-Palacios, A., Navarro, C., Jurado, J., Navarro, R., Lobo, A., 1999. Burnt land mapping at local scale, in: Chuvieco, E. (Ed.), Remote Sensing of Large Wildfires. Springer Berlin Heidelberg, pp. 157-187.

Kull, C., Laris, P., 2009. Fire ecology and fire politics in Mali and Madagascar, Tropical Fire Ecology. Springer Berlin Heidelberg, pp. 171-226.

Lafon, C.W., Grissino-Mayer, H.D., 2007. Spatial patterns of fire occurrence in the central Appalachian Mountains and implications for wildland fire management. Phys Geogr 28, 1-20.

Laris, P.S., 2005. Spatiotemporal problems with detecting and mapping mosaic fire regimes with coarse-resolution satellite data in savanna environments. Remote Sensing of Environment 99, 412-424.

Lentile, L.B., Holden, Z.A., Smith, A.M.S., Falkowski, M.J., Hudak, A.T., Morgan, P., Lewis, A.S., Gessler, P.E., Benson, N.C., 2006. Remote sensing techniques to assess active fire characteristics and post-fire effects. International Journal of Wildland Fire 15, 319.

Lhermitte, S., Verbesselt, J., Verstraeten, W.W., Veraverbeke, S., Coppin, P., 2011. Assessing intra-annual vegetation regrowth after fire using the pixel based regeneration index. ISPRS Journal of Photogrammetry and Remote Sensing 66, 17-27.

Loboda, T., O'Neal, K.J., Csiszar, I., 2007. Regionally adaptable dNBR-based algorithm for burned area mapping from MODIS data. Remote Sensing of Environment 109, 429-442.

Lu, D., Mausel, P., Brondízio, E., Moran, E., 2004. Change detection techniques. International Journal of Remote Sensing 25, 2365-2401.

Miller, J.D., Yool, S.R., 2002. Mapping forest post-fire canopy consumption in several overstory types using multi-temporal Landsat TM and ETM data. Remote Sensing of Environment 82, 481-496.

Pechony, O., Shindell, D.T., 2010. Driving forces of global wildfires over the past millennium and the forthcoming century, in: Sullenberger, D. (Ed.), PNAS. National Academy of Sciences of the United States of America, Washington, DC, pp. 19167-19170.

Pereira, J.M.C., 2003. Remote sensing of burned areas in tropical savannas. International Journal of Wildland Fire 12, 259-270.

Pereira, J.M.C., Sá, A.C.L., Sousa, A.M.O., Silva, J.M.N., Santos, T.N., Carreiras, J.M.B., 1999. Spectral characterisation and discrimination of burnt areas, in: Chuvieco, E. (Ed.), Remote Sensing of Large Wildfires. Springer Berlin Heidelberg, pp. 123-138.

Pricope, N.G., Binford, M.W., 2012. A spatio-temporal analysis of fire recurrence and extent for semi-arid savanna ecosystems in southern Africa using moderate-resolution satellite imagery. Journal of Environmental Management 100, 72-85.

Quintano, C., Fernandez-Manso, A., Fernandez-Manso, O., Shimabukuro, Y.E., 2006. Mapping burned areas in Mediterranean countries using spectral mixture analysis from a uni-temporal perspective. International Journal of Remote Sensing 27, 645-662.

Quintano, C., Fernández-Manso, A., Stein, A., Bijker, W., 2011. Estimation of area burned by forest fires in Mediterranean countries: A remote sensing data mining perspective. Forest Ecology and Management 262, 1597-1607.

Randerson, J.T., Chen, Y., van der Werf, G.R., Rogers, B.M., Morton, D.C., 2012. Global burned area and biomass burning emissions from small fires. J Geophys Res-Biogeo 117.

Roy, D., Landmann, T., 2005. Characterizing the surface heterogeneity of fire effects using multi-temporal reflective wavelength data. International Journal of Remote Sensing 26, 4197-4218.

Roy, D.P., Lewis, P.E., Justice, C.O., 2002. Burned area mapping using multi-temporal moderate spatial resolution data - a bi-directional reflectance model-based expectation approach. Remote Sensing of Environment, 263-286.

Sá, A.C.L., Pereira, J.M.C., Gardner, R.H., 2007. Analysis of the relationship between spatial pattern and spectral detectability of areas burned in southern Africa using satellite data. International Journal of Remote Sensing 28, 3583-3601.

Scaramuzza, P., Micijevic, E., Chander, G., 2004. SLC Gap-Filled Products: Phase One Methodology, Retrieved 4/22, 2011, from http://landsat.usgs.gov/documents/SLC_Gap_Fill_Methodology.pdf.

Smith, A.M.S., Drake, N.A., Wooster, M.J., Hudak, A.T., Holden, Z.A., Gibbons, C.J., 2007. Production of Landsat ETM plus reference imagery of burned areas within Southern African savannahs: comparison of methods and application to MODIS. International Journal of Remote Sensing 28, 2753-2775.

Tansey, K., Grégoire, J.-M., Defourny, P., Leigh, R., Pekel, J.-F., van Bogaert, E., Bartholomé, E., 2008. A new, global, multi-annual (2000–2007) burnt area product at 1 km resolution. Geophys Res Lett 35, L01401.

Thackway, R., Lymburner, L., Guerschman, J.P., 2013. Dynamic land cover information: bridging the gap between remote sensing and natural resource management. Ecol Soc 18.

Trigg, S., Flasse, S., 2001. An evaluation of different bi-spectral spaces for discriminating burned shrub-savannah. International Journal of Remote Sensing 22, 2641-2647.

Vinya, R., Kasumu, E.C., Syampungani, S., Monde, C., Kasubika, R., 2011. Preliminary Study on the Drivers of Deforestation and Potential for REDD+ in Zambia., Lusaka, Zambia.

Zhu, X., Liu, D., Chen, J., 2012. A new geostatistical approach for filling gaps in Landsat ETM+ SLC-off images. Remote Sensing of Environment 124, 49-60.

Zimsky, M., Mupemo, F., Robinson, J., Sekhran, N., 2010. Results of the GEF Biodiversity Portfolio Monitoring and Learning Review Mission, Zambia. Gloabl Environment Facility.

Chapter 2
Mapping Seasonal Fire Progression: Automatic Training Signature Selection for Multitemporal Mapping

2.1 ABSTRACT

The need to monitor the occurrence of fire has prompted a wide range of burned area mapping methods. Single and bitemporal techniques have commonly been applied. However, multitemporal analysis approaches present the opportunity for generation of spatio-temporal burn information in a more efficient way. This paper presents an approach for spatio-temporal mapping of seasonally burned areas. The method relies on the distinctive temporal signatures exhibited by various burn events over a fire season to map burned areas. The spectral-temporal signatures are automatically selected from sampled spectral index data using fuzzy clustering by imposing minimum membership and cluster purity criteria in the selection process and then applied to a Random Forest classifier to derive the required spatio-temporal burned area information. The method was assessed for the 2009 and 2012 fire seasons in eastern Zambia (~8000km^2) using 8 Landsat images in each case. The assessment was conducted over two sites with different land cover distributions to test performance in different landscapes. To account for the random nature of clustering in the training sample selection step, 30 runs were carried out by modifying the seed value of the random process and results averaged to get the final accuracy measures. The use of multiple runs enabled identification of the general trends in overall accuracy with respect to the variation in number of clusters and number of training samples selected. Using over 1000 validation points for each year, we obtained overall accuracies above 92%. While the number of clusters and training samples varied in the 30 runs, the absolute difference in accuracies were not large and do not detract from the overall good performance of the method. The presented approach is data driven and automatic which has the potential to support fire monitoring programs to generate more detailed burned area inventories than are currently possible from coarse datasets such as the MODIS burned area product.

Keywords: Fire, Burned area mapping, Abrupt change, Fuzzy c-means, Landsat, Random Forest.

2.2 INTRODUCTION

Globally, fire is a widespread seasonal phenomenon that has local to regional impacts on ecological and atmospheric processes (Lhermitte et al., 2011; Roy et al., 2002). Because fire impacts can vary with time and space, mapping spatio-temporal fire occurrence is a vital resource for understanding the wide range of fire related impacts (Lhermitte et al., 2011). Information from burn maps can support various environmental studies including atmospheric emission estimation (Smith et al., 2007), and localizing fire related impacts such as erosion and surface runoff, plant mortality, vegetation succession and property loss (Doerr et al., 2006; Flasse et al., 2004). Burned area information can also be used to guide fire and ecosystem management planning (Geraci et al., 2009; Goldammer and De Ronde, 2004). Satellite remote sensing presents the only practical means of monitoring fire occurrence over large areas (Roy et al., 2002) and with regular and repeated observations, satellite sensors present a cost effective and efficient way of collecting consistent data on fire occurrence (Flasse et al., 2004; Kennedy et al., 2007).

Coarse spatial resolution data from sensors such as Advanced Very High Resolution Radiometer (AVHRR), Moderate Resolution Imaging Spectro-radiometer (MODIS) and SPOT VGT have been extensively used to generate burned area information (Boschetti et al., 2009). The higher temporal sampling capability of these sensors systems enables the characterization of the daily and seasonal patterns of burning at regional and global level which is useful in the study of fire patterns and their inter-relation with environmental and anthropogenic factors at regional levels (Archibald et al., 2010; Pricope and Binford, 2012). However, such coarse data are limited for more detailed local mapping of fire, especially in fragmented landscapes were fire sizes tend to be small (Kull and Laris, 2009; Sá et al., 2007). To meet this need, higher spatial resolution data such as Landsat are increasingly being used to generate burned area maps (French et al., 2008; Lentile et al., 2006). These data provide a more detailed view of the landscape thus burn estimates or any dependent estimates such as carbon emissions are more reliable than what is obtained using coarse resolution imagery (Eva and Lambin, 1998; Pereira, 2003). The now free archive of Landsat data can also support seasonal multitemporal burn mapping to derive adequate spatio-temporal information which would enable a better linkage between fire disturbance and pertinent applications such as fire management, ecosystem impacts and carbon emissions assessments (Eva and Lambin, 1998; Korontzi et al., 2003).

Eastern Zambia has very distinct rainy and dry seasons, with 850 - 1050 mm rainfall between November and April, and less than 10mm in the entire dry season of May to October (Celis et al., 1991). Landscape composition varies from wide extents of woodland and grassland to more fragmented landscapes dominated by cropland, scrub and fallow. As the vegetation dries up following the last rainfalls of April, landscape fires become a common occurrence in the fire season, mainly June to November. Since there are no lightning storms during the dry season, fires can be solely attributed to anthropogenic origins. Fires are started for a wide variety of reasons: to clear crop residue and weeds from fields, to prepare new forest land for cultivation, to hunt small game, and to clear undergrowth for safety along forest paths. Such fires frequently burn out of control and cover large areas due to the dry conditions (Frost, 1999; Goldammer et al., 2001). Burned areas remain in a charred state until the advent of significant rains in December when vegetation re-emerges and covers the landscape in green. Much of the landscape is thus touched by fire every year as a seasonally re-occurring event. Given the extensive burning, burned area mapping techniques are needed that can be effective across the broad range of land cover types and scales. It is also critical that the derived burn area information provide information on the temporal patterns of burning since fire intensity (and thus fire impacts) can vary during the fire season (Laris, 2005). Such temporal information on burned areas in various land cover types could inform current Reducing Emissions from Deforestation and Forest Degradation (REDD+) programs (Vinya et al., 2011) and contribute to local scale fire inventory and general fire management.

Burned areas are detected based on the post-fire changes that result in the removal of vegetation and the deposition of charcoal (Flasse et al., 2004). These changes cause spectral contrasts between burned areas and unburned areas in the different portions of the electromagnetic spectrum which enable multispectral remote sensing techniques to be applied (Laris, 2005; Lentile et al., 2006). A variety of burn mapping methods using Landsat data exist, ranging from single-image post-fire classification (Koutsias and Karteris, 2000) to bitemporal change detection approaches based on image thresholding, principal components and spectral mixture analyses (Hudak et al., 1998; Loboda et al., 2007; Smith et al., 2007). While single and bitemporal methods have been successfully applied to map burned areas, they are not efficient for deriving spatio-temporal information especially for longer image sequences. Separate classification of each image or consecutive image pairs in the series tend to suffer from accumulation of error as overall accuracy

is the product of the component accuracies (Bovolo et al., 2012; Demir et al., 2012). The detection of burned areas using one or two images can also be problematic due to the wide spectral and spatial variability of burned areas caused by differences in fire severity, burn completeness, land cover type, phenology and the persistence of the burn signal since fire (Bastarrika et al., 2011; Pereira, 2003; Roy and Landmann, 2005). Burned areas tend to be confused with spectrally similar land covers such as wetlands or with phenological changes leading to less reliable burn information. Further, the need to determine an optimal threshold in some bitemporal methods and the requirement of near anniversary imagery to avoid phenological influences also places further constraints especially if seasonal burn information is sought (Lhermitte et al., 2011; Loboda et al., 2007).

Multitemporal methods, on the other hand, have been found to provide a more efficient way of deriving spatio-temporal burn information as multiple images can be analyzed together (Huang et al., 2010). Multitemporal analysis can provide unambiguous detection of burned areas as tracking through time provides sufficient information for classification. Further, we are freed from the constraint of finding suitable anniversary imagery (Coppin et al., 2004). The use of more than two images for monitoring also affords the ability to identify a greater range of processes of landscape change, including rates and dynamics (Gillanders et al., 2008) which makes multitemporal analysis well suited for dynamic events such as fire. Some studies have attempted to generate seasonal burn information using a series of images. However, none has taken advantage of the full temporal information that multitemporal data provides. Laris (2005) used 5 Landsat ETM+ images over the season in Mali and applied the ISODATA algorithm to cluster each image. Clusters were then visually interpreted for each image and classified as burned or unburned. The overall seasonal burn map was obtained by overlaying the individual classifications. Because of the separate classifications, this approach can suffer from accumulation of error as highlighted earlier. Bastarrika et al. (2011) used a two-step process aimed at minimizing omission and commission errors in which highly probable burn samples were first selected from a database then burn patches were grown using a hybrid contextual algorithm based on logistic regression analysis. Separate classifications of burn samples were also done using rules based on post fire data and bitemporal changes between pre-fire and post-fire images. The approach was tested over a wide range of areas with varying levels of success.

To capitalize on the growing availability of the multitemporal Landsat data, the objective of this study was to develop an effective method for mapping the spatio-temporal progression of seasonal landscape fires. Rather than carry out separate image analyses, the method relies on distinctive temporal signatures exhibited by various burn events over a fire season to map burned areas in a supervised but automatic way. The spectral-temporal signatures are automatically selected using fuzzy clustering by imposing minimum membership and cluster purity criteria in the selection process and then applied to a Random Forest classifier (Breiman, 2001) to derive the required spatio-temporal burned area information. We demonstrate and evaluate the performance of this approach over two sites, with different land cover patterns, in eastern Zambia.

2.3 METHODS

2.3.1 Study area

The study area covers about 8000 km^2 stretching between Magodi and Kazembe chiefdoms in eastern Zambia. The area is characterized by three main physiographic regions with the plateau region (elevation ~1100 m) on the east bordering Malawi, the Luangwa valley floor (elevation ~700 m) to the west, and a hilly transition zone between. The Plateau region is highly settled with landscapes characterized mainly by a patchwork of cropland, forest (mostly open forests or woodland), wetlands and fallow land (Celis et al., 1991; Her and Heatwole, 2008). The Luangwa valley floor is predominantly light forests and grassland and most of the area in our study extent is designated as a Game Management Area which serves as a buffer around national game parks. Settlements and farming activities are mainly confined to areas with alluvial soils that are found along the tributaries of the Luangwa River. Seasonal rainfall occurs between November and April, with May to November typically having little to no rain. Daily temperatures range from 4-35˚C (ECZ, 2001).

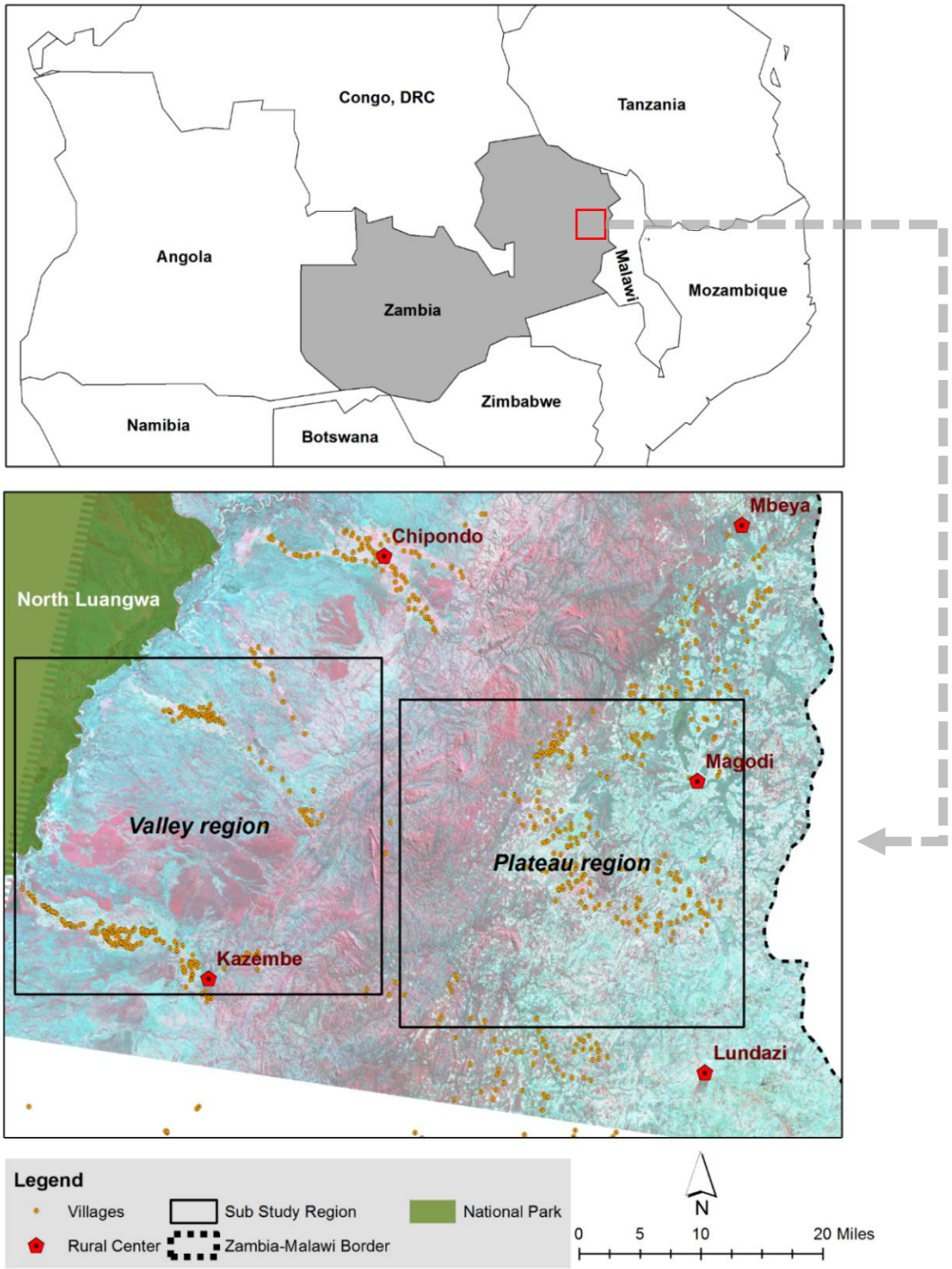

Figure 2.1: Study area in eastern Zambia. The top map highlights the general location of the study area while the bottom map shows a detailed view including the two sub study regions, the Plateau and Valley. A 432 false color Landsat image backdrop is used to provide a sense of the differences in land cover between plateau, hilly transition, and valley regions

2.3.2 Input data and preprocessing

Landsat data (path 169 row 68) for 2009 and 2012 covering the fire season (June – Nov) were downloaded from the USGS Global Visualization Viewer (GLOVIS) website. All images were Standard Terrain Corrected (Level 1T) which involves systematic radiometric and geometric corrections using ground control points and a Digital Elevation Model (DEM) for topographic accuracy (USGS, 2014). We selected fairly clear scenes (<15% cloud cover over study site) from available Landsat 5 and Landsat 7 scenes from May to November in each year. Scenes from May were included to provide a pre-fire reference for the burn mapping analysis. The images acquired for this study are listed in Table 2.1. In addition, high-resolution GeoEye-1, Pleiades and Google Earth Historical imagery were used as validation data.

Table 2.1: Landsat data (path 169 row 68) for 2009 and 2012 used in the analysis

2009			**2012**		
Date of acquisition	*Julian day*	*Sensor*	*Date of acquisition*	*Julian day*	*Sensor*
19-May	139	TM	19-May	140	ETM+
04-Jun	155	TM	06-Jul	188	ETM+
06-Jul	187	TM	22-Jul	204	ETM+
14-Jul	195	ETM+	07-Aug	220	ETM+
15-Aug	227	ETM+	23-Aug	236	ETM+
16-Sep	259	ETM+	24-Sep	268	ETM+
02-Oct	275	ETM+	10-Oct	284	ETM+
03-Nov	307	ETM+	11-Nov	316	ETM+

The detectability of burned areas can be influenced by the spatial pattern of burned areas and the degree of spectral contrast with the background. This in turn is dependent on the land cover distribution and other factors such as the time since fire, weather conditions, and vegetation recovery rate (Pereira, 2003; Sá et al., 2007; Silva et al., 2005). Given the differences in land cover distribution between the plateau and the valley regions in the study area we considered smaller separate areas of interest as a way of assessing the performance of the algorithm to different land cover conditions (Figure 2.1). Landsat data from 2009 was used for a study area in the valley landscape while 2012 data was used for analysis in the plateau region.

Landsat data were converted to surface reflectance using the Landsat Ecosystem Disturbance Adaptive Processing System (LEDAPS) (Masek et al., 2006). Procedures in Jones (2013) were

used to extract cloud, shadow and Landsat 7 ETM+ scan line error gap information from each image. A composite mask was then applied to each image to exclude these pixels from further analysis.

2.3.3 Calculation of MIRBI data

The observation of broad spectral changes associated with burning has motivated the use of various spectral indices (Koutsias et al., 1999; Lentile et al., 2006). Spectral indices are widely used due to conceptual simplicity and the reduced data dimensionality they afford (Veraverbeke et al., 2011; Verstraete and Pinty, 1996). The performance of many spectral indices varies with ecoregion and vegetation type (Epting et al., 2005; Harris et al., 2011). We used the Mid-Infrared Bispectral Index (MIRBI) because it demonstrated superior performance in discriminating burned from unburned areas over similar spectral indices such as normalized burn ratio (NBR) in savanna environments over Botswana and Zambia (Smith et al., 2007). Schepers et al (2014) evaluated a number of spectral indices for their capacity to discriminate burned from unburned areas and also reported highest correlations with burned areas for MIRBI. MIRBI has also been shown to discriminate burned from unburned even longer times since fire (Mohler and Goodin, 2013).

The MIRBI index is based on the concurrent increase in short-wave infrared reflectance after as fire which highly sensitive to spectral changes due to burning and relatively insensitive to intrinsic variability such as vegetation type, the surface heterogeneity and temporal-spectral evolution of burned surfaces (Trigg and Flasse, 2001). After a fire, MIRBI index values abruptly increase (Figure 2.2), and the good discriminative power is partly attributed to use of data from the mid-infrared region which is highly responsive to burning (Trigg and Flasse, 2001). A number of studies have assessed the effectiveness of various spectral indices for burned area mapping and spectral indices that use information from the near-infrared (NIR), the short-wave infrared (SWIR) or thermal-infrared (TIR) bands have been reported to provide greater discrimination between burned and non-burned areas compared to two-dimensional indices that only use visible and NIR bands (Holden et al., 2005; Pereira, 2003; Smith et al., 2007; Veraverbeke et al., 2011).

The MIRBI index was calculated per pixel for each image in the sequence as:

$$MIRBI = 10\rho_{SWIR} - 9.8\rho_{LNIR} + 2.0 \qquad \text{Equation 2.1}$$

where ρ_{SWIR} is the shortwave infrared reflectance (band 7 in Landsat 7) and ρ_{LNIR} is the second shortwave infrared reflectance (band 5 in Landsat 5 and 7) (Smith et al., 2007; Trigg and Flasse, 2001). MIRBI is not a normalized index with known minimum and maximum values as the normalized difference vegetative index (NDVI), thus can have a wide range of values, typically 300-4000 in this study and negative values are possible. For the analysis, MIRBI image data for each year (or fire season) were stacked into a multitemporal dataset.

2.3.4 Algorithm development for training sample selection

Overview

The response of vegetated land cover to fire has been a focus of many studies thus there is a good body of knowledge on the associated spectral signatures (Pereira et al., 1999; Quintano et al., 2010). The removal of vegetation, alteration of vegetation structure, and deposition of charcoal and ash depending on burn completeness results in spectral changes which can be used to differentiate burned from unburned areas (Flasse et al., 2004; Smith et al., 2007). In addition, the persistence of the burn signal over time provides useful distinctive temporal profiles for multitemporal burn mapping (Pereira, 2003). Ancillary structural information associated with these profiles such as gradients and change points (location of abrupt changes in a sequence) can be used to uniquely define fire events by date. Figure 2.2 shows a sample temporal spectral index plot of the MIRBI index over the 2009 fire season in eastern Zambia. Two fire events, one prior to August 15 and the other prior to August 31, can be inferred by the abrupt change in profile values while the unburned samples show little or gradual change in MIRBI values.

By using these properties we can select representative temporal training samples from a multitemporal dataset. To facilitate the selection of training samples, the data are first clustered using an iterative fuzzy clustering process. Training samples are selected from generated clusters and are uniquely labelled based on structural information. The vagueness or non-crisp nature of natural landscapes (Chen et al., 2010; Shih and Chen, 1994) can present challenges for clustering. By allowing different degrees of membership to all clusters, fuzzy clustering enables selection of samples with high membership which contributes to high quality of training samples. The samples selected from the clustering are then available to train a classification model, and we used Random Forests (RF) classifier for this purpose. Given the uncertainty intrinsic to clustering, the performance of the method was assessed over a number of realizations by controlling seed values

of the random process. Multiple realizations enabled assessment of the variation in the number of clusters and its impact on training sample selection and overall classification accuracy. From these results we can identify general trends in overall classification accuracy by plotting the number of clusters against number of samples selected.

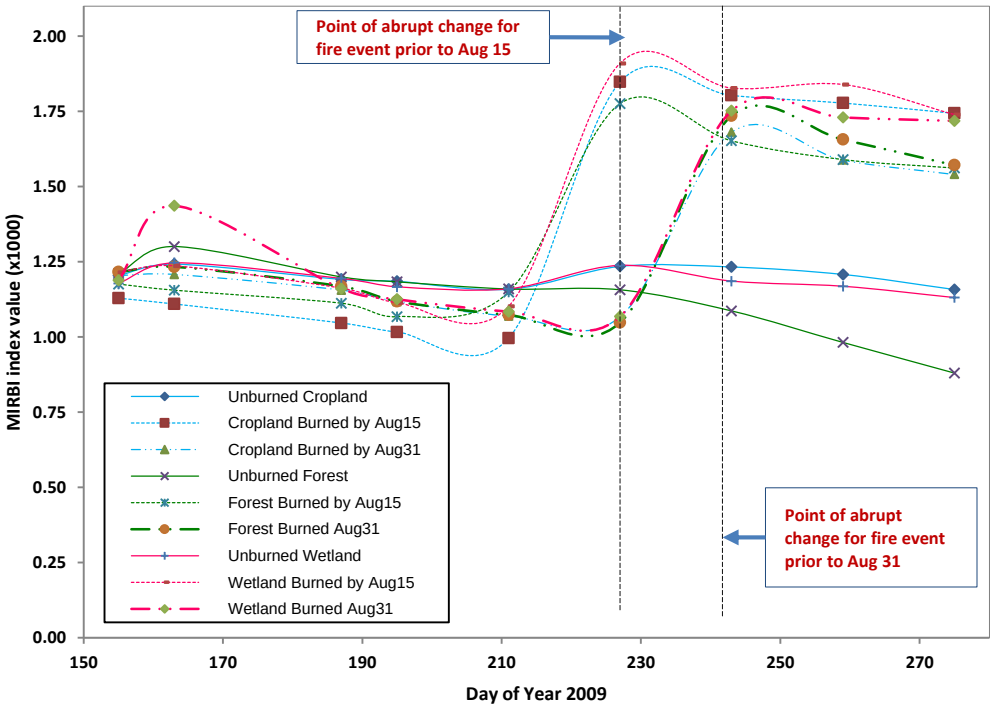

Figure 2.2: Progression of MIRBI values through the fire season in eastern Zambia for 9 pixels sampled from forest, wetland and cropland. Burned profiles have a step function pattern with lower MIRBI values before a fire and higher ones afterward while unburned profiles show a near flat or slowly decreasing trend.

Data sampling for training sample selection

Given the large increase in the MIRBI index after a fire, an approximate burn map can be obtained by thresholding differenced MIRBI data, where pixels above the set threshold are burn candidates and those below are unburned candidates. A suitable threshold can be found by examining differenced MIRBI values of known burned areas and here a threshold of 300 was used. To capture burn samples by date, differences are computed consecutively between two images and any pixels meeting the set threshold for a particular image pair form a separate stratum. Equal random samples are then selected from each of the burn candidate strata while four times that number is selected from unburned candidates. We select a higher number for the unburned candidate category to increase the chance of selecting actual unburned samples as some of the pixels below

the threshold may still be burned. In this way all burn events have a greater chance of being part of the sample which would not be guaranteed by a simple random sampling of the data.

Multitemporal clustering of sampled MIRBI data

Fuzzy c-means (FCM) (Bezdek et al., 1984), a well-known fuzzy clustering algorithm is used for clustering the sampled multitemporal MIRBI data. Fuzzy clustering allows different degrees of membership to all clusters which makes it well suited to handle the non-crisp nature of natural landscapes and the wide spectral variability associated with burned areas (Chen et al., 2010; Shih and Chen, 1994). By allowing varying grades of membership, it allows selection of samples that are more representative of a particular cluster thus high quality training data can be selected. It is also more efficient at dealing with noisy data than non-fuzzy algorithms such as k-means (Schwämmle and Jensen, 2010).

Setting optimal values for the number of clusters and the fuzzy parameter is critical to the application of fuzzy c-means. The use of non-optimal values for these parameters often leads to poorly formed clusters where potentially real clusters are lost or random noise is retained as real clusters (Futschik and Carlisle, 2005; Schwämmle and Jensen, 2010). Following Futschik and Carlisle (2005), an estimate of number of clusters is obtained by iterative clustering of a sample drawn from the main dataset in which the number of clusters is gradually incremented after each run until one or more empty clusters are formed. The number of clusters used just before an empty cluster is detected is taken as the best estimate for the optimal number of clusters. The idea of an empty cluster is used because for fuzzy cluster analysis a threshold or α-cut, such as 0.5, is usually specified to determine to which clusters objects maximally belong (Pedrycz, 2007; Schwämmle and Jensen, 2010). Thus any cluster comprising only objects with membership values less than a set threshold is considered empty or random – resulting from noise in the data. An optimal number of clusters should generate a set of clusters each containing a least one object with a membership meeting the set threshold (Futschik and Carlisle, 2005).

The fuzzy parameter also has to be carefully selected. The fuzzy parameter determines the level of fuzziness in the clustering thus influences the impact of noise on the clustering (Futschik and Carlisle, 2005). High values of the fuzzy parameter usually lead to low membership values, so a compromise value must be set so the fuzzy aspect of the clustering is maintained while real clusters are composed of samples with high membership values. It is desirable to have a fuzzy parameter

that results in membership values greater than 0.5 to weed out noisy samples (Schwämmle and Jensen, 2010). Thus, the fuzzy parameter was determined empirically by making a few clustering runs at different values of the parameter on known number of clusters until membership values in known clusters were greater than 0.5. Once determined, the fuzzy parameter was kept constant for all clustering runs.

To minimize impact of outlying observations and scale biases at different dates (Pedrycz, 2007), the MIRBI data was first normalized using the overall median and median standard deviation values for the whole dataset to give a form of a z-score. Then clustering of the data followed in a two-step procedure. First, the dataset is repeatedly clustered retaining only clusters and pixels per cluster that meet a set membership threshold. The Euclidean distance is used as a (dis)similarity measure between cluster centers and samples. The samples that do not meet the set threshold are then re-clustered separately. Each clustering run updates earlier centroid and fuzzy partition matrices by appending the new centroid and fuzzy partition. This is repeated until a stopping criterion is met: a set maximum number of iterations, or when improvement in the objective function is less than a specified tolerance or the proportion of data for a run falls below 10% of original data. The 10% criterion is applied to prevent clustering noisy data which most likely remains after real clusters have been removed in preceding runs. Second, the final centroid and fuzzy matrix -a summation of all clustering runs – is used as input for a refining step. This step allows for a holistic adjustment of clusters which is possible in the first step since each clustering run uses a different dataset. Membership thresholds are again imposed on clusters to realize the final clustering. Figure 2.3 shows the process flowchart.

Selecting and labeling training profiles per cluster

Training samples are collected per cluster from the final clustering (OCf, OUf in Figure 2.3). It is worth noting that even after repeated clustering and refinement some clusters may still be poorly formed because of the impact of noise in the data. Typically, a valid cluster is compact (members close to each other) and well separated from other clusters (Halkidi et al., 2001; Tan et al., 2005a). To ensure that samples are collected only from valid clusters we impose a minimum per-cluster purity criterion and samples are only selected from clusters with a set minimum level of purity.

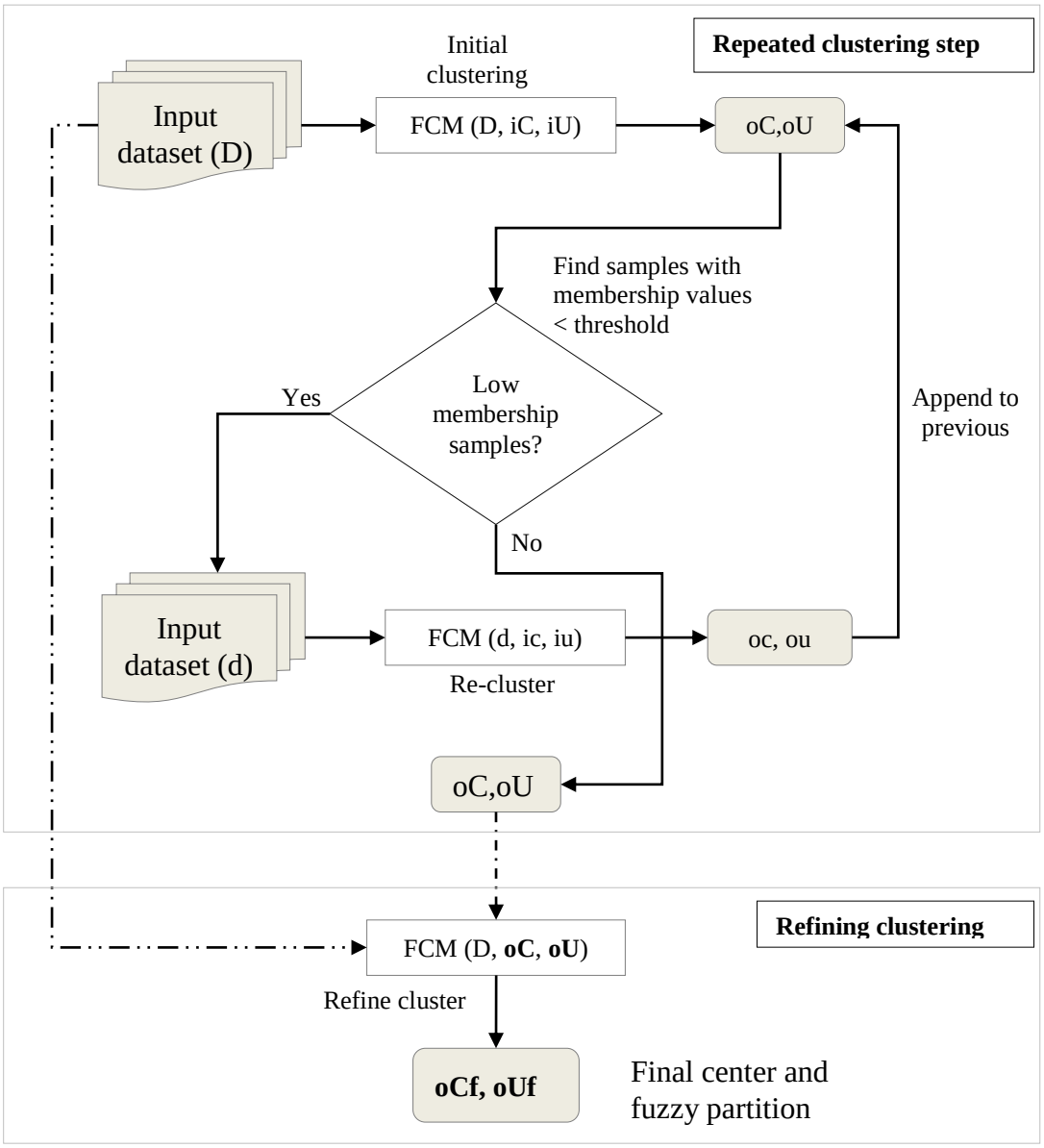

Figure 2.3: Multitemporal clustering using repeated fuzzy c-means. The clustering process starts with input D, initial estimated cluster centers iC and fuzzy partition iU. It then re-clusters any low-membership data d to produce clusters oc and partition ou which are then appended to results from previous clustering runs. If the low-membership condition is not met, oC and oU are retained and used as starting estimates for the refining step to obtain oCf and oUf as final Clusters and fuzzy partition respectively.

Cluster purity is one of the many cluster validity measures that can be used to assess the quality of clusters in a clustering process. An external cluster validity metric measures the extent to which cluster labels match externally supplied class labels, which enables selection of clusters that match

reference characteristics (Halkidi et al., 2001). After Rendón et al (2011), per-cluster purity *P* of a cluster v_k is defined as:

$$P = \max_j(v_k \cap c_j) \times 100/N \qquad \text{Equation 2.2}$$

where c_j is a instance in a set of classes (c_1,c_2,...c_j) and *N* is the total number of samples per cluster. Expressed as a percentage, high purity values such as 90% represent a good match with reference information (high validity) and are preferable. In a fuzzy setup the clustering must be defuzzified in order to get the total number of samples per cluster (*N*). This is done by considering only samples that meet the membership threshold in the calculation.

Class label information is derived by analyzing change points in the temporal profiles of the data. For each temporal profile successive gradient values are calculated by dividing successive MIRBI differences by number of days between the data points. Typically, successive gradient values for unburned profiles fall on or are close to a (zero) horizontal line while for a burned profile there is a noticeable outlier corresponding to the fire event while the rest of the values fall close to the horizontal line as shown in Figure 2.4 a) and b). Therefore, the labeling of the profiles is treated as an outlier detection problem - detection of an outlier signals a burned profile with location of the outlier in the sequence indicating the approximate burn date while non-detection signifies an unburned profile. Note that an actual burn date cannot be determined from 16-day Landsat cycles but is understood to fall between imagery dates that exhibit the point of abrupt change. The Dixon's Q-test (Dean and Dixon, 1951) – an outlier detection test for univariate data, is applied to detect outliers at a set confidence level, typically 95%. The Dixon's Q-test is performed by taking the difference of the suspected value and the value nearest to it, and dividing the difference by the range of the data. If the difference is larger than the tabulated value, the null hypothesis is rejected and the associated value is flagged as an outlier. Since burns are only associated with positive outliers, the detected outlier is further tested to exclude negative outliers which can occur in unburned profiles. This is done by checking if the detected outlier is below or above the mean. Once a cluster has the required purity level, samples are labeled as 'Burned by' and the approximate burn date appended (e.g. 'Burned by Aug15' as in Figure 2.4 a. and b) for pixels burned prior to August 15. Unburned samples as in Figure 2.4 c) and d), are labelled 'Unburned'.

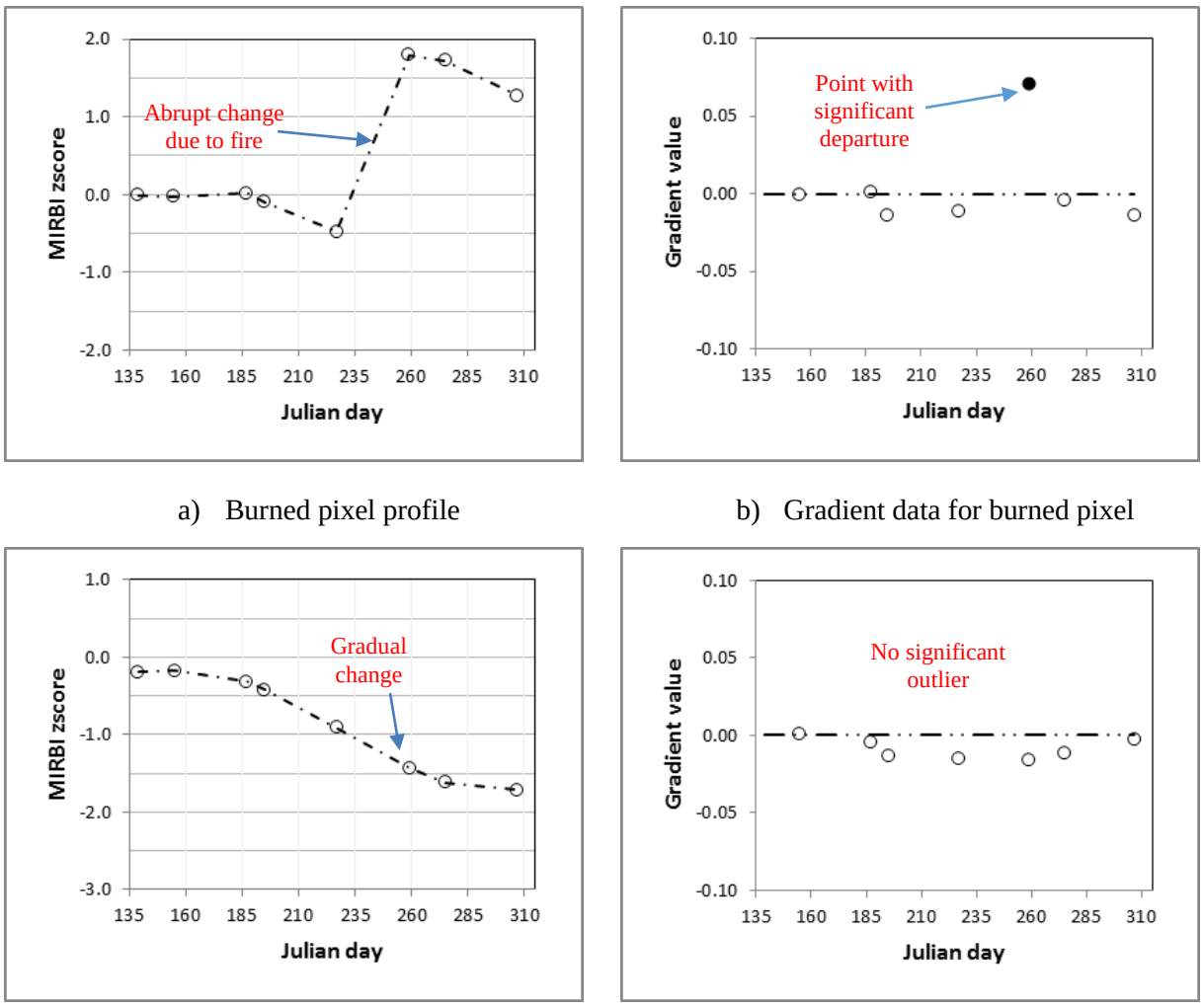

a) Burned pixel profile

b) Gradient data for burned pixel

c) Unburned pixel profile

d) Gradient data for unburned pixel

Figure 2.4: Structural characterization of pixel profiles: a) An example of a burned pixel profile with a fire event between Julian days 227 and 259 and b) Successive gradient values showing a significant departure from the horizontal line at 259 (filled marker) than at other points. c) An unburned pixel profile between days 140-310 and d) Gradient values for unburned pixel showing small departures from the horizontal line indicating no outliers.

2.3.5 Random Forest classification model

RF is an ensemble method for classification and regression which aggregates multiple "weak classifiers" to form a stronger classifier with higher predictive power than individual weak classifiers. RF uses a decision tree as a weak learner and fits a number of trees on various random sub-samples of the dataset. Classification is then based on majority vote of all built decision trees (Breiman, 2001; Tan et al., 2005b). RF makes no assumptions about the statistical distribution of data and on relationships between dependent and independent variables which makes it effective

at capturing the underlying structure of the data and it provides consistently high classification accuracies (Roy et al., 2010; Tan et al., 2005b). RF is also desirable because out-of-bag (OOB) samples - samples not used to build a particular decision tree - can be used to calculate an unbiased error rate and variable importance which avoids the requirement of a test set or cross-validation to estimate generalization error (Breiman, 2001; Prasad et al., 2006).

In training a RF model, dependent and independent variables must be selected and several parameters specified such as the number of decision trees to build, and parameters related to decision tree formation such the split criterion, random sampling and variable importance (Tan et al., 2005b). Most of these parameters can be run at their default levels except the number of decision trees.

2.3.6 Assessment

Parameters for training sample selection

The selection of training samples was based on parameters shown in Table 2.2. The fuzzy factor and the membership thresholds were determined as described previously. The sample sizes were determined based on success in trial runs.

Table 2.2: Parameter settings for training sample selection

Parameter setting	*Plateau area (2009 data)*	*Valley area (2012 data)*
Fuzzy factor	1.6	1.3
Membership threshold	0.5	0.5
Per-cluster purity threshold	85%	85%
Sample size for training sample selection	5500	6600

Training the RF model

To assess the validity of the selected training samples, we used them to train a random forest (RF) model which in turn was used to classify known burn samples. The premise here is that correctly selected training samples should give accurate prediction of known burn samples. To train the RF model the following classification features were used:

a) 8 features representing the normalized MIRBI pixel profile data for each image (see section 0 for details on normalization).

b) 3 features for the minimum, maximum and mean values of normalized MIRBI pixel data.

c) 7 features for the pixel gradient data, $\boldsymbol{g}$ calculated as:

$$g = \Delta MIRBI/\Delta t \qquad \text{Equation 2.3}$$

where $\Delta MIRBI$ is the difference in MIRBI values between any two successive image dates and Δt is the duration in days between the two images.

d) 3 features for the minimum, maximum and mean values of pixel gradient data.

In all 21 classification features were used for an 8-image dataset with 200 trees built for the RF model. The number of trees was determined based on preliminary analyses. OOB accuracy from the trained model was used to assess generalization error and to check for consistency of the selected training data – high overall OOB accuracy (>90) gives high confidence in selected training samples and the built classification model. The model trained in this step is then used to classify the reference burn data.

To gain understanding of the classification features that contribute more to the burn classification, we assessed variable importance using the OOB permuted variable delta error. The importance for a particular variable in the classification is measured by the increase in prediction error when the values of that variable are permuted across the out-of-bag observations. It is calculated over the entire ensemble as the normalized mean of the increase in prediction error from individual trees (Breiman, 2001; MathWorks Inc, 2014).

Classification accuracy and impact of cluster number variability

Accuracy assessment of the classified data was based on reference data from high spatial resolution imagery: GeoEye-1 (2m multispectral ground sample distance, 19 July 2012), Pleiades (2m ground sample distance, 18 October 2012) and Google Earth historical imagery (24 September 2009). The high resolution data provided detailed visual information on burn and unburned condition while the temporal or dating reference information was derived by visual interpretation of the Landsat sequence data itself. The interpretation of the Landsat data was enhanced by using false-color 4-3-2 band combinations (burned areas appear dark) which are effective at discriminating burned from unburned areas (Pereira et al., 1999). Differenced MIRBI images between successive dates, with large increases in the MIRBI index indicative of fire, were also incorporated to aid the interpretation.

For each of the two datasets (2009 and 2012), a stratified random sampling approach was used to select pixels for validation. To ensure the validation sample contained all burn events and covered

all land covers, strata were created by combining 2010 land cover set obtained from Regional Centre for Mapping of Resources for Development (RCMRD)[1] with an approximate burn map (See section 0). The classification scheme for the land cover data comprised six land cover classes: forest, grassland, cropland, settlements, wetland and other. The overall accuracy of the land cover map is 80.4 % (Oduor, 2013). For our analysis, the wetland class was aggregated with grassland, other and settlement classes with cropland to get three generalized classes of forestland, grassland and cropland. Because of the significant effort involved in interpreting validation samples only 15-50 samples were selected for each stratum yet the total number per burn class was adequate to make it statistically representative following recommendations by Congalton (1991). Each sample was visually analyzed to determine the appropriate burn condition and burn date. A summary of validation data collected for the two datasets is shown in Table 2.3 and Table 2.4.

The performance of the overall procedure was assessed using error matrices between reference and predicted burn classes from which the overall, producer and user accuracy measures were derived. The Kappa statistic (Cohen, 1960) was also calculated to determine the level of agreement between the map and the reference information. To account for the random nature of the training, the accuracy assessment was based on multiple realizations of the error matrices. Different realizations of the error matrices can be obtained by varying the seed value of the random number generator which controls the initialization of the cluster process. A random sample of 30 seed values from a pool of 1000 generated random numbers was selected and separate runs were made with each seed value. Accuracy measures were then determined using mean values of the 30 realizations. The multiple realizations also provided a way of assessing the uncertainty of the method which is not possible with one error matrix. Other aspects of the procedure such as the variation of number of clusters and its relationship to the number of training samples selected and overall classification accuracy were also investigated using these multiple results. To assess the relationships, the number of training samples and the overall accuracy were each fitted against the number of clusters and testing was done on the estimated gradient parameters.

[11] RCMRD established in Nairobi – Kenya in 1975 under the auspices of the United Nations Economic Commission for Africa (UNECA) and the then Organization of African Unity (OAU), promotes sustainable development through generation, application and dissemination of Geo-Information and allied ICT services and products in the Member States including Zambia.

Table 2.3: Multitemporal burn validation samples by land cover type for 2009

	Forest	*Grassland*	*Cropland*	*Total*
Unburned	46	44	46	136
Burned by Jun04	17	54	4	75
Burned by Jul06	46	46	44	136
Burned by Jul14	46	49	46	141
Burned by Aug15	46	47	41	134
Burned by Sep16	50	50	44	144
Burned by Oct02	50	50	44	144
Burned by Nov03	45	47	47	139
Total	**346**	**387**	**316**	**1049**

Table 2.4: Multitemporal burn validation samples by land cover type for 2012

	Forest	*Grassland*	*Cropland*	*Total*
Unburned	65	33	36	134
Burned by Jul06	20	21	25	66
Burned by Jul22	42	42	49	133
Burned by Aug07	52	49	49	150
Burned by Aug23	49	55	49	153
Burned by Sep24	47	51	49	147
Burned by Oct10	48	47	48	143
Burned by Nov11	33	25	27	85
Total	**356**	**323**	**332**	**1011**

2.4 RESULTS

2.4.1 Selection of training profiles and model training

With 8 scenes for each of 2009 and 2012, we defined eight (8) burn classes from generated clusters. Table 2.5 gives the breakdown of average number of training samples selected for each pattern over the 30 realizations. The higher numbers of training samples per class for the 2012 dataset are reflective of the larger sample 6600 from which they are selected compared to 5500 for the 2009 dataset. The training profiles corresponding to the eight burn classes for the 2009 dataset are shown in Figure 2.5. Profiles obtained for the 2012 dataset are similar, so are not shown here. Notice the abrupt increase in MIRBI values in profiles corresponding to burned areas and note the differences

in time of these points of abrupt change. These differences make it possible to map the progression of burned areas in the fire season.

Table 2.5: Summary of the average number of training samples selected based on 30 realizations

2009					**2012**				
Class	*Mean*	*Min*	*Max*	*STD*	*Class*	*Mean*	*Min*	*Max*	*STD*
Burned by Aug15	104.1	72	138	12.8	Burned by Aug07	275.6	234	320	22.5
Burned by Jul06	99.3	38	120	18.2	Burned by Aug23	299.1	267	326	15.9
Burned by Jul14	111.6	78	139	15.7	Burned by Jul06	154.3	118	179	14.4
Burned by Jun04	89.9	70	112	9.4	Burned by Jul22	216.2	185	234	11.2
Burned by Nov03	129.0	83	155	17.5	Burned by Nov11	223.3	150	271	30.6
Burned by Oct02	129.9	79	150	16.0	Burned by Oct10	253.6	228	275	10.5
Burned by Sep16	112.2	86	138	12.9	Burned by Sep24	353.3	330	373	12.5
Unburned	74.3	30	119	20.2	Unburned	298.9	258	345	22.6

The trained RF models for 2009 and 2012 had overall OOB accuracy over 99% which shows high consistence among the selected training samples. Figure 2.6 and Figure 2.7 show the variable importance measures for all the variables for each model. The plots shows that features based on successive gradients were more important for the classification of different burn events than features based on normalized MIRBI. All the gradient features had high variable importance scores except *gradient Jun04, minimum, mean and maximum gradient* for 2009. Similar results were obtained for 2012 though the maximum gradient was more important compared to the 2009 case. The high ranking of most gradient features is reflective of the unique points of abrupt change for the burn different classes which reinforces the basis selected for labeling the training data (see section 0).

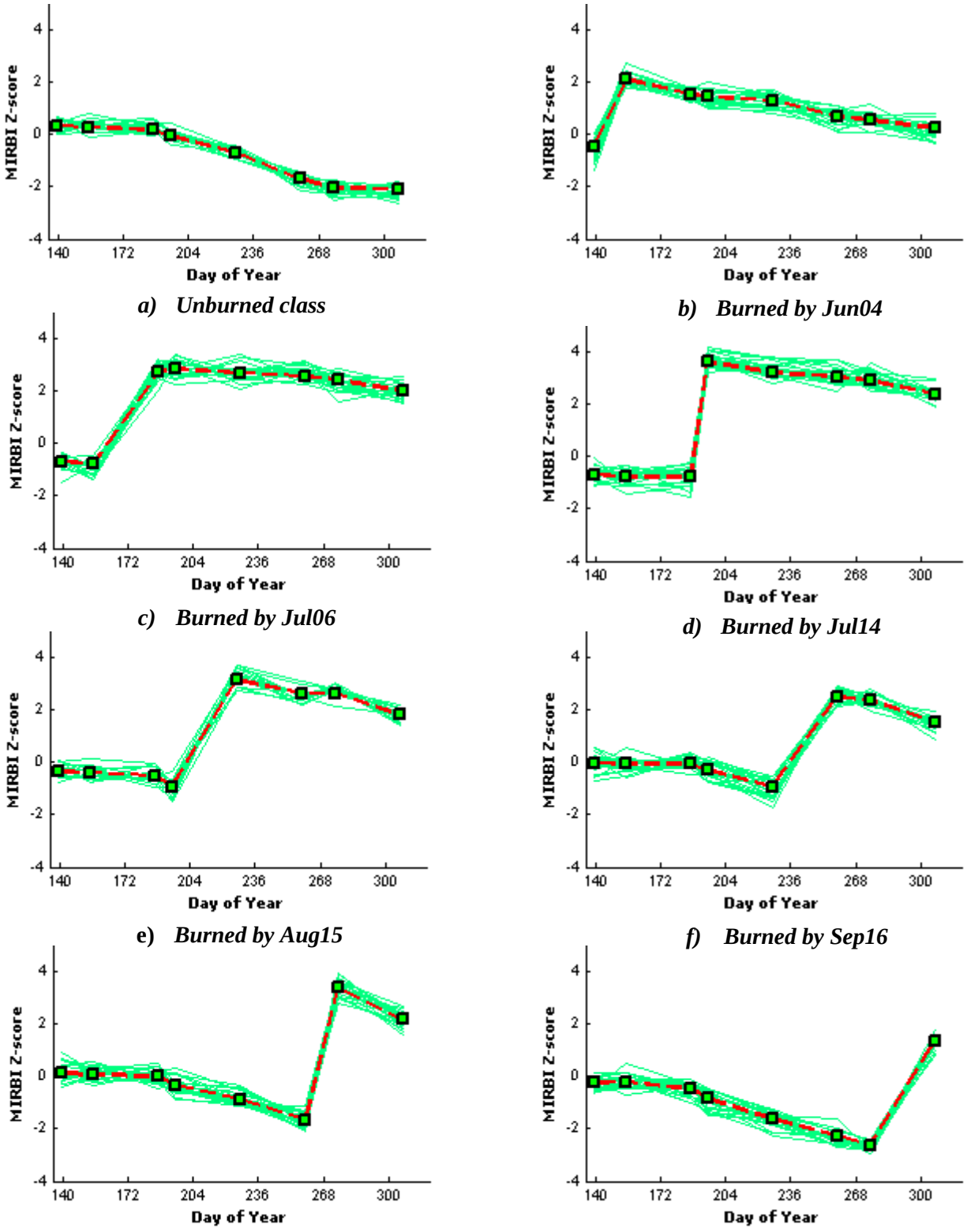

a) Unburned class

b) Burned by Jun04

c) Burned by Jul06

d) Burned by Jul14

e) Burned by Aug15

f) Burned by Sep16

g) Burned by Oct02

h) Burned by Nov03

Figure 2.5: Temporal profiles corresponding to training classes for the 2009 dataset. Clusters centers are represented by the thick dashed line. Abrupt increases in the profiles indicate a response to burning in the interval since the previous image except for the unburned class.

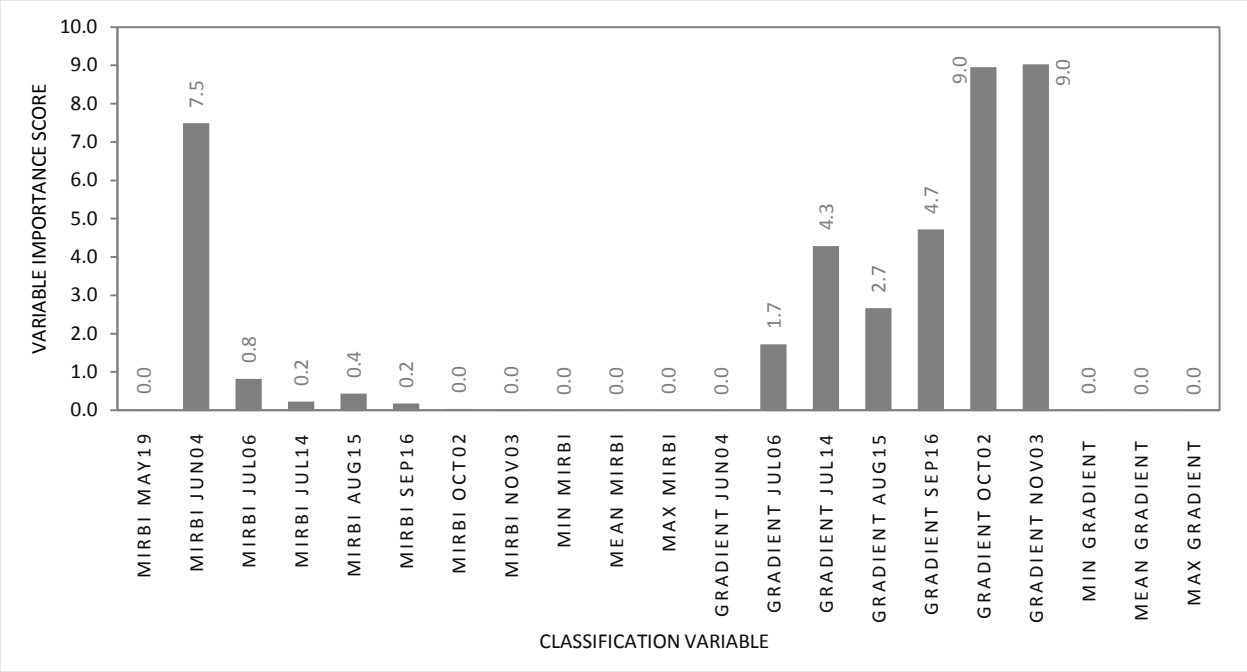

Figure 2.6: Variable importance for 2009 RF model. The higher the variable importance score the more important the variable is for the classification.

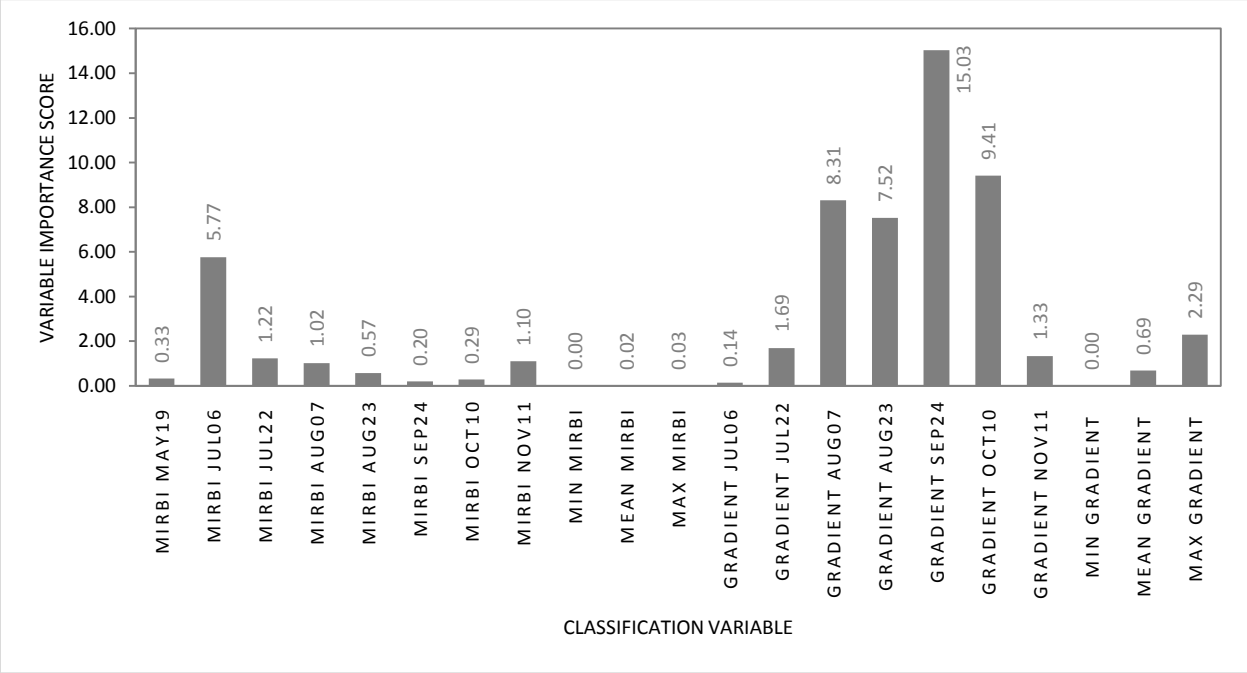

Figure 2.7: Variable importance for 2012 RF model. The higher the variable importance score the more important the variable is for the classification.

2.4.2 Accuracy assessment

Error matrices generated by comparing the validation data with classification results for the two datasets are given in Table 2.7 and Table 2.8. Overall accuracy obtained was 97.3±0.6 % for 2009 data and 92.6±1.6 % for 2012 data. Class specific accuracies are represented by user and producer accuracies with results from the 2009 dataset having higher accuracy values than those from 2012 dataset. On average 97.1% user (UA) and producer accuracies (PA) were achieved for the 2009 dataset compared to 92.1% UA and 92.5% PA for the 2012 dataset. Kappa statistics for the two datasets were 0.972 and 0.912 for 2009 and 2012 respectively showing a high level of agreement between predicted and reference data.

Lower omission and commission errors (0-4 %) were observed in the 2009 dataset than in the 2012 (1-20%). It is not clear why this was the case. Higher misclassification is especially observed for the 2012 dataset in the unburned class, the *Burned by Jul06* and *Burned by Nov11* with a higher number of unburned samples committed to the other two classes. The commission of unburned samples to the other two could be explained by their high similarity in the temporal profiles of the three classes Figure 2.5. Classification features, other than the ones used here such as texture might provide improved discrimination between these classes. A number of studies have reported improved classification by texture information or other spatially oriented features (Gitas et al., 2004; Mitri and Gitas, 2004; Polychronaki and Gitas, 2012).

The distribution of error by land cover shows better performance for samples in the forest land cover class than in grassland and cropland areas. Table 2.6 show the rate of misclassification in the three land cover classes based on the 30 runs. The distribution of error could be attributed to differences in the burn signal in terms of magnitude and signal persistence in the three land cover types - forested areas tend to show larger responses to fire and the signal persists for a longer time than in grassland and cropland areas(Pereira, 2003). Results for 2009 showed lower number of misclassifications by land cover than results from 2012. Given the difference in land cover distribution between the two regions, this may suggest that spatial patterns influence the performance of the algorithm (Silva et al., 2005).

Table 2.6: Burn misclassifications by land cover based on the 30 runs. This analysis only took into account unique incidences, thus pixels misclassified multiple times in the 30 runs was counted only once.

Value	*Total sampled*	*No. associated with misclassified burn validation samples*	*Percentage of total*
		2009	
Cropland	316	36	11.4
Grassland	387	32	8.3
Forest	346	20	5.8
		2012	
Cropland	332	88	26.5
Grassland	323	66	20.4
Forest	356	84	23.6

2.4.3 Sensitivity to randomness of clustering process

The results from the 30 realizations showed that the number of clusters obtained can vary with random seed used. The number of clusters ranged from 53 to 80 for 2009 and 144 to 184 for 2012 data. The mean values were 63.7 with standard deviation of 6.7 and 170.3 and a standard deviation of 9.0, for 2009 and 2012 datasets respectively. Figure 2.8 shows the distribution of the estimated number of clusters for the two datasets. While a similar number of clusters was obtained in a majority of the runs, we must conclude that the procedure is not completely insensitive to the random initialization of the cluster process.

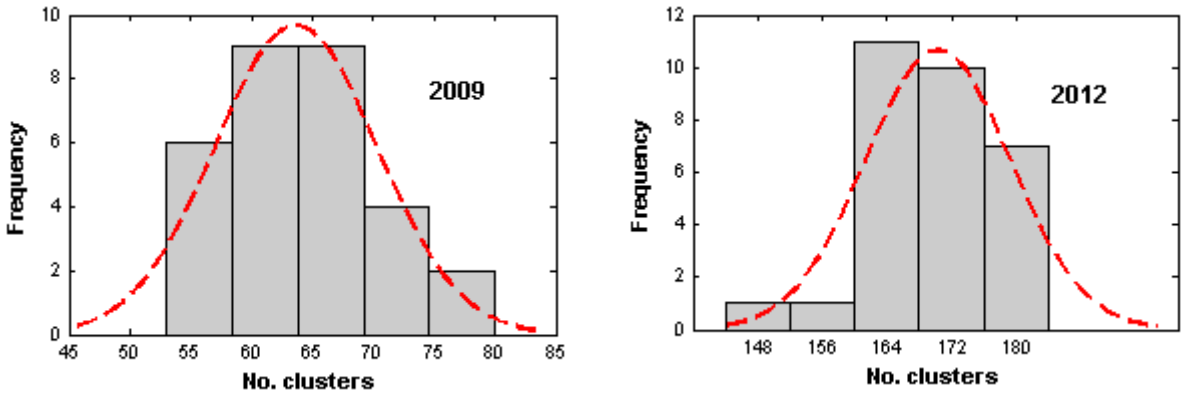

Figure 2.8: Variation of number of clusters created with random seed for 2009 and 2012. The fitted histogram graph, emphasizes the observed variation in the number of clusters selected based on random seed values.

Table 2.7: Contingency table for 2009 result with reference data in columns and predicted class in rows. Overall accuracy 97.3±0.6 %, Kappa 0.972

	Unburned	*Burned by Jun04*	*Burned by Jul06*	*Burned by Jul14*	*Burned by Aug15*	*Burned by Sep16*	*Burned by Oct02*	*Burned by Nov03*	*User Accuracy*	*Producer accuracy*
Unburned	**128.0**	0.9	3.6	0.3	1.4	0.1	0.0	0.0	**95.4**	**94.1**
Burned by Jun04	5.1	**71.1**	0.0	0.4	0.1	0.0	0.0	0.0	**92.8**	**94.8**
Burned by Jul06	1.2	1.9	**128.7**	0.3	0.3	0.1	0.0	0.0	**97.2**	**94.6**
Burned by Jul14	0.0	0.0	0.0	**134.6**	0.0	0.0	0.0	0.0	**100.0**	**95.4**
Burned by Aug15	1.1	0.0	0.7	0.5	**131.9**	0.0	0.0	0.0	**98.3**	**98.5**
Burned by Sep16	0.4	0.0	0.4	0.5	0.0	**143.6**	0.0	0.1	**99.0**	**99.7**
Burned by Oct02	0.0	0.0	1.0	2.0	0.0	0.0	**144.0**	0.0	**98.0**	**100.0**
Burned by Nov03	0.3	1.2	1.6	2.4	0.3	0.2	0.0	**138.9**	**95.8**	**99.9**

Table 2.8: Contingency table for 2012 data with reference data in columns and predicted class in rows. Overall accuracy 92.6±1.6 %, Kappa 0.912

	Unburned	*Burned by Jul06*	*Burned by Jul22*	*Burned by Aug07*	*Burned by Aug23*	*Burned by Sep24*	*Burned by Oct10*	*Burned by Nov11*	*User accuracy*	*Producer accuracy*
Unburned	**89.4**	0.0	4.3	0.0	2.9	0.7	1.3	1.0	**89.6**	**66.7**
Burned by Jul06	0.1	**62.4**	1.0	0.0	0.0	0.0	0.0	1.1	**96.5**	**94.5**
Burned by Jul22	3.9	0.5	**124.0**	0.0	0.0	0.0	0.0	0.0	**96.5**	**93.2**
Burned by Aug07	0.9	1.0	0.0	**149.0**	0.0	0.0	1.6	0.0	**97.7**	**99.3**
Burned by Aug23	4.5	1.6	0.5	0.4	**143.4**	0.0	0.1	0.2	**95.1**	**93.7**
Burned by Sep24	2.0	0.0	0.7	0.4	3.7	**145.1**	0.0	0.5	**95.2**	**98.7**
Burned by Oct10	0.0	0.0	2.0	0.2	0.0	0.0	**139.0**	0.0	**98.4**	**97.2**
Burned by Nov11	33.1	0.5	0.5	0.0	2.9	1.1	0.9	**82.1**	**67.8**	**96.6**

The variation of the number of clusters has a bearing on the number of training samples selected per class and ultimately on the overall accuracy. There was a significant (p-value < 0.001) general decrease in the number of training samples selected with increasing number of clusters in all classes for 2009. However, this trend was not observed with the 2012 dataset. In that case, most of the per-class trend lines did not show any relationship between number of clusters and number of training samples selected. In fact burn classes such as the *Burned by Nov11* and *Burned by Aug23* showed a positive relationship implying that having more clusters resulted in more training samples selected. Figure 2.9 and Figure 2.10 show the variation of training samples with number of clusters while the estimated slope values per class with significance test values are summarized in Table 2.9

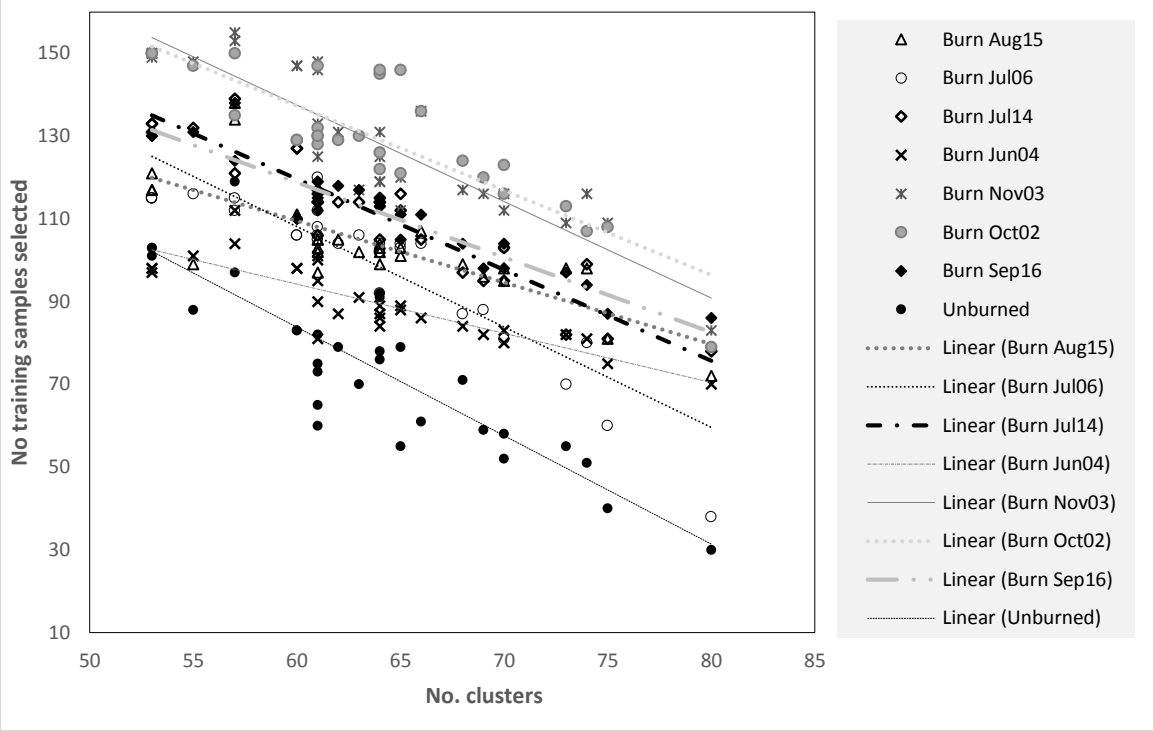

Figure 2.9: Variation of training samples with the number of cluster for 2009. The number of training samples selected decreased with increasing number of clusters

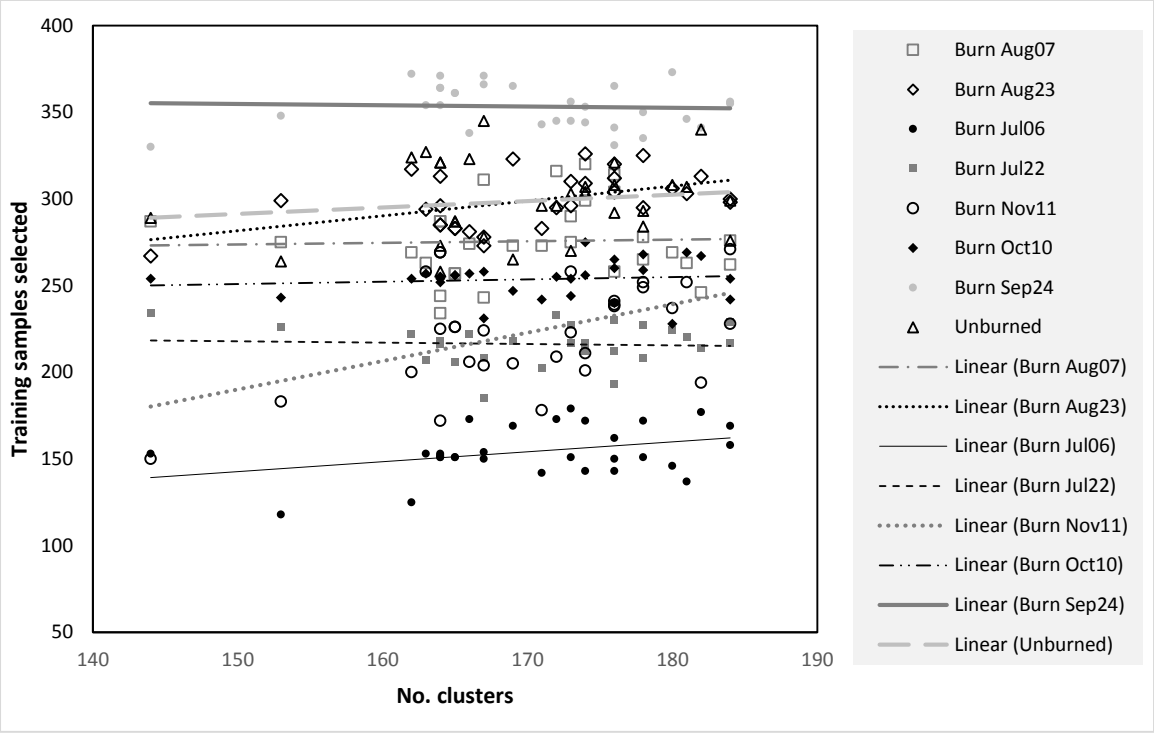

Figure 2.10: Variation of training samples with the number of cluster for 2012. The number of training samples selected for most of the classes did not show any correlation with number of clusters

The fit of the number of clusters against the overall accuracy showed that an increase in the number of clusters resulted in a corresponding decrease in the overall accuracy for 2009 as shown in Figure 2.11. This could be linked to the observed decrease in training samples. This relationship was significant (p-value = 0.0018) at a 0.05 significance level. Results for 2012 also showed a decreasing trend for overall accuracy but the relationship was not statistically significant (p-value = 0.299). This could be attributed to the mixed trends for number of training samples observed in Figure 2.10. The OOB accuracies were higher than the test accuracies in both cases and did not suffer any impact with respect to number of clusters. Higher accuracies from OOB than test samples are expected as the generalization error usually gets worse when applied to test data (Tan et al., 2005b).

In summary, the number of clusters created in the iterative clustering process can have an impact on the number of training samples selected and ultimately on the overall classification accuracy. However, while differences were statistically significant, the absolute difference in accuracies is not large and does not detract from the overall good performance of the method. The reduction in number of training samples selected and classification accuracy for the 2009 data could be

attributed to the over-partitioning or over-fitting of the dataset leading to weakly formed clusters (Tan et al., 2005a). Larger sample sizes could alleviate this as shown by the 2012 case where a larger sample (6600) showed better stability than the 2009 case where a smaller sample (5500) used. Implementation of intermediate merging and splitting steps during the iterative clustering process, as in the ISODATA algorithm (Ball and Hall, 1965), could also improve the stability of the number of clusters.

Table 2.9: Per-class estimated slope values with significance test statistics. P-values less than 0.05 indicate a significant relationship (increasing or decreasing) between the number of clusters and the number of selected training samples. In this case all 2009 classes had a significant decreasing trend while only two (in bold) had significant increasing trend for 2012.

	2009				**2012**		
Burn class	*Slope estimate*	*Std. Error*	*p-value*	*Burn class*	*Slope estimate*	*Std. Error*	*p-value*
Unburned	-2.62	0.28	<.0001	Unburned	0.37	0.47	0.436
Burned by Jun04	-1.19	0.14	<.0001	Burned by Jul06	0.57	0.28	0.051
Burned by Jul06	-2.43	0.23	<.0001	Burned by Jul22	-0.08	0.23	0.741
Burned by Jul14	-2.20	0.16	<.0001	Burned by Aug07	0.09	0.47	0.845
Burned by Aug15	-1.49	0.23	<.0001	**Burned by Aug23**	**0.86**	**0.29**	**0.007**
Burned by Sep16	-1.81	0.12	<.0001	Burned by Sep24	-0.08	0.26	0.775
Burned by Oct02	-2.04	0.24	<.0001	Burned by Oct10	0.13	0.22	0.545
Burned by Nov03	-2.33	0.22	<.0001	**Burned by Nov11**	**1.64**	**0.56**	**0.007**

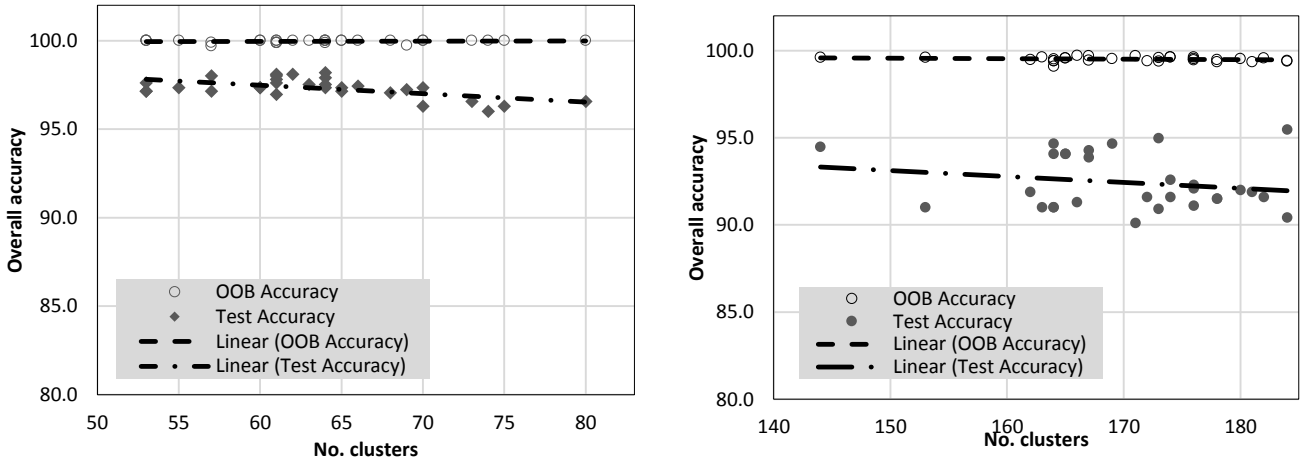

Figure 2.11: Variation of overall accuracy with number of clusters for 2009 and 2012 datasets. Trend lines show there is no systematic relationship between number of clusters and overall OOB and test accuracies.

2.5 DISCUSSION

Because fire disturbance has important implications for vegetation patterns, carbon emission budgets and fire monitoring strategies, information about spatial and temporal occurrence of fire events is required in understanding the wide range of fire effects. The approach presented in this paper presents an effective and efficient approach that can support operational generation of spatio-temporal burned area information. It also contributes to the growing number of multitemporal approaches aimed at characterizing ecosystem disturbance. A common feature in a number of them is the reliance on known spectral-temporal responses of land cover to change processes, such as fire, deforestation and insect infestation, to provide information not only on the type and extent of change but also the timing of the change (Huang et al., 2009; Kennedy et al., 2007). Such detailed information promotes better understanding of linkages between land use and land cover change and impacts upon populations, communities, and the environment as a whole (Gillanders et al., 2008). The other feature is the reliance on known spectral-temporal responses with the goal to automate analyses. This is mainly driven by the increase in the number of images in multitemporal analyses which complicate tasks such as collection of training data or labeling and make them time consuming and expensive (Bovolo et al., 2012; Bruzzone and Prieto, 2001). Automating the training sample selection, as implemented in this study, reduces human intervention which can be error prone, and significantly enhances the generation of required information (Giri et al., 2013; Kennedy et al., 2007).

Classification results obtained for the two sites in eastern Zambia show the effectiveness of the approach in different landscapes. Nevertheless, further testing in other regions is required to establish a more complete perspective of generalization power of the approach. With successful performance shown in mapping burned areas in these savanna environments in eastern Zambia, wider applicability can be expected in many southern Africa countries where such environments exist. The general approach may be adaptable with other burn spectral indices such as the normalized burn ratio (NBR) for application in other environments such as boreal ecosystem, and more broadly, may also be adaptable to applications where abrupt changes are observed such as with deforestation or flooding.

The success of training sample selection and final classification is attributable to a number of steps implemented in the process. A strict iterative clustering procedure in which unsuitable clusters are

excluded by enforcing cluster validity measures was used. The repeated clustering and cluster refining steps reduces variability in the training samples but provides a more inclusive definition of a particular class. Techniques such as guided clustering (Fox and Mayer, 1979; Musy et al., 2006; Wayman, 2000) work under a similar premise of partitioning training data into more homogeneous sub-classes for improved classification accuracy. However, further improvement is needed to ensure stability in the number of clusters created. Merge and split mechanisms as implemented in the ISODATA algorithm could be useful in this regard. The good performance is also a function of the MIRBI index which provides good discrimination between burned and unburned areas (Smith et al., 2007). The robustness of the MIRBI index to land cover type (Trigg and Flasse, 2001) certainly also contributes to the good performance across the three land covers from which samples were selected. The high classification accuracy can be attributed to the reliable training data used and use of a non-parametric Random Forest model. Random Forest is well suited for the abrupt changes in the data while algorithms such as maximum likelihood are not because of the underlining normality assumption (Richards and Jia, 1999). However, other methods such as support vector machines or CART could otherwise be applied. With this flexibility, several classification algorithms can be evaluated and the best one used.

There are a few sources of error and drawbacks that must be highlighted. The approach is sensitive to residual clouds and cloud shadows. From visual inspection of classified data, unfiltered clouds and cloud shadows can cause abrupt changes in the temporal profile of a pixel which impacts the labeling and final burn classification. Clouds and cloud shadows tend to cause sharp changes in band 5 (Kennedy et al., 2007) which has direct impact on MIRBI values. An abrupt increase in the MIRBI due to cloud shadows had an impact especially if it occurred in the last value of a pixel profile. In that case an unburned pixel, as in Figure 2.5 a), would have similar temporal profile as one that burned at the end in the sequence, as in Figure 2.5 h). On the other hand, clouds can cause a decrease in the index which also impacts labeling and burn classification. Implementation of on-the-fly detection techniques of such contaminated pixels could enhance the robustness of the approach. However, the difficulty lies in discriminating abrupt changes due to fire and those due to cloud shadows. A new algorithms called Tmask (Zhu and Woodcock, 2014) with improved capability for detecting residual clouds and cloud shadows by applying multitemporal data has been developed and would provide another option for reducing the impact of residual clouds. Abrupt changes in MIRBI values were also observed in bright open areas such as settlement and

exposed river beds. This also led to some misclassification. These misclassifications could be reduced by masking these areas. The other drawback relates to the efficiency of the analysis. The repeated clustering could be a concern if large samples are involved. Nevertheless, the selection of training samples was done in reasonable time for the samples used in this study. Processing times were within a minute or two using a 2.66 GHz Duo Core processor. Sub-setting large datasets to smaller manageable amounts and applying the process to each at a time would be one way to alleviate the burden of large datasets.

There are also a few challenges and opportunities for operational application of Landsat data for seasonal multitemporal burned area mapping. While current data policies guarantee access to free Landsat data, images spanning the fire seasons may not always be available due to dropped scenes and cloud cover. This could be overcome by applying fusion techniques such as STARFM (Gao et al., 2006) to generate synthetic data for the dropped scenes. The feasibility of such techniques to burn mapping has already been successfully demonstrated (Gao and Masek, 2006). Application of fusion techniques to other environments such as drylands (Walker et al., 2012) also favors the possibility of success in savanna environments. Lastly, instrument errors such as the scan-line corrector (SLC) error hampers the utility of Landsat data. This is even worse for multitemporal analyses as the SLC error gaps may shift with time affecting a larger portion of a study area. Effective gap filling methods, especially one that can recover change information in multitemporal images are required.

2.6 CONCLUSION

While most approaches to mapping burned areas have used one or two images (French et al., 2008; Roy et al., 2002), this study took advantage of the growing temporal depth of Landsat data to develop an effective seasonal burn mapping method that provides information on where and when an area was burned. By detecting burned areas based on general characteristics of temporal profiles, the approach is effective, data driven and can adapt to a particular set of events in the temporal sequences. The automated training sample selection can enhance the capture of necessary spatio-temporal burned area information over large areas which is often time consuming, requires significant human effort and is costly. Further, Landsat data provides adequate spatial detail for monitoring many important land surface dynamics (Giri et al., 2013; Kennedy et al., 2007) and the

multitemporal analysis procedure presented here can contribute to generation of more detailed burned area inventories than currently offered by coarse datasets such as the MODIS burned area product.

2.7 REFERENCES

Archibald, S., Scholes, R.J., Roy, D.P., Roberts, G., Boschetti, L., 2010. Southern African fire regimes as revealed by remote sensing. International Journal of Wildland Fire 19, 861-878.

Ball, G.H., Hall, D.J., 1965. ISODATA, a novel method of data analysis and pattern classification. Stanford research institute, Menlo Park, CA.

Bastarrika, A., Chuvieco, E., Martín, M.P., 2011. Mapping burned areas from Landsat TM/ETM+ data with a two-phase algorithm: Balancing omission and commission errors. Remote Sensing of Environment 115, 1003-1012.

Bezdek, J.C., Ehrlich, R., Full, W., 1984. FCM: The fuzzy c-means clustering algorithm. Comput Geosci-Uk 10, 191-203.

Boschetti, L., Roy, D., Hoffmann, A.A., 2009. MODIS Collection 5 Burned Area Product - MCD45 User's Guide, Retrieved 03/08, 2011, from http://modis-fire.umd.edu/Documents/MODIS_Burned_Area_User_Guide_2.0.pdf.

Bovolo, F., Marchesi, S., Bruzzone, L., 2012. A framework for automatic and unsupervised detection of multiple changes in multitemporal images. Geoscience and Remote Sensing, IEEE Transactions on 50, 2196-2212.

Breiman, L., 2001. Random forests. Machine Learning 45, 5-32.

Bruzzone, L., Prieto, D.F., 2001. Unsupervised retraining of a maximum likelihood classifier for the analysis of multitemporal remote sensing images. Geoscience and Remote Sensing, IEEE Transactions on 39, 456-460.

Celis, R., Milimo, J.T., Wanmali, S., 1991. Adopting improved farm technology: A study of smallholder farmers in Eastern Province, Zambia. International Food Policy Research Institute, Washington, DC.

Chen, C., Li, M.C., Huang, Q.H., Chen, Z.J., Mao, K., 2010. Mapping land cover types as fuzzy sets, in: Yu Liu, Chen, A. (Eds.), 18th International Conference on Geoinformatics. IEEE, Beijing, China.

Cohen, J., 1960. A coefficient of agreement for nominal scales. Educ Psychol Meas 20, 37-46.

Congalton, R.G., 1991. A review of assessing the accuracy of classifications of remotely sensed data. Remote Sensing of Environment 37, 35-46.

Coppin, P., Jonckheere, I., Nackaerts, K., Muys, B., Lambin, E., 2004. Digital change detection methods in ecosystem monitoring: A review. International Journal of Remote Sensing 25, 1565-1596.

Dean, R., Dixon, W., 1951. Simplified statistics for small numbers of observations. Anal Chem 23, 636-638.

Demir, B., Bovolo, F., Bruzzone, L., 2012. Detection of land-cover transitions in multitemporal remote sensing images with active-learning-based compound classification. Geoscience and Remote Sensing, IEEE Transactions on 50, 1930-1941.

Doerr, S.H., Shakesby, R.A., Blake, W.H., Chafer, C.J., Humphreys, G.S., Wallbrink, P.J., 2006. Effects of differing wildfire severities on soil wettability and implications for hydrological response. Journal of Hydrology 319, 295-311.

ECZ, 2001. State of Environment in Zambia 2000. ECZ, Lusaka, Zambia.

Epting, J., Verbyla, D., Sorbel, B., 2005. Evaluation of remotely sensed indices for assessing burn severity in interior Alaska using Landsat TM and ETM+. Remote Sensing of Environment 96, 328-339.

Eva, H., Lambin, E.F., 1998. Remote sensing of biomass burning in tropical regions: Sampling issues and multisensor approach. Remote Sensing of Environment 64, 292-315.

Flasse, S.P., Trigg, S.N., Ceccato, P.N., Perryman, A.H., Hudak, A.T., Thompson, M.W., Brockett, B.H., Dramé, M., Ntabeni, T., Frost, P.E., Landmann, T., Roux, J.L.l., 2004. Remote sensing of vegetation fires and Its contribution to a fire management Information system. Global Fire Management Center, Freiburg.

Fox, L., Mayer, K.E., 1979. Using guided clustering techniques to analyze Landsat data for mapping forest land cover in northern California. Symposium on Machine Processing of Remotely Sensed Data 79CH1430-8MPRSD, Paper 300.

French, N.H.F., Kasischke, E.S., Hall, R.J., Murphy, K.A., Verbyla, D.L., Hoy, E.E., Allen, J.L., 2008. Using Landsat data to assess fire and burn severity in the North American boreal forest region: An overview and summary of results. International Journal of Wildland Fire 17, 443-462.

Frost, P.G.H., 1999. Community-based Management of Fire: Lessons from the Western Province of Zambia, FAO Meeting on Public Policies Affecting Forest Fires. Food & Agriculure Organization, Rome, pp. 341-352.

Futschik, M.E., Carlisle, B., 2005. Noise-robust soft clustering of gene expression time-course data. Journal of Bioinformatics and Computational Biology 03, 965-988.

Gao, F., Masek, J., Schwaller, M., Hall, F., 2006. On the blending of the Landsat and MODIS surface reflectance: Predicting daily Landsat surface reflectance. IEEE Transactions on Geoscience and Remote Sensing 44, 2207-2218.

Gao, F., Masek, J.G., 2006. Mapping Wildland Fire Scar Using Fused Landsat and MODIS Surface Reflectance. 2006 IEEE International Geoscience and Remote Sensing Symposium Vols 1-8, 4172-4175.

Geraci, R., Csiszar, I., Justice, C., Goldammer, J.G., van Lierop, P., Sessa, R., 2009. Fire Disturbance - Assessment of the status of the development of the standards for the Terrestrial Essential Climate Variables. Global Terrrestrial Observing System, Food Agriculture Organization (FAO), Rome, pp. 1-10.

Gillanders, S.N., Coops, N.C., Wulder, M.A., Gergel, S.E., Nelson, T., 2008. Multitemporal remote sensing of landscape dynamics and pattern change: Describing natural and anthropogenic trends. Progress in Physical Geography 32, 503-528.

Giri, C., Pengra, B., Long, J., Loveland, T.R., 2013. Next generation of global land cover characterization, mapping, and monitoring. International Journal of Applied Earth Observation and Geoinformation 25, 30-37.

Gitas, I.Z., Mitri, G.H., Ventura, G., 2004. Object-based image classification for burned area mapping of Creus Cape, Spain, using NOAA-AVHRR imagery. Remote Sensing of Environment 92, 409-413.

Goldammer, J.G., De Ronde, C., 2004. Wildland Fire Management Handbook for Sub-Sahara Africa. Global Fire Management Center, Freiburg.

Goldammer, J.G., Frost, P.G., Jurvélius, M., Kamminga, E.M., Kruger, T., Moody, S.I., Pogeyed, M., 2001. Community participation in integrated forest fire management: Experiences from Africa, Asia and Europe, Communities in Flames. Proceedings of an International Conference on Community Involvement in Fire Management. FAO Regional Office for Asia and the Pacific, Balikpapan, Indonesia, pp. 25-28.

Halkidi, M., Batistakis, Y., Vazirgiannis, M., 2001. On clustering validation techniques. Journal of Intelligent Information Systems 17, 107-145.

Harris, S., Veraverbeke, S., Hook, S., 2011. Evaluating spectral indices for assessing fire severity in chaparral ecosystems (Southern California) using MODIS/ASTER (MASTER) airborne simulator data. Remote Sens-Basel 3, 2403-2419.

Her, Y., Heatwole, C., 2008. Spatial Patterns and Temporal Trends of Lauangwa Valley Fires, OGIS Symposium. OGIS, Virginia Tech, Blacksburg VA.

Holden, Z.A., Smith, A.M.S., Morgan, P., Rollins, M.G., Gessler, P.E., 2005. Evaluation of novel thermally enhanced spectral indices for mapping fire perimeters and comparisons with fire atlas data. International Journal of Remote Sensing 26, 4801-4808.

Huang, C., Coward, S.N., Masek, J.G., Thomas, N., Zhu, Z., Vogelmann, J.E., 2010. An automated approach for reconstructing recent forest disturbance history using dense Landsat time series stacks. Remote Sensing of Environment 114, 183-198.

Huang, C., Goward, S.N., Schleeweis, K., Thomas, N., Masek, J.G., Zhu, Z., 2009. Dynamics of national forests assessed using the Landsat record: Case studies in eastern United States. Remote Sensing of Environment 113, 1430-1442.

Hudak, A.T., Brockett, B.H., Wessman, C.A., 1998. Fire scar mapping in a southern African savanna. Igarss '98 - 1998 International Geoscience and Remote Sensing Symposium, Proceedings Vols 1-5, 1608-1610.

Jones, J.W., Starbuck, M.J., Jenkerson, C.B., 2013. Landsat surface reflectance quality assurance extraction (version 1.7): U.S. Geological Survey Techniques and Methods US Geological Survey, Reston, Virginia.

Kennedy, R.E., Cohen, W.B., Schroeder, T.A., 2007. Trajectory-based change detection for automated characterization of forest disturbance dynamics. Remote Sensing of Environment 110, 370-386.

Korontzi, S., Justice, C.O., Scholes, R.J., 2003. Influence of timing and spatial extent of savanna fires in southern Africa on atmospheric emissions. J Arid Environ 54, 395-404.

Koutsias, N., Karteris, M., 2000. Burned area mapping using logistic regression modeling of a single post-fire Landsat-5 Thematic Mapper image. International Journal of Remote Sensing 21, 673-687.

Koutsias, N., Karteris, M., Fernández-Palacios, A., Navarro, C., Jurado, J., Navarro, R., Lobo, A., 1999. Burnt land mapping at local scale, in: Chuvieco, E. (Ed.), Remote Sensing of Large Wildfires. Springer Berlin Heidelberg, pp. 157-187.

Kull, C., Laris, P., 2009. Fire ecology and fire politics in Mali and Madagascar, Tropical Fire Ecology. Springer Berlin Heidelberg, pp. 171-226.

Laris, P.S., 2005. Spatiotemporal problems with detecting and mapping mosaic fire regimes with coarse-resolution satellite data in savanna environments. Remote Sensing of Environment 99, 412-424.

Lentile, L.B., Holden, Z.A., Smith, A.M.S., Falkowski, M.J., Hudak, A.T., Morgan, P., Lewis, A.S., Gessler, P.E., Benson, N.C., 2006. Remote sensing techniques to assess active fire characteristics and post-fire effects. International Journal of Wildland Fire 15, 319.

Lhermitte, S., Verbesselt, J., Verstraeten, W.W., Veraverbeke, S., Coppin, P., 2011. Assessing intra-annual vegetation regrowth after fire using the pixel based regeneration index. ISPRS Journal of Photogrammetry and Remote Sensing 66, 17-27.

Loboda, T., O'Neal, K.J., Csiszar, I., 2007. Regionally adaptable dNBR-based algorithm for burned area mapping from MODIS data. Remote Sensing of Environment 109, 429-442.

Masek, J.G., Vermote, E.F., Saleous, N.E., Wolfe, R., Hall, F.G., Huemmrich, K.F., Gao, F., Kutler, J., Lim, T.K., 2006. A Landsat surface reflectance dataset for North America, 1990-2000. IEEE Geoscience and Remote Sensing Letters 3, 68-72.

MathWorks Inc, 2014. Variable Importance for Prediction error: R2014b Documentation, Retrieved 11/5, 2014, from http://www.mathworks.com/help/stats/treebagger.oobpermutedvardeltaerror.html.

Mitri, G.H., Gitas, I.Z., 2004. A semi-automated object-oriented model for burned area mapping in the Mediterranean region using Landsat-TM imagery. International Journal of Wildland Fire 13, 367-376.

Mohler, R.L., Goodin, D.G., 2013. Temporal burn scar evolution in tallgrass prairie based on field spectroscopy. International Journal of Remote Sensing 34, 7199-7217.

Musy, R.F., Wynne, R.H., Blinn, C.E., Scrivani, J.A., McRoberts, R.E., 2006. Automated forest area estimation using iterative guided spectral class rejection. Photogrammetric Engineering and Remote Sensing 72, 949-960.

Oduor, P., 2013. US EPA activities supporting national GHG inventory mapping in six ESA countries, Retrieved 11/13, 2013, from http://www.cess.tsinghua.edu.cn/publish/essen/7774/20130716143808193384006/LULC%20presenation_%20UNEP.pdf.

Pedrycz, W.G.F., 2007. Fuzzy systems engineering : toward human-centric computing. John Wiley : IEEE, Hoboken, N.J.

Pereira, J.M.C., 2003. Remote sensing of burned areas in tropical savannas. International Journal of Wildland Fire 12, 259-270.

Pereira, J.M.C., Sá, A.C.L., Sousa, A.M.O., Silva, J.M.N., Santos, T.N., Carreiras, J.M.B., 1999. Spectral characterisation and discrimination of burnt areas, in: Chuvieco, E. (Ed.), Remote Sensing of Large Wildfires. Springer Berlin Heidelberg, pp. 123-138.

Polychronaki, A., Gitas, I.Z., 2012. Burned Area Mapping in Greece Using SPOT-4 HRVIR Images and Object-Based Image Analysis. Remote Sens-Basel 4, 424-438.

Prasad, A., Iverson, L., Liaw, A., 2006. Newer Classification and Regression Tree Techniques: Bagging and Random Forests for Ecological Prediction. Ecosystems 9, 181-199.

Pricope, N.G., Binford, M.W., 2012. A spatio-temporal analysis of fire recurrence and extent for semi-arid savanna ecosystems in southern Africa using moderate-resolution satellite imagery. Journal of Environmental Management 100, 72-85.

Quintano, C., Stein, A., Bijker, W., Fernández-Manso, A., 2010. MODIS Data Mining to Map Burnt Areas 30th EARSeL Symposium: Remote Sensing for Science, Education and Culture, Paris.

Rendón, E., Abundez, I., Arizmendi, A., Quiroz, E.M., 2011. Internal versus External cluster validation indexes. International Journal of Computers and Communications 5, 27-34.

Richards, J.A., Jia, X., 1999. Remote sensing digital image analysis, 5th ed. Springer, New York.

Roy, D., Landmann, T., 2005. Characterizing the surface heterogeneity of fire effects using multi-temporal reflective wavelength data. International Journal of Remote Sensing 26, 4197-4218.

Roy, D.P., Ju, J.C., Kline, K., Scaramuzza, P.L., Kovalskyy, V., Hansen, M., Loveland, T.R., Vermote, E., Zhang, C.S., 2010. Web-enabled Landsat Data (WELD): Landsat ETM plus composited mosaics of the conterminous United States. Remote Sensing of Environment 114, 35-49.

Roy, D.P., Lewis, P.E., Justice, C.O., 2002. Burned area mapping using multi-temporal moderate spatial resolution data - a bi-directional reflectance model-based expectation approach. Remote Sensing of Environment, 263-286.

Sá, A.C.L., Pereira, J.M.C., Gardner, R.H., 2007. Analysis of the relationship between spatial pattern and spectral detectability of areas burned in southern Africa using satellite data. International Journal of Remote Sensing 28, 3583-3601.

Schepers, L., Haest, B., Veraverbeke, S., Spanhove, T., Vanden Borre, J., Goossens, R., 2014. Burned Area Detection and Burn Severity Assessment of a Heathland Fire in Belgium Using Airborne Imaging Spectroscopy (APEX). Remote Sens-Basel 6, 1803-1826.

Schwämmle, V., Jensen, O.N., 2010. A simple and fast method to determine the parameters for fuzzy c–means cluster analysis. Bioinformatics 26, 2841-2848.

Shih, F.Y., Chen, G.P., 1994. Classification of Landsat Remote-Sensing Images by a Fuzzy Unsupervised Clustering-Algorithm. Information Sciences Applications, 1, 97-116.

Silva, J.M.N., Sa, A.C.L., Pereira, J.M.C., 2005. Comparison of burned area estimates derived from SPOT-VEGETATION and Landsat ETM plus data in Africa: Influence of spatial pattern and vegetation type. Remote Sensing of Environment 96, 188-201.

Smith, A.M.S., Drake, N.A., Wooster, M.J., Hudak, A.T., Holden, Z.A., Gibbons, C.J., 2007. Production of Landsat ETM plus reference imagery of burned areas within Southern African savannahs: comparison of methods and application to MODIS. International Journal of Remote Sensing 28, 2753-2775.

Tan, P.-N., Steinbach, M., Kumar, V., 2005a. Cluster Analysis: Basic concepts and Algorithms, Introduction to data mining. Pearson Addison Wesley, Boston.

Tan, P.-N., Steinbach, M., Kumar, V., 2005b. Introduction to data mining. Pearson Addison Wesley, Boston.

Trigg, S., Flasse, S., 2001. An evaluation of different bi-spectral spaces for discriminating burned shrub-savannah. International Journal of Remote Sensing 22, 2641-2647.

USGS, 2014. Landsat Processing Details, Landsat Missions. Retrieved 10/31, 2014, from http://landsat.usgs.gov/Landsat_Processing_Details.php.

Veraverbeke, S., Harris, S., Hook, S., 2011. Evaluating spectral indices for burned area discrimination using MODIS/ASTER (MASTER) airborne simulator data. Remote Sensing of Environment 115, 2702-2709.

Verstraete, M.M., Pinty, B., 1996. Designing optimal spectral indexes for remote sensing applications. IEEE Transactions on Geoscience and Remote Sensing 34, 1254-1265.

Vinya, R., Kasumu, E.C., Syampungani, S., Monde, C., Kasubika, R., 2011. Preliminary Study on the Drivers of Deforestation and Potential for REDD+ in Zambia., Lusaka, Zambia.

Walker, J.J., de Beurs, K.M., Wynne, R.H., Gao, F., 2012. Evaluation of Landsat and MODIS data fusion products for analysis of dryland forest phenology. Remote Sensing of Environment 117, 381-393.

Wayman, J.P., 2000. Landsat TM-based forest area estimation using iterative guided spectral class rejection. Virginia Polytechnic and State University, Blacksburg,VA.

Zhu, Z., Woodcock, C.E., 2014. Automated cloud, cloud shadow, and snow detection in multitemporal Landsat data: An algorithm designed specifically for monitoring land cover change. Remote Sensing of Environment 152, 217-234.

Chapter 3
Profile Based Missing Value Estimation for Abrupt Change Processes

3.1 ABSTRACT

Ease of access to large data stores is facilitating the use of multitemporal imagery analysis to assess changes in natural resources and the environment. However, missing data caused by cloud cover and the scan-line corrector (SLC) error gaps in Landsat 7 imagery confound analysis, and effective estimation methods for gap-filling could greatly improve the usability of these data. Several methods for filling gaps in Landsat data have been proposed but most assume no abrupt or significant change has occurred and that prediction can be based on interpolation from one or two temporally adjacent images. By exploiting longer sequences of multitemporal images we have developed a profile based spatio-temporal k-Nearest Neighbors method, for estimating missing values in spectral index data. Different land cover and changes over time exhibit characteristic temporal profiles. By matching these profiles based on profile shape, reliable estimates of missing values can be obtained. A total of k similar pixel trajectories, both complete and incomplete (with data in points to be estimated), are selected and a weighted average of selected values is used to estimate missing value(s). An alignment pre-step is included to ensure selected pixel profiles match the pixel to be estimated as closely as possible. We tested the profile based approach on an 8-image sequence by simulating between 1 (12.5%) and 6 (75%) missing values per pixel profile in mid-infrared bi-spectral index (MIRBI) data. The profile based approach reliably predicted missing data in the multitemporal data. R^2 values against actual MIRBI ranged from 0.78 to 0.92 indicating high correlation with the actual values. The prediction also showed reasonably high precision with mean absolute error (MAE) values ranging from 55 to 80.9 which represented deviations of 4-7% from actual MIRBI values. The profile based approach was also effective when applied to filling large gaps in multitemporal MIRBI data, generating spatially and temporally consistent filled data even in cases where abrupt changes have occurred.

Keywords: Gap-filling, k-Nearest Neighbors, Multitemporal analysis, Abrupt change, Fire.

3.2 INTRODUCTION

The Landsat satellites have provided an extensive data set for land surface mapping and monitoring at local and global scales (Hansen et al., 2013; Kennedy et al., 2007). However, the utility of these data is often hampered by missing values caused by cloud cover and sensor specific problems such as the scan-line corrector (SLC) error in Landsat 7 (Brooks et al., 2012). The extent of missing data is even higher in multitemporal analyses due to the dynamic nature of cloud cover and SLC gaps, further limiting the amount of usable data. Effective methods for gap-filling are needed to make these data more useful for assessing environmental change. But gap filling methods must be able to restore change information, even abrupt changes such those resulting from deforestation and fire, so that reliable information about landscape dynamics can be derived from the reconstructed datasets.

Several methods for filling missing values in remote sensing data have been proposed, ranging in complexity from temporal image compositing (Roy et al., 2010b), bitemporal local weighted averaging (Chen et al., 2011; Scaramuzza et al., 2004), to geostatistical interpolation (Pringle et al., 2009; Zhu et al., 2012). However, these approaches are limited in that they are formulated with the assumption of gradual or no change in the images being corrected (Chen et al., 2011; Scaramuzza et al., 2004; Zhu et al., 2012), and may be biased towards a particular change or land cover such that they might recover burned areas but distort unburned areas (Barbosa et al., 1998; Roy et al., 2010b). Except for compositing techniques, these methods are mostly bitemporal in nature making them inadequate to reliably model change information over time (Thackway et al., 2013).

Most gap filling methods rely on selection of similar samples to estimate missing values, thus assuming stationarity in the data. This inherent assumption is clearly a weakness in applications where the overall goal is to document change over time. The growing availability of multitemporal image series presents the opportunity to use a sequence of images to better document change over time as it contains more information from which to estimate missing values (Jensen, 2007; Skidmore et al., 2011). The distinctive temporal signatures associated with various land cover types or changes can be exploited in selecting samples by matching the temporal profile of pixel values. Spectral index data provide a good basis for modeling such profiles because the relationships to physical characteristics of the landscape are well defined and indices are more

robust to variability in solar irradiance, atmospheric conditions, land cover variables (canopy background, and canopy structure and composition) than are brightness values (Huete et al., 1999). Abrupt changes associated with disturbances such as fire or deforestation are clearly distinguishable in temporal profile data enabling selection of pixel samples with similar profiles to estimate missing values in a particular pixel.

We present a multitemporal profile-based approach for estimating missing values in spectral index data with the goal of recovering and preserving as much change information, both gradual and abrupt, from the data as possible. To be able to model these changes, we use longer sequences of image data, enabling better temporal definition of the changes, together with local spatial information. The similarity between selected samples and the one being estimated is enhanced through profile alignment, and this leads to better estimates for the missing data. Profile alignment translates the selected samples to the target profile so deviations between them are minimized. Because of the improved similarity, a locally weighted k-Nearest Neighbors method is adequate for estimation, avoiding the need for more complex models. We demonstrate the effectiveness of the method by estimating missing values resulting from the scan-line error, clouds and cloud shadows, in seasonal mid-infrared bi-spectral index data (MIRBI) (Trigg and Flasse, 2001) over a fire season in eastern Zambia. While the application here is based on burn-specific spectral index data, in the development and evaluation of the method we consider the potential for broader applicability to indices used in other disturbance studies, such as drought and deforestation, which exhibit abrupt changes analogous to those of fire.

3.3 APPROACHES FOR GAP-FILLING REMOTE SENSING DATA

Gaps due to missing data in imagery impact the amount of information that can be derived: land cover type information, area estimates, and land cover change estimates (Xiao, 2012). The goal of gap filling methods is to estimate missing values so the derived datasets are spatially and temporally complete to support various applications.

Image compositing is among the many ways bad data or missing data can be corrected in an image. Image compositing techniques aim to replace a missing or bad value with a plausible value from other data obtained over a specified period of time. A missing value is filled based on a set criteria such as a mean, minimum or maximum value of observed vegetation index (Holben, 1986), surface

reflectance (Ql and Kerr, 1997) or surface temperature (Barbosa et al., 1998; Pereira, 2003) values in a temporal sequence. Image compositing is a common processing technique to obtain cloud-free and spatially continuous data and is simple to implement (Xiao, 2012). It is well suited for high temporal resolution data such as that from MODIS or AVHRR. The quality of the recovered data depends on the length of the compositing period – longer periods may not reflect real changes while shorter periods may not be able to filter out clouds. The data generated through these techniques may also be biased toward a particular land cover or phenomenon and degrade others. Barbosa et al.(1998) compared the suitability of five different multitemporal image compositing criteria for burn mapping using AVHRR data. Two were based on maximum value compositing using normalized difference vegetation index (NDVI) and surface temperature while the other three were based on minimum value compositing of channel 1 (visible), 2 (near infrared) and surface Albedo. While results showed minimum-based compositing retained the burn signal better than the others, the vegetation signal was degraded. Therefore, such approaches are more useful if adapted to a specific application or land cover type but may not perform well in general.

A large majority of gap filling methods seek to build a deterministic or statistical relationship between images obtained at different times to predict missing values. Scaramuzza et al (2004) proposed a local histogram matching method for filling SLC gaps in a Landsat 7 ETM+ image based on another existing complete image. By assuming minimal or gradual change in the period between the images, missing values are filled by applying a corrective gain and bias to the pixel values in the complete image over a moving 17-pixel window in the target image. This method performs better in homogenous areas with minimal or no change. However, its performance in heterogeneous areas or areas with significant change is poor (Zeng et al., 2013). Zeng et al (2013) developed a bitemporal gap-filing approach using weighted linear regression. The regression model is built using common existing data in the two images then used to predict missing values in SLC gaps. Another approach by Chen et al (2011) called the neighborhood pixel similar interpolator (NSPI), uses land cover classification information to guide the selection of locally similar pixel between dates. Using an adaptive moving window, the method selects similar pixels in the neighborhood of a gap and estimates the missing value as a weighted average of the selected pixels. Spatially consistent results were obtained in both cases. However, both methods use the underlying assumption that no change has taken place between the two images, so the techniques are not applicable where abrupt change occurs as in cases of deforestation or fire.

Geostatistical interpolation approaches have also been used to fill missing data. These methods model the spatial relationship among observed (non-missing) data to predict values in missing locations (Pringle et al., 2009). Zhu (2012) improved upon the NSPI method (Chen et al., 2011) by applying a geostatistical approach using ordinary Kriging. Improved results were obtained with the geostatistical NSPI approach and had fewer stripping artifacts than the original NSPI method. However, the underlying assumption of stationarity in geostatistical methods is clearly violated when deforestation, fire or other abrupt changes occur (Mariethoz et al., 2012). Other Kriging based methods include those by Pringle et al (2009) who were able to recover missing values in SLC gaps, and filled datasets were smoothly continuous without stripping. However, prediction performance was low in regions of significant change.

The different model-based methods outlined above assume only gradual or no change occurred in the images being corrected. However, land cover is constantly changing and abrupt changes resulting from deforestation and fire often occur in many areas. Thus, a gap-filling method that is able to restore abrupt change in images is desired.

3.4 GAP FILLING USING A PROFILE-BASED APPROACH

3.4.1 Overview and general assumptions

The profile based spatio-temporal k-Nearest Neighbors method relies on translating (offsetting) similarly shaped pixel profiles to a pixel profile being estimated so deviations between them are minimized as much as possible. This assumption is based on the premise that similar land covers show similar temporal profiles (shapes) but only differ in the response level which may be due to differences in structural factors such as percent tree cover, background reflectance, species and so on (Jensen, 2007) (Moody et al., 2005). Therefore, a translation of one to the other will result is a closer fit which can improve the predictive performance of the estimation. Because of the close fit resulting from translation, a locally weighted k-Nearest Neighbors method is adequate for prediction avoiding use of complex models. By analyzing the multitemporal image stack at the same time, missing values are estimated in one step which is more efficient than consecutive processing of several bitemporal image pairs (Huang et al., 2010).

The synergistic use of temporal and spatial information is especially important in resolving ambiguities at points of abrupt change. Figure 3.1a shows a pixel profile with an abrupt change

between the fourth and sixth points (images). However, the fifth point (open diamond) is missing and needs to be estimated. By using the remaining values – points 1-4 and 6-8 as reference in finding similar pixel profiles for estimating the missing value, any of the three cases in b) would qualify as similar pixel profiles. Estimation using all of them would lead to poor prediction for the missing value. To resolve this ambiguity, similar pixels are selected based on the temporal profiles, then local (spatial) information weighted by distance from the target pixel is used to determine the final estimate for the missing value. In that way, local similarity helps tilt the selection toward samples that are more likely to represent the target pixel condition, thus improving the accuracy of the estimate.

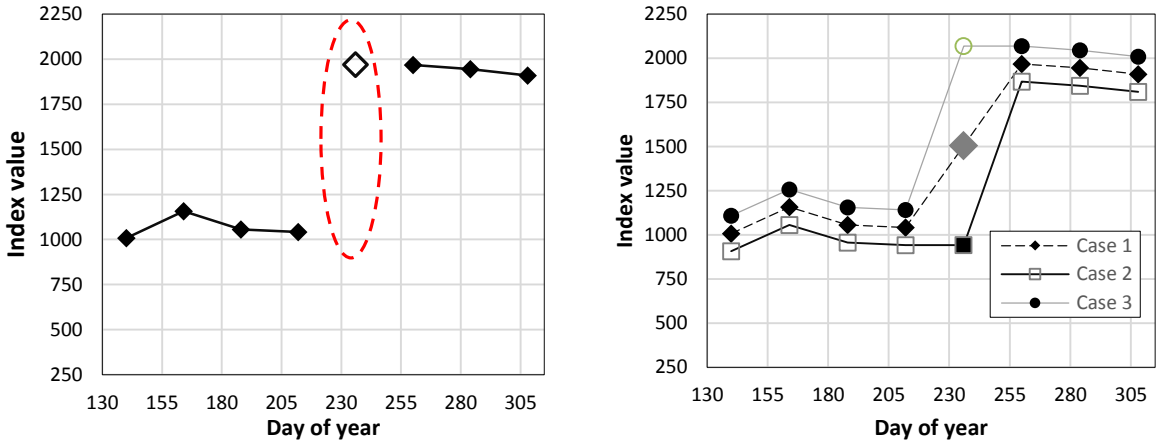

a) b)

Figure 3.1: Ambiguity of missing values when there is abrupt change: a) shows a profile with a missing value from the day 236 image (the dotted oval circle illustrates the range of possible values, with the correct value shown as the open diamond); b) sample trajectories that would qualify as matches for the target profile.

3.4.2 Temporal profile alignment

Let x_i and y_i, $i = 1 \ldots t$, be two pixel temporal profiles in a multitemporal dataset D with similar temporal profiles. Assuming the two profiles only differ in level of response, the one can be mapped onto the other by subtracting an offset. Temporal profile alignment aims to make y_i as similar as possible to x_i by constant translation of y_i onto x_i. Expressing x_i as y_i-T, where T is a constant translation value, T is estimated by minimizing the square error between the two profiles. After Bari and Rueda (2006), T is estimated as:

$$T = \frac{1}{t}\sum_{i=1}^{t}(x_i - y_i) \qquad \text{Equation 3.1}$$

Profile alignment ensures profiles selected are not only close based on distance but are also similar in profile shape. To illustrate, three hypothetical examples in Table 3.1 represent a target pixel (0) and two pixels (1, 2) selected as nearest neighbors based on calculated profile value distances of 966 and 842.3 respectively. Based on this information, pixel 2 would be ranked higher and contribute more to the estimation than pixel 1. But from Figure 3.2, it is clear that pixel 0 and pixel 2 do not have similar profiles. Pixel 1 is similar in shape but is disadvantaged by the large offset from pixel 0. For alignment, the values of T for pixel 1 and pixel 2 will be -337.9 and -12.5 respectively. Subtracting the T value from pixel values gives the translated values in columns 5 and 6 of Table 3.1. The distances between pixel 0 and pixels 1 and 2 are now 142.4 and 841.6 respectively. In this case pixel 1 is correctly selected as a better pixel for the target (pixel 0) than pixel 2. Figure 3.2 shows the profiles before and after translation. From the translated profiles, a similarly shaped profile should contribute better estimates if one of the values of pixel 0 were missing.

Table 3.1: Hypothetical pixel profile values for a target pixel (0) and two nearest-neighbor samples.

	Original values			**Translated values**	
Day of year	*Pixel 0*	*Pixel 1*	*Pixel 2*	*Pixel 1*	*Pixel 2*
140	1008	658	1448	995.9	1460.5
164	1157	900	1230	1237.9	1242.5
188	1056	706	1296	1043.9	1308.5
212	1042	692	1282	1029.9	1294.5
236	1968	1700	1448	2037.9	1460.5
260	1968	1540	1700	1877.9	1712.5
284	1945	1595	1850	1932.9	1862.5
308	1910	1560	1700	1897.9	1712.5

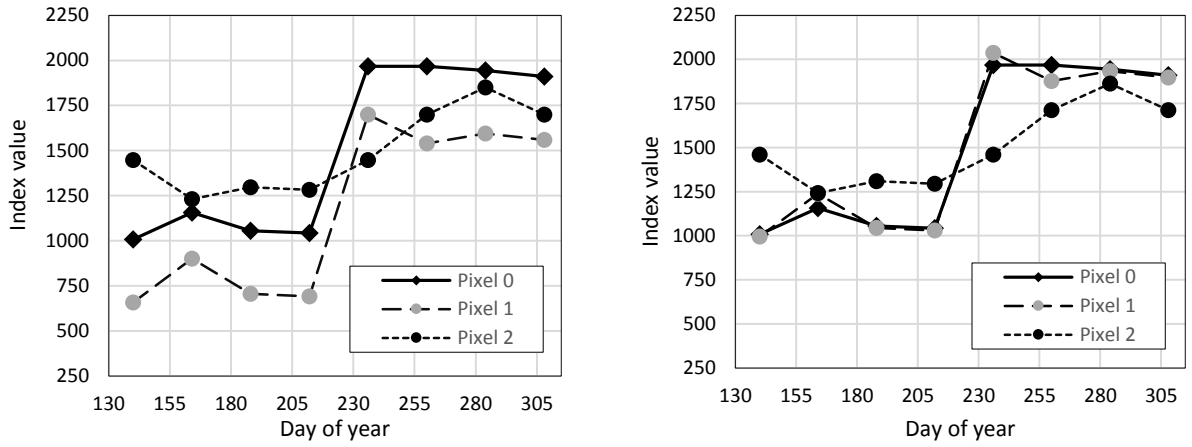

Figure 3.2: An illustration of Profile alignment. a) Original pixel profiles b) Pixel 1 and 2 translated onto pixel 0.

3.4.3 Steps for k-nearest neighbor missing value estimation

The k-Nearest Neighbors algorithm is a non-parametric prediction method that relies on a selected set of samples (k-Nearest Neighbors) to estimate missing values (Keerin et al., 2012). The number of samples, k, is selected using various measures such as the Euclidean distance, Pearson correlation, or cosine distance. Different measures may lead to a different set of k nearest-neighbor samples. The estimation procedure is typically divided into two steps: 1) selection of k nearest neighbor samples and 2) estimation by weighted averaging of the selected samples.

Weighting schemes for estimation depend on the conceptual view of the relationship between observed data and locations to be estimated. There are several ways data can be weighted in the estimation including inverse weighting, exponential or uniform weighting (Atkeson et al., 1997). The type of data – spatial, temporal, and spatial-temporal – influences what weighting is applied in estimating missing data. For spatial data, we assume that farther objects have less influence on the estimation than those closer to the point of interest, while for temporal data, values closer in time are expected to play a bigger role in the estimation than those farther away (Atkeson et al., 1997). Here, we base selection of similar samples on temporal profile similarity, and from those samples an inverse weighting based on spatial Euclidean distance used to estimate the missing value.

Selection of similar profiles for estimation of missing values

Pixels with similar temporal profiles are selected within a set processing window and data common to both the missing pattern and the fill pattern are used to calculate similarity measures. Missing

value(s) may occur anywhere in the temporal sequence; thus there are numerous permutations in which this may happen, and various options in which data can be selected to estimate missing values. To maximize data for the estimation, we use both complete profiles and complementary incomplete profiles. To explain the difference, we define a missing pattern and a fill pattern.

A missing pattern is a logical array of a temporal sequence with 0 and 1 representing missing and observed values respectively. For instance, for a 5-value sequence with fourth missing value, its missing pattern is 11101. A fill pattern is any pattern that has observed values at missing point(s) in the missing pattern. For this 5-value sequence missing pattern (11101), the fill patterns that have a 1 (value) in the fourth place are 11111, 01111, 11110... Further, we describe 11111 as a complete profile, while profiles that have missing values of their own, such as 01111 and 11110, in other positions are called complementary profiles.

Data in the neighborhood defined by a window centered on the pixel to be estimated (target pixel) forms the sample from which similar profiles are selected. Using common data between the target pixel and each pixel in the sample, profiles are translated to the target profile as described previously. Due the potential differences in common data for different fill patterns, use of the Euclidean distance would be problematic as direct comparison is not possible. To avoid this difficulty, the maximum deviation percent, $mdev_j$, was used to define similarity between the target profile and each of the translated profiles, and is calculated as

$$mdev_j = \max_{1 \le i \le p} (100 * |x_i - y_i| / x_i) \qquad \text{Equation 3.2}$$

where x_i the y_i are values of the estimated and fill profiles respectively, p the number of values remaining after excluding missing ones, and j ranges between 1 and N, the number of samples in a given image window.

A pixel profile is selected if it meets a threshold, $mdev_j \le \beta$, and is among the best k nearest neighbor profiles. k is taken as the round value of square root of the number of samples in a given processing window – a rule of thumb which has been found to work well (Duda et al., 2001). If there are no gaps over the processing window, then K is equal to the window size. The value of K

may also be determined through cross-validation approaches but such approaches usually require more computing resources (Atkeson et al., 1997).

Estimating missing values

Estimation of missing data using the k-nearest neighbor method involves taking a weighted average of the selected similar values. For a missing value x_m, and selected similar pixel values x_1, $x_2 \ldots x_K$, the estimate of the missing value, $\hat{x}_m$, is calculated as:

$$\hat{x}_m = \sum_{i=1}^{K} w_i x_i \Big/ \sum_{i=1}^{K} w_i \,; \qquad w_i = 1/ds_i{}^p \qquad \text{Equation 3.3}$$

The weights, w_i, are based on the spatial Euclidean distances, ds_i, of each point from the target pixel location, and p is a positive real number which determines the influence of points on the estimation. Pixels closer to the target pixel contribute more to the estimate that those farther away (Shepard, 1968). Values between 0.5 to 3 are recommended for most implementation of inverse distance weighting (Atkeson et al., 1997).

3.4.4 Implementation of the Profile Based Approach for Generating Filled Data

Due to the shifts in location of SLC gaps and cloud cover from one image scene to the next, very large gaps of missing data may be created in a multitemporal Landsat dataset. Figure 3.3a shows a 400x400 pixel mask for an 8-image MIRBI dataset, where black areas represent pixel locations with complete data after missing values are masked. From inspection of various parts of the data, the gaps of missing data can be as wide as 30 pixels, and over 80 % of the area has some missing data. The distribution of missing values per pixel is given Figure 3.3b. The values in brackets in the legend represent total counts for each case. This high rate of missing data requires a systematic approach to adequately reconstruct the dataset.

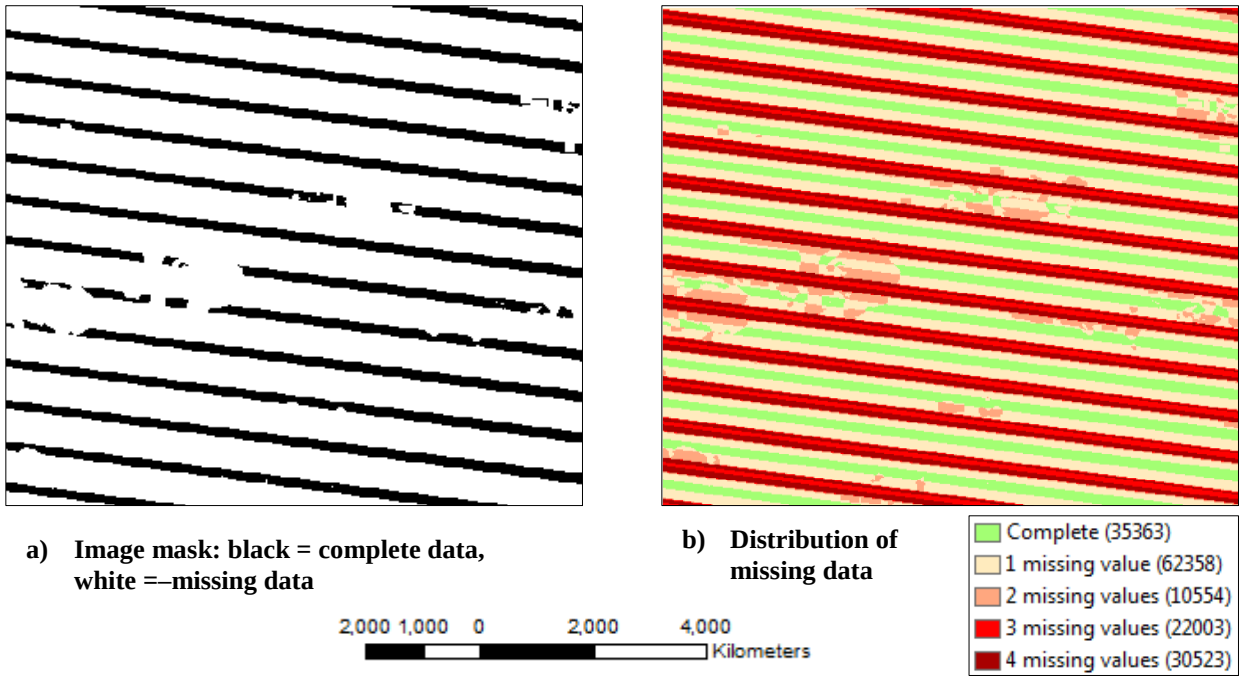

Figure 3.3: Distribution of missing data in a 400x400 pixel area of an 8-image Landsat data stack, a) shows the binary image mask showing missing (white) and complete (black) data, b) shows the number of missing values for each pixel, with the values in brackets in the legend giving the total counts for each case.

To fill these large gaps, the order of the estimation process is managed so adequate spatial and temporal information is available for each missing pattern being estimated. If pixels with complete profiles exist, the estimation process is initialized at the boundaries of the complete data and proceeds outward as in a region growing algorithm. Otherwise, data with the fewest missing values are predicted first and estimation proceeds in a region-growing fashion which enhances consistency with existing complete data and avoids accumulation of error. A morphological dilation on an image mask (Figure 3.3a) is carried out resulting in one-pixel expansion of the regions with complete data. This result is then subtracted from the original image mask to obtain pixels with missing data next to existing complete data or already estimated data. The estimation is then carried out on each of these pixel, updating the image mask each time. The process is iteratively repeated until all missing pixel values are filled.

For each run, an adaptive window size is used with sizes ranging from 5 to 41 pixels to ensure enough samples are selected. Priority is given to pixels with fewer missing values per profile at each run, since the prediction accuracy is expected to be better when there are fewer missing

values. Where the estimation cannot be done such as in the case where pixel profile values are all missing or only one value remains, a local mean of the neighboring pixels in the window is used to fill the missing values. From assessment of the various permutations of missing patterns in the Landsat data used in this study, these cases were found to be quite rare and are expected not to have a significant impact on the final result.

3.5 PERFORMANCE ASSESSMENT

3.5.1 Study area

The study area in eastern Zambia (approximately centered at 12° 1' S and 32°58'E) is a region with widespread human-induced forest disturbance mainly due to shifting cultivation and landscape fires. During the dry season – May to November – landscape fires are common and widespread and our desire to characterize and map this dynamic land cover condition provided both the motivation for developing and the data for testing this new change-preserving gap filling algorithm.

3.5.2 Data and preprocessing

Landsat data (path 169 row 68) for 2009 covering the fire season (May – Nov) were used to evaluate the profile based spatio-temporal k-nearest neighbor method. We obtained fairly clear scenes (<15% cloud cover over the study site) from available Landsat 5 and Landsat 7 archived data (Table 3.2).

Raw Landsat data were calibrated to surface reflectance using the Landsat Ecosystem Disturbance Adaptive Processing System (LEDAPS) (Masek et al., 2006). Pixels affected by clouds, cloud shadows and scan-line error gaps were masked for each image scene following Land Data Operational Products Evaluation (LDOPE) procedures (Jones et al., 2013; USGS, 2011).

We used the MIRBI burn index as the main data input in the performance assessment. MIRBI is highly sensitive to burned areas and retains the burn signal for weeks making detection possible even with 16-day Landsat data. The MIRBI has been used to map burned areas in southern Africa (Smith et al., 2007) and showed better performance than other indices, and is calculated as:

$$MIRBI = 10\rho_{SWIR} - 9.8\rho_{LNIR} + 2.0 \qquad \text{Equation 3.4}$$

where ρ_{SWIR} is the shortwave infrared reflectance (band 7 in Landsat 5 and 7) and ρ_{LNIR} is the second shortwave infrared reflectance (band 5 in Landsat 5 and 7) (Smith et al., 2007). Typically, MIRBI values range from 300 – 4000, although negative values are possible. The MIRBI values for each scene are then stacked into a multitemporal dataset. Figure 3.4 shows a sample of burned area temporal profiles for the multitemporal MIRBI data.

Table 3.2: Landsat images for study area (Path 169, Row 68) used in analysis.

Sensor	Date of acquisition	Julian day 2009
Landsat 5 TM	19-May	139
Landsat 5 TM	04-Jun	155
Landsat 5 TM	06-Jul	187
Landsat 7 ETM+	14-Jul	195
Landsat 7 ETM+	15-Aug	227
Landsat 7 ETM+	16-Sep	259
Landsat 7 ETM+	02-Oct	275
Landsat 7 ETM+	03-Nov	307

3.5.3 Assessing predictive performance

Accuracy testing using simulated missing data

In the absence of independent observed data for validation in the SLC gaps, we assessed performance by simulating missing data in areas with complete data. Since we were working with a multitemporal imagery set with SLC gaps, the areas of complete data were significantly reduced, thus it was not possible to simulate full SLC gaps as has been done in other studies (Chen et al., 2011; Zeng et al., 2013).

The simulation assessment was based on a 5x5 pixel processing window, with the number of k nearest neighbors set at 5, and a similarity cut off threshold of 10%. A total of 1050 randomly selected profiles were used in the assessment. The sampling was stratified according to patterns in Figure 3.4 using an existing multitemporal burn classification. Equal samples (75) were selected for each of the burn temporal profiles and the rest came from the unburned class.

Various missing patterns were simulated by designating some values as missing according to actual missing patterns obtained from the multitemporal dataset. Given the numerous permutations

in which missing value(s) may occur in a pixel profile, we ran 6 simulations based on the total number of missing values per profile to limit the number of cases. Table 3.3 shows the six simulation cases. For each of the six cases, the respective number of missing values were simulated in the 1050 selected profiles with each pattern per case equally allocated to the selected samples. To determine if there were significant differences in performance between the six groups of missing patterns, multiple comparison testing using the Tukey method was carried out. The mean absolute deviation data (described below) obtained for each case of missing values were used to test the difference at a 95% significance level. Cases for pixels with 7 or 8 missing values were not tested because these are estimated by a local mean of neighbors as described in section 0.

Table 3.3: Six simulation cases with varying number of missing values per profiles. In each case 0 represents a missing value in a sequence while 1 represents observed (valid) data.

Simulation case	*Number of missing values simulated*	*Examples of missing patterns for 8-image sequence*	*Total No. values estimated*
1	1	10111111, 01111111, 11111011	1050
2	2	10110111, 01011111, 11011011	2100
3	3	10011101, 01101110, 10111010	3150
4	4	10101100, 00110110, 01101001	4200
5	5	10010100, 00101001, 00010011	5230
6	6	00000110, 00000011, 11000000	6300

The R-squared statistic (R^2) and the mean absolute error (MAE) were used to evaluate the goodness of fit for the prediction. The metrics represent two different aspects of the goodness of fit for the estimated data: that of correlation between predicted and observed values and one of size (precision) of differences between predicted and observed values. Since the two aspects of performance are different, it is usually recommended that models are evaluated on both aspects of performance (Schunn and Wallach, 2005).

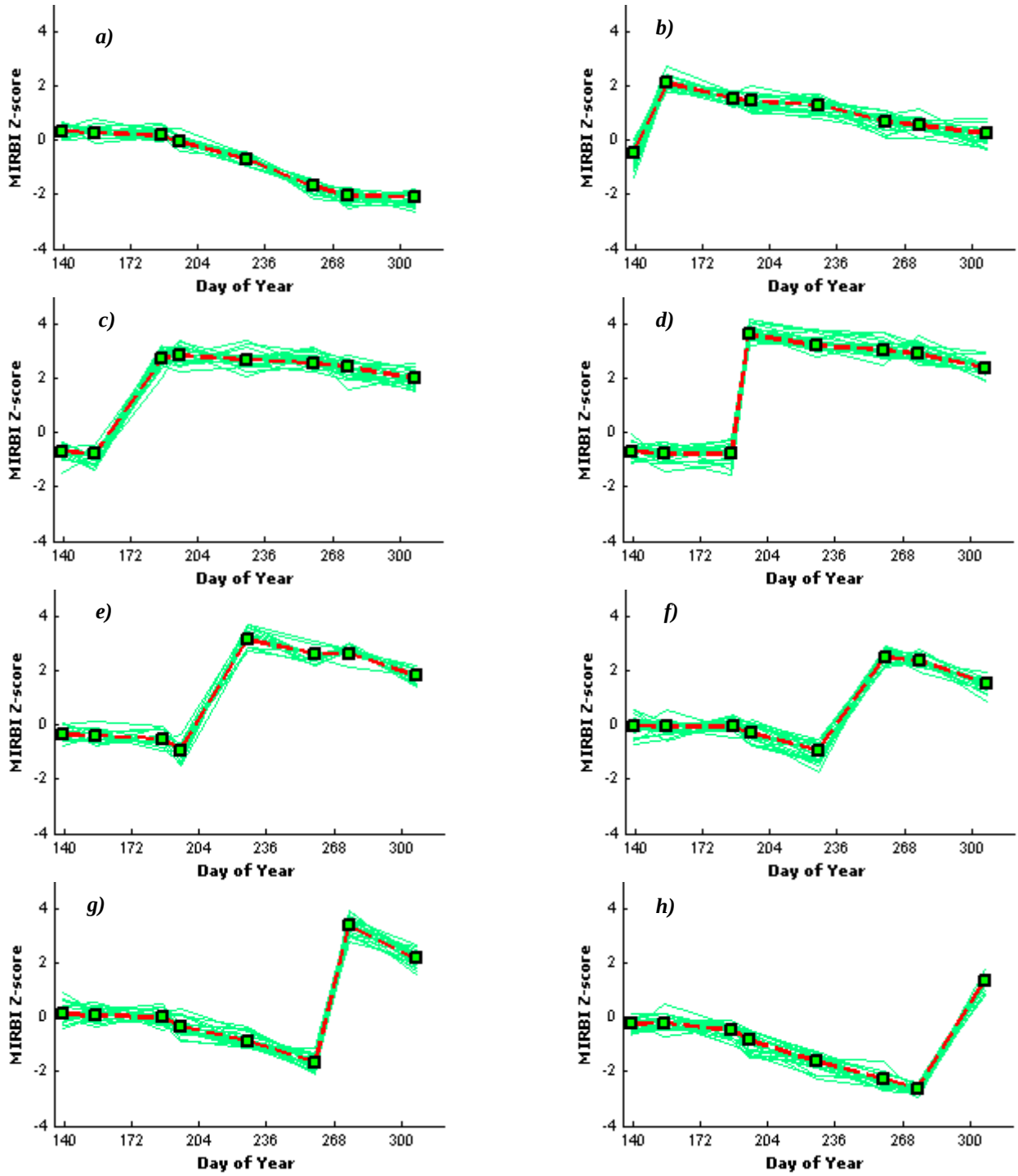

Figure 3.4: Temporal profiles of normalized MIRBI values for groups of pixels (n = 25) from 2009 data: a) Pixel profiles for an unburned area between day of year 139 (May 19) and 307 (November 3); b – h) Pixel profiles from burned areas with different burn times. Abrupt increases in the profiles values indicate a fire occurred in the period between those image dates.

R^2 is a linear regression based metric which measures the degree of association between predicted and actual values - providing information on the direction and relative magnitude between the two sets of data. R^2 varies from 0 to 1 with high values showing higher linear association between predicted and actual values. However, two profiles may have large differences but still have a high R^2, thus high association alone is not enough to define good performance. The mean absolute error (MAE) complements information provided by R^2 with an estimate of the precision of the predicted values, and is commonly expressed in percentage form as mean absolute percentage error (MAPE) (Schunn and Wallach, 2005). These statistics are calculated as:

$$MAE = \frac{1}{N}\sum_{i=1}^{N}|\widehat{x_i} - x_i| \qquad \text{Equation 3.5}$$

$$MAPE = \frac{100}{N}\sum_{i=1}^{N}|\widehat{x_i} - x_i|/x_i \qquad \text{Equation 3.6}$$

where $\widehat{x_i}$ is the predicted value, x_i is the observed value and *N* is the total number of values estimated. MAPE provides a measure of relative comparison even when data vary in magnitude. For both MAE and MAPE, lower values indicate better fit and are preferable.

Qualitative assessment of filled data

The quality of filled data was tested over a 400x400 pixel extent of the study area. Several parts of the area selected had experienced a number of fire events over the sequence of images used. Filled data were assessed qualitatively through visual inspection by looking for inconsistencies in completeness of land cover objects and for evidence of residual stripping effects.

3.6 RESULTS

3.6.1 Accuracy assessment

Table 3.4 shows a summary of results obtained for the different number of missing values per profile. R^2 values between predicted and observed values ranged from 0.78 to 0.92 indicating high correlation with the actual values. Figure 3.5 shows the respective scatter plots for the six simulations. MAE values ranged from 55.9 -80.3 (MIRBI values) representing absolute deviations (MAPE) of 4-7%. As seen in Table 3.4, profiles with fewer missing values (1-3) were estimated more accurately than those with a higher number of missing values (4-6) per profile. Despite the

reduction in predictive accuracy as the number of missing values increases (as would be expected), the high correlation of estimates to actual values, even when most values in a profile are missing, is notable. Thus, in the case where 6 out of 8 values are missing (75% missing), the method still provided fill estimates with an $R^2 = 0.78$ (Table 3.4).

Table 3.4: Summary results on predictive performance of proposed method using simulated data

No. missing per profile	*Ordinary R^2*	*Adjusted R^2*	*MAE*	*MAPE*	*Total values predicted*
1	0.92	0.92	54.9	4.6	1050
2	0.90	0.90	58.0	4.8	2100
3	0.86	0.86	60.4	5.0	3150
4	0.82	0.82	66.1	5.6	4200
5	0.85	0.85	65.8	5.5	5230
6	0.78	0.78	80.3	6.7	6300

Table 3.5: MAE confidence limits between the six groups based on Tukey pairwise comparison

Reference group	*Group compared to*	*Lower 95% confidence limit*	*MAE difference*	*Upper 95% confidence limit*	*Significant difference?*
1	2	-9.3	-3.0	3.3	No
1	3	-11.4	-5.4	0.6	No
1	4	-17.0	-11.2	-5.4	Yes
1	5	-16.6	-10.9	-5.3	Yes
1	6	-31.0	-25.4	-19.8	Yes
2	3	-7.1	-2.4	2.3	No
2	4	-12.6	-8.2	-3.7	Yes
2	5	-12.2	-7.9	-3.6	Yes
2	6	-26.6	-22.4	-18.1	Yes
3	4	-9.7	-5.8	-1.8	Yes
3	5	-9.3	-5.5	-1.7	Yes
3	6	-23.6	-20.0	-16.3	Yes
4	5	-3.2	0.3	3.7	No
4	6	-17.5	-14.2	-10.9	Yes
5	6	-17.6	-14.5	-11.3	Yes

Table 3.5 shows the set of confidence intervals on the differences in MAE between groups obtained by Tukey pairwise comparison. The last column in the table shows which pairs are significantly different thus implying different predictive performance. There was no significant difference in predictive performance for cases with 1 to 3 missing values per profile but performance was poorer

for cases with 4 to 6 missing values. Not surprising, 6 missing values resulted in significantly lower performance compared to all other cases.

3.6.2 Gap filled products

Figure 3.6 shows the test area image with gaps filled using profile based spatio-temporal k-nearest neighbor method. Each row shows the reflectance data, the unfilled MIRBI data and the corresponding filled MIRBI data at a particular date. Reflectance data is displayed with the 4-3-2 false color combination to highlight burned areas in the image. With this combination, burned areas appear black while unburned vegetation appear red (Pereira et al., 1999). Both the unfilled and the filled MIRBI data are displayed using the same continuous color ramp with red and green representing the lowest and highest MIRBI values respectively.

Figure 3.6 a), b) and c) show the scene of July 14, 2009. At this time very little of the area has been burned. A visual comparison of the unfilled and filled data shows the missing data was estimated reasonably well. Given the nature of scan-line error gaps and the fact these are larger in multitemporal data, line artifacts (striping) may form if the interpolation is not done well. In this case, stripping is significantly reduced and is hardly noticeable.

Figure 3.6 d), e) and f) shows the scene of September 16. A larger portion of the image has been affected by fire as indicated by the black regions in Fig. 3.6d. Despite the high number of abrupt changes due to fire, the gap filling was able to restore the missing values in the SLC gaps. By observing the patterns of fire at site A and unburned vegetation at site B (middle row), it can be concluded that there is continuity of the phenomenon (burned or unburned) in the two sites. At each site the gap filling consistently restored the missing values to match the surrounding area. Some stripping effects are noticeable especially in the upper part of the image.

The last row of Figure 3.6 g), h) and i) shows the image of October 2. The increase in area burned since the previous scene is clearly evident. As with the earlier images, the gap filling in most areas provides fill patterns that appear to be representative of the surrounding areas. There are a few locations where the estimated values do not conform to existing patterns in the image, for example at site C (Fig 3.6h), the SLC gap seems to influence the shape of the land cover object. Overall, the gap filling appears to be very good in spite of the large amount of missing data in the multitemporal dataset.

3.7 DISCUSSION

Landsat data are an invaluable resource for earth resources mapping and analysis, but the malfunction of the scan line corrector for Landsat 7 caused approximately 22% loss of data in images captured after 2003 (Scaramuzza et al., 2004). Developing effective methods for filling in the data gaps in these images while maintaining possible change information is important for capitalizing on the historical record of land surface information in this archive. We have demonstrated that by exploiting richer temporal information together with local spatial information, missing data including abrupt changes can be restored with good accuracy.

The rationale for this new gap filling method was to use similarly shaped pixel temporal profiles to guide the estimation of missing values. By exploiting the whole image sequence, missing values can be estimated at any point in the sequence. Some existing approaches (Chen et al., 2011; Pringle et al., 2009) require cloud free or complete images to guide the gap filling process which essentially restricts these methods to forward prediction. In our case, both forward and backward estimation are possible avoiding the need for cloud free or complete scenes. While having complete data in the sequence will improve the prediction, it is not a requirement in the approach described here. The other advantage of this new method is that it processes all images in the multitemporal set at once, thus is more efficient and consistent than doing separate bitemporal processing. Separate analyses are subject to accumulation of error resulting in low overall prediction accuracy which is close to the product of separate prediction accuracies (Bovolo et al., 2012).

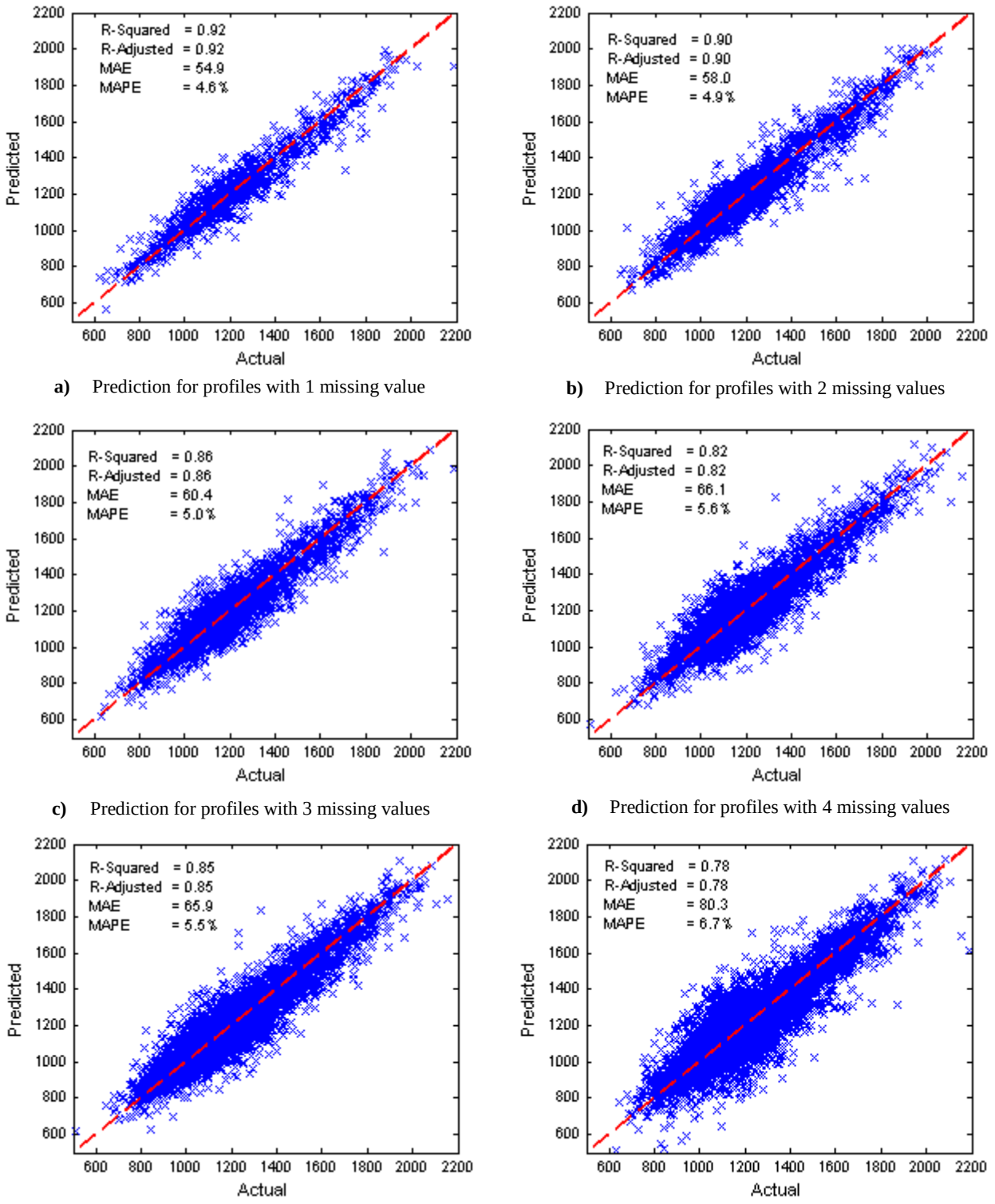

a) Prediction for profiles with 1 missing value

b) Prediction for profiles with 2 missing values

c) Prediction for profiles with 3 missing values

d) Prediction for profiles with 4 missing values

e) Prediction for profiles with 5 missing values

f) Prediction for profiles with 6 missing values

Figure 3.5 Comparison of predictive performance for 1 to 6 missing values in the pixel profile. The plots show predicted versus actual MIRBI values with respective R2, MAE and MAPE values. The red dashed line represents the perfect fit – larger departures from this line indicate poorer estimates.

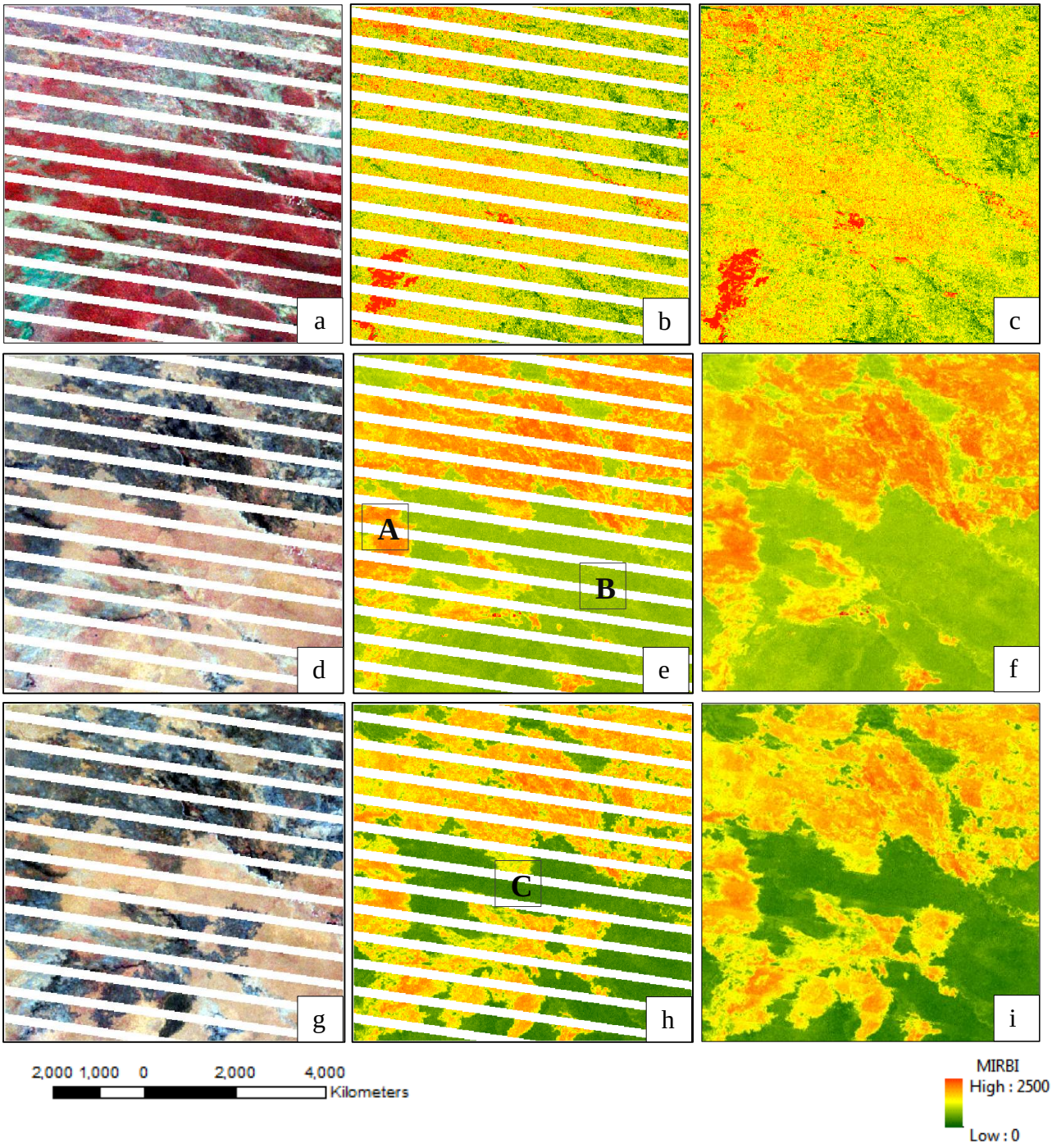

Figure 3.6: Examples of algorithm performance in filling SLC gaps in MIRBI data. The first column (a,d,g) contains surface reflectance data displayed as 432 false color combination, the middle column (b,e,h) is the unfilled MIRBI data, while the last column(c,f,i) shows the gap-filled MIRBI image. The first row (a,b,c) show data on July 14 (minimal fire activity); the second row (d,e,f) show data on September 16 (high fire activity), and the last row (g,h,i) represent data for Oct 2 (highest fire activity). Sites A, B and C are points for comparing visual assessment of the filled product.

Even though the method presented here was applied to fire mapping, it is not limited to this application. Forest disturbances such as deforestation and respective recovery processes show characteristic pixel value trajectories in time (Kennedy et al., 2007) which should also be candidates for estimating missing values in respective vegetation indices such as NDVI or the enhanced vegetation index (EVI). Also, the fact that it was possible to estimate missing values due to abrupt changes from spectral index data shows that there is potential to predict actual reflectance data by using spectral index data as proxy. Work in this direction is underway to enable recovery of the full reflectance product.

The approach used in this application is effective but does have a few limitations. Since missing data are estimated by matching similar pixel profiles, it is possible to recreate unwanted data, particularly if there are remnant clouds or cloud shadows. Therefore, adequate masking of clouds and cloud shadows is necessary for effective application of the approach. New algorithms such Tmask (Zhu and Woodcock, 2014) present improved capability for detecting residual clouds and cloud shadows by applying multitemporal data and would be well suited for application with the approach developed here. With current Landsat 8 data, there is also an opportunity to further enhance cloud detection by applying data from the cirrus band that provides better detection of high-altitude clouds that may not be detected by using traditional bands in Landsat data (Roy et al., 2014). From the efficiency point of view, the calculation of several distances when predicting each missing point, can result in lengthy (inefficient) processing especially if a dataset is large. Processing times are related to the size of the processing window - larger windows demand more computing resources. The current availability of free high speed computing platforms such as Google Earth Engine[2] and Hadoop[3] provide an opportunity of achieving this gap filling goal in more efficient manner. There are also a number of parameters that must be defined such as the number of nearest neighbors and the cut-off similarity threshold. Optimal selection of these parameters and evaluation of their impact on prediction is being evaluated. However, it is quite clear from other studies that the number of nearest neighbors has some impact on estimation – a balance is required between very low and very high numbers (Tan et al., 2005). We set the cut threshold (10%) to weed out bad samples but that could have excluded legitimate samples and compromised the estimation. Choosing an optimal weighting scheme is important for any

[2] https://earthengine.google.org/
[3] hadoop.apache.org/

interpolation method. We choose inverse distance weighting because it is intuitive that farther samples will be less similar to the target point, and this concept is easy to implement. Other weighting schemes, especially those that have a bandwidth parameter should also be evaluated.

Finally, there are opportunities to improve the definition of pixel temporal profiles by incorporating data from other sensors, potentially increasing prediction performance. For instance combining Landsat 8 data with Landsat 7 can improve the temporal sampling to 8 days from the nominal 16 days which would contribute to high prediction accuracy of the developed approach. There is also a wide spectrum of data from other satellites which can be exploited, through fusion techniques, to enhance spatial and temporal information for estimation of missing data. Data from SPOT satellites offer comparable data which can be used to fill Landsat acquisition gaps especially in some African regions where Landsat coverage may be limited (Justice et al., 1986; Roy et al., 2010a). Future missions such as the Sentinel 2 with improved revisit times and wide range of spatial resolutions will also provide even better opportunities for creating spatially and temporal consistent Landsat datasets (Drusch et al., 2012).

3.8 CONCLUSION

Estimation of missing data in remote sensing data is a vital processing step to make the data more usable for Earth resource applications. Although several methods for filling gaps in Landsat data have been proposed, they do not consider the possibility of abrupt changes in the images being corrected. As such, change detection studies face limitations when using images with missing data. By using longer sequence of images and exploiting pixel temporal profile characteristics, we presented an effective approach for estimating missing data in spectral index data with the possibility of preserving change information in the filled data. Results obtained from objective accuracy assessment and subjective observation demonstrate that even abrupt changes occurring in the data gaps can be restored by using this new approach.

3.9 REFERENCES

Atkeson, C.G., Moore, A.W., Schaal, S., 1997. Locally weighted learning for control, Lazy learning. Springer, pp. 75-113.

Barbosa, P.M., Pereira, J.M.C., Gregoire, J.M., 1998. Compositing criteria for burned area assessment using multitemporal low resolution satellite data. Remote Sensing of Environment 65, 38-49.

Bari, A., Rueda, L., 2006. A new profile alignment method for clustering gene expression data, Advances in Artificial Intelligence. Springer, pp. 86-97.

Bovolo, F., Marchesi, S., Bruzzone, L., 2012. A framework for automatic and unsupervised detection of multiple changes in multitemporal images. Geoscience and Remote Sensing, IEEE Transactions on 50, 2196-2212.

Brooks, E.B., Thomas, V.A., Wynne, R.H., Coulston, J.W., 2012. Fitting the multitemporal curve: A fourier series approach to the missing data problem in remote sensing analysis. Geoscience and Remote Sensing, IEEE Transactions on, 1-14.

Chen, J., Zhu, X., Vogelmann, J.E., Gao, F., Jin, S., 2011. A simple and effective method for filling gaps in Landsat ETM+ SLC-off images. Remote Sensing of Environment 115, 1053-1064.

Drusch, M., Del Bello, U., Carlier, S., Colin, O., Fernandez, V., Gascon, F., Hoersch, B., Isola, C., Laberinti, P., Martimort, P., 2012. Sentinel-2: ESA's optical high-resolution mission for GMES operational services. Remote Sensing of Environment 120, 25-36.

Duda, R.O., Hart, P.E., Stork , D.G., 2001. Pattern classification. Wiley, New York.

Hansen, M.C., Potapov, P.V., Moore, R., Hancher, M., Turubanova, S.A., Tyukavina, A., Thau, D., Stehman, S.V., Goetz, S.J., Loveland, T.R., Kommareddy, A., Egorov, A., Chini, L., Justice, C.O., Townshend, J.R.G., 2013. High-Resolution Global Maps of 21st-Century Forest Cover Change. Science 342, 850-853.

Holben, B.N., 1986. Characteristics of maximum-value composite images from temporal AVHRR data. International Journal of Remote Sensing 7, 1417-1434.

Huang, C., Coward, S.N., Masek, J.G., Thomas, N., Zhu, Z., Vogelmann, J.E., 2010. An automated approach for reconstructing recent forest disturbance history using dense Landsat time series stacks. Remote Sensing of Environment 114, 183-198.

Huete, A., Justice, C., Van Leeuwen, W., 1999. MODIS vegetation index (MOD13): Algorithm theoretical basis document, Retrieved 11/10, 2014, from http://vip.arizona.edu/documents/MODIS/MODIS_VI_ATBD.pdf.

Jensen, J.R., 2007. Remote sensing of the environment : An earth resource perspective. Pearson Prentice Hall, Upper Saddle River, NJ.

Jones, J.W., Starbuck, M.J., Jenkerson, C.B., 2013. Landsat surface reflectance quality assurance extraction (version 1.7): U.S. Geological Survey Techniques and Methods US Geological Survey, Reston, Virginia.

Justice, C., Holben, B., Gwynne, M., 1986. Monitoring East African vegetation using AVHRR data. International Journal of Remote Sensing 7, 1453-1474.

Keerin, P., Kurutach, W., Boongoen, T., 2012. Cluster-based KNN missing value imputation for DNA microarray data, Systems, Man, and Cybernetics (SMC), 2012 IEEE International Conference on, pp. 445-450.

Kennedy, R.E., Cohen, W.B., Schroeder, T.A., 2007. Trajectory-based change detection for automated characterization of forest disturbance dynamics. Remote Sensing of Environment 110, 370-386.

Mariethoz, G., McCabe, M.F., Renard, P., 2012. Spatiotemporal reconstruction of gaps in multivariate fields using the direct sampling approach. Water Resour Res 48, W10507.

Masek, J.G., Vermote, E.F., Saleous, N.E., Wolfe, R., Hall, F.G., Huemmrich, K.F., Gao, F., Kutler, J., Lim, T.K., 2006. A Landsat surface reflectance dataset for North America, 1990-2000. Ieee Geoscience and Remote Sensing Letters 3, 68-72.

Moody, E.G., King, M.D., Platnick, S., Schaaf, C.B., Gao, F., 2005. Spatially complete global spectral surface albedos: Value-added datasets derived from Terra MODIS land products. Geoscience and Remote Sensing, IEEE Transactions on 43, 144-158.

Pereira, J.M.C., 2003. Remote sensing of burned areas in tropical savannas. International Journal of Wildland Fire 12, 259-270.

Pereira, J.M.C., Sá, A.C.L., Sousa, A.M.O., Silva, J.M.N., Santos, T.N., Carreiras, J.M.B., 1999. Spectral characterisation and discrimination of burnt areas, in: Chuvieco, E. (Ed.), Remote Sensing of Large Wildfires. Springer Berlin Heidelberg, pp. 123-138.

Pringle, M.J., Schmidt, M., Muir, J.S., 2009. Geostatistical interpolation of SLC-off Landsat ETM+ images. ISPRS Journal of Photogrammetry and Remote Sensing 64, 654-664.

Ql, J., Kerr, Y., 1997. On current compositing algorithms. Remote Sensing Reviews 15, 235-256.

Roy, D., Wulder, M., Loveland, T., CE, W., Allen, R., Anderson, M., Helder, D., Irons, J., Johnson, D., Kennedy, R., 2014. Landsat-8: Science and product vision for terrestrial global change research. Remote Sensing of Environment 145, 154-172.

Roy, D.P., Ju, J., Mbow, C., Frost, P., Loveland, T., 2010a. Accessing free Landsat data via the Internet: Africa's challenge. Remote Sensing Letters 1, 111-117.

Roy, D.P., Ju, J.C., Kline, K., Scaramuzza, P.L., Kovalskyy, V., Hansen, M., Loveland, T.R., Vermote, E., Zhang, C.S., 2010b. Web-enabled Landsat Data (WELD): Landsat ETM plus composited mosaics of the conterminous United States. Remote Sensing of Environment 114, 35-49.

Scaramuzza, P., Micijevic, E., Chander, G., 2004. SLC Gap-Filled Products: Phase One Methodology, Retrieved 4/22, 2011, from http://landsat.usgs.gov/documents/SLC_Gap_Fill_Methodology.pdf.

Schunn, C.D., Wallach, D., 2005. Evaluating goodness-of-fit in comparison of models to data. Psychologie der Kognition: Reden and Vorträge anlässlich der Emeritierung von Werner Tack, 115-154.

Shepard, D., 1968. A two-dimensional interpolation function for irregularly-spaced data, Proceedings of the 1968 23rd ACM national conference. ACM, pp. 517-524.

Skidmore, A.K., Franklin, J., Dawson, T.P., Pilesjö, P., 2011. Geospatial tools address emerging issues in spatial ecology: a review and commentary on the Special Issue. Int J Geogr Inf Sci 25, 337-365.

Smith, A.M.S., Drake, N.A., Wooster, M.J., Hudak, A.T., Holden, Z.A., Gibbons, C.J., 2007. Production of Landsat ETM plus reference imagery of burned areas within Southern African savannahs: comparison of methods and application to MODIS. International Journal of Remote Sensing 28, 2753-2775.

Tan, P.-N., Steinbach, M., Kumar, V., 2005. Introduction to data mining. Pearson Addison Wesley, Boston.

Thackway, R., Lymburner, L., Guerschman, J.P., 2013. Dynamic land cover information: bridging the gap between remote sensing and natural resource management. Ecol Soc 18.

Trigg, S., Flasse, S., 2001. An evaluation of different bi-spectral spaces for discriminating burned shrub-savannah. International Journal of Remote Sensing 22, 2641-2647.

USGS, 2011. LDOPE Tools, LP DAAC : ASTER and MODIS land data products and services, Retrieved 06/10, 2013, from https://lpdaac.usgs.gov/tools/ldope_tools.

Xiao, Z., 2012. Chapter 3 - Compositing, smoothing, and gap-filling techniques, in: Liang, S., Li, X., Wang, J. (Eds.), Advanced Remote Sensing. Academic Press, Boston, pp. 75-90.

Zeng, C., Shen, H.F., Zhang, L.P., 2013. Recovering missing pixels for Landsat ETM plus SLC-off imagery using multi-temporal regression analysis and a regularization method. Remote Sensing of Environment 131, 182-194.

Zhu, X., Liu, D., Chen, J., 2012. A new geostatistical approach for filling gaps in Landsat ETM+ SLC-off images. Remote Sensing of Environment 124, 49-60.

Zhu, Z., Woodcock, C.E., 2014. Automated cloud, cloud shadow, and snow detection in multitemporal Landsat data: An algorithm designed specifically for monitoring land cover change. Remote Sensing of Environment 152, 217-234.

Chapter 4
Fine-scale Seasonal Fire Patterns in Eastern Zambia Derived from Multitemporal Landsat Data

4.1 ABSTRACT

We analyzed patterns of seasonal fire occurrence in eastern Zambia using burned area maps derived from multitemporal Landsat data for 2009 and 2012 fire seasons. The occurrence of fire is widespread in the region with about 60% of the area burned by end of the June to November fire season. Temporally, fire activity is characterized by a unimodal distribution peaking in August and September. Spatially, the early fires occur predominantly in the valley region, but as the season progresses the spatial distribution of fire is similar across all physiographic regions. Comparison of the Landsat derived burned area with the MODIS burned area product revealed high under-estimation by the MODIS product which emphasizes the need for higher spatial resolution data to capture the fine scale burning. Using raster overlay functions, the spatial distribution of fire was analyzed with respect to topography (elevation, slope and aspect), land cover and settlement density. Results show that these landscape factors work in concert to influence fire occurrence. Areas of forest and grassland with higher slopes (>4%), north-facing aspect, and lower settlement densities experience significantly higher fire occurrence. Examining the distribution of burn patch size found that smaller burn patches (<5 ha) predominate although larger patches (>50 ha) contribute more to the total burned area. The size of burn patches in cropland and on the plateau were significantly smaller than for other land covers and landscape regions, reflecting the level of fragmentation of the landscape and the more controlled use of fire in field parcels. The findings have implications for remote sensing data for mapping these fire fragmented landscapes in Zambia. Coarse spatial resolution datasets such as MODIS, are incapable of characterizing such fine-scale fire activity and higher spatial resolution imagery such as Landsat are recommended.

Keywords: Burned area, fire patterns, landscape structure, Landsat, Zambia

4.2 INTRODUCTION

Spatial and temporal patterns in landscape fires has direct impacts on vegetation patterns, carbon emission budgets and fire monitoring strategies (DeBano et al., 1998; Flasse et al., 2004; Korontzi et al., 2003). Variation in fire occurrence is driven by the complex interaction of topography, fuels, weather and ignition sources (Cochrane and Ryan, 2009). The topography of an area can influence the amount of radiant energy transfer during combustion, fuel moisture content due to variable insolation (Lafon and Grissino-Mayer, 2007; Mermoz et al., 2005) and together with wind can restrict fire spread in some directions (Pyne et al., 1996). Land cover controls the amount of available fuels which in turn influences fire intensity and impact of affected areas (Cochrane and Ryan, 2009). Availability of unfragmented fuels supports continuous burning which has implications for sizes of areas burned. Human activity and lightning are the main sources of fire ignition. Human activities such as agriculture, establishing of settlements, and paths and roads also modify fuel sources through fragmentation of the landscape which impacts the occurrence of fire in an area (Archibald et al., 2009). By understanding the interaction of fire occurrence with these factors and associated impacts, researchers can help resource managers and policy makers devise sound natural resource management strategies (Kasischke et al., 2002; Turner, 2010). This understanding also requires appreciation of the spatial and temporal scales over which they occur (Cochrane and Ryan, 2009; Lentile et al., 2006; Pyne et al., 1996).

Fire is widespread across eastern Zambia during the June to November fire season and is characterized mainly by surface fires which burn dead and dying grasses, crop residue, and small trees and shrubs (Frost, 1999; Pereira, 2003; Roy et al., 2005). Fires are mostly linked to rural livelihood activities such as clearing fields for agricultural purposes, improving visibility along paths for safety, hunting, regenerating green vegetation for livestock, and for controlling pests and parasites such as ticks (Baars, 1999; Frost, 1999; Roy et al., 2005; Shea et al., 1996). With the conditions of ready fuel and dry windy weather, fires often burn out of control, ultimately affecting large areas (Archibald et al., 2009; Frost, 1999). These fires are a significant source of carbon emissions that impact regional and global atmospheric chemistry (Cochrane, 2009; Innes et al., 2000). Fires have, over time, also shaped vegetation patterns in the country by expanding grassland extents at the expense of woodland (Lawton, 1978). Information on sizes, patterns and timing of fires and the land covers impacted would be valuable to resource managers to plan fire management in the country and would also inform current REDD+ projects (Vinya et al., 2011).

Scale is an important factor in understanding spatial patterns as it determines what entities on the landscape can be mapped and what spatial relationships can be assessed (Lentile et al., 2006). Fire has extensively been mapped at regional and global scales using coarse imagery such as MODIS (Roy et al., 2006), AVHRR (Barbosa et al., 1997; Giglio et al., 2010) or SPOT VEGETATION (Gregoire et al., 2003). While these datasets have short revisit cycles which enable detailed temporal fire monitoring, their utility for local landscape fire monitoring is limited by their coarse spatial resolution. Depending on the spatial pattern of the landscape and fires, burned areas can be either under-estimated or over-estimated (Sá et al., 2007; Zhang et al., 2011). To address this weakness of coarse data, developed countries such as the United States also collect burned area information using higher spatial resolution imagery such as Landsat (French et al., 2008; Miller and Thode, 2007). However, in developing countries such as Zambia, such programs are not widely implemented leading to a gap in information for studying such disturbances at local scale (Goldammer and De Ronde, 2004; Pricope and Binford, 2012). The use of free available Landsat data would meet this information need and would enable better understanding of the scale of fire activity that occurs in landscapes in Zambia.

To address this gap in the availability of higher resolution burn mapping products, Malambo and Heatwole (2015a) developed a multitemporal burn mapping procedure to analyze a sequence of images spanning the fire season with procedures of gap-filling the Landsat-7 missing data (Malambo and Heatwole, 2015b). The burned area mapping procedure is based on automatic selection of temporal training signatures using fuzzy clustering and classification using Random Forest (Breiman, 2001). The method provides an effective way of deriving the spatial and temporal distribution of burned areas within a fire season. Generation of burned area information is enhanced by an effective gap-filling method that estimates missing data in Landsat scenes due to clouds and the scan-line error gaps. The gap-filling method exploits longer sequences of multitemporal images to estimate missing data using characteristic land cover temporal profiles. Both gradual and abrupt changes can be estimated using this procedure making it well suited for applications such as for burned area mapping.

Eastern Zambia is characterized by three physiographic regions – a plateau region with an average elevation of 1100 m adjacent to the border with Malawi, the Luangwa valley floor (average elevation 700 m) to the west, and a hilly transition zone in the middle (Celis et al., 1991). The three regions present distinct topographic, demographic and fuel patterns that may contribute to

variation in fire activity. The plateau region is a highly settled with landscapes characterized by a patchwork of cropland, forest (mostly open forests or woodland), wetlands and fallow land (Celis et al., 1991; Her and Heatwole, 2008). The Luangwa valley floor is predominated by light forests and grassland and most of the area is reserved for a game management area which is a buffer area around the national game parks. Settlements and farming in the valley region are mainly confined to areas of alluvial soils formed by rivers tributary to the Luangwa River. The annual landscape fires cover extensive portions of the landscape as we have observed from numerous visits to the region. However because of the limited spatial resolution of the existing burn inventories, the extent and relationship of fires to characteristics of the region are not known. The objective of this study was to apply the multitemporal analysis tools of Malambo and Heatwole (2015a, b) to characterize the spatio-temporal burn patterns in eastern Zambia, to compare similarity of burn extent and patterns between two years, to highlight the improved burn detection with respect to MODIS burned area data (Roy et al., 2006), and to analyze the relationship between fires and physiographic region, land cover, population presence, and fire size. Specific questions we wanted to address in this analysis were to examine: 1) the occurrence of fire with respect to land cover, topography and settlement density, and 2) the distribution of burn patch sizes by land cover and physiographic region.

4.3 METHODS

4.3.1 Study area

The study area is located in the eastern part of Zambia between latitude 11°32’ and 12° 20’ S and longitude 32°18’E and 33°18’E representing a total area of 7677 square kilometers. The region has a tropical climate with very distinct wet/dry seasons, with the dry season generally extending from May to November and the rainy season from November to April. Mean daily temperatures range from 15 to 36°C and depend on the elevation of the area – the Luangwa valley region which is part of the study area has some of the hottest temperatures in the country. Generally, cooler temperatures (12-15°C) are prevalent in June and July while temperatures above 30°C mainly occur September through November (Astle et al., 1969). Annual rainfall, mainly driven by the Inter-tropical Convergence Zone (ITCZ), ranges from 850 to 1050 millimeters (Celis et al., 1991)

and is concentrated in the months December to March. The valley area in the study area receives relatively lower rainfall compared to the plateau regions (ECZ, 2001).

Miombo is the principal vegetation type in the area characterized by an intermingling of woodland and grasses (Pereira, 2003). It is a type of savanna woodland which is composed of two-storied canopy with trees 10-12 m high (ECZ, 2001). There is widespread human induced forest disturbance mainly due to shifting cultivation and landscape fires. Fire incidences are prevalent in the dry season with peak fire activity from August through October. Fire occurs almost everywhere affecting all land cover types including cropland, forests, and wetlands.

4.3.2 Data and preprocessing

Data sources

Landsat data (path 169 row 68) for the 2009 and 2012 fire seasons (May to Nov) were used to derive burned areas for each of the image dates. All images were Standard Terrain Corrected (Level 1T) which involves systematic radiometric and geometric corrections using ground control points and a Digital Elevation Model (DEM) for topographic accuracy (USGS, 2014). Fairly clear scenes (<15% cloud cover over study site) were obtained from the USGS website from available Landsat 5 and Landsat 7 scenes from May to November in each year. The list of images acquired for this study is given in Table 4.1.

Other data used for the study include a land cover map and the 90m Shuttle Radar Topographic Mission (SRTM) elevation data. The 2010 land cover dataset was obtained from the Regional Center for Mapping Resources for Development (RCMRD), Kenya. These data were created as part of the US Environmental Protection Agency (EPA) effort to support greenhouse gas (GHG) inventory reporting in selected east and southern African countries including Zambia. The classification scheme - based on IPCC guidelines for land cover mapping and greenhouse gas emission estimation - comprise six land cover classes: forest, grassland, cropland, settlements, wetland and other. The overall accuracy of the land cover map is 80.4 % (Oduor, 2013). We also digitized settlement locations with the aid of ArcGIS® online high resolution base map imagery for use in estimating settlement density.

Preprocessing Landsat data

The raw Landsat data were calibrated to surface reflectance using the Landsat Ecosystem Disturbance Adaptive Processing System (LEDAPS) (Masek et al., 2006). The LEDAPS processing chain also includes cloud masking. We used procedures described in Jones (2013) to mask pixels affected by clouds, cloud shadows and scan-line error gaps. The procedure used quality information derived in the LEDAPS processing chain to identify pixels affected by clouds, cloud shadows and scan-line error. These routines are much less computationally intensive than programs such as Fmask (Zhu and Woodcock, 2012) and provide reasonable detection of clouds and cloud shadows.

Table 4.1: Landsat images selected for the study.

2009			**2012**		
Sensor	*Date of acquisition*	*Julian day 2009*	*Sensor*	*Date of acquisition*	*Julian day 2012*
TM	19-May	139	ETM+	19-May	140
TM	04-Jun	155	ETM+	06-Jul	188
TM	06-Jul	187	ETM+	22-Jul	204
ETM+	14-Jul	195	ETM+	07-Aug	220
ETM+	15-Aug	227	ETM+	23-Aug	236
ETM+	16-Sep	259	ETM+	24-Sep	268
ETM+	02-Oct	275	ETM+	10-Oct	284
ETM+	03-Nov	307	ETM+	11-Nov	316

Generation of MIRBI multitemporal dataset

The MIRBI index was used for mapping burned areas, and is calculated for each image using the expression:

$$MIRBI = 10\rho_{SWIR} - 9.8\rho_{LNIR} + 2.0 \qquad \text{Equation 4.1}$$

where ρ_{SWIR} is the shortwave infrared reflectance (band 7 in Landsat 5 and 7) and ρ_{LNIR} is the second shortwave infrared reflectance (band 5 in Landsat 5 and 7) (Smith et al., 2007). All calculated data were then stacked into one multitemporal dataset arranged in ascending order by acquisition date.

Missing (masked) data in areas affected by clouds, shadows and the SLC gaps were estimated using a trajectory based spatio-temporal imputation procedure described by Malambo and Heatwole (2015b). The procedure uses pixel data with similar temporal profiles to estimate

missing values in a target pixel trajectory. The procedure has been evaluated by simulating missing data in known pixel trajectories and showed good performance in recovering the missing values.

4.3.3 Burned area classification

Seasonal burned area data was derived for the two years by classifying the multitemporal MIRBI data using a procedure of Malambo and Heatwole (2015a). Burned areas are classified by burn date using trained Random forests (Breiman, 2001) models for each year. Overall mapping accuracies for the 2009 and 2012 models are 97.3±0.6 and 92.6±1.6 percent respectively. Full details on the training and validation procedures of these models are given in Malambo and Heatwole (2015a).

To enhance spatial coherency and reduce speckle in the classified data, isolated pixels (1-3 pixels) were reassigned to their nearest neighbors. These isolated pixel represented about 1% of the total area so this reassignment is not expected to have a significant change of the burn distribution. The derived burned area information was then edited to mask identifiable errors such as those resulting from the residual clouds and other outliers in the dataset. For comparison of burned area patterns, all masked locations were applied to both datasets so that the same areas were considered in each year.

We evaluated general characteristics of fire activity including the extent of burned area by date, total burned area for the whole season, and burned area size distribution. Burned area by date represents the area burned prior to the date of the Landsat image acquisition. The total area burned over the fire season was then calculated by summing these individual contributions. The difference in total burned area between the two years was tested using the two sample test for proportions. The McNemar test (McNemar, 1947)– a statistical test of paired nominal data used to compare paired proportions, was also used to test the general patterns of burned area between the two years. Each pixel's burn state (burned or unburned) in 2009 and 2012 was used to compare paired proportions and to test the general patterns of burned area between the two years at 0.05 significance level.

Table 4.2: Temporal aggregation of MODIS burned area data.

2009		2012	
Landsat date range (Julian days)	*Fire season class*	*Landsat date range (Julian days)*	*Fire season class*
139 - 195	Early	140 - 204	Early
196 - 259	Mid	205 - 268	Mid
260 - 307	Late	269 – 316	Late

4.3.4 Comparison with MODIS Burned Area Product

Burned area data from the MODIS Burned Area Product were obtained for the years 2009 and 2012 from the University of Maryland[4]. The data covered May through November which coincided with the Landsat time span. To compare the two products the MODIS burned area data was temporally aggregated over date ranges defined by the Landsat data. The fire season was divided into early, mid and late season as shown in Table 4.2. For each part of the season the total burned area was calculated.

4.3.5 Assessing variation of fire occurrence as a function of landscape factors

To facilitate the combination with burn maps and comparisons between categories, appropriate categorical data were created from the continuous dataset representing elevation, slope, aspect, and settlement density. Datasets generated included the following:

a) Elevation data ranged from 581 to 1365 m and was grouped into 5 ranges: 581-670 m, 671 – 750 m, 751 – 935 m, 936 – 1060 m and >1060 m.

b) Percent slope data, derived from the elevation data, ranged from 0 to 69.80% and was classified in 4 categories: 0-4%, 4.01 – 8.00%, 8.01 - 15.00% and >15%.

c) Slope aspect data, also derived from elevation, were classified into 8 aspects classes representing the 8 cardinal directions. Flat areas were not included in the analysis.

d) Settlement density, calculated as the number of settlements per unit area, ranged from 0-5.34 and was recoded into 4 categories: 0 (Unsettled), 0.01 - 1.00, 1.01 – 3.00 and >3.00.

[4] MODIS Burned Area Product. ftp://ba1.geog.umd.edu/ Accessed 10/10/2014.

e) The land cover data was reclassified into three broad categories of forest, grassland and cropland by aggregating the ‘wetland’ class with ‘grassland’, and the ‘settlement’ and ‘other’ classes with ‘cropland’.

The categorized datasets were then spatially combined using standard raster overlay operations with the total burned area maps for each year to get a cross-tabulation of each group with burned data. The percentage of area burned for each class/category for each was calculated with respect to the total available area in that class. Our aim was to identify the classes that have significantly higher or lower fire occurrences, thus differences among proportions in each case were tested using the analysis of means for proportions (Nelson, 2005). This statistical test is not a pair-wise comparison but compares each group mean to the overall average of all the groups

4.3.6 Assessing burn patch size distribution

For burned area size analyses, individual burn patches were extracted from the two seasonal burn datasets using 8-pixel connectivity to define patches. The extracted data was used to assess the general distribution of burn patch size, with comparison between burn patch size, land cover, and physiographic region. Because the burn patch size distribution did not satisfy normality assumptions, non-parametric tests were used for analysis. To test for differences in burn patch size between the years, among land cover classes and physiographic regions we used the Kruskal-Wallis test - a non-parametric version of one-way analysis of variance (ANOVA) (Rice, 2006). Pairwise comparisons of mean burn patch size were done using the Steel-Dwass test (also non-parametric) controlling the experiment-wise error rate at 0.05.

Physiographic regions were defined by grouping the elevation dataset. Earlier studies define the Plateau region to lie at elevations above 1000 m above sea level while the valley floor was defined to lie between 400 and 700 m (Astle et al., 1969; Celis et al., 1991). Using available land cover and hillshade analysis as auxiliary information to accurately define the boundaries, these ranges were adjusted so the valley floor was lay between 581 and 760 m, the hilly transition between 761 and 960 m and the plateau between 960 and 1365 m above sea level. Figure 4.1 shows the map for the three regions. Inconsistent low or high elevation islands in each region were edited to make the regions uniform.

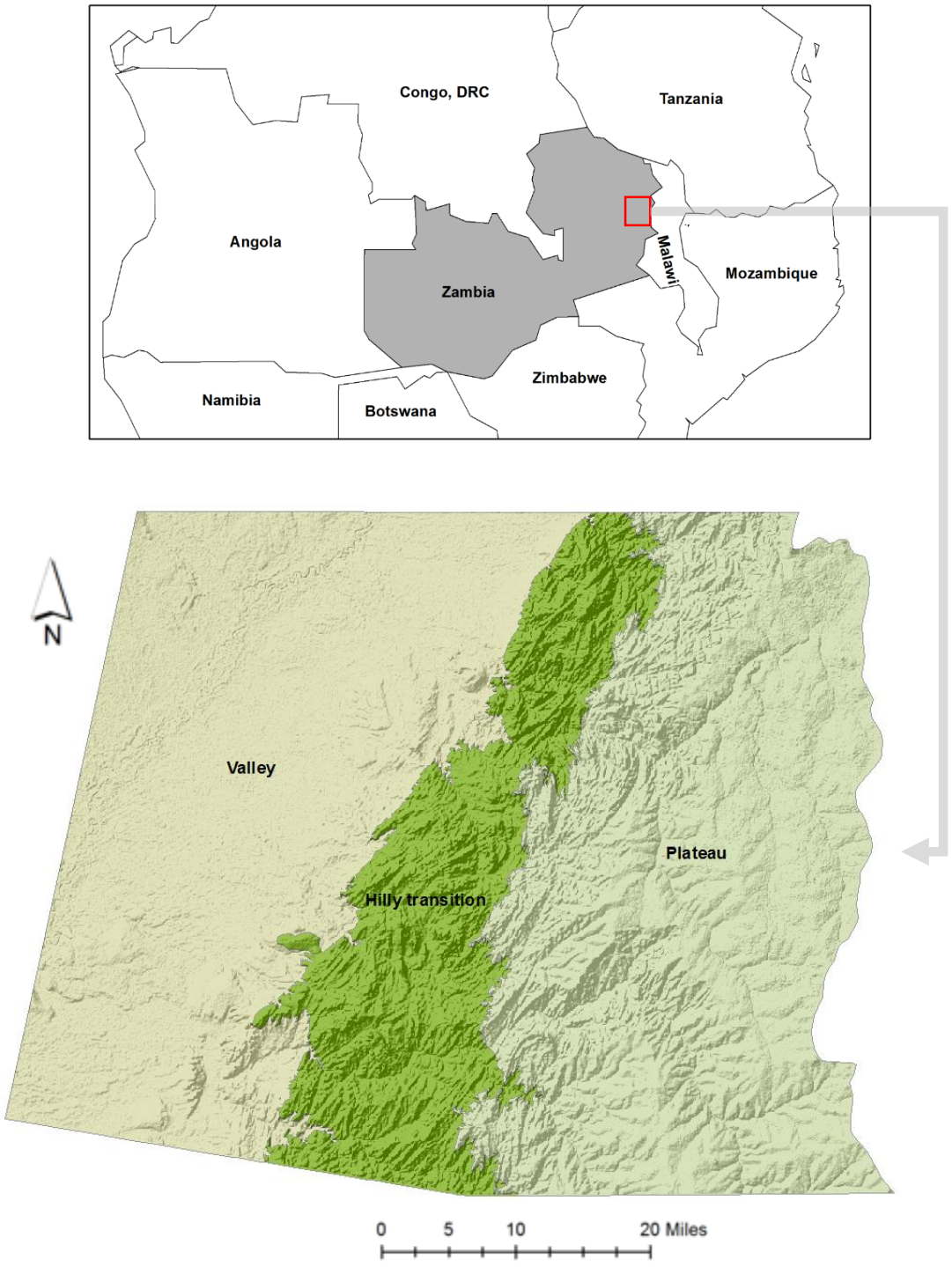

Figure 4.1: The three physiographic regions in eastern Zambia: Valley floor between 581 and 760 m, the hilly transition between 761 and 960 m and the plateau between 960 and 1365 m above sea level.

4.4 RESULTS

4.4.1 Spatial and temporal distribution of burned area

Of the 7677 km^2 in the study area, 60% on average had burned by November in both years. A total of 4596 km^2 was mapped as burned for 2009 while 4649 km^2 was mapped for 2012 representing burn proportions of 59.9% and 60.6% respectively. The two sample test for proportions (p-value < 0.0001) showed that the proportion of burned area in the two years was different. McNemar test (χ^2 = 1275.96, df = 1, p-value < 0.0001) also indicated that there was a significant difference in the pixels that burned (or did not burn) between the two years. This means that amount and the actual areas affected by fire varied from 2009 to 2012. This disparity could be partly attributed to the different end dates for the two image sequences used – since there reasonably could be unmapped burned areas for 2009 between November 3 and November 16, last date in the 2012 sequence. Table 4.3 shows details of contingency table for the two datasets.

Table 4.3: Summary of agreement and discordant pairs between burned area maps for 2009 and 2012

Pair Combination	*2009*	*2012*	*Count*	*Percent*
Pairs in agreement (Burned)	Burned	Burned	3772319	42.2
Discordant pairs	Burned	Unburned	1334296	15.6
Pair in agreement (Unburned)	Unburned	Unburned	2030912	23.6
Discordant pairs	Unburned	Burned	1393290	16.3

Figure 4.2 shows the temporal distribution of total burned area from May to November for the two years. The burned area exhibits a unimodal distribution with the majority of fires occurring between August and September (days 213 – 273). The peak burning period accounts for nearly 75 percent of the total burned area. While the results from the two years are not directly comparable because of the different image dates, the graphs show that the temporal burning trends for the two years are similar.

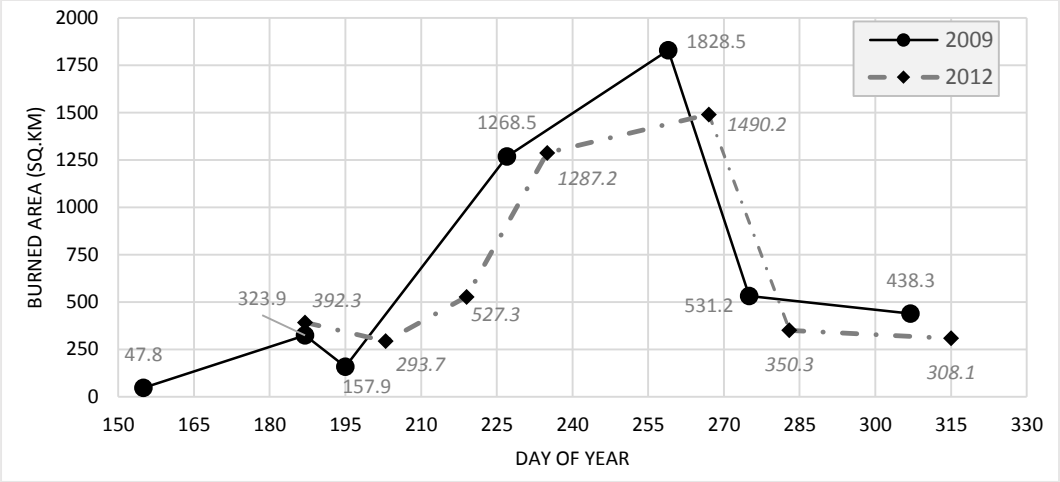

Figure 4.2: Temporal progression of fire in the 2009 and 2012 fire seasons in eastern Zambia. Data labels for 2012 are italicized to differentiate them from 2009 data labels. The temporal distribution of burned area is unimodal with the amount of burned area initially lower, in June and July (days 152 - 212), is highest between August and September (days 213 – 273) and then drops again in October through November (days 274 - 315).

Figure 4.3 summarizes the distribution of burned area over the three physiographic regions during the 2012 fire seasons. The trend in burning is also spatially depicted by the seasonal burn maps for the two years in Figure 4.4 and Figure 4.5. Most of the early fire activity (before August) occurs on the Luangwa valley floor. However as the fire season reaches peak activity there is a more even spatial distribution of burned area between the three regions.

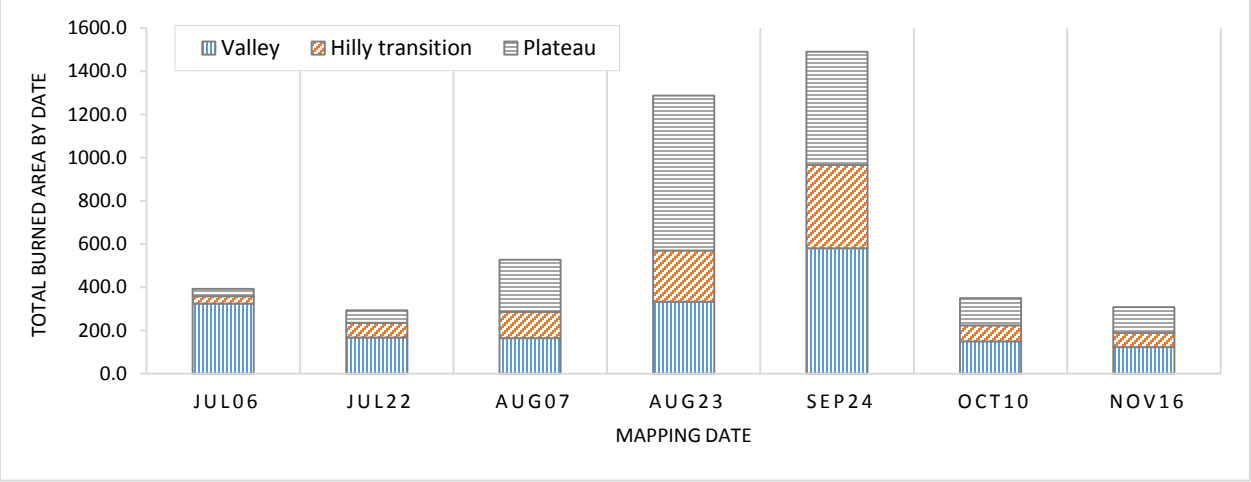

Figure 4.3: Distribution of burned areas during by physiographic region for the 2012 fire season in eastern Zambia. Similar trends were observed for 2009 but are not displayed here for space

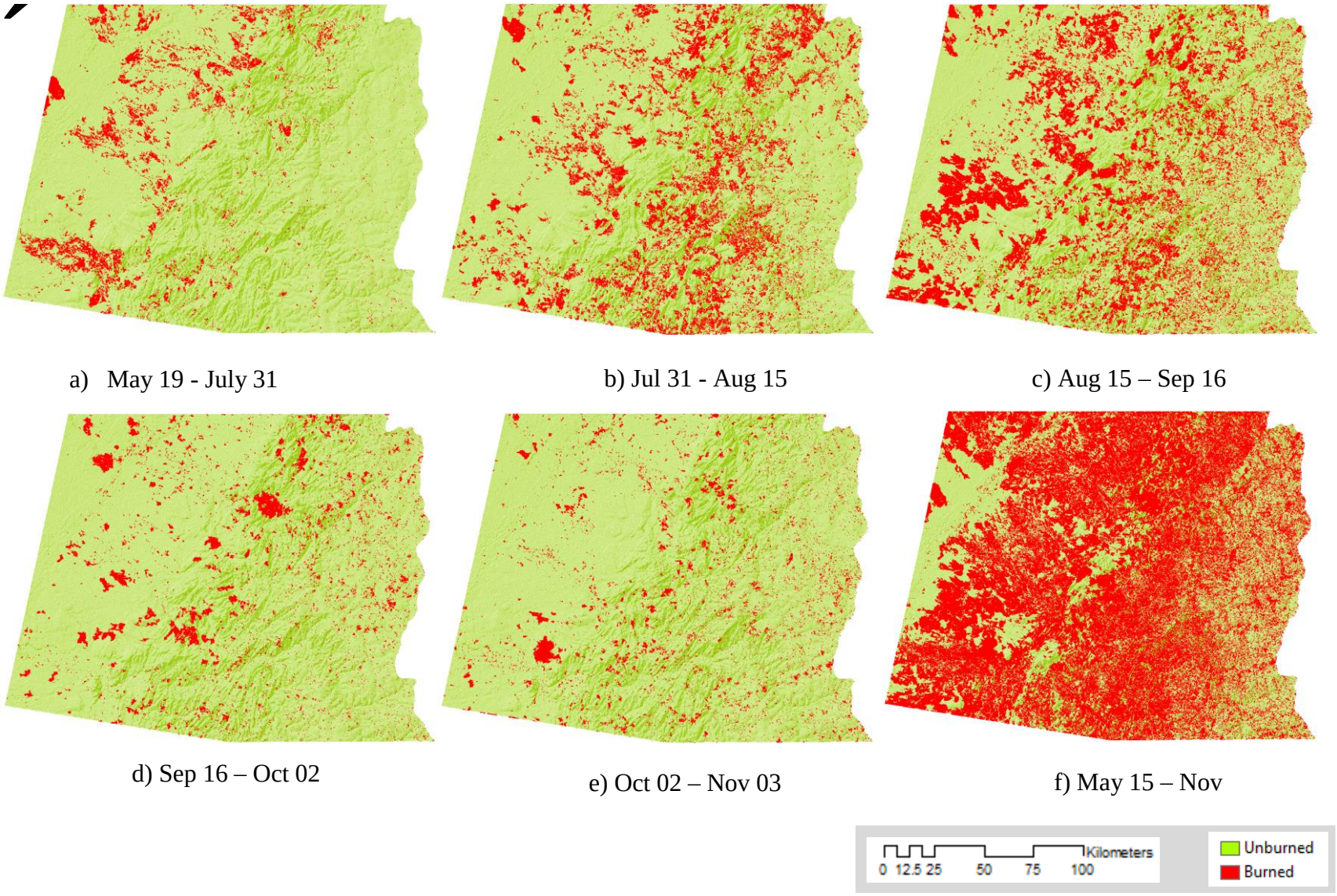

Figure 4.4: Progression of burned area during the 2009 fire season in eastern Zambia. The first five maps show incremental areas burned between two image dates while the last (in row 2, column 3) show the overall burned area during the fire season.

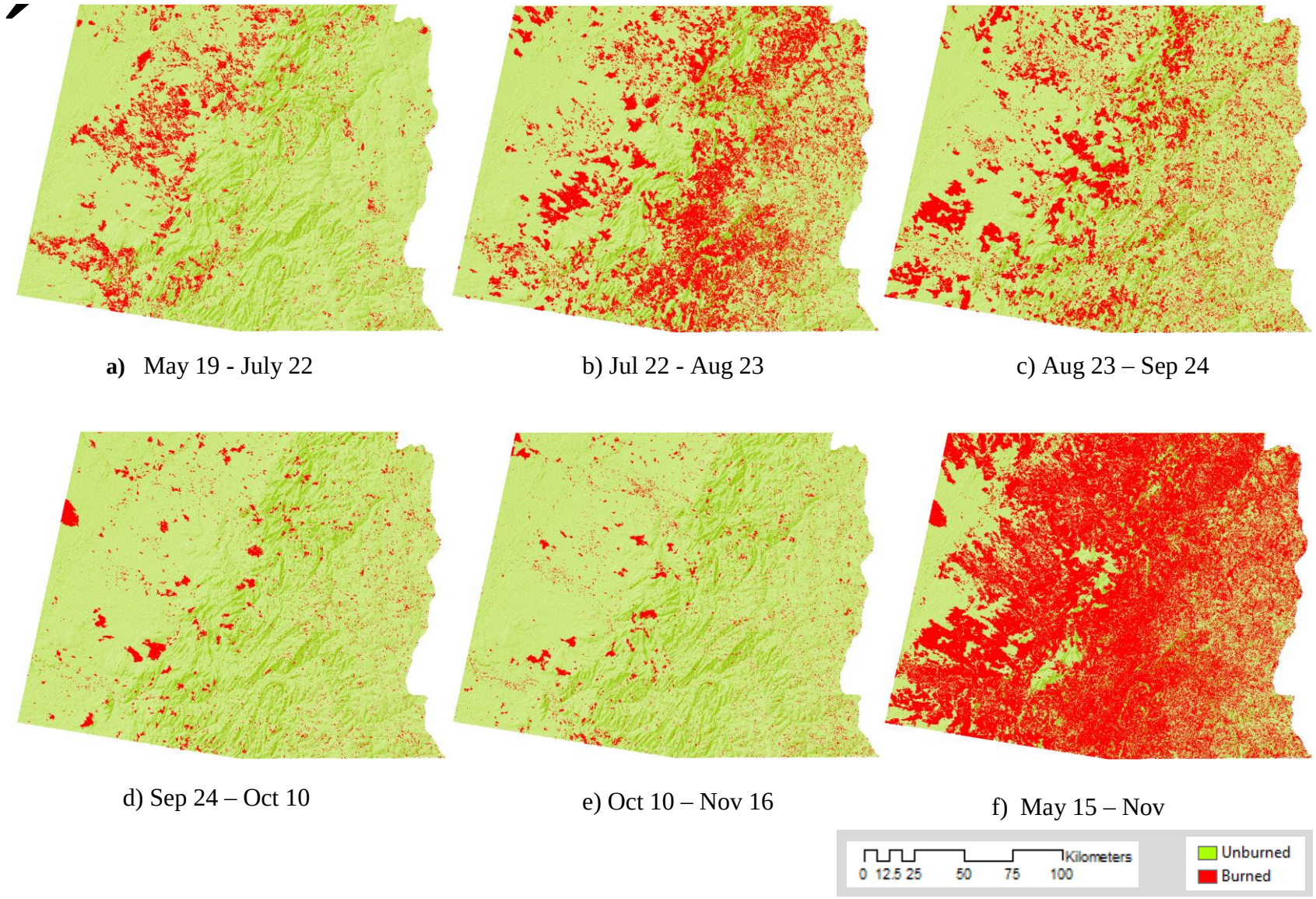

Figure 4.5: Progression of burned area during the 2012 fire season in eastern Zambia. The first five maps show incremental areas burned between two image dates while the last (in row 2, column 3) show the overall burned area during the fire season.

4.4.2 Comparison of Landsat burn extent with MODIS burned area product.

Table 4.4 shows the burn extent in each part of the fire season for the two datasets. Compared to the 60% burn extent between the two years, the MODIS data only showed 20% of the area had burned by the end of the season. The disparity between Landsat and MODIS is greater at the beginning and end of the fire season compared to mid-season. There was also a higher level of agreement on detections between the Landsat and MODIS data in the valley and transition regions. However, most of the burned areas on the plateau were undetected by the MODIS data. Burned area maps for the three parts of the season are shown in Figure 4.6.

Table 4.4: Comparison of Landsat with MODIS derived burned area for 2009 and 2012 fire seasons in eastern Zambia. Area figures are in square kilometers and percentages are based on the total area of 7677 square kilometers.

		2009		
Fire season	*Landsat burned area*	*Percent burned*	*MODIS burned area*	*Percent burned*
Early	529.5	6.9	106.5	1.4
Mid	3097.0	40.3	1232.1	16.0
Late	969.4	12.6	238.5	3.1
Total	**4596.0**	**59.9**	**1577.0**	**20.5**

		2012		
Fire season	*Landsat burned area*	*Percent burned*	*MODIS burned area*	*Percent burned*
Early	686.0	8.9	170.2	2.2
Mid	3304.7	43.0	1169.5	15.2
Late	658.4	8.6	152.5	2.0
Total	**4649.0**	**60.6**	**1492.1**	**19.4**

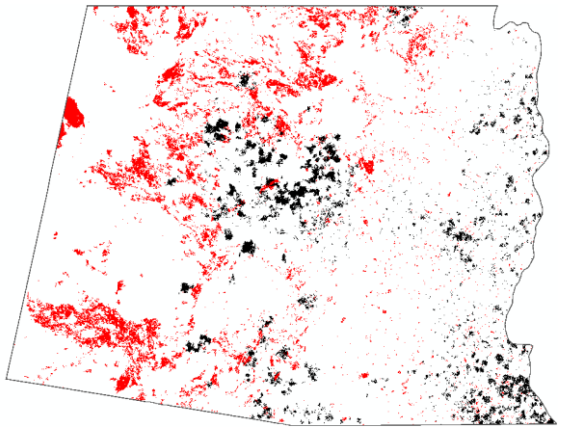

a) Early season - Landsat

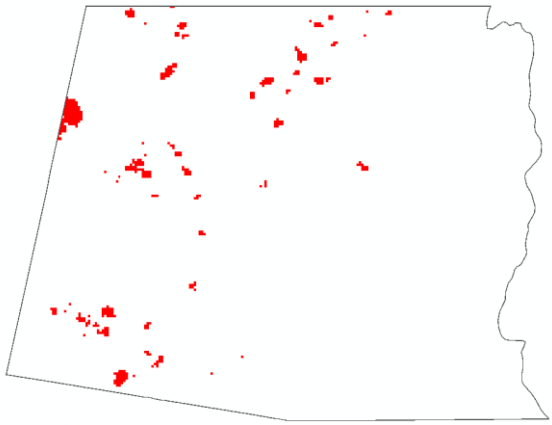

b) Early season - MODIS

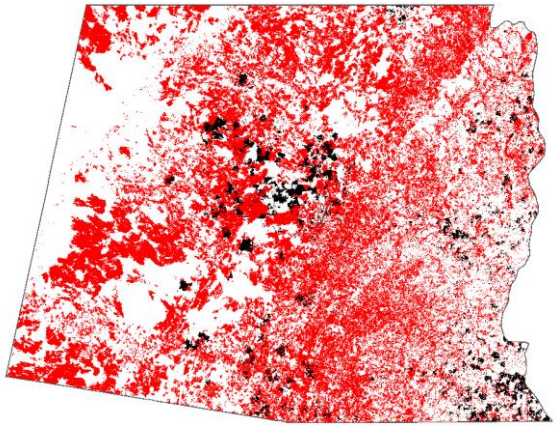

c) Mid-season - Landsat

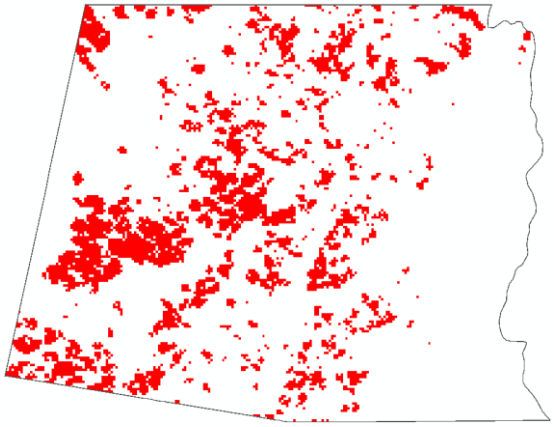

d) Mid-season - MODIS

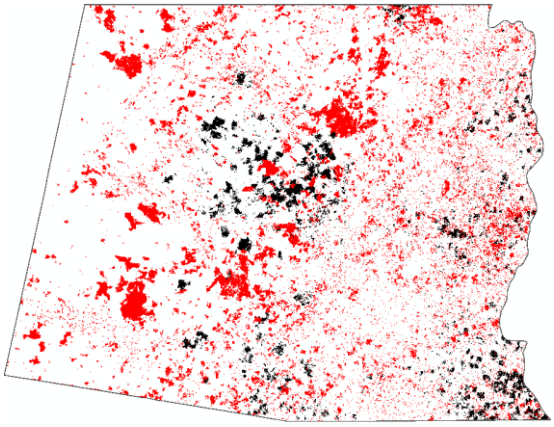

e) Late season - Landsat

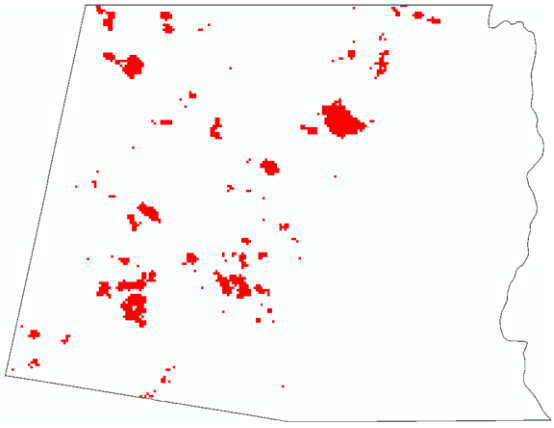

f) Late season - MODIS

Figure 4.6: (a-f) Burned area maps based on Landsat and MODIS data for 2009 fire season in eastern Zambia. Black areas in the Landsat maps represent areas masked because of clouds.

4.4.3 Spatial distribution of fires as a function of land cover, topography and settlement density

Spatial distribution of burned area by land cover

Figure 4.7 shows the distribution of burned area by land cover. The relative percent of burned area in each land cover type, shown as bar charts in the figure, was 64-67% for forestland, 56-58% for grassland and 42-53% for cropland. The analyses of means for proportions showed that fire occurrence in forest land was significantly higher while fire occurrence in cropland and grassland was significantly lower than average fire occurrence. Results for the two years were consistent (Table 4.5).

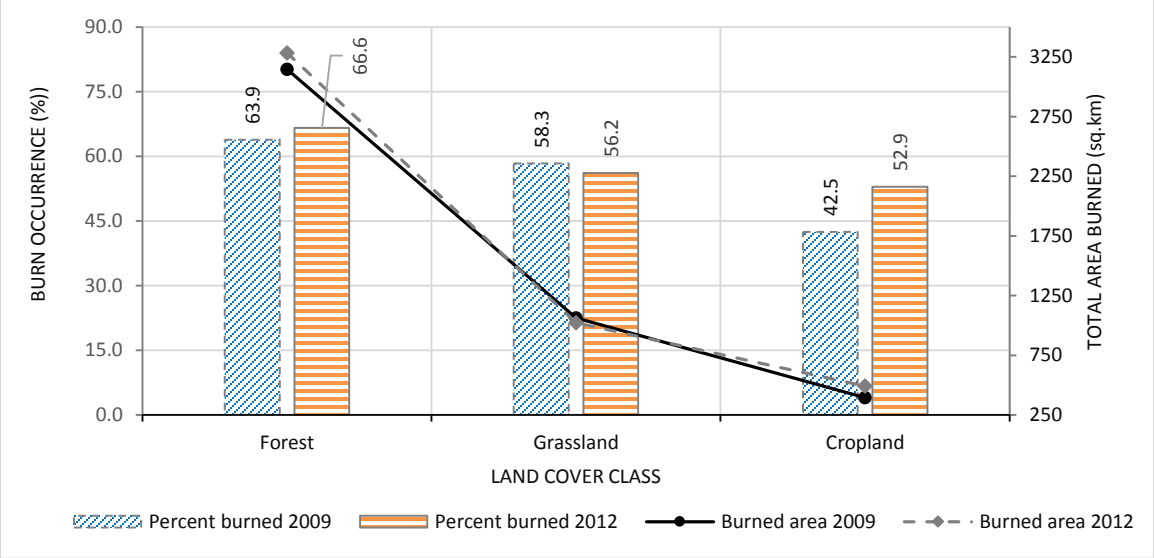

Figure 4.7: Fire occurrence by land cover category for 2009 and 2012 fire seasons in eastern Zambia. The total burned area in each land cover category is represented by the linear graphs

Table 4.5: Analysis of fire occurrence by land cover for the 2009 and 2012 fire seasons in eastern Zambia. Any individual group proportion not contained in the lower and upper limit interval is deemed significant - larger than the overall average of all group proportions if it lies above the upper decision line and smaller if it lies below the lower limit.

			2009		
Level	*Group N*	*Lower Limit*	*Group Proportion*	*Upper Limit*	*Limit Exceeded*
Cropland	1032282	0.598	0.422	0.600	Lower
Forest	5474734	0.598	0.638	0.599	Upper
Grassland	2023801	0.598	0.583	0.599	Lower
			2012		
Cropland	1032282	0.604	0.506	0.607	Lower
Forest	5474734	0.605	0.645	0.606	Upper
Grassland	2023801	0.605	0.550	0.606	Lower

Spatial distribution of burned area as a function of topography

Figure 4.8 shows the percent fire occurrence as a function of elevation. Elevations from 670 to 1060m showed significantly higher fire occurrences than elevations below 670 or above 1060m. A summary of the test is given in

Table 4.6. Elevation ranges with higher fire occurrence correspond with areas in the valley and hilly transition that have large extents of grassland and forest while the ones with lower fire occurrence lie the plateau and valley floor where fuels are scattered and continuous spread of fire is limited.

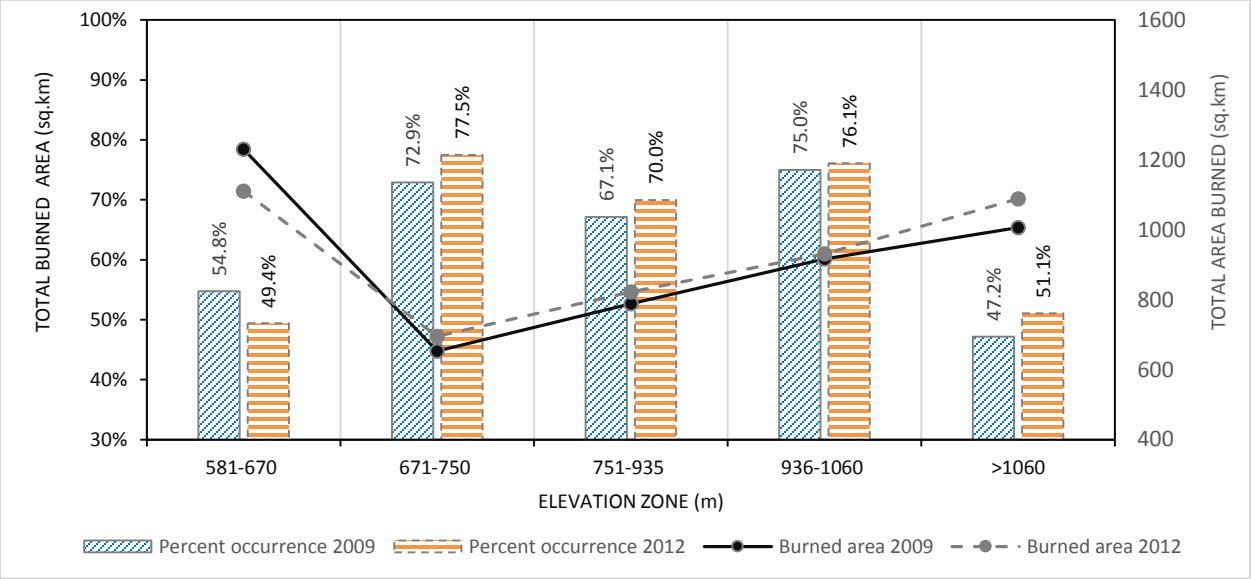

Figure 4.8: Fire occurrence by elevation category for 2009 and 2012 fire seasons in eastern Zambia. The total burned area in each elevation category is represented by the linear graphs. Note that the total available area in the 671-750 category was much lower than the other categories causing a dip in the linear plots.

Table 4.6: Analysis of fire occurrence by elevation for the 2009 and 2012 fire seasons in eastern Zambia. Any individual group proportion not contained in the lower and upper limit interval is deemed significant - larger than the overall average of all group proportions if it lies above the upper decision line and smaller if it lies below the lower limit.

2009					
Level	*Group N*	*Lower Limit*	*Group Proportion*	*Upper Limit*	*Limit Exceeded*
>1060	263293	0.597	0.472	0.601	Lower
581-670	277379	0.597	0.548	0.601	Lower
671-750	110681	0.595	0.729	0.602	Upper
751-935	144961	0.596	0.671	0.602	Upper
936-1060	150994	0.596	0.750	0.602	Upper
2012					
Level	*Group N*	*Lower Limit*	*Group Proportion*	*Upper Limit*	*Limit Exceeded*
>1060	263266	0.604	0.511	0.608	Lower
581-670	277556	0.604	0.494	0.608	Lower
671-750	110758	0.602	0.775	0.609	Upper
751-935	145070	0.602	0.700	0.608	Upper
936-1060	151066	0.603	0.761	0.608	Upper

Figure 4.9 shows the variation of burned areas as a function of slope. The fire occurrence was significantly lower than average in the 0-4% slope range while the other slope ranges have significantly higher fire occurrences than average. These gentle slopes are mainly located on the plateau where most of the human activity is concentrated and some parts of the valley near the Luangwa River with less vegetation.

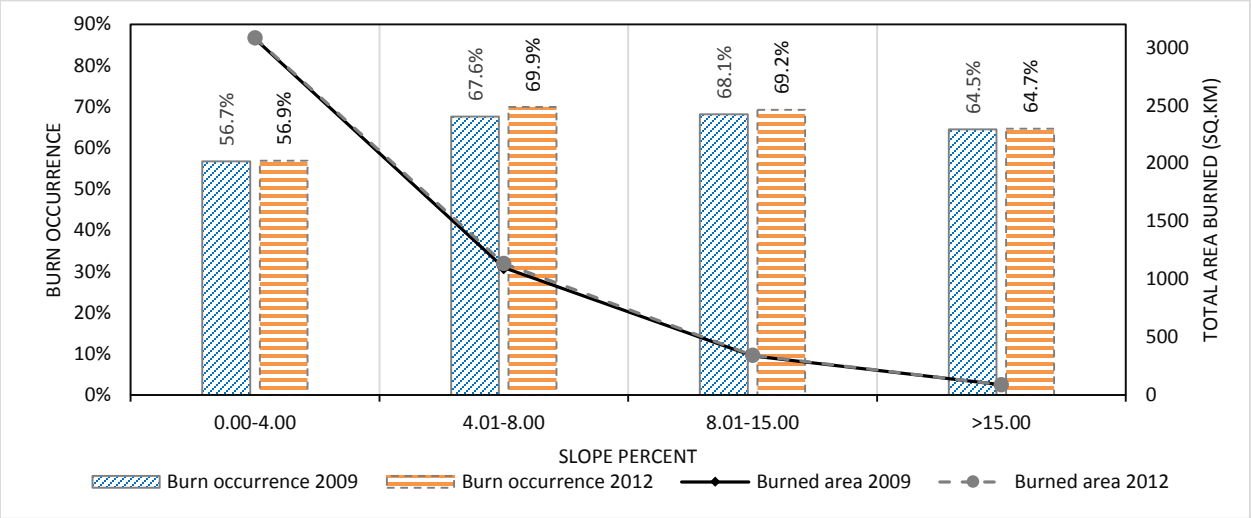

Figure 4.9: Fire occurrence by slope category for 2009 and 2012 fire seasons in eastern Zambia. The total burned area in each slope category is represented by the linear graphs.

Table 4.7: Analysis of fire occurrence by slope for the 2009 and 2012 fire seasons in eastern Zambia. Any individual group proportion not contained in the lower and upper limit interval is deemed significant - larger than the overall average of all group proportions if it lies above the upper decision line and smaller if it lies below the lower limit.

2009					
Level	*Group N*	*Lower Limit*	*Group Proportion*	*Upper Limit*	*Limit Exceeded*
0.00-4.00	669383	0.598	0.567	0.600	Lower
4.01-8.00	200541	0.597	0.676	0.601	Upper
8.01-15.00	60899	0.594	0.681	0.604	Upper
>15.00	16485	0.590	0.645	0.608	Upper
2012					
Level	*Group N*	*Lower Limit*	*Group Proportion*	*Upper Limit*	*Limit Exceeded*
0.00-4.00	669732	0.605	0.569	0.606	Lower
4.01-8.00	200616	0.603	0.699	0.608	Upper
8.01-15.00	60896	0.601	0.692	0.610	Upper
>15.00	16472	0.596	0.647	0.615	Upper

The analysis of fire activity against slope aspect showed that the distribution of fire is dominated by slopes facing North, West, Northwest and Southwest. Burned area in these directions accounted for over 60% of the total mapped burned area from both datasets.

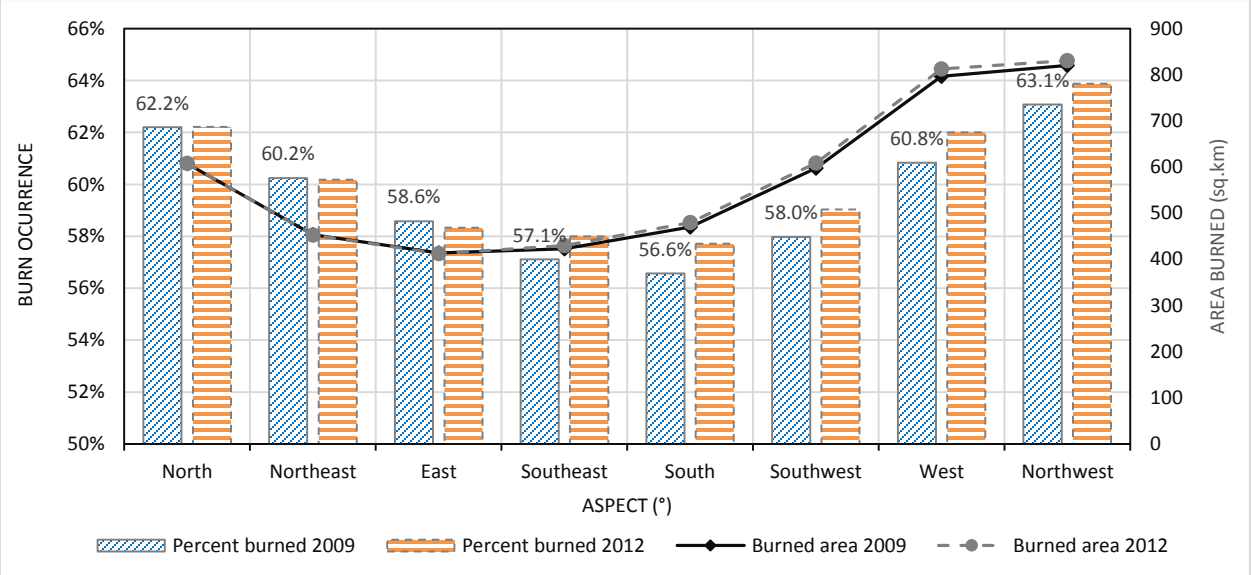

Figure 4.10: Fire occurrence by slope aspect category for 2009 and 2012 fire seasons in eastern Zambia. The total burned area in each slope aspect category is represented by the linear graphs.

Table 4.8: Analysis of fire occurrence by aspect for the 2009 and 2012 fire seasons in eastern Zambia. Any individual group proportion not contained in the lower and upper limit interval is deemed significant - larger than the overall average of all group proportions if it lies above the upper decision line and smaller if it lies below the lower limit.

2009					
Level	*Group N*	*Lower Limit*	*Group Proportion*	*Upper Limit*	*Limit Exceeded*
East	87189	0.595	0.586	0.603	Lower
North	120586	0.595	0.622	0.603	Upper
Northeast	92931	0.595	0.602	0.603	
Northwest	160532	0.596	0.631	0.602	Upper
South	102595	0.595	0.566	0.603	Lower
Southeast	91417	0.595	0.571	0.603	Lower
Southwest	127301	0.596	0.580	0.603	Lower
West	161688	0.596	0.608	0.602	Upper
2012					
Level	*Group N*	*Lower Limit*	*Group Proportion*	*Upper Limit*	*Limit Exceeded*
East	87301	0.602	0.583	0.610	Lower
North	120711	0.602	0.622	0.609	Upper
Northeast	92928	0.602	0.602	0.610	
Northwest	160583	0.603	0.640	0.609	Upper
South	102562	0.602	0.577	0.610	Lower
Southeast	91497	0.602	0.580	0.610	Lower
Southwest	127273	0.602	0.590	0.609	Lower
West	161787	0.603	0.620	0.609	Upper

Distribution of burned area as a function of settlement density

Figure 4.11 shows the variation of fire occurrence with settlement density. Areas with higher settlement densities (greater than 1) had relatively lower fire occurrence than those with lower settlement densities for both years. Of all settlement categories, only 0.01 – 1.00 had significantly higher fire occurrence than average. The other categories had significantly lower fire occurrence.

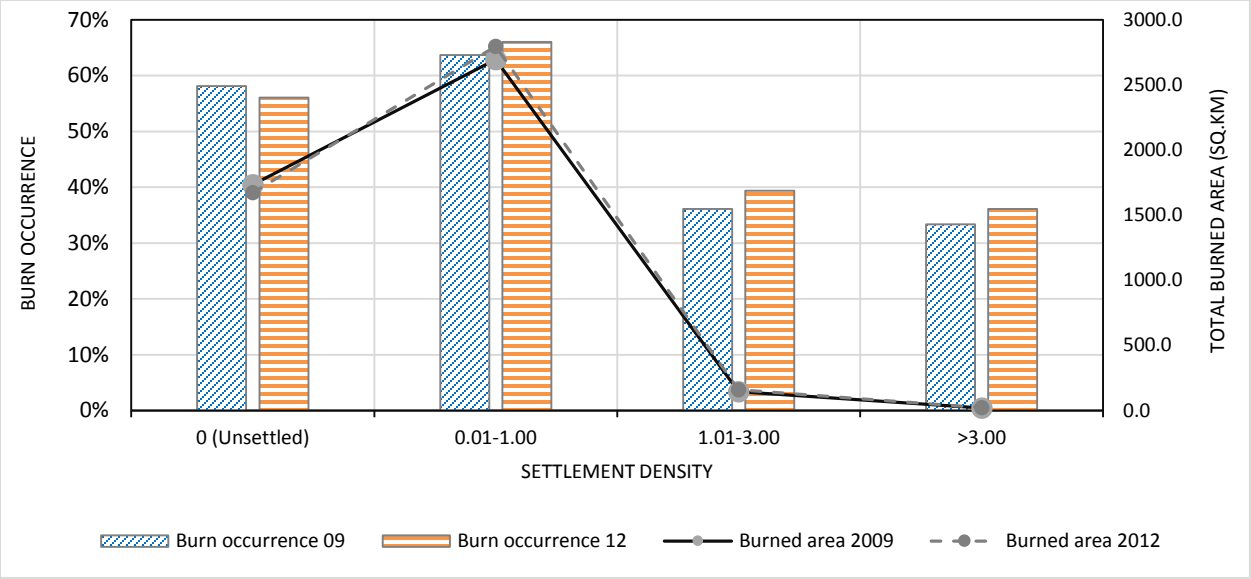

Figure 4.11: Fire occurrence by settlement density for 2009 and 2012 fire seasons in eastern Zambia. The total burned area in each settlement density category is represented by the linear graphs.

Table 4.9: Analysis of fire occurrence by settlement density for the 2009 and 2012 fire seasons in eastern Zambia. Any individual group proportion not contained in the lower and upper limit interval is deemed significant - larger than the overall average of all group proportions if it lies above the upper decision line and smaller if it lies below the lower limit.

2009					
Level	*Group N*	*Lower Limit*	*Group Proportion*	*Upper Limit*	*Limit Exceeded*
>3.00	64739	0.5939	0.3338	0.6033	Lower
0.01-1.00	4702070	0.5982	0.6370	0.5990	Upper
1.01-3.00	447041	0.5969	0.3614	0.6003	Lower
Unsettled	3316967	0.5981	0.5813	0.5991	Lower
2012					
Level	*Group N*	*Lower Limit*	*Group Proportion*	*Upper Limit*	*Limit Exceeded*
>3.00	64739	0.6009	0.3609	0.6102	Lower
0.01-1.00	4702070	0.6052	0.6606	0.6059	Upper
1.01-3.00	447041	0.6038	0.3938	0.6073	Lower
Unsettled	3316967	0.6050	0.5608	0.6060	Lower

4.4.4 Burn patch size distribution

General distribution of burn patch size

A total of 46546 and 55916 individual burn patches were extracted from the 2009 and 2012 burn maps respectively. Mean patch size significantly differed between the two years (Kruskal-Wallis[5] test, $\chi^2 = 38.4$, df =1, $p < 0.001$). Table 4.10 summarizes the descriptive statistics of individual burn patches. The minimum individual burned area size was 0.4 ha and the maximum, which occurred in 2009, is 20530.8 ha. The mean burned area size for the two years is 9.1 ha with a large average standard deviation of 116.7 ha, indicative of high variability in burned patch sizes. The median size was much lower than the mean in both cases indicating a very skewed distribution of burn patch size dominated by smaller burn patches.

Table 4.10: Descriptive statistics of burn patch size by year in eastern Zambia. All areas are expressed in hectares

	Overall statistics		**Individual burn statistics**				
Year	*Burn patch count*	*Total burned area*	*Minimum*	*Median*	*Mean*	*Maximum*	*Standard deviation*
2009	46546	459600.0	0.4	1.3	9.9	20530.8	130.9
2012	55916	464900.0	0.4	1.2	8.3	13727.3	102.4
Mean	**51231**	**462200.5**	**0.4**	**1.22**	**9.1**	**17129.1**	**116.7**

Figure 4.12 shows the burned area size distribution for the two years categorized in a number of patch size ranges. The dominance of burn patches up to 5 ha is quite evident – these relatively small burn patches represented on average 83.5% of the total number of burn patches. However, patches greater than 50 ha contributed more - 60 percent - to the total burned area in the two fire seasons despite their lower frequencies. The contribution of each patch category is given in Figure 4.13.

[5] The Kruskal-Wallis is the same as the Wilcoxon test when the variable being tested only has two levels- in this case 'year' has two levels 2009 and 2012.

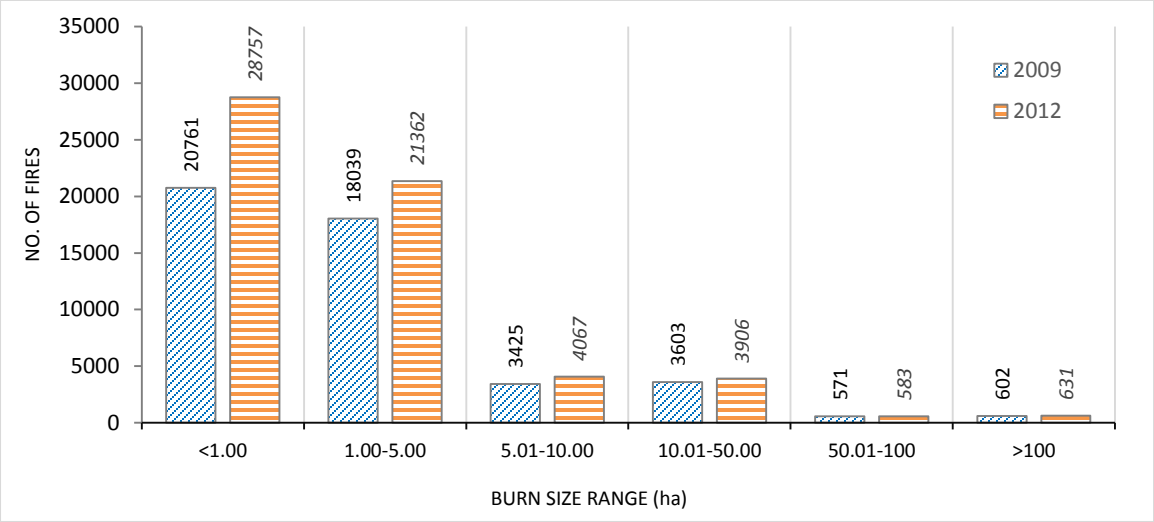

Figure 4.12: Burned area size distribution for the 2009 and 2012 fire seasons in eastern Zambia. For the two years, fires with sizes up to 5 ha were more frequent (over 80 percent) than those larger than 50 ha.

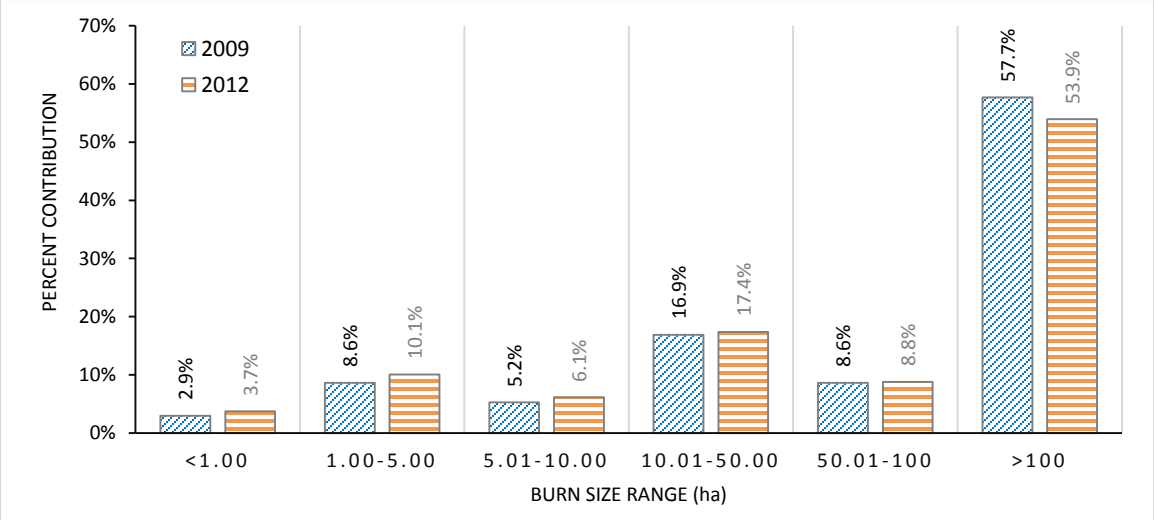

Figure 4.13: Contribution to total burned area by burn patch size for the 2009 and 2012 fire seasons in eastern Zambia. A larger proportion of the total burned area is contributed by fire with sizes larger than 50 ha despite their lower frequencies as shown in Figure 4.12

Distribution of burn patch size by land cover

The variation of burn patch size for the three land covers is shown in Figure 4.14. In forest and grassland the largest contribution comes from patches with sizes greater than 100 ha while patches 1 – 5 ha contributed more to total burned area in the cropland class. Patches less than a hectare are more prevalent in cropland than in the other two classes. In general, cropland patches showed decreasing proportional representation with increasing patch size compared to forestland and

grassland which showed increasing trends. The last two classes (50.01 – 100 and >100) are virtually absent in the cropland class indicating that the large fires occur in forest and grassland areas.

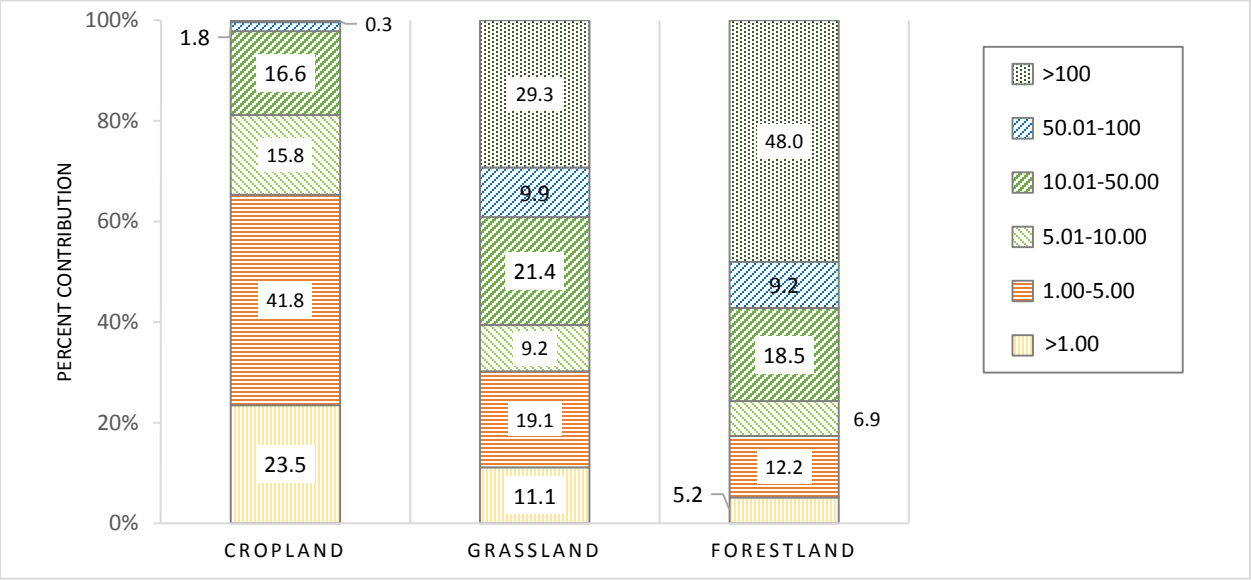

Figure 4.14: Overall burn patch size variation with land cover in eastern Zambia

The significant differences in burn patch sizes among the land covers was confirmed by the Kruskal-Wallis test (Kruskal-Wallis test, χ^2 = 3720.9, df =2, p-value < 0.0001) but the difference in burn patch sizes between the two years was found to be insignificant (Kruskal-Wallis6 test, χ^2 = 0.7600, df =1, p-value = 0.3833). Pair-wise comparisons using the Steel-Dwass test (Table 4.11) revealed that forest land burn patch sizes (5.96 ± 57.91 ha) are significantly larger than cropland (1.56 ± 3.00 ha) and grassland (3.20 ± 27.36 ha). In addition, grassland burn patches are significantly larger than cropland burn patches. Variability in burn patch size is greater in forestland and grassland as shown by their respective high standard deviations.

[6] The Kruskal-Wallis is the same as the Wilcoxon test when the variable being tested only has two levels- in this case 'year' has two levels 2009 and 2012.

Table 4.11: Non-parametric pairwise comparison of burn patch size by land cover using Steel-Dwass test. (A positive score mean difference between levels indicates that the second level (-Level) is smaller than the first (Level) and vice versa. Small p-values (<0.0001) in each case indicate significant pairwise differences in mean burn patch size.)

Level	*- Level*	*Score Mean Difference*	*Standard Error Difference*	*Z score*	*p-Value*
Forestland	Cropland	520.65	28.48	18.28	<.0001
Grassland	Cropland	221.44	18.98	11.67	<.0001
Grassland	Forestland	-273.51	25.99	-10.52	<.0001

Variation of burn patch size by physiographic region

Figure 4.15 shows the proportional representation of burn patch sizes in each region. The plateau showed a decreasing proportional representation with increasing size while increasing trends were observed for the other two regions. This implies that larger fires are rare on the plateau than in the valley or the hilly transition zone.

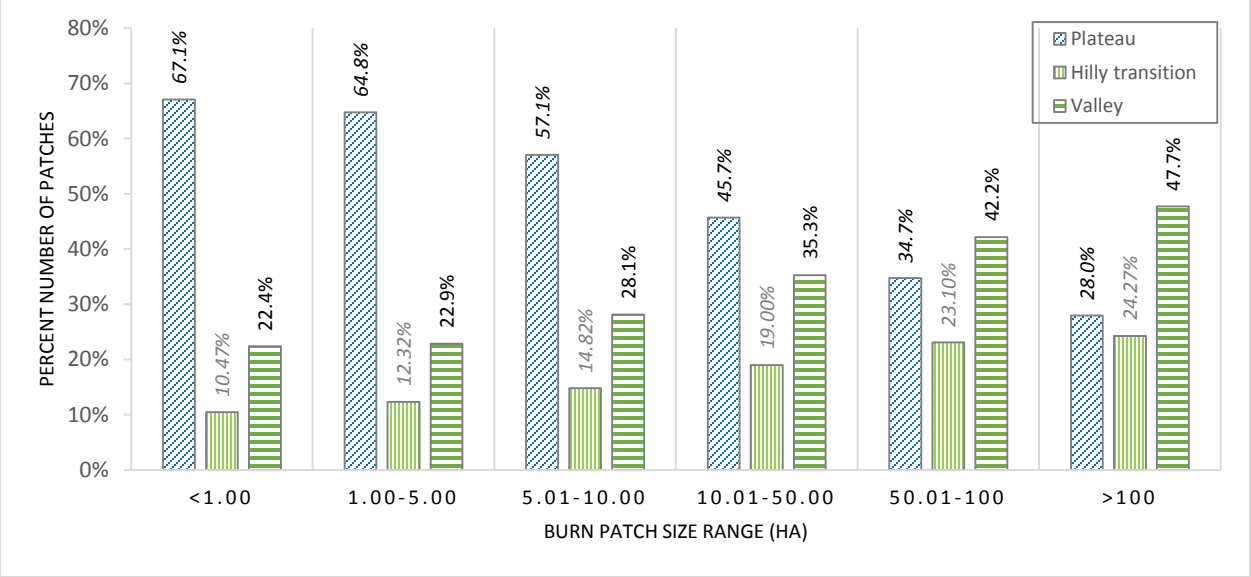

Figure 4.15: Distribution of burn patch size by physiographic region

Table 4.12 shows the descriptive statistics for burn patch size for the two years. Statistical testing showed that the mean burn patches sizes were significantly different by year (χ^2 = 39.17, df = 1, p-value < 0.0001) and by physiographic region (Kruskal-Wallis test, χ^2 = 456.18, df =2, p-value < 0.0001 for 2009 and χ^2 = 634.55, df =2, p-value < 0.0001 for 2012) with the Hilly transition having the largest mean burn patch sizes, followed by the valley and then plateau for 2009. Results for 2012 were similar, and details of the pairwise comparison are given in Table 4.13. As with the

results in the previous section there is high variability in the size of burn patches as shown by the high standard deviations.

Table 4.12: Burn patch statistics by physiographic region for the 2009 and 2012 fire seasons in eastern Zambia

	2009			**2012**		
Level	*Number*	*Mean*	*Std Dev*	*Number*	*Mean*	*Std Dev*
Hilly transition	6523	14.7284	88.955	6296	15.6766	107.396
Plateau	29200	5.8756	57.238	36955	4.6646	48.272
Valley	11724	14.0825	105.056	13565	13.5672	117.788

Table 4.13: Pairwise comparison of mean burn patch size in the three physiographic regions. (A positive score mean difference between levels indicates that the second level (-Level) is smaller than the first (Level) and vice versa. Small p-values (<0.0001) in each case indicate significant pairwise differences in mean burn patch size.)

2009					
Level	*- Level*	*Score Mean Difference*	*Standard Error Difference*	*Z*	*p-Value*
Valley	Plateau	2531.6	149.6	16.92	<.0001
Valley	Hilly transition	-570.1	211.3	-2.70	0.0209
Plateau	Hilly transition	-3101.8	187.4	-16.55	<.0001
2012					
Level	*- Level*	*Score Mean Difference*	*Standard Error Difference*	*Z*	*p-Value*
Valley	Plateau	3188.0	164.4	19.38	<.0001
Valley	Hilly transition	-1190.1	249.8	-4.76	<.0001
Plateau	Hilly transition	-4378.2	223.4	-19.60	<.0001

4.5 DISCUSSION

Understanding how landscape patterns influence fire processes and vice versa is vital for both fire and vegetation management (Rollins et al., 2002). This study assessed patterns of seasonal fire with respect to landscape characteristics in eastern Zambia using seasonal burned area information derived from multitemporal Landsat data. The relative fire activity for different levels of landscape factors was assessed by determining fractions of burned area in each level.

Seasonal burn mapping showed that fire is widespread in the region with 60% of the area burning by the end of the dry season. This would not come as a surprise to researchers that are familiar with fire regimes in southern African countries, especially Zambia. Fire activity has been reported

to be widespread in many regions of Zambia. Archibald et al (2010), using MODIS burned area product, estimated over 50% of the area burned in many parts of Zambia every year. Another study estimated between 40 – 85% in the western part of the country (Pricope and Binford, 2012). Considering the under-estimation as shown by the comparison between Landsat and MODIS derived burned area data, these estimates could be considered conservative. The high fire occurrence may be a reflection of ineffective or non-existent fire management policies in Zambia. Research by Pricope and Binford (2012) indicated that countries with better organized fire management programs such as Botswana and Zimbabwe showed lower fire incidences.

Seasonal fire activity is characterized by peak activity around August and September with lower fire activity earlier in June and July and late in October to November. These results conform to reports from other studies (Archibald et al., 2010; Roy et al., 2005). The peak fire activity generally coincides with the availability of dead and dry leaf matter along with hot, dry and windy weather that encourage extensive burning of the landscape. Spatially, the valley floor had a higher percentage of the early fires in the two seasons analyzed, but as the fire season progressed the distribution of fire events across all regions (valley, plateau, and hills) was similar. This spatial trend in likely reflective of different crops and agricultural practices in the valley and plateau which influence the timing of burning and clearing fields. Maize is predominately grown on the plateau and is usually harvested from May to June, while the millet and sorghum crops grown in the valley are harvested from March to May (FAO, 2014).

Fire occurrence was found to be higher in forestland and grassland, in elevation between 671 and 1060 m, in areas with slopes greater than 4% and settlement densities from up to 1 per square km. These patterns in fire occurrence highlight the roles played by human activity, fuel availability and landscape fragmentation. Areas with higher human activity as reflected by the high settlement density tended to have lower fire occurrences. Considering that fire activity in eastern Zambia is mainly anthropogenic, this finding might seem counter intuitive. However, research shows that higher settlement density entails higher landscape fragmentation due to increased agriculture and infrastructure such as roads (Archibald et al., 2009). This limits the extent of land for burning and areas around settlements and roads act as fire breaks either physically or through suppression by people (DeWilde and Chapin III, 2006). The location of the forest and grassland also coincides with less settled areas (valley and hilly transition) compared to cropland which is mostly located near highly settled areas on the plateau. The variation of fire occurrence with elevation and slope

showed similar correspondence. Despite the differences among the land cover types, the proportion of area in each land cover category that burns is quite high, underscoring the widespread extent of fire activity in the area.

The distribution of burn patch size is dominated by small fires up to 5 ha. However, large fires contribute more to the total burned area. Large fires comprised less than 5% of the total number of areas (pixel groups) burned in the two fire seasons but accounted for more than 60% of the total burned area. This has been observed in many fire regimes (Lafon and Grissino-Mayer, 2007). Burn patches in cropland were significantly smaller than in forest and grassland. The size of crop fields places a limitation of how large fires in this land cover class can spread (McCarty et al., 2009). The average agricultural holding in eastern Zambia is about 3 ha but holdings less that a hectare are quite common (Sitko et al., 2011). On the other hand, the large expanse of forest and grassland enables uninhibited burning in these cover types resulting in higher mean burn patch size. Analysis of burn patch sizes by physiographic region also reflects the difficulty placed on fire spread by landscape fragmentation. Small fires less than 5 ha are more frequent on the plateau than in the other regions. This has been observed in other studies which found that areas of higher human activity and landscape fragmentation had relatively smaller burn patches (Sá et al., 2007).

The burn patch size distribution observed in this study has implications for remote sensing data to use in mapping fire in Zambia. While large burn patches may be reliably mapped with coarse resolution data such as Moderate Resolution Imaging Spectro-radiometer (MODIS) most of the smaller fires are missed. Missing these small fires can have a large impact on burned area estimation and on derived information such as biomass emission estimates. Randerson et.al (2012) accounted for the influence of small fires by combining 1-km thermal anomalies (active fires) with 500 m MODIS burned area observations. Small fires significantly increased the total burned area by as much as 157% in some continental-scale regions and by as much as 35% globally. This increase in burned area substantially increased the estimated biomass emissions by as much as 35%. The new multitemporal Landsat data in this study enabled the quantification of these small fire providing a more detailed view of fire activity in eastern Zambia.

4.6 CONCLUSION

With the benefit of analysis at a higher spatial resolution, this study showed the fine-scale incidence of burning in eastern Zambia where about 60% of the area burned by end of the fire season in November. The burning pattern is characterized by a distinct spatial trend in which the valley region burns earlier than the plateau and transition regions. The burning is also characterized by small and dispersed fires earlier in the season and larger more homogenous fires occurring in the mid of the season. The study also showed the inadequacy of coarse spatial resolution MODIS data in characterizing the fine-scale fire activity and adds to earlier studies that have documented this limitation (Laris, 2005; Sá et al., 2007; Silva et al., 2005). Most of the fire activity, for example on the plateau region, was missed by the MODIS burned area product because of its coarse spatial resolution which is inadequate to map small fires associated with the higher level of fragmentation. Thus, to gain a better understanding of fire activity in such landscapes, it is of critical importance that higher resolution data such as Landsat data are used.

This study relates fires, spatially and temporally, with landscape factors that modify fire behavior. The imagery analysis can now confirm how human activity and landscape structure interact to influence the spatial and temporal patterns of fire in eastern Zambia. The high fire occurrence observed in forest and grassland, in elevation between 671 and 1060 m, in areas with slopes greater than 4%, and in low settlement areas provide immediate insight on where fire management efforts must be directed. Higher human activity on the plateau has caused fragmentation of the landscape which provides some control on fire activity and might be considered a lower priority area.

Lastly, this study demonstrated how available free earth observation data can be leveraged to address resource management issues such as fire disturbance in developing countries. Given the difficulties faced by developing countries in allocating budgets for resource management, the use of earth observation data presents a cost effective and efficient way of deriving relevant information about natural resources and the environment. This application provides a baseline for comparison with future studies in other areas of Zambia. Such studies are needed to provide resource managers with detailed and more specific information on sizes, patterns and timing of fires and the land covers impacted to plan fire management activities. The analysis was made possible by new tools developed to capitalize on the growing multitemporal Landsat data: 1) The multitemporal analysis with automatic training sample selection that makes the analysis data-

driven and simple to implement, and produced greater than 92% accuracy in classification (Malambo and Heatwole, 2015a). Such automatic tools help reduce cost of training tasks that may require substantial human effort and support operational generation of relevant information, 2) The gap-filling tool that preserves change information, thus opens the archive of Landsat 7 imagery to meaningful multitemporal analysis (Malambo and Heatwole, 2015b). Land cover is in constant flux in many developing countries such as Zambia (Hansen et al., 2013) and spatially and temporally consistent data afforded by such tools can contribute to the assessment of various disturbances including deforestation, drought and fire.

4.7 REFERENCES

Archibald, S., Roy, D.P., van Wilgen, B.W., Scholes, R.J., 2009. What limits fire? An examination of drivers of burnt area in Southern Africa. Global Change Biology 15, 613-630.

Archibald, S., Scholes, R.J., Roy, D.P., Roberts, G., Boschetti, L., 2010. Southern African fire regimes as revealed by remote sensing. International Journal of Wildland Fire 19, 861-878.

Astle, W.L., Webster, R., Lawrance, C.J., 1969. Land Classification for Management Planning in the Luangwa Valley of Zambia. J Appl Ecol 6, 143-169.

Baars, R., 1999. The effect of rangeland fires on cattle tick infestation in western Zambia. Tropical Animal health and production 31, 275-278.

Barbosa, P.M., Gregoire, J.M., Pereira, J.M.C., 1997. Detection of burned areas in Africa using a multitemporal multithreshold analysis of NOAA-AVHRR-GAC data. Earth Surface Remote Sensing 3222, 67-75.

Breiman, L., 2001. Random forests. Machine Learning 45, 5-32.

Celis, R., Milimo, J.T., Wanmali, S., 1991. Adopting improved farm technology: A study of smallholder farmers in Eastern Province, Zambia. International Food Policy Research Institute, Washington, DC.

Cochrane, M., Ryan, K., 2009. Fire and fire ecology: Concepts and principles, Tropical Fire Ecology. Springer Berlin Heidelberg, pp. 25-62.

Cochrane, M.A., 2009. Tropical fire ecology : climate change, land use, and ecosystem dynamics. Springer ; Published in association with Praxis Pub., Berlin; New York; Chichester, UK.

DeBano, L.F., Neary, D.G., Folliott, P.F., 1998. Fire's effects on ecosystems. J. Wiley, New York.

DeWilde, L.o., Chapin III, F.S., 2006. Human impacts on the fire regime of interior Alaska: interactions among fuels, ignition sources, and fire suppression. Ecosystems 9, 1342-1353.

ECZ, 2001. State of Environment in Zambia 2000. ECZ, Lusaka, Zambia.

FAO, 2014. Crop Calendar, Retrieved 9/15, 2014, from http://www.fao.org/agriculture/seed/cropcalendar/welcome.do.

Flasse, S.P., Trigg, S.N., Ceccato, P.N., Perryman, A.H., Hudak, A.T., Thompson, M.W., Brockett, B.H., Dramé, M., Ntabeni, T., Frost, P.E., Landmann, T., Roux, J.L.l., 2004. Remote sensing of vegetation fires and Its contribution to a fire management Information system. Global Fire Management Center, Freiburg, Germany.

French, N.H.F., Kasischke, E.S., Hall, R.J., Murphy, K.A., Verbyla, D.L., Hoy, E.E., Allen, J.L., 2008. Using Landsat data to assess fire and burn severity in the North American boreal forest region: An overview and summary of results. International Journal of Wildland Fire 17, 443-462.

Frost, P.G.H., 1999. Community-based Management of Fire: Lessons from the Western Province of Zambia, FAO Meeting on Public Policies Affecting Forest Fires. Food & Agriculure Organization, Rome, pp. 341-352.

Giglio, L., Randerson, J.T., van der Werf, G.R., Kasibhatla, P.S., Collatz, G.J., Morton, D.C., DeFries, R.S., 2010. Assessing variability and long-term trends in burned area by merging multiple satellite fire products. Biogeosciences 7, 1171-1186.

Goldammer, J.G., De Ronde, C., 2004. Wildland Fire Management Handbook for Sub-Sahara Africa. Global Fire Management Center, Freiburg, Germany.

Gregoire, J.M., Tansey, K., Silva, J.M.N., 2003. The GBA2000 initiative: developing a global burnt area database from SPOT-VEGETATION imagery. International Journal of Remote Sensing 24, 1369-1376.

Hansen, M.C., Potapov, P.V., Moore, R., Hancher, M., Turubanova, S.A., Tyukavina, A., Thau, D., Stehman, S.V., Goetz, S.J., Loveland, T.R., Kommareddy, A., Egorov, A., Chini, L., Justice, C.O., Townshend, J.R.G., 2013. High-Resolution Global Maps of 21st-Century Forest Cover Change. Science 342, 850-853.

Her, Y., Heatwole, C., 2008. Spatial Patterns and Temporal Trends of Lauangwa Valley Fires, OGIS Symposium. OGIS, Virginia Tech, Blacksburg VA.

Innes, J.L., Beniston, M., Verstraete, M.M., 2000. Biomass burning and its inter-relationships with the climate system. Kluwer Academic Publishers, Dordrecht; Boston.

Jones, J.W., Starbuck, M.J., Jenkerson, C.B., 2013. Landsat surface reflectance quality assurance extraction (version 1.7): U.S. Geological Survey Techniques and Methods US Geological Survey, Reston, Virginia.

Kasischke, E.S., Williams, D., Barry, D., 2002. Analysis of the patterns of large fires in the boreal forest region of Alaska. International Journal of Wildland Fire 11, 131-144.

Korontzi, S., Justice, C.O., Scholes, R.J., 2003. Influence of timing and spatial extent of savanna fires in southern Africa on atmospheric emissions. J Arid Environ 54, 395-404.

Lafon, C.W., Grissino-Mayer, H.D., 2007. Spatial patterns of fire occurrence in the central Appalachian Mountains and implications for wildland fire management. Phys Geogr 28, 1-20.

Laris, P.S., 2005. Spatiotemporal problems with detecting and mapping mosaic fire regimes with coarse-resolution satellite data in savanna environments. Remote Sensing of Environment 99, 412-424.

Lawton, R.M., 1978. A Study of the Dynamic Ecology of Zambian Vegetation. J Ecol 66, 175-198.

Lentile, L.B., Holden, Z.A., Smith, A.M.S., Falkowski, M.J., Hudak, A.T., Morgan, P., Lewis, A.S., Gessler, P.E., Benson, N.C., 2006. Remote sensing techniques to assess active fire characteristics and post-fire effects. International Journal of Wildland Fire 15, 319.

Malambo, L., Heatwole, C., D, 2015a. Mapping seasonal fire progression: Automatic training signature selection for multitemporal mapping. Virginia Polytechnic & State University, Blacksburg, VA. Unpublished

Malambo, L., Heatwole, C., D, 2015b. Profile based Missing Value Estimation for Abrupt Change Processes. Virginia Polytechnic & State University, Blacksburg, VA. Unpublished

Masek, J.G., Vermote, E.F., Saleous, N.E., Wolfe, R., Hall, F.G., Huemmrich, K.F., Gao, F., Kutler, J., Lim, T.K., 2006. A Landsat surface reflectance dataset for North America, 1990-2000. IEEE Geoscience and Remote Sensing Letters 3, 68-72.

McCarty, J.L., Korontzi, S., Justice, C.O., Loboda, T., 2009. The spatial and temporal distribution of crop residue burning in the contiguous United States. Sci Total Environ 407, 5701-5712.

McNemar, Q., 1947. Note on the sampling error of the difference between correlated proportions or percentages. Psychometrika 12, 153-157.

Mermoz, M., Kitzberger, T., Veblen, T.T., 2005. Landscape influences on occurrence and spread of wildfires in Patagonian forests and shrublands. Ecology 86, 2705-2715.

Miller, J.D., Thode, A.E., 2007. Quantifying burn severity in a heterogeneous landscape with a relative version of the delta Normalized Burn Ratio (dNBR). Remote Sensing of Environment 109, 66-80.

Nelson, P.R.W.P.C.K.A.F., 2005. The analysis of means : a graphical method for comparing means, rates and proportions. Society for Industrial and Applied Mathematics, Philadelphia, Pa.

Oduor, P., 2013. US EPA activities supporting national GHG inventory mapping in six ESA countries, Retrieved 11/13, 2013, from http://www.cess.tsinghua.edu.cn/publish/essen/7774/20130716143808193384006/LULC%20presenation_%20UNEP.pdf.

Pereira, J.M.C., 2003. Remote sensing of burned areas in tropical savannas. International Journal of Wildland Fire 12, 259-270.

Pricope, N.G., Binford, M.W., 2012. A spatio-temporal analysis of fire recurrence and extent for semi-arid savanna ecosystems in southern Africa using moderate-resolution satellite imagery. Journal of Environmental Management 100, 72-85.

Pyne, S.J., Andrews, P.L., Laven, R.D., 1996. Introduction to wildland fire. Wiley, New York.

Randerson, J.T., Chen, Y., van der Werf, G.R., Rogers, B.M., Morton, D.C., 2012. Global burned area and biomass burning emissions from small fires. J Geophys Res-Biogeo 117.

Rice, J., 2006. Mathematical statistics and data analysis. Cengage Learning.

Rollins, M., Morgan, P., Swetnam, T., 2002. Landscape-scale controls over 20th century fire occurrence in two large Rocky Mountain (USA) wilderness areas. Landscape Ecol 17, 539-557.

Roy, D.P., Boschetti, L., Justice, C., 2006. Global mapping of fire-affected areas using multitemporal MODIS data: the MCD45 product. 2006 Ieee International Geoscience and Remote Sensing Symposium, Vols 1-8, 4165-4168.

Roy, D.P., Frost, P.G.H., Justice, C.O., Landmann, T., Le Roux, J.L., Gumbo, K., Makungwa, S., Dunham, K., Du Toit, R., Mhwandagara, K., Zacarias, A., Tacheba, B., Dube, O.P., Pereira, J.M.C., Mushove, P., Morisette, J.T., Vannan, S.K.S., Davies, D., 2005. The Southern Africa

Fire Network (SAFNet) regional burned-area product-validation protocol. International journal of remote sensing 26, 4265-4292.

Sá, A.C.L., Pereira, J.M.C., Gardner, R.H., 2007. Analysis of the relationship between spatial pattern and spectral detectability of areas burned in southern Africa using satellite data. International Journal of Remote Sensing 28, 3583-3601.

Shea, R.W., Shea, B.W., Kauffman, J.B., Ward, D.E., Haskins, C.I., Scholes, M.C., 1996. Fuel biomass and combustion factors associated with fires in savanna ecosystems of South Africa and Zambia. Journal of Geophysical Research: Atmospheres (1984–2012) 101, 23551-23568.

Silva, J.M.N., Sa, A.C.L., Pereira, J.M.C., 2005. Comparison of burned area estimates derived from SPOT-VEGETATION and Landsat ETM plus data in Africa: Influence of spatial pattern and vegetation type. Remote Sensing of Environment 96, 188-201.

Sitko, N., Chapoto, A., Kabwe, S., Tembo, S., Hichaambwa, M., Lubinda, R., Chiwawa, H., Mataa, M., Heck, S., Nthani, D., 2011. Technical Compendium: Descriptive Agricultural Statistics and Analysis for Zambia in Support of the USAID Mission's Feed the Future Strategic Review.

Smith, A.M.S., Drake, N.A., Wooster, M.J., Hudak, A.T., Holden, Z.A., Gibbons, C.J., 2007. Production of Landsat ETM plus reference imagery of burned areas within Southern African savannahs: comparison of methods and application to MODIS. International Journal of Remote Sensing 28, 2753-2775.

Turner, M.G., 2010. Disturbance and landscape dynamics in a changing world1. Ecology 91, 2833-2849.

USGS, 2014. Landsat Processing Details, Landsat Missions. Retrieved 10/31, 2014, from http://landsat.usgs.gov/Landsat_Processing_Details.php.

Vinya, R., Kasumu, E.C., Syampungani, S., Monde, C., Kasubika, R., 2011. Preliminary Study on the Drivers of Deforestation and Potential for REDD+ in Zambia., Lusaka, Zambia.

Zhang, X., Kondragunta, S., Quayle, B., 2011. Estimation of Biomass Burned Areas Using Multiple-Satellite-Observed Active Fires. IEEE Transactions on Geoscience and Remote sensing 49, 4469-4482.

Zhu, Z., Woodcock, C.E., 2012. Object-based cloud and cloud shadow detection in Landsat imagery. Remote Sensing of Environment 118, 83-94.

Chapter 5
Summary and Conclusions

Fire burns extensive areas of vegetated landscapes across Zambia each year, a problem recognized as a major disturbance to biodiversity in the country. However, little has been done to manage the frequent occurrence of fires and there are very few studies on the dynamics of landscape fires. A few regional studies (Archibald et al., 2010; Pricope and Binford, 2012) that included Zambia were carried out using coarse (500m ground sample distance) spatial resolution data. Access to multitemporal Landsat data has created the opportunity for mapping and monitoring fire disturbance at spatial resolutions adequate to capture the small and dispersed burn patches which characterize fire activity in Zambia. Research presented in the preceding chapters demonstrate the benefits and effectiveness of using multitemporal analysis for seasonal burn mapping, gap filling and in characterizing the spatial-temporal fire patterns in eastern Zambia.

The first objective of this research was to develop and evaluate a multitemporal method for seasonal burned area mapping. While most methods use one or two images to map burned areas (French et al., 2008; Roy et al., 2002), this study capitalized on the growing temporal depth of Landsat data to develop a method providing information on where and when an area was burned and at a spatial resolution appropriate for monitoring many important land surface dynamics (Giri et al., 2013; Kennedy et al., 2007). We used eight images per sequence (over the May-Nov fire season) and detected burned areas based on characteristic temporal profiles is a new approach for Landsat based burned area mapping. The method also has potential to support fire monitoring programs and development of burn area inventories at higher spatial resolutions especially in developing countries such as Zambia where such inventories are currently lacking. By providing a timeline of when an area was burned, derived fire disturbance information can more explicitly applied to address fire management objectives, ecosystem impacts and carbon emissions (Eva and Lambin, 1998; Korontzi et al., 2003). The abrupt effect of burning on land cover spectral properties is shared by other disturbances such as deforestation and drought. Thus there is potential to adapt the method to map these disturbances as well. Other adaptations could also include the use of burn spectral indices other than the MIRBI used here and thus be better suited for environments where such indices are more effective.

The rich depth of temporal information was also used in developing a method for estimating missing values in multitemporal MIRBI data (Chapter 3). Again, existing approaches have mostly used two images to fill gaps in Landsat data based on the assumption of insignificant changes between the two images. To address the possibility of significant change due to fire, we used eight multitemporal images in estimating missing values. This study found that both spatial and temporal information are essential for adequate estimation of missing data when abrupt phenomena such as fire are involved. The similarity in phenological responses for broad classes of land cover was further exploited in profile alignment which enhanced the prediction of the missing values. Despite high levels of missing data, reasonably accurate estimates were obtained for all missing values which we attribute to use of the longer sequence of images. While the application here was based on burn-specific spectral index data, in the development and evaluation of the method we considered the potential for broader applicability to indices used in other disturbance studies, such as drought and deforestation, which exhibit abrupt changes with similarities to those of fire.

Having developed methods for multitemporal burn mapping and the estimation of missing data in the first two objectives, the third objective sought to broaden our understanding of fire patterns in the study area by examining the correlation between derived seasonal burned areas with respect to land scape factors such as topography, land cover and settlement density. While a few regional studies (Archibald et al., 2010; Pricope and Binford, 2012) included Zambia in assessing fire patterns, these studies used coarse spatial resolution data which cannot capture the fine scale burn activity taking place in land cover such as cropland. The use of Landsat-based burn information enabled quantification of burn patterns with high spatial detail. Results suggest that human activity and landscape structure interact to influence the spatial and temporal patterns of fire. The human factor has implications for fire management as highlighted by other studies. The use of fire is highly entrenched with many cultural and livelihood practices, thus any fire management strategies should involve local people (Eriksen, 2007). Different fire occurrence patterns by land cover were observed with forest land showing higher incidences for fire and larger burn patch sizes. However, the fire occurrence in cropland, though lower, is not insignificant. The impact of burning in each land cover type on carbon emissions must be appreciated even for current REDD+ programs in Zambia (Kokwe and Mickels-Kokwe, 2012; Vinya et al., 2011). As observed by Barlow et al (2012), REDD+ programs tend to focus narrowly on avoiding deforestation but overlook the impact of fire which may have consequences on reaching long-term emission reduction goals.

This research has demonstrated the effectiveness of multitemporal analysis for both extracting burn information and for estimating missing data, and has also contributed to knowledge of spatial and temporal patterns of fire in eastern Zambia. One opportunity for further research is the evaluation of fused datasets, such as those derived using STARFM, to improve the temporal resolution of the image sequence. The use of fused datasets would improve the reliability of burn detection and gap-filling in cases where Landsat data are not adequate. Fusion techniques could also be applied to comparable data such as that from SPOT satellites to enhance spatial and temporal information for estimation of missing data and for spatial-temporal mapping change detection. Future missions such as the Sentinel 2 will also offer even better opportunities for creating spatially and temporal consistent Landsat datasets because of their wide range of spatial and temporal resolutions (Drusch et al., 2012). The other opportunity for further research concerns the evaluation of the imputation method developed here in estimating actual reflectance. Recovering actual reflectance data would support an even wider range of earth science applications.

5.1 REFERENCES

Archibald, S., Scholes, R.J., Roy, D.P., Roberts, G., Boschetti, L., 2010. Southern African fire regimes as revealed by remote sensing. International Journal of Wildland Fire 19, 861-878.

Barlow, J., Parry, L., Gardner, T.A., Ferreira, J., Aragão, L.E., Carmenta, R., Berenguer, E., Vieira, I.C., Souza, C., Cochrane, M.A., 2012. The critical importance of considering fire in REDD+ programs. Biol Conserv 154, 1-8.

Drusch, M., Del Bello, U., Carlier, S., Colin, O., Fernandez, V., Gascon, F., Hoersch, B., Isola, C., Laberinti, P., Martimort, P., 2012. Sentinel-2: ESA's optical high-resolution mission for GMES operational services. Remote Sensing of Environment 120, 25-36.

Eriksen, C., 2007. Why do they burn the 'bush'? Fire, rural livelihoods, and conservation in Zambia. Geographical Journal 173, 242-256.

Eva, H., Lambin, E.F., 1998. Remote sensing of biomass burning in tropical regions: Sampling issues and multisensor approach. Remote Sensing of Environment 64, 292-315.

French, N.H.F., Kasischke, E.S., Hall, R.J., Murphy, K.A., Verbyla, D.L., Hoy, E.E., Allen, J.L., 2008. Using Landsat data to assess fire and burn severity in the North American boreal forest region: An overview and summary of results. International Journal of Wildland Fire 17, 443-462.

Giri, C., Pengra, B., Long, J., Loveland, T.R., 2013. Next generation of global land cover characterization, mapping, and monitoring. International Journal of Applied Earth Observation and Geoinformation 25, 30-37.

Kennedy, R.E., Cohen, W.B., Schroeder, T.A., 2007. Trajectory-based change detection for automated characterization of forest disturbance dynamics. Remote Sensing of Environment 110, 370-386.

Kokwe, M., Mickels-Kokwe, G., 2012. Forest management practices with potential for REDD+ in Zambia. Ministry of Lands, Natural Resources and Environmental Protection, Lusaka, Zambia.

Korontzi, S., Justice, C.O., Scholes, R.J., 2003. Influence of timing and spatial extent of savanna fires in southern Africa on atmospheric emissions. J Arid Environ 54, 395-404.

Pricope, N.G., Binford, M.W., 2012. A spatio-temporal analysis of fire recurrence and extent for semi-arid savanna ecosystems in southern Africa using moderate-resolution satellite imagery. Journal of Environmental Management 100, 72-85.

Roy, D.P., Lewis, P.E., Justice, C.O., 2002. Burned area mapping using multi-temporal moderate spatial resolution data - a bi-directional reflectance model-based expectation approach. Remote Sensing of Environment, 263-286.

Vinya, R., Kasumu, E.C., Syampungani, S., Monde, C., Kasubika, R., 2011. Preliminary Study on the Drivers of Deforestation and Potential for REDD+ in Zambia., Lusaka, Zambia.

Appendices

Appendix A: Code for Performance Assessment of Burned Area Mapping Method (Chapter 2)

MATLAB code to perform accuracy assessment, gather cluster sensitivity and variable importance data. The code requires MATLAB Statistics, Fuzzy Logic and Parallel Computing toolboxes.

```
% ************************ Prepare input data ***************************
%
clc;clear;close all
load sample2009 % load preselected sample for training sample selection
minmf=0.5; % minimum membership cut-off
ffactor=1.6; %fuzzy exponent
jd=[139 155 187 195 227 259 275 307]; % Image acquisiotn dates -Julian 2009
dtxt={'May19' 'Jun04' 'Jul06' 'Jul14' 'Aug15' 'Sep16' 'Oct02' 'Nov03'};

% /### for 2012 use:
%   load sample2012; minmf=0.5;ffactor=1.3;
%   jd=[140 188 204 220 236 268 284 316]; % Julian days 2012
%  dtxt={'May19' 'Jul06' 'Jul22' 'Aug07' 'Aug23' 'Sep24' 'Oct10' 'Nov11'};
% ###/

% *************** Transform data to zscores/pre-allocate ******************
%
[nr,ncol]=size(X);X=X(:);sd = mad(X,1);mn=median(X);
X=(X-repmat(mn,size(X,1),1))./sd; X=reshape(X,nr,ncol);

% seed values to control random processes
s=[815,906,127,914,633,98,279,547,958,965,158,971,958,486,801,142,422,...
    916,793,960,656,36,850,934,679,758,744,393,656,172];
% pre-allocate matrices
vlmat=zeros(length(s),6); % holds performance metrics
confmat=zeros(8,8,length(s));% N-D confusion matrix for all 30 runs
trainmat=zeros(8,length(s)); % keeps track of no. train samples/class
labelmat=cell(size(trainmat));% keeps track of corresponding class labels
varImp=zeros(30,21); % variable importance matrix

% *************** Run following stes for each seed value ****************
%
for z=1:length(s)
    rng(s(z))

    % Repeated clustering and refinement clustering
    [center, mfmat, ~] = repeatedClustering(X, ffactor,minmf);
    [ocenter, o_mfmat, ~] = refiningfcm(X, mfmat, ffactor,minmf);

    % Select training signatures from refined clustering
    esh=85;
    [trData,trLabels, trClass] = selectTrainSamples(X,ocenter,o_mfmat,...
                                                    minmf,esh,jd,dtxt);
    d=tabulate(trLabels);
    % triain RF
    if ~matlabpool('size')
```

```
        matlabpool open
    end
    trdata=prepareData(trData,jd); % calculate
    RandStream.setGlobalStream(RandStream('mlfg6331_64','seed',s(z)));
    options = statset('UseParallel','always',...
        'Streams',RandStream.getGlobalStream,...
        'UseSubStreams','always'); % settings for parallel computing
    ntrees=200;
    mdl = TreeBagger(ntrees,trdata,trLabels,'options',options,'OOBPred',...
                'On', 'oobvarimp','on','NVarToSample','all');
    varImp(z,:)=mdl.OOBPermutedVarDeltaError; % get variable importance
    % Assess accuracy using out of bag samples
    [lbl1OOB, pscore] = oobPredict(mdl);
    [conf,classorder] = confusionmat(trLabels,lbl1OOB,'order',trClass);
    %disp(dataset({conf,classorder{:}},'obsnames',classorder));
    occ=sum(diag(conf))/sum(conf(:))*100; % OOB overall accuracy

    % Validate model with independent reference data
    %
    load Valdata2009 % loads validation data
    [nr,ncol]=size(Y);
    Y=Y(:);
    Y=(Y-repmat(mn,size(Y,1),1))./sd;
    Y=reshape(Y,nr,ncol);
    Y=prepareData(Y,jd);
    [predClass, Class_Score] = predict(mdl,Y);
    [conf1,classorder1] = confusionmat(BurnClass,predClass,'order',...
        {'Unburned' 'BurnJun04' 'BurnJul06' 'BurnJul14'...
        'BurnAug15' 'BurnSep16' 'BurnOct02' 'BurnNov03'});
    occa=sum(diag(conf1))/sum(conf1(:))*100; % overall test accuracy
    index = cellfun(@strcmp, BurnClass, predClass);
    rg=1:length(BurnClass);rg=rg';
   xsx=table(rg(not(index)),BurnClass(not(index)),predClass(not(index)),...
                                        LC(not(index)),'VariableNames',...
                            {'Index' 'Reference' 'Predicted' 'Landcover'});
    if z==1
        T=xsx;
    else
        T=[T;xsx]; %#ok<*AGROW>
    end
    % Capture performance metrics
    confmat(:,:,z)=conf1; % multi-dimensional confusion matrix
    vlmat(z,:)=[z s(z) size(ocenter,1) length(trLabels) occ occa];
    [st,lx]=sort(d(:,1)); labelmat(:,z)=st;trainmat(:,z)=cell2mat(d(lx,2));
end
```

Supporting functions for Performance Assessment Code (Chapter 2)

MATLAB function for repeated clustering step

MATLAB code for repeated fuzzy clustering as described in section 2.3.4 and Figure 2.3

```
function [center, mfmat, remp] = repeatedClustering(X, ffactor,minmf)
% repeatedClustering Dataset clustering using repeated fuzzy c-means
%
%   [center, mfmat, remp] = repeatedClustering(X, ffactor,minmf) repeatedly
```

```
%   clusters dataset X using fuzzy c-means by imposing min. membership,
%   minmf  to return the cumulative center matrix,center and
%   partition matrix,mfmat.
%       X  - is nxp matrix,
%       ffactor - is scalar representing the fuzzifying paramter
%       minmf - scalar representing min. membership
%       center - kxp matrix, k is cumulative no. clusters
%       mfmat -kxn cumulative fuzzy patrttion matrix
%       remp - remainder unclustered samples
%
%  Lonesome Malambo, 11/8/2014
dtm=X; [nr,~]=size(X);i=1; n=0;lmp=nr;ctrtmp=0;
while not(ctrtmp)
    if i==1
        % determine optimal number of clusters
        noClusters = getOptimalClusters(dtm,
ffactor,minmf);%round(sqrt(size(dtm,1)/2));
        % do fuzzy partitions
        [center,mfmat,~]=fcm(dtm,noClusters,[ffactor,200,0.00001,0]);
        tw=(mfmat>=minmf);
        sm=sum(tw,2);
        ex=sm<=1;
        if max(ex)>0 % delete low membership clusters
            center(ex,:)=[];
            mfmat(ex,:)=[];
        end
    else
        % determine if there lower membership profiles in previous clustering
        mxm=max(mfmat,[],1);
        lmp=find(mxm<minmf);% low membership profiles

        dtm=X(lmp,:);
        % determine optimal number of clusters
        if (n==length(lmp))
            noClusters = getOptimalClusters(dtm,
ffactor,minmf)+1;%round(sqrt(size(dtm,1)/2)+5);
        else
            noClusters = getOptimalClusters(dtm,
ffactor,minmf);%round(sqrt(size(dtm,1)/2));
        end
        % stop if no of cluster is greater than data volume or is no of
        % low membership profiles is less than 10pct of data

        % Recluster low membership profiles only
        [ctr,fmt,~]=fcm(dtm,noClusters,[ffactor,200,0.00001,0]);

        mf=zeros(noClusters,nr)+0.00000001;
        mf(:,lmp)=fmt;
        % Update fuzzy matrix and center profiles
        mfmat=[mfmat;mf];%#ok<*AGROW> % final membership matrix
        center=[center;ctr];

        tw=(mfmat>=minmf);
        sm=sum(tw,2);
        ex=sm<=1;
        if max(ex)>0 % delete low membership clusters
            center(ex,:)=[];
```

```
            mfmat(ex,:)=[];
        end

%isempty(lmp)||(n==length(lmp))(length(lmp)<noClusters)||(length(lmp)<0.15*nr
)
        ctrtmp=(isempty(lmp))||(length(lmp)<0.10*nr)||...
            (n==length(lmp))||(length(lmp)<noClusters);
    end
n=length(lmp);
i=i+1;

end
% final clean up
remp=lmp;
end
```

MATLAB function for refining fuzzy clustering step

MATLAB code for repeated fuzzy clustering as described in section 2.3.4 and Figure 2.3

```
function [ocenter, o_mfmat, obj_fcn] = refiningfcm(data, mfmat,
ffactor,minmf)
%FCM_MR Data set clustering using fuzzy c-means clustering with specified
% partition matrix.
%%   [center, mfmat, obj_fcn] = fcm_mr(data, mfmat, ffactor,minmf) clusters
%   data into k clusters based on fuzzy partition matrix mfmat.
%       data - is mxn matrix, m is no. of data points, n is no. variables
%       mfmat - pxm matrix for the fuzzy partition matrix
%       ffactor - scalar for fuzzy paramter
%       minmf - scalar for min. membership
%       center - kxn center matrix, k==p is no deletions
%       mfmat -  kxm output fuzzy partition matrix
%   Lonesome Malambo, 11/09/2014
%   stepfcm is function in Fuzzy Logic Toolbox, The MathWorks,Inc.1994-2014

max_iter = 200;         % Max. iteration

obj_fcn = zeros(max_iter, 1); % Array for objective function

% Main loop
cluster_n=size(mfmat,1);
for i = 1:max_iter,
      [mfmat, ocenter, obj_fcn(i)] = stepfcm(data, mfmat, cluster_n,
ffactor);
      % check termination condition
      if i > 1,
            if abs(obj_fcn(i) - obj_fcn(i-1)) < 0.00001, break; end,
      end
end
iter_n = i; % Actual number of iterations
obj_fcn(iter_n+1:max_iter) = [];
% Delete low membership clusters if exist
tw=(mfmat>=minmf); sm=sum(tw,2); ex=sm<=0; o_mfmat=mfmat;
if max(ex)>0
    ocenter(ex,:)=[];
    o_mfmat(ex,:)=[];
end
```

MATLAB function for training sample selection and labeling

MATLAB code for training sample selection and labeling as described in section 2.3.4 and Figure 2.4

```
function [trData,trLabels, trClass] =
selectTrainSamples(X,center,mfmat,minmf,esh,jd,dtxt)
% selectTrainSamples selects training samples based on cluster purity of a
% cluster core using changepoints as class labels.

% X - input data
% center - cluster centers
% mfmat - fuzzy partition matrix
% minmf - minimum membership value
% esh - minimum purity value for cluster to be taken as pure and fit for
% training purposes.
% jd - sequence of image acquisition dates in julian calendar

% convert to gradient values
XX=diff(X,1,2); jdd=diff(jd); nn=round(mean(jdd));
jdn=min(jd):nn:min(jd)+(length(jd)-1)*nn; % make uniform
jddn=diff(jdn); XX= (XX./repmat(jddn,size(XX,1),1)); % gradient data

% updated center gradient profiles
ctrg=diff(center,1,2); ctrg= ctrg./repmat(jdd,size(ctrg,1),1);

trD=zeros(size(XX,1),1); % training sample index vector
trL=trD;% training sample label vector

z=0; [nc,~]=size(ctrg); [hh,ss]=sort(mfmat,2,'descend');%sort by column
selmat=zeros(nc,3);
% characterize cluster quality
for i=1:size(ctrg,1)
    cc=hh(i,:);
    ix=find(cc>=minmf,100,'first'); tt=ss(i,:); ix=tt(ix);% core indices

    if ~isempty(ix)&&(length(ix)>=3) % core must >= 3
        bot=zeros(length(ix),1);% per cluster purity matrix
    else
        selmat(i,:)=[100 0 1];
        continue
    end
    for j=1:length(ix)
        r=ix(j);
        ctr=XX(r,:);
        [outlier_point,~] = dixonQtest(ctr,95);
        if ~isempty(outlier_point)
            mnc=mean(ctr);
            if mnc<ctr(outlier_point)
                bot(j)=outlier_point;% if +ve outlier then burned
            elseif mnc<0
                bot(j)=0; % if -ve outlier then unburned
            else
                bot(j)=-9;
            end
        else
```

```
            mnc=mean(ctr);
            if mnc<0
                bot(j)=0;% if no outlier then unburned
            else
                bot(j)=-9;% if no outlier then unburned
            end
        end
    end

    e=entropyc(bot);
    if e(2)<esh
        del=1; % do not use for training selection
    else
        del=0;mlb=mode(bot); % mode label
        ts=bot==mlb;ix=ix(ts); % exclude discordant samples
        xx=(z+1):(z+length(ix));trD(xx,:)=ix'; trL(xx,:)=mlb;z=xx(end);
    end
    selmat(i,:)=[e del];
end
trD(z+1:end)=[];trL(z+1:end)=[]; trainData=unique([trD trL],'rows');

% Label training data
class=sort(unique(trainData(:,2))); trc=cell(size(trainData(:,2)));
classorder=cell(size(class));
for i=1:length(class)
    cid=class(i);
    tf=trainData(:,2)==cid;
    if cid>0
        lb={['Burn' dtxt{cid+1}]};
    elseif cid==0
        lb={'Unburned'};
    else
        lb={'trash'};
    end
    trc(tf)=lb;
    classorder(i)=lb;

end
% restrict to valid data
gx=trainData(:,2)>=0;td=trainData(:,1);gx1=td(gx);trData=X(gx1,:);
trLabels=trc(gx,:);

ht= ~cellfun(@(x) strcmp(x,'trash'),classorder); % indices for non-crop
trClass=classorder(ht);

end
```

Miscellaneous MATLAB supporting functions (Chapter 2)

```
function [outlier_point,outlier_value] = dixonQtest(X,conf)
% dixoQtest Outlier detection using Dixon Q test for 3<=N<=10
%
%  [outlier_point,outlier_value] = dixonQtest(X,conf) finds the positive
%  outlier in X at a conf confidence level and returns the outlier
%  position in X, outlier_point, and the corresponding outlier value,
%  outlier_value.
%       X - nx1 or 1xn vector
```

```
%       conf - scalar for confidence level valid values=[90,95,99]
%       outlier_point - scalar if outlier is detected, otherwise is empty
%       outlier_value - scalar if outlier is detected, otherwise is empty
%
%  Lonesome Malambo 11/08/2014
%
%  References:
%       http://www.chem.uoa.gr/applets/AppletQtest/Appl_Qtest2.html
%
%       Rorabacher, D.B. (1991). Statistical Treatment for Rejection of
%       Deviant Values: Critical Values of Dixon Q Parameter and Related
%       Subrange Ratios at the 95 percent Confidence Level. Anal. Chem.
%       83, 2, 139-146.

% Critical values of Q,90,95 and 99% CL by column
Qtable=[3 0.941 0.970 0.994;
    4 0.765 0.829 0.926;
    5 0.642 0.710 0.821;
    6 0.560 0.625 0.740;
    7 0.507 0.568 0.680;
    8 0.468 0.526 0.634;
    9 0.437 0.493 0.598;
    10 0.412 0.466 0.568;];

if ~ismember(conf,[90,95,99])
    error('Only 90, 95 or 99 are valid values for confidence interval')
end
if ~isvector(X)
    error('X must be a vector')
end
if length(X)<3||length(X)>10
    error('X must be length 3-10')
end

[xs,id]=sort(X); % sort values
q=(xs(end)-xs(end-1))/range(xs); % q statistic
n=length(X);
if conf==90
    tf=ismember(Qtable(:,1),n);
    qt=Qtable(tf,2);
elseif conf==95
    tf=ismember(Qtable(:,1),n);
    qt=Qtable(tf,3);
else
    tf=ismember(Qtable(:,1),n);
    qt=Qtable(tf,4);
end
% Q test
if q>qt % then its an outlier
    outlier_point=id(end);
    outlier_value=xs(end);
else
    outlier_point=[];
    outlier_value=[];
end

end
```

```
function noClusters = estimateNumberClusters(X, ffactor,minmf)
% estimateNumberClusters estimates the number of clusters,noClusters,by
% repeatedly clustering a samples of the dataset X until one or more empty
% clusters are detected following:
% Futschik, M. E. and B. Carlisle (2005).
%   "Noise-robust soft clustering of gene expression time-course data."
%   Journal of Bioinformatics and Computational Biology 03(04): 965-988.
%
% ffactor - scalar for the fuzzifying parameter
% minmf - scalar for min. membership

[nr,~]=size(X);
if nr>1000 % get a 40% radom sample if data is large.
    smp=floor(0.4*nr);
    y = datasample(1:nr,smp,'Replace',false);
    X=X(y,:);
end
nc=3:50;
    for i=1:length(nc)
            [~,fmat,~]=fcm_m(X,nc(i),[ffactor,100,0.001,0]);
            tw=(fmat>=minmf);
            sm=sum(tw,2);
            %ec=max(fmat,[],2);

            nec=numel(find(sm(sm<2)));
            if nec>0 % if empty cluster found
                noClusters=nc(i)-1;
                break
            else
                noClusters=nc(i);
            end
    end

end

function enty = entropyc( bot )
%ENTROPYC calculates the entropy and cluster purity of cluster using
% change point label frequencies

uv=unique(bot);
ent=zeros(length(uv),1);
pcnt=zeros(length(uv),1);
for i=1:length(uv)
   id=uv(i);
   ix=find(bot==id);
   pcnt(i)=length(ix);
   p=length(ix)/length(bot);
   ent(i)=-p*log2(p);
end
enty=[sum(ent),max(pcnt)/length(bot)*100];
end


function [ data ] = prepareData(X,jd)
%prepareData calculate features from data X for classification
% jd is the sequence of julian days
```

```
% Fetaures calculated include the min,max,mean and successive gradients of
% X
mnmx_X=[min(X,[],2) mean(X,2) max(X,[],2)];
% gradient data
XX=diff(X,1,2);
jdd=diff(jd);
nn=round(mean(jdd));
jdn=min(jd):nn:min(jd)+(length(jd)-1)*nn;
jddn=diff(jdn);
XX= 100*(XX./repmat(jddn,size(XX,1),1)); % gradient data
mnmx_grad=[min(XX,[],2) mean(XX,2) max(XX,[],2)];

data=[X mnmx_X XX mnmx_grad]; %all data

end
```

APPENDIX B: VALIDATION DATA FOR BURNED AREA MAPPING (CHAPTER 2)

Validation points for 2009 used in Chapter 2, with X and Y coordinates (WGS 1984 UTM Zone 36S), burn class and associated land cover type. The Burn class labels have been shortened due to space limitation e.g. *BurnJun06* instead of *Burn by Jun06* used in Chapter 2.

ID	X	Y	Land cover	Burn class	ID	X	Y	Land cover	Burn class
1	445845	8694145	Grassland	Unburned	**526**	450345	8656225	Grassland	BurnJul06
2	446505	8693155	Grassland	Unburned	**527**	446565	8655805	Grassland	BurnJul06
3	451065	8692315	Grassland	Unburned	**528**	448215	8655415	Grassland	BurnJul06
4	439095	8692255	Grassland	Unburned	**529**	454395	8652535	Grassland	BurnJul06
5	454215	8691865	Grassland	Unburned	**530**	451575	8651005	Grassland	BurnJul06
6	442665	8691655	Grassland	Unburned	**531**	459015	8694235	Forest	BurnJul06
7	461235	8690815	Grassland	Unburned	**532**	460425	8693995	Forest	BurnJul06
8	448605	8690755	Grassland	Unburned	**533**	460215	8693905	Forest	BurnJul06
9	438765	8690305	Grassland	Unburned	**534**	462945	8692735	Forest	BurnJul06
10	459435	8690155	Grassland	Unburned	**535**	461895	8692735	Forest	BurnJul06
11	440955	8689945	Grassland	Unburned	**536**	452325	8692225	Forest	BurnJul06
12	450165	8689555	Grassland	Unburned	**537**	465525	8689165	Forest	BurnJul06
13	436635	8688715	Grassland	Unburned	**538**	455595	8688805	Forest	BurnJul06
14	456945	8687695	Grassland	Unburned	**539**	465375	8688295	Forest	BurnJul06
15	440055	8687215	Grassland	Unburned	**540**	447765	8688025	Forest	BurnJul06
16	462135	8686915	Grassland	Unburned	**541**	465285	8684335	Forest	BurnJul06
17	443445	8686615	Grassland	Unburned	**542**	461805	8683975	Forest	BurnJul06
18	439275	8686255	Grassland	Unburned	**543**	461835	8683915	Forest	BurnJul06
19	442005	8684845	Grassland	Unburned	**544**	467505	8682175	Forest	BurnJul06
20	434535	8684065	Grassland	Unburned	**545**	459105	8681275	Forest	BurnJul06
21	447165	8683225	Grassland	Unburned	**546**	467445	8677315	Forest	BurnJul06

ID	X	Y	Land cover	Burn class	ID	X	Y	Land cover	Burn class
22	439215	8682445	Grassland	Unburned	**547**	446625	8673445	Forest	BurnJul06
23	437775	8681605	Grassland	Unburned	**548**	462885	8672995	Forest	BurnJul06
24	436965	8678755	Grassland	Unburned	**549**	464835	8671795	Forest	BurnJul06
25	457995	8678665	Grassland	Unburned	**550**	465285	8671585	Forest	BurnJul06
26	435765	8677975	Grassland	Unburned	**551**	465075	8666635	Forest	BurnJul06
27	443505	8677795	Grassland	Unburned	**552**	464475	8665885	Forest	BurnJul06
28	437625	8677675	Grassland	Unburned	**553**	466335	8662705	Forest	BurnJul06
29	437925	8677675	Grassland	Unburned	**554**	455325	8660335	Forest	BurnJul06
30	439365	8677435	Grassland	Unburned	**555**	455235	8660245	Forest	BurnJul06
31	454215	8677165	Grassland	Unburned	**556**	463485	8660215	Forest	BurnJul06
32	447615	8676145	Grassland	Unburned	**557**	438435	8658835	Forest	BurnJul06
33	452415	8675485	Grassland	Unburned	**558**	448395	8657455	Forest	BurnJul06
34	453165	8674345	Grassland	Unburned	**559**	459555	8656795	Forest	BurnJul06
35	434025	8673265	Grassland	Unburned	**560**	476235	8656165	Forest	BurnJul06
36	471255	8665855	Grassland	Unburned	**561**	453885	8655685	Forest	BurnJul06
37	443055	8663215	Grassland	Unburned	**562**	447285	8655625	Forest	BurnJul06
38	465435	8658955	Grassland	Unburned	**563**	447405	8655565	Forest	BurnJul06
39	464115	8657905	Grassland	Unburned	**564**	455355	8655415	Forest	BurnJul06
40	462135	8656345	Grassland	Unburned	**565**	450645	8655085	Forest	BurnJul06
41	464745	8655025	Grassland	Unburned	**566**	476355	8654245	Forest	BurnJul06
42	450315	8652205	Grassland	Unburned	**567**	472395	8653945	Forest	BurnJul06
43	444525	8651995	Grassland	Unburned	**568**	472005	8653885	Forest	BurnJul06
44	445035	8651005	Grassland	Unburned	**569**	473445	8653615	Forest	BurnJul06
45	439395	8693185	Cropland	Unburned	**570**	472755	8652955	Forest	BurnJul06
46	449595	8692585	Cropland	Unburned	**571**	472665	8652865	Forest	BurnJul06
47	436845	8692525	Cropland	Unburned	**572**	473325	8652805	Forest	BurnJul06
48	456975	8692525	Cropland	Unburned	**573**	472755	8652715	Forest	BurnJul06
49	476265	8692495	Cropland	Unburned	**574**	441285	8652625	Forest	BurnJul06
50	438315	8692315	Cropland	Unburned	**575**	462915	8652325	Forest	BurnJul06
51	458805	8692225	Cropland	Unburned	**576**	453825	8651575	Forest	BurnJul06
52	459495	8692075	Cropland	Unburned	**577**	449085	8688865	Cropland	BurnJul06
53	476055	8691775	Cropland	Unburned	**578**	436665	8688595	Cropland	BurnJul06
54	475395	8691685	Cropland	Unburned	**579**	437325	8662945	Cropland	BurnJul06
55	476355	8691535	Cropland	Unburned	**580**	440805	8660425	Cropland	BurnJul06
56	456855	8691535	Cropland	Unburned	**581**	436155	8660275	Cropland	BurnJul06
57	476025	8691535	Cropland	Unburned	**582**	443295	8660215	Cropland	BurnJul06
58	476595	8691445	Cropland	Unburned	**583**	436095	8660185	Cropland	BurnJul06
59	475515	8689825	Cropland	Unburned	**584**	443235	8660125	Cropland	BurnJul06
60	435555	8689825	Cropland	Unburned	**585**	443445	8660035	Cropland	BurnJul06
61	476355	8689615	Cropland	Unburned	**586**	445005	8659795	Cropland	BurnJul06

ID	X	Y	Land cover	Burn class	ID	X	Y	Land cover	Burn class
62	475215	8688955	Cropland	Unburned	**587**	447915	8659525	Cropland	BurnJul06
63	474195	8688835	Cropland	Unburned	**588**	447945	8659495	Cropland	BurnJul06
64	451935	8687305	Cropland	Unburned	**589**	441525	8659495	Cropland	BurnJul06
65	435435	8686915	Cropland	Unburned	**590**	441915	8659405	Cropland	BurnJul06
66	444375	8686525	Cropland	Unburned	**591**	442035	8659405	Cropland	BurnJul06
67	439215	8684395	Cropland	Unburned	**592**	441375	8659375	Cropland	BurnJul06
68	471285	8682415	Cropland	Unburned	**593**	442485	8659345	Cropland	BurnJul06
69	439845	8682295	Cropland	Unburned	**594**	452895	8658775	Cropland	BurnJul06
70	433845	8681155	Cropland	Unburned	**595**	452715	8658715	Cropland	BurnJul06
71	437835	8679565	Cropland	Unburned	**596**	452745	8658685	Cropland	BurnJul06
72	438705	8677555	Cropland	Unburned	**597**	446205	8657785	Cropland	BurnJul06
73	438855	8677555	Cropland	Unburned	**598**	446745	8657695	Cropland	BurnJul06
74	438435	8677555	Cropland	Unburned	**599**	446535	8657695	Cropland	BurnJul06
75	438795	8677555	Cropland	Unburned	**600**	440355	8657665	Cropland	BurnJul06
76	438645	8677525	Cropland	Unburned	**601**	446925	8657665	Cropland	BurnJul06
77	438885	8677525	Cropland	Unburned	**602**	440055	8657635	Cropland	BurnJul06
78	438525	8677525	Cropland	Unburned	**603**	446625	8657635	Cropland	BurnJul06
79	438465	8677525	Cropland	Unburned	**604**	448155	8657425	Cropland	BurnJul06
80	435315	8677105	Cropland	Unburned	**605**	445785	8656915	Cropland	BurnJul06
81	442005	8677045	Cropland	Unburned	**606**	445335	8656915	Cropland	BurnJul06
82	433695	8671405	Cropland	Unburned	**607**	445725	8656885	Cropland	BurnJul06
83	468615	8670265	Cropland	Unburned	**608**	445725	8656855	Cropland	BurnJul06
84	433755	8669485	Cropland	Unburned	**609**	446115	8656825	Cropland	BurnJul06
85	445005	8657935	Cropland	Unburned	**610**	446205	8656795	Cropland	BurnJul06
86	462915	8656375	Cropland	Unburned	**611**	445515	8656795	Cropland	BurnJul06
87	449985	8655265	Cropland	Unburned	**612**	446475	8656765	Cropland	BurnJul06
88	449685	8655175	Cropland	Unburned	**613**	446565	8656765	Cropland	BurnJul06
89	450525	8653195	Cropland	Unburned	**614**	446235	8656735	Cropland	BurnJul06
90	450285	8653135	Cropland	Unburned	**615**	446895	8656705	Cropland	BurnJul06
91	436185	8691715	Forest	Unburned	**616**	446835	8656675	Cropland	BurnJul06
92	472755	8691145	Forest	Unburned	**617**	446595	8656615	Cropland	BurnJul06
93	435495	8688865	Forest	Unburned	**618**	446985	8656585	Cropland	BurnJul06
94	438675	8688385	Forest	Unburned	**619**	441585	8656435	Cropland	BurnJul06
95	445125	8685505	Forest	Unburned	**620**	443565	8656105	Cropland	BurnJul06
96	463455	8683645	Forest	Unburned	**621**	474315	8693035	Forest	BurnSep16
97	436935	8682745	Forest	Unburned	**622**	473445	8692105	Forest	BurnSep16
98	437985	8682595	Forest	Unburned	**623**	464595	8688535	Forest	BurnSep16
99	452025	8682385	Forest	Unburned	**624**	469305	8687845	Forest	BurnSep16
100	446895	8681185	Forest	Unburned	**625**	455745	8686915	Forest	BurnSep16
101	473985	8678215	Forest	Unburned	**626**	469335	8686735	Forest	BurnSep16

ID	X	Y	Land cover	Burn class	ID	X	Y	Land cover	Burn class
102	476355	8677765	Forest	Unburned	**627**	468435	8685865	Forest	BurnSep16
103	433965	8677195	Forest	Unburned	**628**	472365	8683285	Forest	BurnSep16
104	437115	8675875	Forest	Unburned	**629**	461205	8681065	Forest	BurnSep16
105	455955	8675035	Forest	Unburned	**630**	444105	8679715	Forest	BurnSep16
106	438165	8674645	Forest	Unburned	**631**	441855	8679115	Forest	BurnSep16
107	473235	8672515	Forest	Unburned	**632**	462015	8678125	Forest	BurnSep16
108	473805	8670445	Forest	Unburned	**633**	461235	8677255	Forest	BurnSep16
109	464085	8669875	Forest	Unburned	**634**	453255	8675275	Forest	BurnSep16
110	452085	8668675	Forest	Unburned	**635**	454905	8675095	Forest	BurnSep16
111	431235	8667805	Forest	Unburned	**636**	443685	8673925	Forest	BurnSep16
112	470805	8666725	Forest	Unburned	**637**	457575	8673865	Forest	BurnSep16
113	436335	8666125	Forest	Unburned	**638**	450135	8673835	Forest	BurnSep16
114	450495	8665975	Forest	Unburned	**639**	445335	8673625	Forest	BurnSep16
115	453465	8665555	Forest	Unburned	**640**	470565	8672695	Forest	BurnSep16
116	467205	8664385	Forest	Unburned	**641**	443535	8671885	Forest	BurnSep16
117	470475	8664085	Forest	Unburned	**642**	458115	8671675	Forest	BurnSep16
118	443445	8664025	Forest	Unburned	**643**	443145	8670955	Forest	BurnSep16
119	468255	8663245	Forest	Unburned	**644**	449295	8670115	Forest	BurnSep16
120	459675	8662645	Forest	Unburned	**645**	443535	8669905	Forest	BurnSep16
121	459135	8661625	Forest	Unburned	**646**	437145	8669875	Forest	BurnSep16
122	469725	8661115	Forest	Unburned	**647**	440295	8669515	Forest	BurnSep16
123	470475	8660965	Forest	Unburned	**648**	442005	8669155	Forest	BurnSep16
124	457515	8660095	Forest	Unburned	**649**	444135	8667835	Forest	BurnSep16
125	473175	8658565	Forest	Unburned	**650**	438345	8663845	Forest	BurnSep16
126	458055	8658025	Forest	Unburned	**651**	471675	8663845	Forest	BurnSep16
127	464775	8657995	Forest	Unburned	**652**	466185	8663515	Forest	BurnSep16
128	464625	8657965	Forest	Unburned	**653**	464535	8662915	Forest	BurnSep16
129	467925	8657425	Forest	Unburned	**654**	464655	8662855	Forest	BurnSep16
130	440535	8656615	Forest	Unburned	**655**	432405	8662765	Forest	BurnSep16
131	476595	8654245	Forest	Unburned	**656**	473685	8662465	Forest	BurnSep16
132	442095	8653525	Forest	Unburned	**657**	475905	8662345	Forest	BurnSep16
133	437865	8653075	Forest	Unburned	**658**	472395	8661805	Forest	BurnSep16
134	465555	8653045	Forest	Unburned	**659**	449565	8661145	Forest	BurnSep16
135	458145	8651995	Forest	Unburned	**660**	430545	8659135	Forest	BurnSep16
136	470715	8651125	Forest	Unburned	**661**	472035	8658715	Forest	BurnSep16
137	455745	8691685	Grassland	BurnAug15	**662**	460575	8658445	Forest	BurnSep16
138	464895	8691445	Grassland	BurnAug15	**663**	448215	8658355	Forest	BurnSep16
139	473205	8691115	Grassland	BurnAug15	**664**	442425	8657245	Forest	BurnSep16
140	446265	8690185	Grassland	BurnAug15	**665**	470865	8657095	Forest	BurnSep16
141	460335	8689105	Grassland	BurnAug15	**666**	436995	8656135	Forest	BurnSep16

ID	X	Y	Land cover	Burn class	ID	X	Y	Land cover	Burn class
142	474735	8689045	Grassland	BurnAug15	**667**	457575	8655955	Forest	BurnSep16
143	475695	8687815	Grassland	BurnAug15	**668**	438435	8655865	Forest	BurnSep16
144	474705	8687815	Grassland	BurnAug15	**669**	461745	8655505	Forest	BurnSep16
145	452505	8686345	Grassland	BurnAug15	**670**	462045	8653465	Forest	BurnSep16
146	455445	8685775	Grassland	BurnAug15	**671**	472755	8693035	Grassland	BurnSep16
147	452205	8685355	Grassland	BurnAug15	**672**	467745	8690035	Grassland	BurnSep16
148	466095	8685175	Grassland	BurnAug15	**673**	455985	8689705	Grassland	BurnSep16
149	454905	8684995	Grassland	BurnAug15	**674**	470265	8689555	Grassland	BurnSep16
150	467835	8684875	Grassland	BurnAug15	**675**	448755	8687935	Grassland	BurnSep16
151	458235	8684395	Grassland	BurnAug15	**676**	469815	8687545	Grassland	BurnSep16
152	466065	8684305	Grassland	BurnAug15	**677**	471705	8687485	Grassland	BurnSep16
153	466575	8684215	Grassland	BurnAug15	**678**	473325	8687185	Grassland	BurnSep16
154	456915	8683645	Grassland	BurnAug15	**679**	465915	8686165	Grassland	BurnSep16
155	457845	8683465	Grassland	BurnAug15	**680**	453555	8686105	Grassland	BurnSep16
156	468615	8683045	Grassland	BurnAug15	**681**	471165	8683465	Grassland	BurnSep16
157	460875	8682025	Grassland	BurnAug15	**682**	453615	8683225	Grassland	BurnSep16
158	469155	8681965	Grassland	BurnAug15	**683**	440385	8683135	Grassland	BurnSep16
159	464835	8680495	Grassland	BurnAug15	**684**	464415	8682565	Grassland	BurnSep16
160	465945	8679505	Grassland	BurnAug15	**685**	473655	8682025	Grassland	BurnSep16
161	472275	8679355	Grassland	BurnAug15	**686**	448125	8681035	Grassland	BurnSep16
162	460215	8677405	Grassland	BurnAug15	**687**	450525	8680795	Grassland	BurnSep16
163	461625	8675185	Grassland	BurnAug15	**688**	449685	8680735	Grassland	BurnSep16
164	464025	8674855	Grassland	BurnAug15	**689**	445185	8679445	Grassland	BurnSep16
165	447705	8672185	Grassland	BurnAug15	**690**	467385	8679295	Grassland	BurnSep16
166	444765	8667835	Grassland	BurnAug15	**691**	467475	8678125	Grassland	BurnSep16
167	441375	8667385	Grassland	BurnAug15	**692**	455175	8678035	Grassland	BurnSep16
168	441855	8666305	Grassland	BurnAug15	**693**	468975	8677975	Grassland	BurnSep16
169	436875	8663005	Grassland	BurnAug15	**694**	442335	8677915	Grassland	BurnSep16
170	436635	8654305	Grassland	BurnAug15	**695**	449325	8677885	Grassland	BurnSep16
171	436725	8654305	Grassland	BurnAug15	**696**	456465	8677825	Grassland	BurnSep16
172	455505	8654275	Grassland	BurnAug15	**697**	450645	8677765	Grassland	BurnSep16
173	436575	8654275	Grassland	BurnAug15	**698**	463995	8677585	Grassland	BurnSep16
174	436695	8654245	Grassland	BurnAug15	**699**	442665	8676865	Grassland	BurnSep16
175	436575	8654215	Grassland	BurnAug15	**700**	443745	8676775	Grassland	BurnSep16
176	436575	8654185	Grassland	BurnAug15	**701**	445845	8676535	Grassland	BurnSep16
177	435825	8653435	Grassland	BurnAug15	**702**	451215	8675695	Grassland	BurnSep16
178	435765	8653405	Grassland	BurnAug15	**703**	454605	8675155	Grassland	BurnSep16
179	442815	8653375	Grassland	BurnAug15	**704**	443415	8674885	Grassland	BurnSep16
180	435825	8653345	Grassland	BurnAug15	**705**	448185	8674075	Grassland	BurnSep16
181	458475	8653015	Grassland	BurnAug15	**706**	452505	8673415	Grassland	BurnSep16

ID	X	Y	Land cover	Burn class	ID	X	Y	Land cover	Burn class
182	458955	8652985	Grassland	BurnAug15	**707**	460905	8673355	Grassland	BurnSep16
183	447195	8651695	Grassland	BurnAug15	**708**	455445	8673055	Grassland	BurnSep16
184	473775	8691025	Cropland	BurnAug15	**709**	448815	8671105	Grassland	BurnSep16
185	474435	8689015	Cropland	BurnAug15	**710**	473715	8669425	Grassland	BurnSep16
186	449085	8688805	Cropland	BurnAug15	**711**	448005	8669275	Grassland	BurnSep16
187	455865	8687785	Cropland	BurnAug15	**712**	458895	8664595	Grassland	BurnSep16
188	451335	8686495	Cropland	BurnAug15	**713**	445035	8660905	Grassland	BurnSep16
189	468285	8683045	Cropland	BurnAug15	**714**	458985	8659705	Grassland	BurnSep16
190	468915	8681995	Cropland	BurnAug15	**715**	456435	8658115	Grassland	BurnSep16
191	468615	8681065	Cropland	BurnAug15	**716**	441705	8656435	Grassland	BurnSep16
192	469815	8666005	Cropland	BurnAug15	**717**	435825	8655325	Grassland	BurnSep16
193	431385	8663845	Cropland	BurnAug15	**718**	442515	8654275	Grassland	BurnSep16
194	435285	8662255	Cropland	BurnAug15	**719**	442005	8651515	Grassland	BurnSep16
195	444375	8662015	Cropland	BurnAug15	**720**	438945	8651035	Grassland	BurnSep16
196	434565	8661445	Cropland	BurnAug15	**721**	462075	8692795	Cropland	BurnSep16
197	434655	8661415	Cropland	BurnAug15	**722**	472335	8690095	Cropland	BurnSep16
198	439035	8660755	Cropland	BurnAug15	**723**	472635	8690065	Cropland	BurnSep16
199	438975	8660725	Cropland	BurnAug15	**724**	474375	8689795	Cropland	BurnSep16
200	440595	8660545	Cropland	BurnAug15	**725**	474315	8689795	Cropland	BurnSep16
201	440655	8660485	Cropland	BurnAug15	**726**	469725	8689765	Cropland	BurnSep16
202	439305	8659825	Cropland	BurnAug15	**727**	469875	8689525	Cropland	BurnSep16
203	439065	8659825	Cropland	BurnAug15	**728**	469575	8689525	Cropland	BurnSep16
204	439215	8659825	Cropland	BurnAug15	**729**	459885	8689135	Cropland	BurnSep16
205	439245	8659795	Cropland	BurnAug15	**730**	468855	8688745	Cropland	BurnSep16
206	439275	8659765	Cropland	BurnAug15	**731**	468945	8687755	Cropland	BurnSep16
207	445515	8659735	Cropland	BurnAug15	**732**	464805	8687395	Cropland	BurnSep16
208	441885	8659285	Cropland	BurnAug15	**733**	453015	8687305	Cropland	BurnSep16
209	464295	8658925	Cropland	BurnAug15	**734**	472845	8687185	Cropland	BurnSep16
210	444975	8658925	Cropland	BurnAug15	**735**	473655	8687125	Cropland	BurnSep16
211	444825	8658925	Cropland	BurnAug15	**736**	455955	8685865	Cropland	BurnSep16
212	446625	8658685	Cropland	BurnAug15	**737**	470055	8684725	Cropland	BurnSep16
213	446955	8658565	Cropland	BurnAug15	**738**	459615	8682325	Cropland	BurnSep16
214	442005	8658385	Cropland	BurnAug15	**739**	466935	8682235	Cropland	BurnSep16
215	443445	8658145	Cropland	BurnAug15	**740**	459855	8681395	Cropland	BurnSep16
216	441045	8657515	Cropland	BurnAug15	**741**	453435	8676325	Cropland	BurnSep16
217	450825	8657155	Cropland	BurnAug15	**742**	431505	8662885	Cropland	BurnSep16
218	450915	8657095	Cropland	BurnAug15	**743**	436245	8662165	Cropland	BurnSep16
219	451275	8657035	Cropland	BurnAug15	**744**	436425	8662165	Cropland	BurnSep16
220	447405	8656675	Cropland	BurnAug15	**745**	436365	8662105	Cropland	BurnSep16
221	448005	8656525	Cropland	BurnAug15	**746**	446385	8661685	Cropland	BurnSep16

ID	X	Y	Land cover	Burn class	ID	X	Y	Land cover	Burn class
222	448095	8656375	Cropland	BurnAug15	**747**	434415	8661415	Cropland	BurnSep16
223	443445	8656135	Cropland	BurnAug15	**748**	442155	8661295	Cropland	BurnSep16
224	450795	8655145	Cropland	BurnAug15	**749**	438075	8660965	Cropland	BurnSep16
225	449475	8693545	Forest	BurnAug15	**750**	446565	8660575	Cropland	BurnSep16
226	467565	8692915	Forest	BurnAug15	**751**	439305	8658715	Cropland	BurnSep16
227	459255	8692165	Forest	BurnAug15	**752**	447195	8658655	Cropland	BurnSep16
228	462705	8686675	Forest	BurnAug15	**753**	440685	8658595	Cropland	BurnSep16
229	461475	8685865	Forest	BurnAug15	**754**	440565	8658595	Cropland	BurnSep16
230	458235	8685415	Forest	BurnAug15	**755**	447495	8658475	Cropland	BurnSep16
231	464055	8679775	Forest	BurnAug15	**756**	447945	8658475	Cropland	BurnSep16
232	470325	8678665	Forest	BurnAug15	**757**	449025	8658385	Cropland	BurnSep16
233	459615	8677405	Forest	BurnAug15	**758**	442605	8658355	Cropland	BurnSep16
234	472335	8676415	Forest	BurnAug15	**759**	441885	8657485	Cropland	BurnSep16
235	469515	8675875	Forest	BurnAug15	**760**	443235	8657245	Cropland	BurnSep16
236	468435	8675035	Forest	BurnAug15	**761**	449205	8655385	Cropland	BurnSep16
237	471165	8674705	Forest	BurnAug15	**762**	449295	8655295	Cropland	BurnSep16
238	473445	8674255	Forest	BurnAug15	**763**	451665	8653045	Cropland	BurnSep16
239	466575	8673295	Forest	BurnAug15	**764**	454215	8652535	Cropland	BurnSep16
240	439845	8671465	Forest	BurnAug15	**765**	452475	8694145	Grassland	BurnOct02
241	447345	8671375	Forest	BurnAug15	**766**	459585	8691205	Grassland	BurnOct02
242	447435	8671375	Forest	BurnAug15	**767**	443355	8690545	Grassland	BurnOct02
243	447435	8671285	Forest	BurnAug15	**768**	456675	8689585	Grassland	BurnOct02
244	445935	8669635	Forest	BurnAug15	**769**	442485	8688715	Grassland	BurnOct02
245	433965	8668375	Forest	BurnAug15	**770**	467535	8687875	Grassland	BurnOct02
246	467175	8667445	Forest	BurnAug15	**771**	468345	8687755	Grassland	BurnOct02
247	467895	8667205	Forest	BurnAug15	**772**	443775	8687665	Grassland	BurnOct02
248	436635	8663155	Forest	BurnAug15	**773**	464445	8687575	Grassland	BurnOct02
249	438015	8657965	Forest	BurnAug15	**774**	444525	8687515	Grassland	BurnOct02
250	440955	8657605	Forest	BurnAug15	**775**	440895	8686015	Grassland	BurnOct02
251	467115	8657485	Forest	BurnAug15	**776**	440835	8686015	Grassland	BurnOct02
252	474795	8657455	Forest	BurnAug15	**777**	475575	8685895	Grassland	BurnOct02
253	456615	8656195	Forest	BurnAug15	**778**	475725	8685775	Grassland	BurnOct02
254	473445	8655685	Forest	BurnAug15	**779**	446835	8685265	Grassland	BurnOct02
255	474885	8655505	Forest	BurnAug15	**780**	453585	8685205	Grassland	BurnOct02
256	442755	8654245	Forest	BurnAug15	**781**	447255	8685205	Grassland	BurnOct02
257	472965	8653855	Forest	BurnAug15	**782**	451125	8684545	Grassland	BurnOct02
258	441435	8653465	Forest	BurnAug15	**783**	447465	8684185	Grassland	BurnOct02
259	474255	8653465	Forest	BurnAug15	**784**	467145	8684185	Grassland	BurnOct02
260	447075	8652775	Forest	BurnAug15	**785**	467745	8683915	Grassland	BurnOct02
261	466065	8652715	Forest	BurnAug15	**786**	454605	8681995	Grassland	BurnOct02

ID	X	Y	Land cover	Burn class	ID	X	Y	Land cover	Burn class
262	469485	8652235	Forest	BurnAug15	**787**	454425	8681995	Grassland	BurnOct02
263	470385	8652235	Forest	BurnAug15	**788**	455085	8681935	Grassland	BurnOct02
264	471465	8652175	Forest	BurnAug15	**789**	456675	8681785	Grassland	BurnOct02
265	431925	8652055	Forest	BurnAug15	**790**	454335	8681095	Grassland	BurnOct02
266	471075	8651995	Forest	BurnAug15	**791**	454575	8680975	Grassland	BurnOct02
267	432435	8651845	Forest	BurnAug15	**792**	456705	8680645	Grassland	BurnOct02
268	467745	8651635	Forest	BurnAug15	**793**	458775	8680555	Grassland	BurnOct02
269	469455	8651245	Forest	BurnAug15	**794**	452025	8680495	Grassland	BurnOct02
270	450675	8651185	Forest	BurnAug15	**795**	459615	8680345	Grassland	BurnOct02
271	449655	8659285	Cropland	BurnJun04	**796**	452355	8679385	Grassland	BurnOct02
272	450735	8654215	Cropland	BurnJun04	**797**	453855	8679175	Grassland	BurnOct02
273	450735	8654185	Cropland	BurnJun04	**798**	451995	8678605	Grassland	BurnOct02
274	450765	8654155	Cropland	BurnJun04	**799**	452355	8678395	Grassland	BurnOct02
275	458685	8691235	Grassland	BurnJun04	**800**	467685	8676235	Grassland	BurnOct02
276	445695	8689345	Grassland	BurnJun04	**801**	468585	8669185	Grassland	BurnOct02
277	448425	8688925	Grassland	BurnJun04	**802**	450105	8668075	Grassland	BurnOct02
278	448545	8688895	Grassland	BurnJun04	**803**	469215	8667955	Grassland	BurnOct02
279	448425	8688895	Grassland	BurnJun04	**804**	450195	8667895	Grassland	BurnOct02
280	448035	8688865	Grassland	BurnJun04	**805**	450435	8666845	Grassland	BurnOct02
281	448575	8688835	Grassland	BurnJun04	**806**	470625	8666755	Grassland	BurnOct02
282	448665	8688805	Grassland	BurnJun04	**807**	453405	8666605	Grassland	BurnOct02
283	447435	8688115	Grassland	BurnJun04	**808**	449445	8666095	Grassland	BurnOct02
284	447405	8688055	Grassland	BurnJun04	**809**	450165	8665975	Grassland	BurnOct02
285	457785	8687575	Grassland	BurnJun04	**810**	447405	8659555	Grassland	BurnOct02
286	450015	8686675	Grassland	BurnJun04	**811**	454875	8659345	Grassland	BurnOct02
287	468045	8669275	Grassland	BurnJun04	**812**	454155	8658445	Grassland	BurnOct02
288	466455	8668435	Grassland	BurnJun04	**813**	456525	8657215	Grassland	BurnOct02
289	437535	8667925	Grassland	BurnJun04	**814**	442815	8652415	Grassland	BurnOct02
290	449235	8667115	Grassland	BurnJun04	**815**	457575	8690455	Cropland	BurnOct02
291	450045	8666995	Grassland	BurnJun04	**816**	457155	8689645	Cropland	BurnOct02
292	448995	8666245	Grassland	BurnJun04	**817**	444465	8689435	Cropland	BurnOct02
293	448875	8666215	Grassland	BurnJun04	**818**	453495	8689165	Cropland	BurnOct02
294	448965	8666185	Grassland	BurnJun04	**819**	453525	8689135	Cropland	BurnOct02
295	448875	8666155	Grassland	BurnJun04	**820**	453585	8689075	Cropland	BurnOct02
296	448425	8665345	Grassland	BurnJun04	**821**	453645	8689015	Cropland	BurnOct02
297	449085	8664205	Grassland	BurnJun04	**822**	453735	8688985	Cropland	BurnOct02
298	448965	8664205	Grassland	BurnJun04	**823**	449655	8687725	Cropland	BurnOct02
299	449025	8664205	Grassland	BurnJun04	**824**	454035	8687155	Cropland	BurnOct02
300	448965	8664175	Grassland	BurnJun04	**825**	476205	8685835	Cropland	BurnOct02
301	449025	8664175	Grassland	BurnJun04	**826**	475425	8685775	Cropland	BurnOct02

ID	X	Y	Land cover	Burn class	ID	X	Y	Land cover	Burn class
302	444285	8663995	Grassland	BurnJun04	**827**	476205	8685775	Cropland	BurnOct02
303	444255	8663935	Grassland	BurnJun04	**828**	475455	8685745	Cropland	BurnOct02
304	444405	8663845	Grassland	BurnJun04	**829**	475875	8685745	Cropland	BurnOct02
305	444555	8663845	Grassland	BurnJun04	**830**	475305	8685745	Cropland	BurnOct02
306	445095	8662735	Grassland	BurnJun04	**831**	475905	8685745	Cropland	BurnOct02
307	434955	8662405	Grassland	BurnJun04	**832**	475395	8685715	Cropland	BurnOct02
308	435525	8662225	Grassland	BurnJun04	**833**	449655	8685685	Cropland	BurnOct02
309	447735	8661475	Grassland	BurnJun04	**834**	457545	8682715	Cropland	BurnOct02
310	433035	8660695	Grassland	BurnJun04	**835**	457605	8682685	Cropland	BurnOct02
311	448575	8660425	Grassland	BurnJun04	**836**	460275	8682295	Cropland	BurnOct02
312	449445	8660245	Grassland	BurnJun04	**837**	433815	8670415	Cropland	BurnOct02
313	449865	8660185	Grassland	BurnJun04	**838**	444585	8661025	Cropland	BurnOct02
314	449595	8660155	Grassland	BurnJun04	**839**	444555	8660995	Cropland	BurnOct02
315	433335	8659705	Grassland	BurnJun04	**840**	444645	8660965	Cropland	BurnOct02
316	434805	8659405	Grassland	BurnJun04	**841**	444795	8660905	Cropland	BurnOct02
317	449325	8659315	Grassland	BurnJun04	**842**	444555	8660875	Cropland	BurnOct02
318	449385	8659285	Grassland	BurnJun04	**843**	444555	8660845	Cropland	BurnOct02
319	449415	8659225	Grassland	BurnJun04	**844**	434925	8659465	Cropland	BurnOct02
320	448875	8659225	Grassland	BurnJun04	**845**	443565	8659105	Cropland	BurnOct02
321	449415	8659195	Grassland	BurnJun04	**846**	444345	8659045	Cropland	BurnOct02
322	439785	8657635	Grassland	BurnJun04	**847**	439335	8658775	Cropland	BurnOct02
323	451845	8657005	Grassland	BurnJun04	**848**	452925	8658715	Cropland	BurnOct02
324	452235	8656825	Grassland	BurnJun04	**849**	439995	8658715	Cropland	BurnOct02
325	452145	8656795	Grassland	BurnJun04	**850**	452895	8658715	Cropland	BurnOct02
326	452205	8656765	Grassland	BurnJun04	**851**	439905	8658685	Cropland	BurnOct02
327	451305	8654995	Grassland	BurnJun04	**852**	452865	8658685	Cropland	BurnOct02
328	453435	8653645	Grassland	BurnJun04	**853**	440175	8658625	Cropland	BurnOct02
329	460695	8693005	Forest	BurnJun04	**854**	440085	8658625	Cropland	BurnOct02
330	442485	8664265	Forest	BurnJun04	**855**	441225	8658445	Cropland	BurnOct02
331	449115	8664205	Forest	BurnJun04	**856**	443355	8658085	Cropland	BurnOct02
332	442335	8664205	Forest	BurnJun04	**857**	451035	8657995	Cropland	BurnOct02
333	442425	8664175	Forest	BurnJun04	**858**	451035	8654035	Cropland	BurnOct02
334	442515	8664145	Forest	BurnJun04	**859**	464175	8693365	Forest	BurnOct02
335	442215	8664145	Forest	BurnJun04	**860**	469305	8692615	Forest	BurnOct02
336	442305	8664145	Forest	BurnJun04	**861**	467835	8687065	Forest	BurnOct02
337	444375	8663995	Forest	BurnJun04	**862**	468225	8686945	Forest	BurnOct02
338	444315	8663995	Forest	BurnJun04	**863**	456705	8681665	Forest	BurnOct02
339	449085	8661265	Forest	BurnJun04	**864**	454905	8680975	Forest	BurnOct02
340	460905	8660485	Forest	BurnJun04	**865**	456945	8680825	Forest	BurnOct02
341	451305	8658955	Forest	BurnJun04	**866**	457845	8680645	Forest	BurnOct02

ID	X	Y	Land cover	Burn class	ID	X	Y	Land cover	Burn class
342	452775	8657725	Forest	BurnJun04	**867**	453525	8679175	Forest	BurnOct02
343	452355	8656915	Forest	BurnJun04	**868**	472875	8673445	Forest	BurnOct02
344	454275	8655595	Forest	BurnJun04	**869**	474975	8673265	Forest	BurnOct02
345	448935	8655355	Forest	BurnJun04	**870**	474405	8673145	Forest	BurnOct02
346	445095	8693365	Grassland	BurnNov03	**871**	463215	8671855	Forest	BurnOct02
347	468615	8691715	Grassland	BurnNov03	**872**	471045	8671795	Forest	BurnOct02
348	469635	8690515	Grassland	BurnNov03	**873**	464415	8671735	Forest	BurnOct02
349	466275	8690155	Grassland	BurnNov03	**874**	470235	8671015	Forest	BurnOct02
350	446385	8689225	Grassland	BurnNov03	**875**	437775	8670865	Forest	BurnOct02
351	453765	8689165	Grassland	BurnNov03	**876**	474645	8670385	Forest	BurnOct02
352	442635	8688685	Grassland	BurnNov03	**877**	474405	8670295	Forest	BurnOct02
353	452115	8688415	Grassland	BurnNov03	**878**	475125	8670235	Forest	BurnOct02
354	458895	8687365	Grassland	BurnNov03	**879**	454185	8668375	Forest	BurnOct02
355	476385	8686675	Grassland	BurnNov03	**880**	473685	8668345	Forest	BurnOct02
356	437625	8686585	Grassland	BurnNov03	**881**	450465	8667925	Forest	BurnOct02
357	448455	8685835	Grassland	BurnNov03	**882**	433005	8667595	Forest	BurnOct02
358	470955	8685475	Grassland	BurnNov03	**883**	474525	8667325	Forest	BurnOct02
359	448605	8684935	Grassland	BurnNov03	**884**	456225	8667085	Forest	BurnOct02
360	462645	8684875	Grassland	BurnNov03	**885**	451755	8666785	Forest	BurnOct02
361	469065	8684845	Grassland	BurnNov03	**886**	473205	8666635	Forest	BurnOct02
362	450585	8684575	Grassland	BurnNov03	**887**	453165	8666635	Forest	BurnOct02
363	454815	8683885	Grassland	BurnNov03	**888**	454305	8666275	Forest	BurnOct02
364	456525	8683735	Grassland	BurnNov03	**889**	475065	8666155	Forest	BurnOct02
365	472875	8683255	Grassland	BurnNov03	**890**	451785	8665675	Forest	BurnOct02
366	454845	8682895	Grassland	BurnNov03	**891**	446865	8665555	Forest	BurnOct02
367	469995	8682865	Grassland	BurnNov03	**892**	472365	8665555	Forest	BurnOct02
368	471315	8682595	Grassland	BurnNov03	**893**	474105	8665285	Forest	BurnOct02
369	467955	8681035	Grassland	BurnNov03	**894**	445515	8664685	Forest	BurnOct02
370	468525	8681005	Grassland	BurnNov03	**895**	446805	8664445	Forest	BurnOct02
371	469425	8678965	Grassland	BurnNov03	**896**	474225	8664295	Forest	BurnOct02
372	463455	8673865	Grassland	BurnNov03	**897**	431235	8663935	Forest	BurnOct02
373	471945	8669755	Grassland	BurnNov03	**898**	464895	8657785	Forest	BurnOct02
374	451605	8662885	Grassland	BurnNov03	**899**	432465	8656765	Forest	BurnOct02
375	438525	8662885	Grassland	BurnNov03	**900**	442275	8656345	Forest	BurnOct02
376	451605	8662855	Grassland	BurnNov03	**901**	430575	8656075	Forest	BurnOct02
377	451725	8662825	Grassland	BurnNov03	**902**	475725	8655355	Forest	BurnOct02
378	453345	8662615	Grassland	BurnNov03	**903**	472695	8654875	Forest	BurnOct02
379	453195	8662615	Grassland	BurnNov03	**904**	466935	8654545	Forest	BurnOct02
380	453345	8662555	Grassland	BurnNov03	**905**	475245	8652295	Forest	BurnOct02
381	453165	8662555	Grassland	BurnNov03	**906**	464865	8651905	Forest	BurnOct02

ID	X	Y	Land cover	Burn class	ID	X	Y	Land cover	Burn class
382	438165	8661925	Grassland	BurnNov03	**907**	451035	8651185	Forest	BurnOct02
383	454185	8661505	Grassland	BurnNov03	**908**	431535	8651005	Forest	BurnOct02
384	453975	8661505	Grassland	BurnNov03	**909**	467985	8693905	Forest	BurnJul14
385	454125	8661475	Grassland	BurnNov03	**910**	462555	8689705	Forest	BurnJul14
386	454215	8661445	Grassland	BurnNov03	**911**	463605	8689675	Forest	BurnJul14
387	460365	8660485	Grassland	BurnNov03	**912**	462975	8689615	Forest	BurnJul14
388	456075	8660125	Grassland	BurnNov03	**913**	463785	8689435	Forest	BurnJul14
389	453855	8659465	Grassland	BurnNov03	**914**	468255	8688835	Forest	BurnJul14
390	447345	8658625	Grassland	BurnNov03	**915**	468495	8687875	Forest	BurnJul14
391	450405	8658085	Grassland	BurnNov03	**916**	455175	8686795	Forest	BurnJul14
392	432375	8655835	Grassland	BurnNov03	**917**	456825	8686585	Forest	BurnJul14
393	464745	8692465	Cropland	BurnNov03	**918**	473175	8675395	Forest	BurnJul14
394	476265	8690635	Cropland	BurnNov03	**919**	465255	8674615	Forest	BurnJul14
395	469545	8690575	Cropland	BurnNov03	**920**	441405	8673205	Forest	BurnJul14
396	469725	8690545	Cropland	BurnNov03	**921**	475725	8673085	Forest	BurnJul14
397	476145	8689795	Cropland	BurnNov03	**922**	464565	8663995	Forest	BurnJul14
398	475965	8689795	Cropland	BurnNov03	**923**	443445	8662165	Forest	BurnJul14
399	476115	8689765	Cropland	BurnNov03	**924**	443115	8662165	Forest	BurnJul14
400	476355	8689735	Cropland	BurnNov03	**925**	443715	8662045	Forest	BurnJul14
401	476145	8689705	Cropland	BurnNov03	**926**	463185	8659225	Forest	BurnJul14
402	475935	8689615	Cropland	BurnNov03	**927**	450885	8659075	Forest	BurnJul14
403	474135	8686945	Cropland	BurnNov03	**928**	435855	8658355	Forest	BurnJul14
404	471645	8686555	Cropland	BurnNov03	**929**	449475	8658205	Forest	BurnJul14
405	472365	8686405	Cropland	BurnNov03	**930**	440565	8657575	Forest	BurnJul14
406	472095	8686285	Cropland	BurnNov03	**931**	456345	8657275	Forest	BurnJul14
407	472125	8686225	Cropland	BurnNov03	**932**	476505	8655295	Forest	BurnJul14
408	471255	8685475	Cropland	BurnNov03	**933**	469245	8655205	Forest	BurnJul14
409	471105	8685445	Cropland	BurnNov03	**934**	443865	8655175	Forest	BurnJul14
410	471195	8685445	Cropland	BurnNov03	**935**	444975	8655055	Forest	BurnJul14
411	471255	8685415	Cropland	BurnNov03	**936**	446865	8654725	Forest	BurnJul14
412	454305	8664415	Cropland	BurnNov03	**937**	470415	8654035	Forest	BurnJul14
413	454425	8664415	Cropland	BurnNov03	**938**	460425	8653735	Forest	BurnJul14
414	454365	8664385	Cropland	BurnNov03	**939**	460755	8653555	Forest	BurnJul14
415	454275	8664355	Cropland	BurnNov03	**940**	468195	8653345	Forest	BurnJul14
416	452835	8662735	Cropland	BurnNov03	**941**	471105	8653105	Forest	BurnJul14
417	452985	8662705	Cropland	BurnNov03	**942**	471255	8652925	Forest	BurnJul14
418	452925	8662705	Cropland	BurnNov03	**943**	459525	8652865	Forest	BurnJul14
419	452895	8662675	Cropland	BurnNov03	**944**	460005	8652835	Forest	BurnJul14
420	439665	8661595	Cropland	BurnNov03	**945**	455175	8652595	Forest	BurnJul14
421	470985	8660965	Cropland	BurnNov03	**946**	474975	8652595	Forest	BurnJul14

ID	X	Y	Land cover	Burn class	ID	X	Y	Land cover	Burn class
422	471105	8660965	Cropland	BurnNov03	**947**	474765	8652505	Forest	BurnJul14
423	471045	8660935	Cropland	BurnNov03	**948**	454965	8652415	Forest	BurnJul14
424	471105	8660875	Cropland	BurnNov03	**949**	443925	8652115	Forest	BurnJul14
425	437835	8660005	Cropland	BurnNov03	**950**	458055	8652055	Forest	BurnJul14
426	437865	8659915	Cropland	BurnNov03	**951**	473865	8651815	Forest	BurnJul14
427	439125	8659825	Cropland	BurnNov03	**952**	474555	8651725	Forest	BurnJul14
428	439815	8659615	Cropland	BurnNov03	**953**	457755	8651185	Forest	BurnJul14
429	444255	8658985	Cropland	BurnNov03	**954**	459105	8650885	Forest	BurnJul14
430	444885	8658865	Cropland	BurnNov03	**955**	445305	8689405	Cropland	BurnJul14
431	439665	8658745	Cropland	BurnNov03	**956**	456075	8685685	Cropland	BurnJul14
432	439425	8658715	Cropland	BurnNov03	**957**	437805	8683555	Cropland	BurnJul14
433	442275	8658415	Cropland	BurnNov03	**958**	433185	8662645	Cropland	BurnJul14
434	444915	8657875	Cropland	BurnNov03	**959**	436665	8662135	Cropland	BurnJul14
435	452625	8657695	Cropland	BurnNov03	**960**	436725	8662045	Cropland	BurnJul14
436	447345	8657635	Cropland	BurnNov03	**961**	444135	8662015	Cropland	BurnJul14
437	442095	8657395	Cropland	BurnNov03	**962**	443535	8661985	Cropland	BurnJul14
438	452355	8655775	Cropland	BurnNov03	**963**	444225	8661985	Cropland	BurnJul14
439	456525	8653195	Cropland	BurnNov03	**964**	439545	8661655	Cropland	BurnJul14
440	457665	8684665	Forest	BurnNov03	**965**	439365	8661655	Cropland	BurnJul14
441	464355	8681485	Forest	BurnNov03	**966**	433575	8661565	Cropland	BurnJul14
442	463035	8673805	Forest	BurnNov03	**967**	438705	8660845	Cropland	BurnJul14
443	469215	8671975	Forest	BurnNov03	**968**	433245	8660695	Cropland	BurnJul14
444	450675	8671855	Forest	BurnNov03	**969**	441495	8660455	Cropland	BurnJul14
445	451065	8671735	Forest	BurnNov03	**970**	435105	8660425	Cropland	BurnJul14
446	451155	8671705	Forest	BurnNov03	**971**	437295	8660125	Cropland	BurnJul14
447	451185	8671675	Forest	BurnNov03	**972**	443595	8659195	Cropland	BurnJul14
448	453435	8670325	Forest	BurnNov03	**973**	443985	8659105	Cropland	BurnJul14
449	447915	8666335	Forest	BurnNov03	**974**	443715	8659045	Cropland	BurnJul14
450	472515	8664535	Forest	BurnNov03	**975**	450555	8659045	Cropland	BurnJul14
451	444945	8663905	Forest	BurnNov03	**976**	450585	8659015	Cropland	BurnJul14
452	452775	8663755	Forest	BurnNov03	**977**	450555	8658955	Cropland	BurnJul14
453	453675	8663575	Forest	BurnNov03	**978**	450075	8658235	Cropland	BurnJul14
454	453675	8663485	Forest	BurnNov03	**979**	443025	8658235	Cropland	BurnJul14
455	454635	8663395	Forest	BurnNov03	**980**	450045	8658175	Cropland	BurnJul14
456	451455	8662855	Forest	BurnNov03	**981**	450225	8658175	Cropland	BurnJul14
457	451575	8662795	Forest	BurnNov03	**982**	449835	8658145	Cropland	BurnJul14
458	451485	8662765	Forest	BurnNov03	**983**	450195	8658115	Cropland	BurnJul14
459	452625	8662705	Forest	BurnNov03	**984**	450195	8658085	Cropland	BurnJul14
460	452535	8662675	Forest	BurnNov03	**985**	450045	8658055	Cropland	BurnJul14
461	452685	8662645	Forest	BurnNov03	**986**	450225	8658025	Cropland	BurnJul14

ID	X	Y	Land cover	Burn class	ID	X	Y	Land cover	Burn class
462	453795	8662405	Forest	BurnNov03	**987**	445125	8657995	Cropland	BurnJul14
463	454095	8662405	Forest	BurnNov03	**988**	444315	8657995	Cropland	BurnJul14
464	474915	8662255	Forest	BurnNov03	**989**	445185	8657965	Cropland	BurnJul14
465	453045	8661655	Forest	BurnNov03	**990**	445095	8657965	Cropland	BurnJul14
466	473865	8661475	Forest	BurnNov03	**991**	445155	8657935	Cropland	BurnJul14
467	473835	8661415	Forest	BurnNov03	**992**	445185	8657875	Cropland	BurnJul14
468	473775	8661385	Forest	BurnNov03	**993**	439965	8657695	Cropland	BurnJul14
469	471015	8661025	Forest	BurnNov03	**994**	441465	8657545	Cropland	BurnJul14
470	451215	8660935	Forest	BurnNov03	**995**	441405	8657545	Cropland	BurnJul14
471	473355	8660755	Forest	BurnNov03	**996**	449055	8657425	Cropland	BurnJul14
472	467085	8660605	Forest	BurnNov03	**997**	448995	8657335	Cropland	BurnJul14
473	472695	8660575	Forest	BurnNov03	**998**	449025	8657305	Cropland	BurnJul14
474	475335	8660155	Forest	BurnNov03	**999**	448815	8657305	Cropland	BurnJul14
475	464475	8660065	Forest	BurnNov03	**1000**	451155	8653045	Cropland	BurnJul14
476	453075	8659645	Forest	BurnNov03	**1001**	454065	8693845	Grassland	BurnJul14
477	469725	8658325	Forest	BurnNov03	**1002**	468105	8693845	Grassland	BurnJul14
478	461235	8657455	Forest	BurnNov03	**1003**	454545	8692945	Grassland	BurnJul14
479	459465	8654665	Forest	BurnNov03	**1004**	454995	8692735	Grassland	BurnJul14
480	474945	8654605	Forest	BurnNov03	**1005**	459165	8690155	Grassland	BurnJul14
481	466965	8653765	Forest	BurnNov03	**1006**	461085	8690065	Grassland	BurnJul14
482	452475	8651965	Forest	BurnNov03	**1007**	460935	8690065	Grassland	BurnJul14
483	462795	8651335	Forest	BurnNov03	**1008**	468825	8689795	Grassland	BurnJul14
484	451575	8651155	Forest	BurnNov03	**1009**	461475	8689795	Grassland	BurnJul14
485	459375	8694205	Grassland	BurnJul06	**1010**	461565	8689765	Grassland	BurnJul14
486	452505	8692285	Grassland	BurnJul06	**1011**	463935	8689525	Grassland	BurnJul14
487	453825	8691955	Grassland	BurnJul06	**1012**	452985	8689255	Grassland	BurnJul14
488	449385	8691595	Grassland	BurnJul06	**1013**	468645	8688925	Grassland	BurnJul14
489	445665	8691295	Grassland	BurnJul06	**1014**	463305	8688685	Grassland	BurnJul14
490	452145	8691265	Grassland	BurnJul06	**1015**	449715	8688625	Grassland	BurnJul14
491	454125	8690965	Grassland	BurnJul06	**1016**	453405	8688235	Grassland	BurnJul14
492	445125	8690425	Grassland	BurnJul06	**1017**	443085	8687665	Grassland	BurnJul14
493	452175	8690365	Grassland	BurnJul06	**1018**	455265	8686975	Grassland	BurnJul14
494	445455	8690215	Grassland	BurnJul06	**1019**	455655	8686855	Grassland	BurnJul14
495	442155	8689765	Grassland	BurnJul06	**1020**	456945	8684725	Grassland	BurnJul14
496	454815	8688835	Grassland	BurnJul06	**1021**	456915	8684605	Grassland	BurnJul14
497	455355	8687905	Grassland	BurnJul06	**1022**	457185	8684515	Grassland	BurnJul14
498	441885	8686825	Grassland	BurnJul06	**1023**	457305	8683705	Grassland	BurnJul14
499	454425	8685985	Grassland	BurnJul06	**1024**	473025	8683105	Grassland	BurnJul14
500	449175	8685805	Grassland	BurnJul06	**1025**	468705	8682925	Grassland	BurnJul14
501	463725	8684665	Grassland	BurnJul06	**1026**	472755	8675305	Grassland	BurnJul14

ID	X	Y	Land cover	Burn class	ID	X	Y	Land cover	Burn class
502	464385	8684605	Grassland	BurnJul06	**1027**	467235	8675275	Grassland	BurnJul14
503	464355	8684545	Grassland	BurnJul06	**1028**	465375	8674585	Grassland	BurnJul14
504	464355	8684515	Grassland	BurnJul06	**1029**	440625	8674315	Grassland	BurnJul14
505	464835	8684485	Grassland	BurnJul06	**1030**	441465	8673265	Grassland	BurnJul14
506	461775	8684005	Grassland	BurnJul06	**1031**	437475	8660935	Grassland	BurnJul14
507	456555	8683795	Grassland	BurnJul06	**1032**	433755	8660575	Grassland	BurnJul14
508	459855	8683225	Grassland	BurnJul06	**1033**	433605	8660575	Grassland	BurnJul14
509	462915	8682775	Grassland	BurnJul06	**1034**	462885	8659225	Grassland	BurnJul14
510	457935	8682655	Grassland	BurnJul06	**1035**	442965	8658265	Grassland	BurnJul14
511	462195	8676925	Grassland	BurnJul06	**1036**	449715	8658205	Grassland	BurnJul14
512	443715	8670955	Grassland	BurnJul06	**1037**	462345	8657425	Grassland	BurnJul14
513	466635	8669545	Grassland	BurnJul06	**1038**	456075	8657185	Grassland	BurnJul14
514	433635	8662585	Grassland	BurnJul06	**1039**	469335	8656225	Grassland	BurnJul14
515	434475	8660395	Grassland	BurnJul06	**1040**	456075	8653225	Grassland	BurnJul14
516	442005	8660395	Grassland	BurnJul06	**1041**	454485	8652685	Grassland	BurnJul14
517	442065	8660365	Grassland	BurnJul06	**1042**	455625	8652535	Grassland	BurnJul14
518	448395	8660335	Grassland	BurnJul06	**1043**	457785	8652145	Grassland	BurnJul14
519	455745	8660305	Grassland	BurnJul06	**1044**	458625	8652055	Grassland	BurnJul14
520	433905	8659525	Grassland	BurnJul06	**1045**	458535	8651935	Grassland	BurnJul14
521	455415	8659345	Grassland	BurnJul06	**1046**	448365	8651455	Grassland	BurnJul14
522	456195	8659105	Grassland	BurnJul06	**1047**	459525	8650765	Grassland	BurnJul14
523	453555	8657635	Grassland	BurnJul06	**1048**	459585	8650735	Grassland	BurnJul14
524	441255	8656435	Grassland	BurnJul06	**1049**	460125	8650705	Grassland	BurnJul14
525	449055	8656285	Grassland	BurnJul06					

Validation points for 2012 used in Chapter 2, with X and Y coordinates (WGS 1984 UTM Zone 36S), burn class and associated land cover type. The Burn class labels have been shortened due to space limitation e.g. *BurnOct10* instead of *Burn by Oct10* as used in Chapter 2.

ID	X	Y	Land cover	Burn class	ID	X	Y	Land cover	Burn class
1	512445	8681695	Forest	Unburned	**507**	519165	8678485	Grassland	BurnOct10
2	521985	8681665	Forest	Unburned	**508**	519735	8678455	Grassland	BurnOct10
3	504225	8681305	Forest	Unburned	**509**	520095	8677795	Grassland	BurnOct10
4	521985	8680795	Forest	Unburned	**510**	521265	8677585	Grassland	BurnOct10
5	512835	8680615	Forest	Unburned	**511**	515685	8677375	Grassland	BurnOct10
6	502215	8680285	Forest	Unburned	**512**	521595	8677225	Grassland	BurnOct10
7	522495	8680195	Forest	Unburned	**513**	521955	8677075	Grassland	BurnOct10
8	488085	8679505	Forest	Unburned	**514**	521745	8677045	Grassland	BurnOct10

ID	X	Y	Land cover	Burn class	ID	X	Y	Land cover	Burn class
9	510405	8679445	Forest	Unburned	**515**	506235	8676685	Grassland	BurnOct10
10	522525	8679325	Forest	Unburned	**516**	516195	8676265	Grassland	BurnOct10
11	522045	8679235	Forest	Unburned	**517**	516165	8676265	Grassland	BurnOct10
12	522285	8679025	Forest	Unburned	**518**	521145	8675905	Grassland	BurnOct10
13	513285	8678575	Forest	Unburned	**519**	502545	8675665	Grassland	BurnOct10
14	518655	8677885	Forest	Unburned	**520**	521235	8675215	Grassland	BurnOct10
15	501315	8677525	Forest	Unburned	**521**	521295	8675155	Grassland	BurnOct10
16	509025	8677105	Forest	Unburned	**522**	521535	8674615	Grassland	BurnOct10
17	503205	8676595	Forest	Unburned	**523**	521175	8674285	Grassland	BurnOct10
18	521445	8676115	Forest	Unburned	**524**	522495	8674105	Grassland	BurnOct10
19	523125	8676085	Forest	Unburned	**525**	514065	8673955	Grassland	BurnOct10
20	511275	8675965	Forest	Unburned	**526**	522435	8673595	Grassland	BurnOct10
21	520275	8675695	Forest	Unburned	**527**	504285	8673415	Grassland	BurnOct10
22	520485	8675275	Forest	Unburned	**528**	516315	8673385	Grassland	BurnOct10
23	517095	8674945	Forest	Unburned	**529**	518895	8673355	Grassland	BurnOct10
24	513855	8674705	Forest	Unburned	**530**	516795	8673265	Grassland	BurnOct10
25	516045	8674225	Forest	Unburned	**531**	515385	8673205	Grassland	BurnOct10
26	504495	8674105	Forest	Unburned	**532**	522855	8672485	Grassland	BurnOct10
27	520875	8673985	Forest	Unburned	**533**	511665	8672095	Grassland	BurnOct10
28	500025	8672725	Forest	Unburned	**534**	523035	8672035	Grassland	BurnOct10
29	514245	8672395	Forest	Unburned	**535**	500775	8672005	Grassland	BurnOct10
30	521415	8671615	Forest	Unburned	**536**	517875	8669785	Grassland	BurnOct10
31	518625	8671585	Forest	Unburned	**537**	507135	8668795	Grassland	BurnOct10
32	517575	8671525	Forest	Unburned	**538**	501975	8668315	Grassland	BurnOct10
33	517155	8671525	Forest	Unburned	**539**	519975	8667535	Grassland	BurnOct10
34	517485	8671495	Forest	Unburned	**540**	517575	8665795	Grassland	BurnOct10
35	513285	8671135	Forest	Unburned	**541**	517455	8663455	Grassland	BurnOct10
36	514005	8670985	Forest	Unburned	**542**	518925	8662675	Grassland	BurnOct10
37	504915	8670475	Forest	Unburned	**543**	515625	8681305	Grassland	BurnAug07
38	506085	8669905	Forest	Unburned	**544**	514545	8680735	Grassland	BurnAug07
39	505845	8668945	Forest	Unburned	**545**	506355	8680735	Grassland	BurnAug07
40	517785	8668765	Forest	Unburned	**546**	518925	8680375	Grassland	BurnAug07
41	512235	8668345	Forest	Unburned	**547**	507975	8678845	Grassland	BurnAug07
42	519555	8668195	Forest	Unburned	**548**	500175	8677705	Grassland	BurnAug07
43	518265	8668165	Forest	Unburned	**549**	499815	8677075	Grassland	BurnAug07
44	499155	8667925	Forest	Unburned	**550**	499395	8676565	Grassland	BurnAug07
45	518685	8667685	Forest	Unburned	**551**	520485	8676505	Grassland	BurnAug07
46	502755	8667475	Forest	Unburned	**552**	520575	8676295	Grassland	BurnAug07
47	520905	8667355	Forest	Unburned	**553**	520515	8676145	Grassland	BurnAug07
48	521415	8666845	Forest	Unburned	**554**	521025	8676055	Grassland	BurnAug07

ID	X	Y	Land cover	Burn class	ID	X	Y	Land cover	Burn class
49	523035	8666455	Forest	Unburned	**555**	520875	8676025	Grassland	BurnAug07
50	504975	8666095	Forest	Unburned	**556**	520545	8675995	Grassland	BurnAug07
51	519855	8665855	Forest	Unburned	**557**	516165	8675635	Grassland	BurnAug07
52	511005	8665855	Forest	Unburned	**558**	521025	8674825	Grassland	BurnAug07
53	518865	8665705	Forest	Unburned	**559**	522885	8673985	Grassland	BurnAug07
54	498945	8665075	Forest	Unburned	**560**	515715	8673475	Grassland	BurnAug07
55	504525	8664175	Forest	Unburned	**561**	522915	8673295	Grassland	BurnAug07
56	494685	8663755	Forest	Unburned	**562**	522885	8673295	Grassland	BurnAug07
57	517845	8663755	Forest	Unburned	**563**	504105	8672905	Grassland	BurnAug07
58	522615	8663725	Forest	Unburned	**564**	503445	8672305	Grassland	BurnAug07
59	506505	8663305	Forest	Unburned	**565**	495825	8671765	Grassland	BurnAug07
60	517725	8663275	Forest	Unburned	**566**	509145	8671435	Grassland	BurnAug07
61	513405	8663215	Forest	Unburned	**567**	523395	8671375	Grassland	BurnAug07
62	514875	8663065	Forest	Unburned	**568**	520065	8670655	Grassland	BurnAug07
63	521145	8662975	Forest	Unburned	**569**	509145	8670475	Grassland	BurnAug07
64	521625	8662735	Forest	Unburned	**570**	504525	8670475	Grassland	BurnAug07
65	522255	8662555	Forest	Unburned	**571**	519615	8670085	Grassland	BurnAug07
66	511125	8681005	Forest	BurnOct10	**572**	496185	8669785	Grassland	BurnAug07
67	511455	8680945	Forest	BurnOct10	**573**	500385	8669695	Grassland	BurnAug07
68	506655	8680585	Forest	BurnOct10	**574**	518175	8669215	Grassland	BurnAug07
69	521805	8680315	Forest	BurnOct10	**575**	513735	8669065	Grassland	BurnAug07
70	522975	8680045	Forest	BurnOct10	**576**	495825	8668855	Grassland	BurnAug07
71	522795	8680015	Forest	BurnOct10	**577**	519285	8668735	Grassland	BurnAug07
72	518295	8678215	Forest	BurnOct10	**578**	509265	8667385	Grassland	BurnAug07
73	503505	8677135	Forest	BurnOct10	**579**	494235	8667115	Grassland	BurnAug07
74	519825	8676775	Forest	BurnOct10	**580**	516195	8666935	Grassland	BurnAug07
75	502725	8676685	Forest	BurnOct10	**581**	492915	8666875	Grassland	BurnAug07
76	509715	8676535	Forest	BurnOct10	**582**	520575	8666305	Grassland	BurnAug07
77	498495	8676295	Forest	BurnOct10	**583**	510585	8665585	Grassland	BurnAug07
78	505515	8676235	Forest	BurnOct10	**584**	509655	8665495	Grassland	BurnAug07
79	505425	8675815	Forest	BurnOct10	**585**	513165	8665315	Grassland	BurnAug07
80	504555	8675425	Forest	BurnOct10	**586**	511125	8665255	Grassland	BurnAug07
81	510855	8675155	Forest	BurnOct10	**587**	510735	8665015	Grassland	BurnAug07
82	504315	8675095	Forest	BurnOct10	**588**	517185	8664625	Grassland	BurnAug07
83	514095	8674345	Forest	BurnOct10	**589**	521565	8663905	Grassland	BurnAug07
84	503205	8674225	Forest	BurnOct10	**590**	509085	8663875	Grassland	BurnAug07
85	514875	8673535	Forest	BurnOct10	**591**	493695	8663815	Grassland	BurnAug07
86	518805	8673205	Forest	BurnOct10	**592**	505545	8681815	Grassland	BurnJul22
87	499065	8672935	Forest	BurnOct10	**593**	519345	8681455	Grassland	BurnJul22
88	508215	8672875	Forest	BurnOct10	**594**	516015	8681245	Grassland	BurnJul22

ID	X	Y	Land cover	Burn class	ID	X	Y	Land cover	Burn class
89	517575	8671915	Forest	BurnOct10	**595**	514365	8681185	Grassland	BurnJul22
90	522915	8671885	Forest	BurnOct10	**596**	515955	8681185	Grassland	BurnJul22
91	522735	8671795	Forest	BurnOct10	**597**	517035	8675905	Grassland	BurnJul22
92	512895	8671735	Forest	BurnOct10	**598**	508365	8675845	Grassland	BurnJul22
93	490005	8671675	Forest	BurnOct10	**599**	517575	8675425	Grassland	BurnJul22
94	512595	8669815	Forest	BurnOct10	**600**	518055	8675365	Grassland	BurnJul22
95	523455	8668165	Forest	BurnOct10	**601**	505785	8675155	Grassland	BurnJul22
96	522495	8667535	Forest	BurnOct10	**602**	521475	8673775	Grassland	BurnJul22
97	518355	8666515	Forest	BurnOct10	**603**	521085	8673685	Grassland	BurnJul22
98	523185	8666305	Forest	BurnOct10	**604**	516465	8672995	Grassland	BurnJul22
99	508215	8665945	Forest	BurnOct10	**605**	519615	8672755	Grassland	BurnJul22
100	514365	8665735	Forest	BurnOct10	**606**	517845	8672425	Grassland	BurnJul22
101	494925	8665045	Forest	BurnOct10	**607**	519135	8672215	Grassland	BurnJul22
102	519765	8664955	Forest	BurnOct10	**608**	519075	8671855	Grassland	BurnJul22
103	520455	8664955	Forest	BurnOct10	**609**	517935	8671855	Grassland	BurnJul22
104	518505	8663935	Forest	BurnOct10	**610**	518475	8671765	Grassland	BurnJul22
105	513795	8663905	Forest	BurnOct10	**611**	518715	8671615	Grassland	BurnJul22
106	506385	8663875	Forest	BurnOct10	**612**	509115	8671495	Grassland	BurnJul22
107	520875	8663515	Forest	BurnOct10	**613**	520815	8671495	Grassland	BurnJul22
108	521265	8663425	Forest	BurnOct10	**614**	517245	8671105	Grassland	BurnJul22
109	497175	8663425	Forest	BurnOct10	**615**	517005	8670955	Grassland	BurnJul22
110	518235	8663305	Forest	BurnOct10	**616**	503655	8670265	Grassland	BurnJul22
111	506955	8663215	Forest	BurnOct10	**617**	517995	8669965	Grassland	BurnJul22
112	520095	8662975	Forest	BurnOct10	**618**	520035	8669785	Grassland	BurnJul22
113	518625	8662705	Forest	BurnOct10	**619**	521355	8669665	Grassland	BurnJul22
114	512835	8681725	Forest	BurnAug07	**620**	519105	8669065	Grassland	BurnJul22
115	515475	8681665	Forest	BurnAug07	**621**	517755	8668885	Grassland	BurnJul22
116	507885	8681215	Forest	BurnAug07	**622**	519465	8668765	Grassland	BurnJul22
117	514155	8680915	Forest	BurnAug07	**623**	518385	8668465	Grassland	BurnJul22
118	518745	8680315	Forest	BurnAug07	**624**	518415	8668435	Grassland	BurnJul22
119	513645	8679895	Forest	BurnAug07	**625**	517665	8668345	Grassland	BurnJul22
120	489255	8679655	Forest	BurnAug07	**626**	515745	8667895	Grassland	BurnJul22
121	511935	8678875	Forest	BurnAug07	**627**	514785	8667655	Grassland	BurnJul22
122	511755	8678845	Forest	BurnAug07	**628**	518835	8667205	Grassland	BurnJul22
123	494025	8677975	Forest	BurnAug07	**629**	516615	8666875	Grassland	BurnJul22
124	494535	8677885	Forest	BurnAug07	**630**	523095	8663125	Grassland	BurnJul22
125	521475	8677615	Forest	BurnAug07	**631**	504945	8663095	Grassland	BurnJul22
126	501195	8677435	Forest	BurnAug07	**632**	523005	8663065	Grassland	BurnJul22
127	505155	8675305	Forest	BurnAug07	**633**	504105	8662375	Grassland	BurnJul22
128	519405	8675215	Forest	BurnAug07	**634**	523455	8678905	Grassland	BurnNov11

ID	X	Y	Land cover	Burn class	ID	X	Y	Land cover	Burn class
129	523185	8674945	Forest	BurnAug07	**635**	512295	8675245	Grassland	BurnNov11
130	503865	8672935	Forest	BurnAug07	**636**	514785	8674405	Grassland	BurnNov11
131	516285	8672905	Forest	BurnAug07	**637**	519045	8674285	Grassland	BurnNov11
132	516165	8672755	Forest	BurnAug07	**638**	518865	8674285	Grassland	BurnNov11
133	491715	8672365	Forest	BurnAug07	**639**	519015	8674225	Grassland	BurnNov11
134	512445	8672305	Forest	BurnAug07	**640**	521625	8673205	Grassland	BurnNov11
135	505575	8670865	Forest	BurnAug07	**641**	522345	8673175	Grassland	BurnNov11
136	493185	8670865	Forest	BurnAug07	**642**	522435	8673175	Grassland	BurnNov11
137	506595	8670775	Forest	BurnAug07	**643**	522285	8673145	Grassland	BurnNov11
138	507165	8670625	Forest	BurnAug07	**644**	522375	8673085	Grassland	BurnNov11
139	509355	8670325	Forest	BurnAug07	**645**	523215	8672875	Grassland	BurnNov11
140	486255	8670265	Forest	BurnAug07	**646**	502935	8672725	Grassland	BurnNov11
141	504555	8669905	Forest	BurnAug07	**647**	522615	8672575	Grassland	BurnNov11
142	503895	8669605	Forest	BurnAug07	**648**	492615	8671945	Grassland	BurnNov11
143	514005	8669605	Forest	BurnAug07	**649**	492705	8671945	Grassland	BurnNov11
144	501135	8669005	Forest	BurnAug07	**650**	492735	8671915	Grassland	BurnNov11
145	518895	8668795	Forest	BurnAug07	**651**	519855	8670505	Grassland	BurnNov11
146	489945	8668735	Forest	BurnAug07	**652**	498525	8670085	Grassland	BurnNov11
147	522255	8667385	Forest	BurnAug07	**653**	517635	8668585	Grassland	BurnNov11
148	506625	8667235	Forest	BurnAug07	**654**	517845	8668525	Grassland	BurnNov11
149	509745	8666815	Forest	BurnAug07	**655**	517965	8668495	Grassland	BurnNov11
150	521985	8666365	Forest	BurnAug07	**656**	517995	8668465	Grassland	BurnNov11
151	517755	8666335	Forest	BurnAug07	**657**	518055	8665045	Grassland	BurnNov11
152	506385	8666245	Forest	BurnAug07	**658**	488655	8662705	Grassland	BurnNov11
153	506925	8665855	Forest	BurnAug07	**659**	519885	8676385	Grassland	BurnJul06
154	506685	8665825	Forest	BurnAug07	**660**	517185	8672485	Grassland	BurnJul06
155	506295	8665345	Forest	BurnAug07	**661**	517515	8669275	Grassland	BurnJul06
156	491985	8665045	Forest	BurnAug07	**662**	517485	8669215	Grassland	BurnJul06
157	508575	8664985	Forest	BurnAug07	**663**	517515	8669215	Grassland	BurnJul06
158	506505	8664955	Forest	BurnAug07	**664**	517335	8669215	Grassland	BurnJul06
159	487065	8664235	Forest	BurnAug07	**665**	517305	8669185	Grassland	BurnJul06
160	493695	8664205	Forest	BurnAug07	**666**	517455	8669155	Grassland	BurnJul06
161	521505	8663725	Forest	BurnAug07	**667**	517425	8669095	Grassland	BurnJul06
162	516135	8663455	Forest	BurnAug07	**668**	517455	8669095	Grassland	BurnJul06
163	512925	8663275	Forest	BurnAug07	**669**	517485	8669095	Grassland	BurnJul06
164	520875	8662975	Forest	BurnAug07	**670**	517515	8669095	Grassland	BurnJul06
165	517635	8662825	Forest	BurnAug07	**671**	517395	8669095	Grassland	BurnJul06
166	500625	8681845	Forest	BurnSep24	**672**	517455	8669065	Grassland	BurnJul06
167	488715	8681695	Forest	BurnSep24	**673**	522975	8668165	Grassland	BurnJul06
168	503535	8681455	Forest	BurnSep24	**674**	523095	8667145	Grassland	BurnJul06

ID	X	Y	Land cover	Burn class	ID	X	Y	Land cover	Burn class
169	513555	8681305	Forest	BurnSep24	**675**	523245	8667145	Grassland	BurnJul06
170	503025	8681155	Forest	BurnSep24	**676**	517185	8665015	Grassland	BurnJul06
171	503385	8681065	Forest	BurnSep24	**677**	514695	8662705	Grassland	BurnJul06
172	511245	8680885	Forest	BurnSep24	**678**	514665	8662675	Grassland	BurnJul06
173	505245	8680825	Forest	BurnSep24	**679**	514695	8662645	Grassland	BurnJul06
174	488445	8680735	Forest	BurnSep24	**680**	520905	8680615	Cropland	Unburned
175	509205	8680615	Forest	BurnSep24	**681**	518475	8680555	Cropland	Unburned
176	507225	8680495	Forest	BurnSep24	**682**	506385	8677045	Cropland	Unburned
177	488985	8680345	Forest	BurnSep24	**683**	517185	8676445	Cropland	Unburned
178	513165	8680015	Forest	BurnSep24	**684**	510345	8676205	Cropland	Unburned
179	513855	8679955	Forest	BurnSep24	**685**	500715	8675575	Cropland	Unburned
180	506805	8678995	Forest	BurnSep24	**686**	522315	8674885	Cropland	Unburned
181	499035	8678215	Forest	BurnSep24	**687**	519135	8674825	Cropland	Unburned
182	514485	8677555	Forest	BurnSep24	**688**	518925	8674195	Cropland	Unburned
183	491445	8675395	Forest	BurnSep24	**689**	508365	8673475	Cropland	Unburned
184	497355	8675185	Forest	BurnSep24	**690**	509985	8673295	Cropland	Unburned
185	514545	8674285	Forest	BurnSep24	**691**	519255	8672815	Cropland	Unburned
186	515955	8673715	Forest	BurnSep24	**692**	519915	8672755	Cropland	Unburned
187	506445	8673715	Forest	BurnSep24	**693**	515835	8672455	Cropland	Unburned
188	501585	8672905	Forest	BurnSep24	**694**	514035	8672065	Cropland	Unburned
189	490875	8672515	Forest	BurnSep24	**695**	514935	8670835	Cropland	Unburned
190	509025	8672395	Forest	BurnSep24	**696**	520785	8670685	Cropland	Unburned
191	495135	8670895	Forest	BurnSep24	**697**	518835	8670535	Cropland	Unburned
192	503295	8670625	Forest	BurnSep24	**698**	521685	8670535	Cropland	Unburned
193	513135	8670145	Forest	BurnSep24	**699**	514425	8670355	Cropland	Unburned
194	513555	8669845	Forest	BurnSep24	**700**	498765	8670055	Cropland	Unburned
195	523485	8668435	Forest	BurnSep24	**701**	501705	8669545	Cropland	Unburned
196	513555	8668225	Forest	BurnSep24	**702**	520455	8669095	Cropland	Unburned
197	521235	8667895	Forest	BurnSep24	**703**	521625	8668975	Cropland	Unburned
198	503775	8667625	Forest	BurnSep24	**704**	502155	8668885	Cropland	Unburned
199	523155	8667595	Forest	BurnSep24	**705**	523005	8668765	Cropland	Unburned
200	500085	8667205	Forest	BurnSep24	**706**	498195	8668135	Cropland	Unburned
201	504795	8667115	Forest	BurnSep24	**707**	519735	8667955	Cropland	Unburned
202	497295	8666305	Forest	BurnSep24	**708**	502545	8665855	Cropland	Unburned
203	494385	8666065	Forest	BurnSep24	**709**	522315	8665705	Cropland	Unburned
204	505005	8665885	Forest	BurnSep24	**710**	515715	8665555	Cropland	Unburned
205	505485	8665465	Forest	BurnSep24	**711**	516465	8664985	Cropland	Unburned
206	506115	8664385	Forest	BurnSep24	**712**	517575	8664955	Cropland	Unburned
207	507675	8664145	Forest	BurnSep24	**713**	521925	8664685	Cropland	Unburned
208	510585	8663665	Forest	BurnSep24	**714**	520815	8663695	Cropland	Unburned

ID	X	Y	Land cover	Burn class	ID	X	Y	Land cover	Burn class
209	522825	8663395	Forest	BurnSep24	**715**	504585	8662585	Cropland	Unburned
210	522645	8662915	Forest	BurnSep24	**716**	513915	8681875	Cropland	BurnSep24
211	520065	8662915	Forest	BurnSep24	**717**	515145	8681755	Cropland	BurnSep24
212	514185	8662765	Forest	BurnSep24	**718**	509115	8681245	Cropland	BurnSep24
213	496545	8681515	Forest	BurnAug23	**719**	498645	8681185	Cropland	BurnSep24
214	522135	8681095	Forest	BurnAug23	**720**	520845	8681185	Cropland	BurnSep24
215	502155	8680705	Forest	BurnAug23	**721**	515265	8679715	Cropland	BurnSep24
216	502875	8680225	Forest	BurnAug23	**722**	508755	8679655	Cropland	BurnSep24
217	510345	8680105	Forest	BurnAug23	**723**	521325	8679145	Cropland	BurnSep24
218	491505	8679985	Forest	BurnAug23	**724**	518625	8679115	Cropland	BurnSep24
219	501615	8679745	Forest	BurnAug23	**725**	500685	8678935	Cropland	BurnSep24
220	522285	8679685	Forest	BurnAug23	**726**	521055	8678605	Cropland	BurnSep24
221	490065	8679505	Forest	BurnAug23	**727**	518655	8678245	Cropland	BurnSep24
222	502005	8679385	Forest	BurnAug23	**728**	517605	8678005	Cropland	BurnSep24
223	499095	8679145	Forest	BurnAug23	**729**	513765	8677945	Cropland	BurnSep24
224	502425	8679055	Forest	BurnAug23	**730**	523125	8677735	Cropland	BurnSep24
225	503835	8679025	Forest	BurnAug23	**731**	522945	8677435	Cropland	BurnSep24
226	523185	8678965	Forest	BurnAug23	**732**	522765	8677405	Cropland	BurnSep24
227	493905	8678965	Forest	BurnAug23	**733**	522375	8677165	Cropland	BurnSep24
228	496665	8677585	Forest	BurnAug23	**734**	522375	8677105	Cropland	BurnSep24
229	505545	8676895	Forest	BurnAug23	**735**	513315	8675665	Cropland	BurnSep24
230	509715	8676295	Forest	BurnAug23	**736**	503865	8675065	Cropland	BurnSep24
231	491955	8675305	Forest	BurnAug23	**737**	508725	8674765	Cropland	BurnSep24
232	517845	8674345	Forest	BurnAug23	**738**	522525	8674645	Cropland	BurnSep24
233	522195	8673475	Forest	BurnAug23	**739**	509505	8674375	Cropland	BurnSep24
234	493815	8673055	Forest	BurnAug23	**740**	510915	8674045	Cropland	BurnSep24
235	522735	8672125	Forest	BurnAug23	**741**	507975	8673955	Cropland	BurnSep24
236	494325	8671675	Forest	BurnAug23	**742**	516615	8673865	Cropland	BurnSep24
237	490425	8671615	Forest	BurnAug23	**743**	506955	8672755	Cropland	BurnSep24
238	513405	8671375	Forest	BurnAug23	**744**	499545	8672245	Cropland	BurnSep24
239	502815	8671135	Forest	BurnAug23	**745**	498885	8672005	Cropland	BurnSep24
240	486885	8671135	Forest	BurnAug23	**746**	507435	8671585	Cropland	BurnSep24
241	486075	8669305	Forest	BurnAug23	**747**	517815	8671405	Cropland	BurnSep24
242	503625	8669245	Forest	BurnAug23	**748**	522225	8670805	Cropland	BurnSep24
243	505305	8669095	Forest	BurnAug23	**749**	521265	8670145	Cropland	BurnSep24
244	491715	8668435	Forest	BurnAug23	**750**	499095	8668975	Cropland	BurnSep24
245	501735	8668345	Forest	BurnAug23	**751**	517425	8668585	Cropland	BurnSep24
246	490755	8668285	Forest	BurnAug23	**752**	517215	8667805	Cropland	BurnSep24
247	505095	8667985	Forest	BurnAug23	**753**	516045	8667325	Cropland	BurnSep24
248	495645	8667895	Forest	BurnAug23	**754**	519585	8666875	Cropland	BurnSep24

ID	X	Y	Land cover	Burn class	ID	X	Y	Land cover	Burn class
249	505455	8667415	Forest	BurnAug23	**755**	502785	8666515	Cropland	BurnSep24
250	498435	8666515	Forest	BurnAug23	**756**	519165	8665195	Cropland	BurnSep24
251	505635	8665945	Forest	BurnAug23	**757**	521865	8665165	Cropland	BurnSep24
252	518085	8664835	Forest	BurnAug23	**758**	519945	8665135	Cropland	BurnSep24
253	499005	8664055	Forest	BurnAug23	**759**	520725	8664985	Cropland	BurnSep24
254	508605	8664025	Forest	BurnAug23	**760**	518235	8664475	Cropland	BurnSep24
255	502785	8663905	Forest	BurnAug23	**761**	513645	8663845	Cropland	BurnSep24
256	490335	8663425	Forest	BurnAug23	**762**	517065	8663605	Cropland	BurnSep24
257	496395	8663395	Forest	BurnAug23	**763**	517575	8662585	Cropland	BurnSep24
258	506205	8663305	Forest	BurnAug23	**764**	523485	8662465	Cropland	BurnSep24
259	519375	8663095	Forest	BurnAug23	**765**	496395	8681545	Cropland	BurnAug23
260	521895	8662585	Forest	BurnAug23	**766**	514665	8681395	Cropland	BurnAug23
261	497475	8662315	Forest	BurnAug23	**767**	515355	8680705	Cropland	BurnAug23
262	518655	8681725	Forest	BurnNov11	**768**	513795	8680585	Cropland	BurnAug23
263	504075	8681065	Forest	BurnNov11	**769**	519795	8680315	Cropland	BurnAug23
264	512025	8680435	Forest	BurnNov11	**770**	520305	8680165	Cropland	BurnAug23
265	517035	8680405	Forest	BurnNov11	**771**	507285	8679505	Cropland	BurnAug23
266	511305	8680285	Forest	BurnNov11	**772**	521625	8679355	Cropland	BurnAug23
267	522315	8680225	Forest	BurnNov11	**773**	520305	8679055	Cropland	BurnAug23
268	506685	8680015	Forest	BurnNov11	**774**	522525	8678365	Cropland	BurnAug23
269	522405	8679205	Forest	BurnNov11	**775**	522075	8678185	Cropland	BurnAug23
270	516285	8678605	Forest	BurnNov11	**776**	520725	8677765	Cropland	BurnAug23
271	514905	8677765	Forest	BurnNov11	**777**	522315	8677675	Cropland	BurnAug23
272	511395	8676715	Forest	BurnNov11	**778**	521715	8677555	Cropland	BurnAug23
273	522735	8675455	Forest	BurnNov11	**779**	512325	8676775	Cropland	BurnAug23
274	522795	8675425	Forest	BurnNov11	**780**	509925	8675515	Cropland	BurnAug23
275	519345	8674585	Forest	BurnNov11	**781**	518115	8674975	Cropland	BurnAug23
276	517695	8674015	Forest	BurnNov11	**782**	521955	8674345	Cropland	BurnAug23
277	514305	8673985	Forest	BurnNov11	**783**	521175	8672905	Cropland	BurnAug23
278	520245	8673775	Forest	BurnNov11	**784**	520575	8672245	Cropland	BurnAug23
279	494685	8672635	Forest	BurnNov11	**785**	521685	8672065	Cropland	BurnAug23
280	520185	8671915	Forest	BurnNov11	**786**	495885	8670805	Cropland	BurnAug23
281	513855	8671615	Forest	BurnNov11	**787**	513615	8670655	Cropland	BurnAug23
282	520815	8667265	Forest	BurnNov11	**788**	522675	8670475	Cropland	BurnAug23
283	503925	8666665	Forest	BurnNov11	**789**	514005	8670415	Cropland	BurnAug23
284	516195	8665765	Forest	BurnNov11	**790**	513285	8669725	Cropland	BurnAug23
285	518115	8665285	Forest	BurnNov11	**791**	508215	8669635	Cropland	BurnAug23
286	497295	8664325	Forest	BurnNov11	**792**	517665	8669245	Cropland	BurnAug23
287	519075	8664265	Forest	BurnNov11	**793**	507345	8669095	Cropland	BurnAug23
288	522555	8664235	Forest	BurnNov11	**794**	513495	8668705	Cropland	BurnAug23

ID	X	Y	Land cover	Burn class	ID	X	Y	Land cover	Burn class
289	520755	8664115	Forest	BurnNov11	**795**	504525	8668075	Cropland	BurnAug23
290	519555	8664055	Forest	BurnNov11	**796**	494265	8668075	Cropland	BurnAug23
291	498135	8663545	Forest	BurnNov11	**797**	494835	8668015	Cropland	BurnAug23
292	497175	8662735	Forest	BurnNov11	**798**	502125	8667895	Cropland	BurnAug23
293	503295	8662525	Forest	BurnNov11	**799**	518055	8666995	Cropland	BurnAug23
294	523215	8662315	Forest	BurnNov11	**800**	519255	8666725	Cropland	BurnAug23
295	512955	8681605	Forest	BurnJul06	**801**	500655	8666695	Cropland	BurnAug23
296	513135	8681575	Forest	BurnJul06	**802**	508065	8666605	Cropland	BurnAug23
297	513255	8681545	Forest	BurnJul06	**803**	517785	8665525	Cropland	BurnAug23
298	513345	8681515	Forest	BurnJul06	**804**	517065	8664985	Cropland	BurnAug23
299	517095	8672575	Forest	BurnJul06	**805**	516555	8664445	Cropland	BurnAug23
300	517125	8672515	Forest	BurnJul06	**806**	510945	8664175	Cropland	BurnAug23
301	518085	8671045	Forest	BurnJul06	**807**	517515	8664115	Cropland	BurnAug23
302	518025	8671015	Forest	BurnJul06	**808**	492555	8663395	Cropland	BurnAug23
303	517935	8670985	Forest	BurnJul06	**809**	511395	8663275	Cropland	BurnAug23
304	518205	8670955	Forest	BurnJul06	**810**	493395	8663275	Cropland	BurnAug23
305	518235	8670925	Forest	BurnJul06	**811**	513675	8663185	Cropland	BurnAug23
306	517935	8670865	Forest	BurnJul06	**812**	510495	8662735	Cropland	BurnAug23
307	518205	8670835	Forest	BurnJul06	**813**	511935	8662495	Cropland	BurnAug23
308	517995	8670835	Forest	BurnJul06	**814**	510375	8681785	Cropland	BurnAug07
309	518055	8670805	Forest	BurnJul06	**815**	517605	8680735	Cropland	BurnAug07
310	509565	8665525	Forest	BurnJul06	**816**	507705	8680405	Cropland	BurnAug07
311	511695	8665105	Forest	BurnJul06	**817**	509595	8680255	Cropland	BurnAug07
312	511755	8665075	Forest	BurnJul06	**818**	503145	8680195	Cropland	BurnAug07
313	511995	8665045	Forest	BurnJul06	**819**	516705	8680105	Cropland	BurnAug07
314	511815	8665015	Forest	BurnJul06	**820**	519645	8676835	Cropland	BurnAug07
315	512835	8681635	Forest	BurnJul22	**821**	523005	8676385	Cropland	BurnAug07
316	513045	8681575	Forest	BurnJul22	**822**	518085	8676325	Cropland	BurnAug07
317	519315	8681125	Forest	BurnJul22	**823**	501315	8674885	Cropland	BurnAug07
318	518895	8680495	Forest	BurnJul22	**824**	517575	8674675	Cropland	BurnAug07
319	515625	8680345	Forest	BurnJul22	**825**	519705	8674525	Cropland	BurnAug07
320	486945	8677705	Forest	BurnJul22	**826**	522645	8674135	Cropland	BurnAug07
321	519975	8675815	Forest	BurnJul22	**827**	522615	8673745	Cropland	BurnAug07
322	517785	8675425	Forest	BurnJul22	**828**	522765	8673745	Cropland	BurnAug07
323	518055	8675095	Forest	BurnJul22	**829**	515685	8673445	Cropland	BurnAug07
324	511035	8673835	Forest	BurnJul22	**830**	516045	8673265	Cropland	BurnAug07
325	505035	8673385	Forest	BurnJul22	**831**	518025	8672365	Cropland	BurnAug07
326	518475	8672965	Forest	BurnJul22	**832**	515475	8671735	Cropland	BurnAug07
327	520335	8672635	Forest	BurnJul22	**833**	520725	8670505	Cropland	BurnAug07
328	518055	8672605	Forest	BurnJul22	**834**	521955	8669755	Cropland	BurnAug07

ID	X	Y	Land cover	Burn class	ID	X	Y	Land cover	Burn class
329	517755	8672365	Forest	BurnJul22	**835**	514125	8669725	Cropland	BurnAug07
330	520635	8672035	Forest	BurnJul22	**836**	496035	8669485	Cropland	BurnAug07
331	516315	8671945	Forest	BurnJul22	**837**	518295	8669305	Cropland	BurnAug07
332	518445	8671585	Forest	BurnJul22	**838**	521085	8668645	Cropland	BurnAug07
333	521085	8671405	Forest	BurnJul22	**839**	517935	8667685	Cropland	BurnAug07
334	517155	8671165	Forest	BurnJul22	**840**	510765	8667205	Cropland	BurnAug07
335	517245	8670955	Forest	BurnJul22	**841**	517545	8667205	Cropland	BurnAug07
336	521235	8670865	Forest	BurnJul22	**842**	517755	8667115	Cropland	BurnAug07
337	517275	8670805	Forest	BurnJul22	**843**	517725	8666305	Cropland	BurnAug07
338	519075	8670625	Forest	BurnJul22	**844**	518295	8666245	Cropland	BurnAug07
339	517905	8670445	Forest	BurnJul22	**845**	510225	8666095	Cropland	BurnAug07
340	519765	8670355	Forest	BurnJul22	**846**	521085	8666065	Cropland	BurnAug07
341	519315	8670265	Forest	BurnJul22	**847**	513105	8665795	Cropland	BurnAug07
342	518895	8670055	Forest	BurnJul22	**848**	511605	8665555	Cropland	BurnAug07
343	515595	8670055	Forest	BurnJul22	**849**	509325	8665255	Cropland	BurnAug07
344	519435	8669485	Forest	BurnJul22	**850**	510795	8665225	Cropland	BurnAug07
345	519075	8669215	Forest	BurnJul22	**851**	510615	8664925	Cropland	BurnAug07
346	505725	8668945	Forest	BurnJul22	**852**	509355	8664895	Cropland	BurnAug07
347	521085	8668825	Forest	BurnJul22	**853**	503445	8664775	Cropland	BurnAug07
348	519315	8668825	Forest	BurnJul22	**854**	513885	8664445	Cropland	BurnAug07
349	522705	8668345	Forest	BurnJul22	**855**	515085	8664235	Cropland	BurnAug07
350	515055	8667355	Forest	BurnJul22	**856**	512835	8663995	Cropland	BurnAug07
351	520605	8664535	Forest	BurnJul22	**857**	513285	8663995	Cropland	BurnAug07
352	518895	8663905	Forest	BurnJul22	**858**	514005	8663425	Cropland	BurnAug07
353	519165	8663905	Forest	BurnJul22	**859**	516195	8663095	Cropland	BurnAug07
354	505035	8663215	Forest	BurnJul22	**860**	512985	8663035	Cropland	BurnAug07
355	515355	8662555	Forest	BurnJul22	**861**	513465	8662795	Cropland	BurnAug07
356	515865	8662315	Forest	BurnJul22	**862**	512805	8662615	Cropland	BurnAug07
357	510285	8681425	Grassland	BurnAug23	**863**	517755	8679385	Cropland	BurnJul22
358	511965	8680585	Grassland	BurnAug23	**864**	517905	8679355	Cropland	BurnJul22
359	521775	8679445	Grassland	BurnAug23	**865**	515595	8678695	Cropland	BurnJul22
360	520485	8679445	Grassland	BurnAug23	**866**	518985	8677435	Cropland	BurnJul22
361	523335	8679325	Grassland	BurnAug23	**867**	517785	8677345	Cropland	BurnJul22
362	521895	8679145	Grassland	BurnAug23	**868**	519405	8677285	Cropland	BurnJul22
363	498375	8678845	Grassland	BurnAug23	**869**	518085	8677255	Cropland	BurnJul22
364	521865	8678425	Grassland	BurnAug23	**870**	517275	8677165	Cropland	BurnJul22
365	519435	8678365	Grassland	BurnAug23	**871**	517995	8677015	Cropland	BurnJul22
366	522735	8678065	Grassland	BurnAug23	**872**	518145	8676745	Cropland	BurnJul22
367	522405	8678035	Grassland	BurnAug23	**873**	518775	8676745	Cropland	BurnJul22
368	522465	8678005	Grassland	BurnAug23	**874**	518745	8676625	Cropland	BurnJul22

ID	X	Y	Land cover	Burn class	ID	X	Y	Land cover	Burn class
369	521445	8677975	Grassland	BurnAug23	**875**	519315	8676475	Cropland	BurnJul22
370	505935	8677795	Grassland	BurnAug23	**876**	519315	8676385	Cropland	BurnJul22
371	515445	8677735	Grassland	BurnAug23	**877**	517905	8675965	Cropland	BurnJul22
372	521115	8677195	Grassland	BurnAug23	**878**	518055	8675905	Cropland	BurnJul22
373	520695	8677135	Grassland	BurnAug23	**879**	519375	8675755	Cropland	BurnJul22
374	520785	8677105	Grassland	BurnAug23	**880**	519195	8675695	Cropland	BurnJul22
375	491655	8677015	Grassland	BurnAug23	**881**	520635	8674075	Cropland	BurnJul22
376	520185	8676445	Grassland	BurnAug23	**882**	520455	8673895	Cropland	BurnJul22
377	519975	8676415	Grassland	BurnAug23	**883**	520695	8673565	Cropland	BurnJul22
378	520185	8676415	Grassland	BurnAug23	**884**	520995	8673415	Cropland	BurnJul22
379	521355	8674675	Grassland	BurnAug23	**885**	521325	8672725	Cropland	BurnJul22
380	521355	8673715	Grassland	BurnAug23	**886**	503295	8672665	Cropland	BurnJul22
381	518625	8673535	Grassland	BurnAug23	**887**	517635	8672425	Cropland	BurnJul22
382	503745	8673535	Grassland	BurnAug23	**888**	517605	8672395	Cropland	BurnJul22
383	521505	8673415	Grassland	BurnAug23	**889**	519075	8671525	Cropland	BurnJul22
384	511875	8673025	Grassland	BurnAug23	**890**	520785	8671405	Cropland	BurnJul22
385	522135	8671225	Grassland	BurnAug23	**891**	521265	8671015	Cropland	BurnJul22
386	514305	8670715	Grassland	BurnAug23	**892**	517815	8670775	Cropland	BurnJul22
387	513315	8669875	Grassland	BurnAug23	**893**	516645	8670715	Cropland	BurnJul22
388	517605	8669575	Grassland	BurnAug23	**894**	517095	8670565	Cropland	BurnJul22
389	509055	8669395	Grassland	BurnAug23	**895**	517155	8670565	Cropland	BurnJul22
390	502995	8669335	Grassland	BurnAug23	**896**	520875	8670355	Cropland	BurnJul22
391	504195	8669185	Grassland	BurnAug23	**897**	520065	8670025	Cropland	BurnJul22
392	506655	8669155	Grassland	BurnAug23	**898**	519225	8669995	Cropland	BurnJul22
393	504615	8669125	Grassland	BurnAug23	**899**	518265	8669965	Cropland	BurnJul22
394	507615	8669005	Grassland	BurnAug23	**900**	519915	8669935	Cropland	BurnJul22
395	507585	8668765	Grassland	BurnAug23	**901**	519975	8669755	Cropland	BurnJul22
396	507345	8668705	Grassland	BurnAug23	**902**	518865	8669755	Cropland	BurnJul22
397	512295	8668015	Grassland	BurnAug23	**903**	519015	8669665	Cropland	BurnJul22
398	496035	8667385	Grassland	BurnAug23	**904**	521145	8668405	Cropland	BurnJul22
399	518715	8667235	Grassland	BurnAug23	**905**	515025	8667655	Cropland	BurnJul22
400	518955	8667205	Grassland	BurnAug23	**906**	514815	8667625	Cropland	BurnJul22
401	517875	8665675	Grassland	BurnAug23	**907**	514935	8667505	Cropland	BurnJul22
402	508035	8665615	Grassland	BurnAug23	**908**	516285	8667415	Cropland	BurnJul22
403	508005	8665615	Grassland	BurnAug23	**909**	516555	8667085	Cropland	BurnJul22
404	517215	8665225	Grassland	BurnAug23	**910**	516285	8663485	Cropland	BurnJul22
405	504195	8665195	Grassland	BurnAug23	**911**	518475	8662765	Cropland	BurnJul22
406	498495	8665045	Grassland	BurnAug23	**912**	504945	8681905	Cropland	BurnOct10
407	523245	8664625	Grassland	BurnAug23	**913**	521025	8681365	Cropland	BurnOct10
408	498675	8664085	Grassland	BurnAug23	**914**	517245	8680645	Cropland	BurnOct10

ID	X	Y	Land cover	Burn class	ID	X	Y	Land cover	Burn class
409	488745	8663995	Grassland	BurnAug23	**915**	520335	8680465	Cropland	BurnOct10
410	494295	8662855	Grassland	BurnAug23	**916**	521205	8679955	Cropland	BurnOct10
411	513975	8662705	Grassland	BurnAug23	**917**	516465	8679145	Cropland	BurnOct10
412	505845	8681485	Grassland	Unburned	**918**	515085	8678995	Cropland	BurnOct10
413	519975	8681305	Grassland	Unburned	**919**	505725	8678155	Cropland	BurnOct10
414	518895	8681065	Grassland	Unburned	**920**	513645	8675695	Cropland	BurnOct10
415	512925	8681035	Grassland	Unburned	**921**	513645	8675665	Cropland	BurnOct10
416	521355	8680855	Grassland	Unburned	**922**	508485	8675455	Cropland	BurnOct10
417	518985	8680825	Grassland	Unburned	**923**	514035	8675335	Cropland	BurnOct10
418	521235	8680435	Grassland	Unburned	**924**	513795	8675065	Cropland	BurnOct10
419	522105	8680135	Grassland	Unburned	**925**	512595	8674915	Cropland	BurnOct10
420	518445	8679475	Grassland	Unburned	**926**	519465	8674165	Cropland	BurnOct10
421	521385	8679025	Grassland	Unburned	**927**	513105	8673775	Cropland	BurnOct10
422	511425	8678995	Grassland	Unburned	**928**	502005	8672815	Cropland	BurnOct10
423	519225	8678665	Grassland	Unburned	**929**	500715	8672695	Cropland	BurnOct10
424	517035	8678005	Grassland	Unburned	**930**	519975	8672305	Cropland	BurnOct10
425	516615	8677795	Grassland	Unburned	**931**	519945	8672275	Cropland	BurnOct10
426	518445	8677645	Grassland	Unburned	**932**	519945	8672245	Cropland	BurnOct10
427	520635	8677015	Grassland	Unburned	**933**	508695	8671855	Cropland	BurnOct10
428	511425	8676895	Grassland	Unburned	**934**	512265	8671825	Cropland	BurnOct10
429	506085	8675575	Grassland	Unburned	**935**	520875	8671735	Cropland	BurnOct10
430	521355	8675215	Grassland	Unburned	**936**	522165	8670505	Cropland	BurnOct10
431	517455	8675065	Grassland	Unburned	**937**	511635	8668855	Cropland	BurnOct10
432	505905	8674795	Grassland	Unburned	**938**	515955	8668855	Cropland	BurnOct10
433	521445	8674105	Grassland	Unburned	**939**	519975	8668675	Cropland	BurnOct10
434	521355	8673415	Grassland	Unburned	**940**	510975	8668495	Cropland	BurnOct10
435	519375	8673355	Grassland	Unburned	**941**	506595	8667835	Cropland	BurnOct10
436	522105	8672485	Grassland	Unburned	**942**	520995	8667745	Cropland	BurnOct10
437	510885	8671165	Grassland	Unburned	**943**	521415	8667685	Cropland	BurnOct10
438	511965	8671075	Grassland	Unburned	**944**	523455	8667655	Cropland	BurnOct10
439	517965	8669575	Grassland	Unburned	**945**	521565	8667505	Cropland	BurnOct10
440	513645	8666725	Grassland	Unburned	**946**	519795	8667085	Cropland	BurnOct10
441	514845	8666245	Grassland	Unburned	**947**	520215	8666545	Cropland	BurnOct10
442	510045	8665765	Grassland	Unburned	**948**	520425	8666545	Cropland	BurnOct10
443	510345	8664745	Grassland	Unburned	**949**	513105	8666215	Cropland	BurnOct10
444	518715	8663395	Grassland	Unburned	**950**	510105	8666125	Cropland	BurnOct10
445	514335	8681365	Grassland	BurnSep24	**951**	518145	8665735	Cropland	BurnOct10
446	504795	8681275	Grassland	BurnSep24	**952**	518205	8665585	Cropland	BurnOct10
447	515835	8681005	Grassland	BurnSep24	**953**	502785	8665465	Cropland	BurnOct10
448	505605	8680855	Grassland	BurnSep24	**954**	514365	8665015	Cropland	BurnOct10

ID	X	Y	Land cover	Burn class	ID	X	Y	Land cover	Burn class
449	505635	8680765	Grassland	BurnSep24	**955**	515145	8664595	Cropland	BurnOct10
450	514395	8680765	Grassland	BurnSep24	**956**	520395	8664085	Cropland	BurnOct10
451	509745	8680135	Grassland	BurnSep24	**957**	521925	8663815	Cropland	BurnOct10
452	521655	8680045	Grassland	BurnSep24	**958**	520365	8663215	Cropland	BurnOct10
453	521865	8679925	Grassland	BurnSep24	**959**	520275	8663125	Cropland	BurnOct10
454	518355	8679895	Grassland	BurnSep24	**960**	509625	8672665	Cropland	BurnJul06
455	517965	8679895	Grassland	BurnSep24	**961**	509685	8672635	Cropland	BurnJul06
456	521385	8679895	Grassland	BurnSep24	**962**	517185	8672575	Cropland	BurnJul06
457	514815	8679805	Grassland	BurnSep24	**963**	517155	8672515	Cropland	BurnJul06
458	521895	8679655	Grassland	BurnSep24	**964**	512505	8671885	Cropland	BurnJul06
459	521745	8679025	Grassland	BurnSep24	**965**	520065	8671765	Cropland	BurnJul06
460	504495	8679025	Grassland	BurnSep24	**966**	520035	8671705	Cropland	BurnJul06
461	523425	8678935	Grassland	BurnSep24	**967**	519975	8671675	Cropland	BurnJul06
462	521535	8678545	Grassland	BurnSep24	**968**	519945	8671615	Cropland	BurnJul06
463	513105	8678455	Grassland	BurnSep24	**969**	519165	8670985	Cropland	BurnJul06
464	521325	8678395	Grassland	BurnSep24	**970**	517995	8670865	Cropland	BurnJul06
465	508605	8678305	Grassland	BurnSep24	**971**	518025	8670865	Cropland	BurnJul06
466	511125	8677945	Grassland	BurnSep24	**972**	518115	8670835	Cropland	BurnJul06
467	518835	8677885	Grassland	BurnSep24	**973**	518295	8670835	Cropland	BurnJul06
468	499275	8677735	Grassland	BurnSep24	**974**	518325	8670805	Cropland	BurnJul06
469	513705	8677675	Grassland	BurnSep24	**975**	518415	8670775	Cropland	BurnJul06
470	521205	8677675	Grassland	BurnSep24	**976**	521265	8669635	Cropland	BurnJul06
471	521055	8677375	Grassland	BurnSep24	**977**	517185	8669545	Cropland	BurnJul06
472	506055	8676805	Grassland	BurnSep24	**978**	522495	8669095	Cropland	BurnJul06
473	512595	8676775	Grassland	BurnSep24	**979**	522495	8669005	Cropland	BurnJul06
474	506685	8676445	Grassland	BurnSep24	**980**	522285	8668165	Cropland	BurnJul06
475	520275	8676355	Grassland	BurnSep24	**981**	517125	8665675	Cropland	BurnJul06
476	520395	8676115	Grassland	BurnSep24	**982**	517155	8665675	Cropland	BurnJul06
477	510975	8675965	Grassland	BurnSep24	**983**	517125	8665615	Cropland	BurnJul06
478	512955	8674855	Grassland	BurnSep24	**984**	517065	8665615	Cropland	BurnJul06
479	521685	8674195	Grassland	BurnSep24	**985**	500325	8681635	Cropland	BurnNov11
480	521955	8673835	Grassland	BurnSep24	**986**	518175	8677135	Cropland	BurnNov11
481	521115	8673325	Grassland	BurnSep24	**987**	513765	8676955	Cropland	BurnNov11
482	516765	8673175	Grassland	BurnSep24	**988**	519375	8676835	Cropland	BurnNov11
483	522015	8673085	Grassland	BurnSep24	**989**	519375	8676805	Cropland	BurnNov11
484	515505	8672815	Grassland	BurnSep24	**990**	508845	8676445	Cropland	BurnNov11
485	513225	8671105	Grassland	BurnSep24	**991**	510345	8676445	Cropland	BurnNov11
486	514215	8671015	Grassland	BurnSep24	**992**	521625	8676145	Cropland	BurnNov11
487	515505	8670865	Grassland	BurnSep24	**993**	521625	8676115	Cropland	BurnNov11
488	522825	8669365	Grassland	BurnSep24	**994**	521715	8675695	Cropland	BurnNov11

ID	X	Y	Land cover	Burn class	ID	X	Y	Land cover	Burn class
489	519285	8668855	Grassland	BurnSep24	**995**	518475	8675215	Cropland	BurnNov11
490	518205	8668435	Grassland	BurnSep24	**996**	496545	8675185	Cropland	BurnNov11
491	518745	8666875	Grassland	BurnSep24	**997**	508485	8674795	Cropland	BurnNov11
492	515955	8666455	Grassland	BurnSep24	**998**	522615	8674735	Cropland	BurnNov11
493	517815	8665015	Grassland	BurnSep24	**999**	519555	8674255	Cropland	BurnNov11
494	517515	8663245	Grassland	BurnSep24	**1000**	496665	8673595	Cropland	BurnNov11
495	498345	8662945	Grassland	BurnSep24	**1001**	511455	8672935	Cropland	BurnNov11
496	518355	8681845	Grassland	BurnOct10	**1002**	522855	8671675	Cropland	BurnNov11
497	518325	8681815	Grassland	BurnOct10	**1003**	510105	8670355	Cropland	BurnNov11
498	523305	8681665	Grassland	BurnOct10	**1004**	522945	8668585	Cropland	BurnNov11
499	519345	8680645	Grassland	BurnOct10	**1005**	503925	8667325	Cropland	BurnNov11
500	519555	8680615	Grassland	BurnOct10	**1006**	512805	8667235	Cropland	BurnNov11
501	522045	8680405	Grassland	BurnOct10	**1007**	516585	8664325	Cropland	BurnNov11
502	521775	8680225	Grassland	BurnOct10	**1008**	514485	8662765	Cropland	BurnNov11
503	515955	8680225	Grassland	BurnOct10	**1009**	518565	8662435	Cropland	BurnNov11
504	521055	8680015	Grassland	BurnOct10	**1010**	497115	8662405	Cropland	BurnNov11
505	519405	8678785	Grassland	BurnOct10	**1011**	520995	8662375	Cropland	BurnNov11
506	519705	8678635	Grassland	BurnOct10					